Synthesis and Evaluation of Nanoparticle-Polymer Composites

Evita Chundoo

Doctor of Philosophy

Aston University

May 2012

Evita Chundoo, 2012

Evita Chundoo asserts her moral right to be identified as the author of this thesis

Aston University

Synthesis and Evaluation of Nanoparticle-Polymer Composites

Evita Chundoo

Doctor of Philosophy

2012

This thesis describes the synthesis of functionalised polymeric material by a variety of free-radical mediated polymerisation techniques including dispersion, emulsion, seeded emulsion, suspension and bulk polymerisation reactions.

Organic fluorophores and nanoparticles such as quantum dots were incorporated within polymeric materials, in particular, thiol-functionalised polymer microspheres, which were fluorescently labelled either during synthesis or by covalent attachment post synthesis. The resultant fluorescent polymeric conjugates were then assessed for their utility in biological systems as an analytical tool for cells or biological structures.

Quantum dot labelled, thiol-functionalised microspheres were assessed for their utility in the visualisation and tracking of red blood cells. Determination of the possible internalisation of fluorescent microspheres into red blood cells was required before successful tracking of red blood cells could take place. Initial work appeared to indicate the presence of fluorescent microspheres inside red blood cells by the process of beadfection. A range of parameters were also investigated in order to optimise beadfection.

Thiol-functionalised microspheres labelled successfully with organic fluorophores were used to image the tear film of the eye. A description of problems encountered with the covalent attachment of hydrophilic, thiol-reactive fluorescent dyes to a variety of modified polymer microspheres is also included in this section. Results indicated large microspheres were particularly useful when tracking the movement of fluid along the tear meniscus.

Functional bulk polymers were synthesised for assessment of their interaction with titanium dioxide nanoparticles. Thiol-functionalised polymethyl methacrylate and spin-coated thiouronium-functionalised polystyrene appeared to facilitate the attachment of titanium dioxide nanoparticles. Interaction assays included the use of XPS analysis and processes such as centrifugation. Attempts to synthesise 4-vinyl catechol, a compound containing hydroxyl moieties with potential for coordination with titanium dioxide nanoparticles, were also carried out using 3,4-dihydroxybenzaldehyde as the starting material.

To my family whom I am indebted to eternally

Acknowledgements

I would like to thank my supervisor, Dr Andrew Sutherland for his continuous help, patience, guidance and invaluable input throughout my last three years of study.

I would also like to thank Dr Laura Leslie, Professor Geoff Tansley, Dr Lindsay Marshall and Dr Anna Hine for their expertise and assistance in carrying out studies in relation to red blood cells and Paramdeep Bilkhu and Professor James Wolffsohn for their expertise and assistance in performing tear film studies.

I am grateful to Dr Mike Perry for his help and guidance with NMR spectroscopy and his endless humour and catalogue of jokes! I am also grateful to Mr Nick May, Dr Chi Wai Tsang and Mrs Karen Farrow for their assistance in performing high resolution mass spectrometry.

I would also like to thank Charlotte Bland and Dr David Nagel for their tireless efforts and patience in the analysis of samples by Confocal and Fluorescent microscopy.

Thank you to past members of the Sutherland group, in particular, Dr Jonathan Behrendt for his expertise and guidance which were of great value to this project and current members including Gwendolen Chimonides for her help, humour and support.

I would also like to thank my good friends Amandeep Panaser and Selma Riasat for their valued support, advice and comic relief. Thank you to Nicola Pullan and the resident technical genius, Arun Sohdi, for their help and support.

Finally, I would like to thank my Mum, Dad, Shima and Kash for their unconditional support, patience and love. This thesis is dedicated to them.

Abbreviations

4-VBTU	4-Vinylbenzyl isothiouronium chloride
4-VBC	4-Vinylbenzyl chloride
AFM	Atomic Force Microscopy
AIBN	Azobis-*iso*-butyronitrile
APS	Aminopropylsilane
ATP	Adenosine Triphosphate
CdQDs	Cadmium-containing Quantum Dots
CFQDs	Cadmium-free Quantum Dots
CMC	Critical Micelle Concentration
DAPI	4',6-Diamino-2-phenylindole
DBU	1,8-Diazabicyclo[5.4.0]undec-7-ene
DCM	Dichloromethane
DMF	*N-N*-Dimethylformamide
DVB	Divinylbenzene
FACS	Fluorescence Activated Cell Sorting
FTIR	Fourier Transform Infrared Spectroscopy
GFP	Green Fluorescent Protein
HeLa	Human cervical cancer cells
HOMO	Highest Occupied Molecular Orbital
LUMO	Lowest Unoccupied Molecular Orbital
MMA	Methyl Methacrylate
MTT	(3-(4,5-Dimethylthiazol-2-yl)-2,5-diphenyltetrazolium bromide

NIR	Near Infrared
NMR	Nuclear Magnetic Resonance
NSC	Neural Stem Cells
PAA	Polyacrylic acid
PBS	Phosphate Buffered Saline
PEI	Polyethyleneimine
PET	Polyethylene terephthalate
PVA	Polyvinyl alcohol
PVDC	Polyvinylidende chloride
PVP	Polyvinylpyrrolidone
PyMPO	1-(2-Maleimidylethyl)-4-(5-(4-Methoxyphenyl)Oxazol-2-yl)Pyridinium Methanesulfonate
QDs	Quantum Dots
RBCs	Red Blood Cells
ROS	Reactive Oxygen Species
SDS	Sodium Dodecyl Sulfate
TBAF	Tetra-*n*-ammonium fluoride solution
TBDMS-Cl	*Tert*-butyldimethylchlorosilane
TBTU	O-(Benzotriazol-1-yl)-*N*,*N*,*N'*,*N'*-tetramethyluronium tetrafluoroborate
TEOS	Tetraethylorthosilicate
TFA	Trifluoroacetic acid
TLC	Thin Layer Chromatography
TMAOH	Tetramethylammonium hydroxide solution
TMEDA	Tetramethylethylenediamine

TMS	Tetramethylsilane
TFI	Thin Film Interferometry
THF	Tetrahydrofuran
UV	Ultraviolet
XPS	X-ray Photoelectron Spectroscopy

Chapter 1

Introduction 20

Chapter 2

Results and Discussion

10

Chapter 5
References 179

List of Tables

List of Figures

List of Schemes

Chapter 1
Introduction

1.1. Free radical polymerisation

Free radicals are molecules or part of a molecule which possess an unpaired electron[1]. They can be formed by electron-transfer reactions or homolytic bond fission. This unpaired electron is a highly reactive entity which significantly increases the reactivity of the molecule[1].

Free radical polymerisation consists of a reaction mechanism following a series of three steps summarised in Scheme 1[2].

Initiation

$$I \longrightarrow 2I\bullet$$

Propagation

$$I\bullet + M \longrightarrow IM\bullet$$

$$IM\bullet + M \longrightarrow M_{n+1}\bullet$$

Termination

a) Disproportionation $\quad M_{n+1}\bullet + M_{n+1}\bullet \longrightarrow P + M=M_{n+1}$

b) Chain transfer $\quad M_{n+1}\bullet + M \longrightarrow P + M\bullet$

c) Recombination $\quad M_{n+1}\bullet + I\bullet / IM\bullet \longrightarrow P$

I = initiator, M = monomer, IM$\bullet$ = monomer radical,

$M_{n+1}\bullet$ = propagating radical chain, P = polymer

Scheme 1: Summary of the general mechanism for free radical polymerisation[2, 4]

The first step, initiation, involves the generation of a free radical species from a non-free radical molecule by either thermal or photolytic decomposition[2-4]. The free radical species then reacts with the double bond of a monomer unit to form a monomer radical. This monomer radical continues to react rapidly with other monomer units *via* their double bond, propagating the chain. Termination of the growth of the polymer chain occurs in three ways, recombination, disproportionation or chain transfer[3, 4]. When the growing oligomer radical reacts with another monomer radical

or initiator radical, the two radicals combine, thus terminating the propagation of the chain. As the combination of the two radicals is energetically favourable, only a low level of energy is required and the reaction proceeds quickly[1]. Disproportionation occurs when a propagating radical chain abstracts a β-hydrogen from a neighbouring propagating radical chain so that it no longer has any unpaired electrons. The second propagating radical chain will then have two unpaired electrons which subsequently form a double bond[1]. Chain transfer occurs when the radical on a propagating chain transfers to a neighbouring monomer, polymer or solvent.

A commonly used free-radical initiator is azobis-*iso*-butyronitrile, AIBN. Thermolytic fission of AIBN occurs at 70 °C to yield cyano*iso*propyl free radicals[2].

Methods of free radical polymerisation reactions utilised in this project are dispersion, emulsion, seeded emulsion, suspension and bulk polymerisation.

1.1.1. Dispersion polymerisation

The mechanism for free-radical initiated dispersion polymerisation, summarised in Figure 1, involves four stages; initiation, propagation, nucleation and particle formation[5].

Initially, the reaction mixture is a homogeneous solution consisting of a monomer, cross-linker, polymer based stabiliser and initiator[6-10]. The solvent medium selected is one in which the reactants are soluble and the eventual product is insoluble[8, 10, 11].

The reaction mixture is heated to initiate the decomposition of AIBN which induces the formation of free radicals[5, 8]. These radicals initiate the growth of polymer chains by reaction with monomer units[6-8]. The solubility of the polymer chains decreases as the chains increase in molecular weight, until they reach the critical chain length upon which the polymer chains are no longer soluble in the solvent and precipitate out[6, 7, 9]. The insoluble polymer chains then aggregate with other insoluble chains to form spherical structures referred to as nuclei[11]. The size of the nuclei is further increased by addition of free monomer particles which also aggregate with the nuclei[9].

Nuclei are then prevented from further aggregation by the absorbance of a stabiliser which sterically stabilises the growth of the nuclei and leads to the formation of the final polymer particles, polymer microspheres[6-8]. The stabiliser also aids particle formation by adsorbing onto the entire surface of the polymer particle, thus preventing

further adsorption of insolubles or free monomer[12]. A commonly used stabiliser in dispersion polymerisation is polyvinylpyrrolidone (PVP). PVP is an amphiphilic polymer because of its polar amide group and hydrophobic hydrocarbon polymer backbone. This amphiphilic nature is particularly useful in stabilising polymer particles in polar media as the hydrophobic region of the stabiliser is able to interact with the polymer particle, leaving the hydrophilic region projecting outwards into the solution enabling the polymer particles to form stable suspensions in polar solvent media[9].
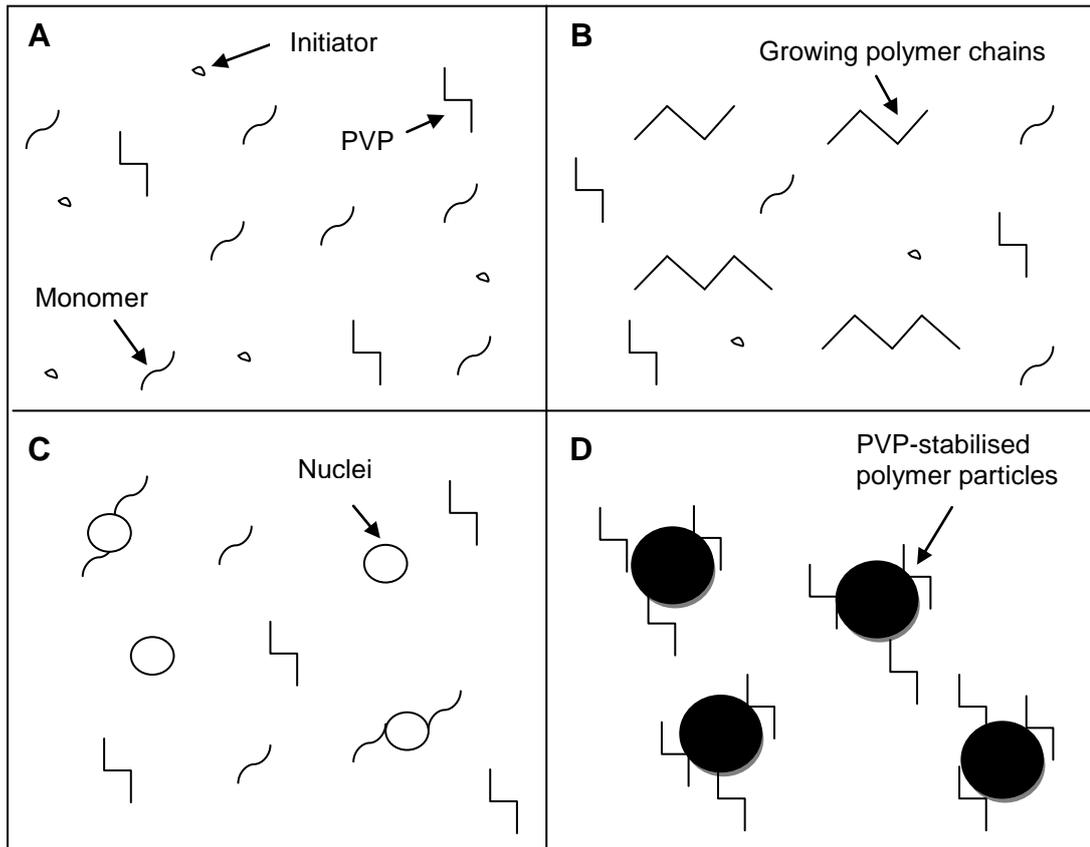
A Initiation: Homogeneous solution of initiator, monomer, and stabiliser. Polymerisation initiated by increasing the temperature of the solution.

B Propagation: Growth of polymer chains until they reach the critical chain length.

C Nucleation: Insoluble polymer chains aggregate into nuclei. The size of nuclei increases due to the addition of free monomer.

D Particle formation: The growth of nuclei is sterically stabilised by the attachment of PVP molecules to form the final polymer particles.

Figure 1: Schematic representation of the mechanistic stages of dispersion polymerisation

The dispersion polymerisation reaction takes place under an inert atmosphere to prevent the polymerisation from being inhibited by the presence of oxygen. The diameter of particles synthesised from this polymerisation technique is generally 1-10 μm and typically possess a narrow size distribution[6, 9-11].

1.1.2. Emulsion polymerisation

Emulsion polymerisation is a heterogeneous system[13] in which the reagents required are monomer, surfactant and a water-soluble initiator[14].

Early models for the mechanism of emulsion polymerisation were proposed by Harkins and a quantitative form of this mechanism was developed by Smith-Ewart[13-16]. A graphical depiction of the polymerisation rate during the stages of emulsion polymerisation is shown in Figure 2.
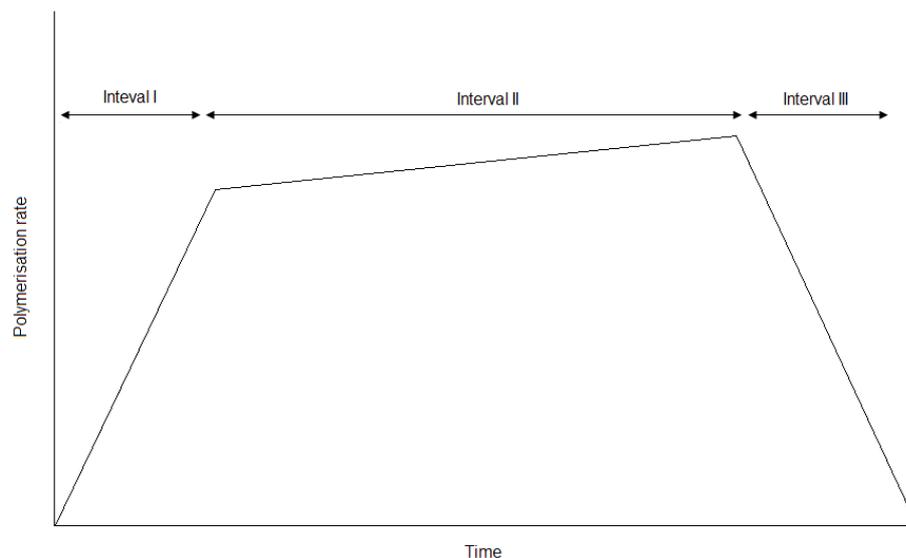
Figure 2: The rate of emulsion polymerisation against time, which is divided into three intervals in accordance with Harkins and Smith-Ewart mechanisms

The mechanism of particle formation and growth is defined by three intervals[13, 16]. Interval I relates to particle formation[16], in which the monomer is suspended in surfactant-rich aqueous media and exists as large, reservoir-like droplets[14]. Above the critical micelle concentration (CMC), excess surfactant aggregates and surrounds the monomer reservoirs. These reservoirs then partition into smaller droplets surrounded by surfactant to form micelles[14], thus solubilising the monomer droplets within the aqueous phase[15]. Free radicals, formed from the decomposition of the

initiator in the aqueous phase[10, 13], react with monomer molecules in the aqueous phase to form monomer radicals. The monomer radicals continue to react with other monomer molecules in the aqueous phase, propagating the chain. Once the chain reaches the critical chain length, it is hydrophobic enough to enter a micelle[14, 16]. The oligomeric radical migrates to the locus of polymerisation in the micelles and continues to propagate with the monomer inside[16].

The micelles can only contain one monomer radical at a time and the entry of another monomer radical into the micelle will terminate propagation[13, 14]. The number of monomer-swollen micelles increases[16] as more oligomeric radicals migrate from the aqueous phase into micelles, this, in turn, leads to an increase in the polymerisation rate as more monomer units are polymerised[13]. As the number and size of micelles increases, more surfactant is used up as it is absorbed onto the growing surface of the micelles[16] until there is no longer any free surfactant present. This marks the end of Interval I.

The number of particles remains constant in Interval II[16], whilst the growth of the micelles continues until all of the monomer droplets have been absorbed by the micelles which signifies the end of Interval II[13]. There is a slight increase in the rate of polymerisation during Interval II due to the Trommsdorff effect[16]. The Trommsdorff effect, also known as the "gel effect", is described as the autoacceleration of free radical polymerisation which occurs due to an increase in the viscosity of the system[17]. Accelerated polymerisation occurs due to difficulties in the termination of polymerisation as the movement of a radical into a micelle is restricted due to the increased viscosity[3, 18, 19]. The movement of monomer molecules within micelles is not restricted hence the propagation of the polymer chains within micelles can continue which leads to an overall increase in the rate of polymerisation[20].

The number of particles also remains the same in Interval III, however the polymerisation rate decreases in accordance with the depleting level of monomer in the micelles as the monomer is being polymerised[13, 15, 16]. Termination of the polymerisation reaction occurs upon entry of a monomer radical into the micelle which reacts with the radical centre in the propagating chain[16].
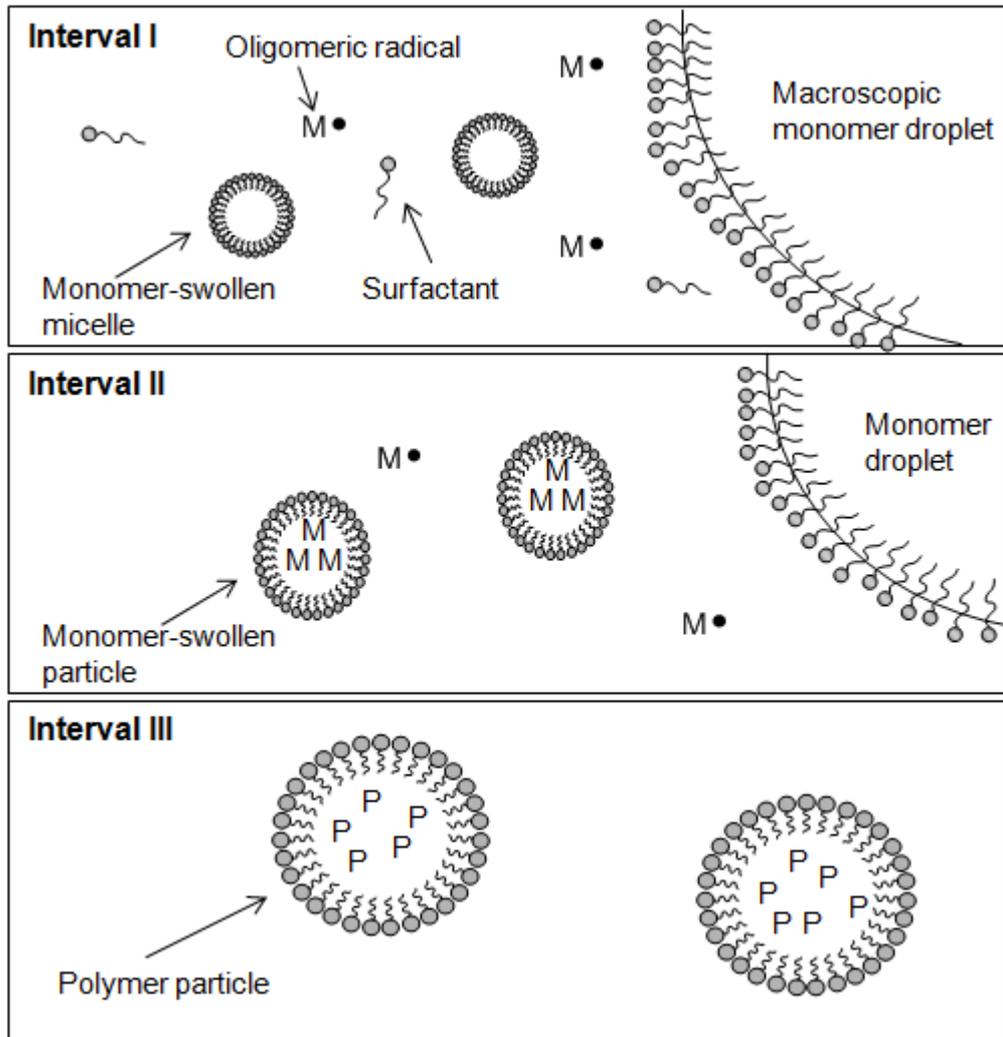
Figure 3: Schematic representation of the three stages of emulsion polymerisation

1.1.3. Suspension polymerisation

Suspension polymerisation reaction conditions typically require monomer, a water-soluble stabiliser and an oil-soluble initiator[21, 22]. The reaction mixture is a heterogeneous solution, consisting of a monomer phase which is dispersed into small droplets in a larger volume of aqueous phase by vigorous stirring[23]. Coalescence may have an impact on the dispersion of droplets at the beginning of the reaction, when monomer is initially dispersed into the aqueous phase. It may also be a factor whilst the polymerisation proceeds, as the formation of polymer particles can also be followed by the agglomeration of these particles[21]. The droplets are prevented from coalescing by vigorous agitation[5], as well as the presence of a stabilising agent[23]. A common stabilising agent is polyvinyl alcohol (PVA), in which PVA possesses a hydrocarbon backbone which surrounds the monomer droplets, with the hydroxyl

groups enabling suspension in aqueous medium[23]. The concentration of stabilising agent used is typically 0.1 wt %[21], which is significantly less than the concentration used in emulsion polymerisations (usually 1-5 wt %)[24]. The stabiliser agent(s) do not form micelles in solution as in emulsion polymerisation, instead it forms a thin film at the monomer-water interface to prevent the monomer droplets from coalescing[25]. This low stabiliser concentration is reflected in the large size of the polymer particles synthesised by this polymerisation reaction.

This type of polymerisation reaction gives rise to spherical polymer particles, usually with a broad size distribution often between a range of 10-500 µm[6, 21, 25]. Droplet size is dependent on the type of monomer used, speed of agitation, type and concentration of stabiliser and the viscosities of the dispersed and continuous phase[21, 23, 25]. It is also affected by the rate of droplet break up and coalescence[23, 25].

The kinetics of suspension polymerisation reactions are similar to that of bulk polymerisation reactions[10, 22] in that the monomer droplets formed from the suspension of monomer in the aqueous phase contain a large number of free radicals, roughly a figure of 10^8[21, 26], each serving as a loci of polymerisation[21, 25, 26]. Termination follows the mechanisms of bulk polymerisation, in which two propagating radicals combine or chain transfer occurs[26].

Water acts as a heat-transfer agent in this reaction, ensuring the efficient distribution and dissipation of heat where required throughout the reaction mixture[27, 28]. This also reduces the impact of the Trommsdorff effect as water is able to effectively dissipate heat from any hot spots which can occur.

1.1.4. Bulk polymerisation

Bulk polymerisation only requires the presence of a monomer and initiator. No solvent is present in this polymerisation. The highly exothermic nature of the reaction, the impact of the Trommsdorff effect and the high activation energies required mean that heat dissipation is difficult and hot spots can occur[19, 24, 29]. The reaction mixture can also become quite viscous making stirring problematic[29].

Bulk polymerisation is best suited to step polymerisations, where low activation energy is required and the molecular weight of the polymer increases slowly, reducing the possibility of hot spots and the Trommsdorff effect[24]. Exceptions to this rule are the chain polymerisations of styrene and methyl methacrylate.

1.1.5. Seeded emulsion polymerisation

In emulsion polymerisation, the size of the final polymer particles is determined by the micellular nucleation stage and the stabilisation of micelle growth[14]. The rate of emulsion polymerisation is dependent on the surface area and number of micelles present in the system as well as the generation of monomer radicals. Seeded emulsion polymerisation overcomes factors that can affect the polymerisation rate of emulsion polymerisation, by the addition of seed particles in the reaction mixture[30]. These seed particles are generally pre-formed polymer particles. The seed particles are swollen with monomer and serve as nuclei, around which monomer can polymerise. This method of polymerisation allows control over the size and number of the final latex particles formed[27]. The end-product from this polymerisation process is typically core-shell particles in which a layer of polymeric shell has been synthesised around the core seed particles[14, 31]. Core-shell particles synthesised by seeded emulsion polymerisation have been investigated by Jose et al[32] and Kobayashi and Senna[33].

1.1.6. Comparison of polymerisation techniques

Table 1: Summary of dispersion, emulsion and suspension polymerisation techniques

| | Polymerisation type | | |
	Dispersion	**Emulsion**	**Suspension**
Solution type	Homogeneous	Heterogeneous	Heterogeneous
Monomer solubility	Soluble in solvent	Insoluble in water	Insoluble in water
Initiator solubility	Soluble in monomer	Soluble in water	Soluble in monomer
Stabiliser	Soluble in solvent	Soluble in water	Soluble in water
Solvent	Organic solvents or water	Water	Water
Particle diameter (μm)	0.5-10	0.1-1	1-100

Table 2: Advantages and disadvantages of dispersion, emulsion and suspension polymerisation techniques

Polymerisation type	Advantages	Disadvantages
Dispersion	Control over heat dissipation Low viscosity of polymer[19]	Washing of polymer required to remove un-reacted monomer
Emulsion	Organic solvents not required for polymerisation[19] High molecular weight polymer and fast polymerisation rate[14] Polymer obtained does not require washing/filtration as most of the monomer polymerises	Water-soluble monomers cannot be used
Suspension	Easy to dissipate heat[21] Organic solvents not required for polymerisation[19]	Washing of polymer required to remove un-reacted monomer / excess surfactant Removal of water required to isolate polymer Efficient stirring required Broad size distribution[21]
Bulk	Simple set-up No solvent required	Heat transfer is difficult Possible local hot spots, broad molecular weight, degradation[24] Slow polymerisation rate[14]

1.2. Quantum dots

Quantum dots (QDs) are crystalline, nanometre-sized structures composed of a metal semi-conductor core[34], coated with a layer of inorganic material, all of which is further coated by an organic ligand layer and is summarised in Figure 4. The organic layer stabilises the structure and additionally enables attachment of entities such as polymer microspheres[35].
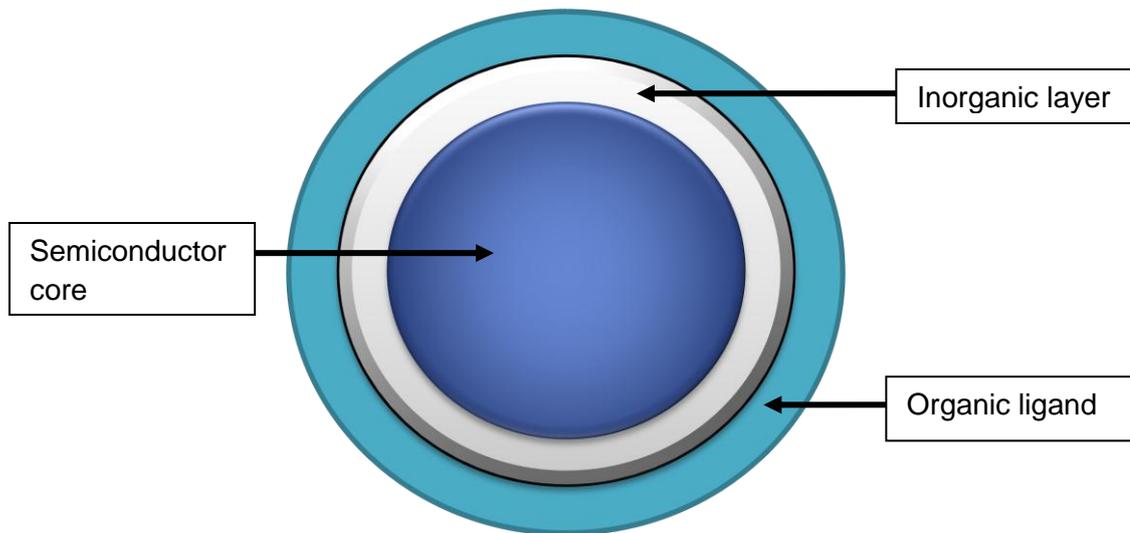
Figure 4: A diagrammatic representation of the structure of a QD

Typically, QDs have a size range of 1-10 nm[36]. The high surface area to volume ratio of these particles imbues them with unique properties which are absent in bulk materials[36]. This is largely due to the quantum confinement effect exhibited by QDs which can be explained by looking in more detail at the relevance of the band gap in the semiconductor material[37].

1.2.1. Band gap

The band gap is the energy difference between the valence band and the conduction band[38, 39]. The electrons which exist on energy levels below this energy gap are known as valence band electrons and electrons above are conduction band electrons. Electrons reside in the valence band as they do not possess the required amount of energy to traverse the band gap. When QDs absorb UV light, electrons become excited and are able to jump from the valence band to the conduction band, leaving a positively charged "hole" in the valence band[40] which is collectively known as an

exciton[41] or an electron-hole pair[42] as depicted in Figure 5. They can also be described as charge carriers.
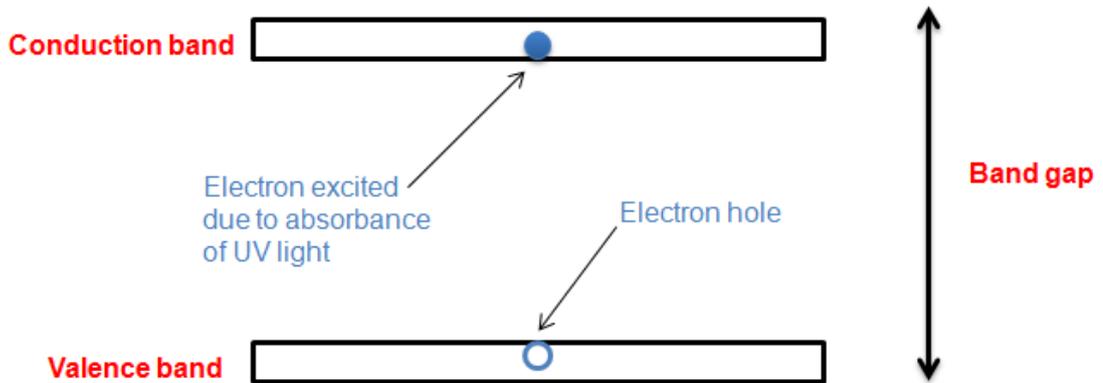
Figure 5: A schematic representation of the promotion of an electron from the valence band to the conduction band after the absorbance of UV light

The electron and the positively charged hole are free to move independently of each other resulting in electrical conductivity. However, the positively charged hole is only temporary and unless the electron and hole are separated, the electron will eventually fall back to the valence band, resulting in the emission of electromagnetic radiation with a wavelength which corresponds to the energy dissipated during electron transfer.

In bulk materials, the band gap is of a fixed position; therefore the wavelength of electromagnetic radiation emitted will not change. In contrast, the band gap is flexible in nano-sized QDs, meaning the wavelength of emission can be changed.

In a QD system, the Exciton Bohr Radius of the semi conductor material, which is the distance between the electron and electron hole in an exciton, is generally larger than the QD itself[35, 39, 43]. Thus, the energy levels in QDs are discrete, and a notable separation between energy levels is apparent, as opposed to bulk materials, in which energy levels are continuous[38]. This breaks the laws of quantum mechanics and these conditions are known as quantum confinement[35]. As a result, the charge carriers assume a higher energy state which requires greater energy to confine the exciton[43]. This leads to an increase in the width of the band gap. As QDs decrease in diameter, the energy needed for confinement increases. This is why QDs shift to blue emission as their size decreases[43].

If the diameter of the QD is modified, this will have an effect on the boundaries of the band gap and consequently a change in wavelength of the radiation emitted from the QD can be observed. This tuneable range of energies means that a range of emission wavelengths can be obtained as demonstrated in Figure 6[44].

Figure 6: A photograph of a range of QDs (all formed from the same semiconductor core) with different emissive properties, are shown to be excited at the same time by a single light source[44]

1.2.2. Properties of quantum dots

One of the most exploitable properties of QDs is their capacity to exhibit optical effects. QDs are characterised by a high quantum yield (80-90 %), high photo-stability, resistance to photo-bleaching and a narrow emission spectrum which is size-tuneable[45, 46]. The narrow emissive properties of QDs are in stark contrast to conventional fluorophores. QDs also have a large absorption spectrum (spanning from NIR to UV), a long fluorescent lifetime (>10 ns)[44] and a large effective Stokes shift[47, 48.] These highly sought-after photo-physical properties make QDs a desirable material for use in many imaging and light-emission based applications.

1.2.3. Quantum dot toxicity

The heavy metal core of a QD generally contains a mixture of cadmium selenide (CdSe) or cadmium telluride (CdTe), both of which are considered to be highly toxic and carcinogenic. To enhance stability and further protect the CdSe or CdTe core, it is often passivated with a zinc selenide layer (ZnSe)[49, 50].

There is still some uncertainty as to the exact nature of the damaging effects caused by QDs and the mechanisms by which these effects occur. One of the effects highlighted in literature is the generation of Reactive Oxygen Species (ROS), possibly due to energy or electron transfer from QDs to oxygen molecules[50, 51]. This can lead

to the degradation and oxidation of QDs. Studies have linked the release of Cd^{2+} with increased cytotoxicity[50] and porphyria[52].

These findings suggest that QDs could be potentially harmful, *in-vivo*, as their surface may be prone to degradation. Consequently, this could lead to the release of the toxic heavy metal ions contained in the core.

1.3. Organic fluorophores

Molecules that possess alternating single and double bonds are conjugated molecules. Conjugation in organic molecules imbues the molecules with individual features, in particular, fluorescence.

Organic fluorophores are generally aromatic, conjugated structures which possess a delocalised π-electronic system[1]. They also usually contain electron donor atoms such as oxygen or nitrogen.

When a fluorophore is irradiated with electromagnetic energy, most of this energy is transmitted; however a small amount of energy is absorbed by the molecule. This energy is distributed across the entire molecule. The conjugated nature of organic fluorophores means that upon absorption of electromagnetic radiation, a ground state electron is promoted from a lower energy bonding (π) molecular orbital (HOMO) to a higher energy anti-bonding (π*) molecular orbital (LUMO)[1], as shown in Figure 7.
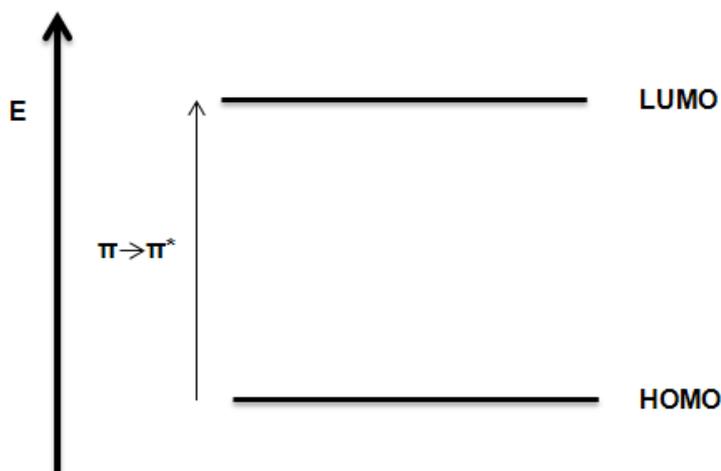
Figure 7: A schematic representation of the energy gap between the HOMO and LUMO states

When the excited electron relaxes to ground state, it emits a photon of light[53].

The energy required for the promotion of an electron relates to the energy gap between the HOMO and LUMO states. This energy gap is analogous to the band gap present in QDs. The energy gap is affected by the level of conjugation in the molecule. The greater the conjugation, the smaller the energy gap between HOMO and LUMO, which means that a smaller amount of energy is required for fluorescence to occur[54]. Therefore, molecules with a high level of conjugation emit light in the red region of the visible spectrum and molecules with a low level of conjugation will emit in the blue region[53, 55].

Organic fluorophores typically have a narrow absorption spectrum which is dependent on the structure of the fluorophore, a broad emission spectrum and are not photo-stable enough for long-term imaging[56]. Photo-bleaching is a major disadvantage when using organic fluorophores. Prolonged photoexcitation renders the fluorophore ineffective and it can no longer emit fluorescence, which limits the imaging capacity of organic fluorophores[56]. Moreover, the broadband emission profiles typically possessed by organic fluorophores can cause problematic overlaps in emission wavelengths if many organic fluorophores are excited at one time[57].

1.3.1. Comparison of fluorescent structures

Table 3: Comparative summary of the optical properties of QDs and fluorescent dyes

	Fluorescent dyes	QDs
Susceptibility to photo-bleaching	High	Low
Photo-stability	Low	High
Emission spectrum	Broad	Narrow
Absorption spectrum	Narrow	Broad

Table 4: Advantages and disadvantages of the use of QDs and organic fluorophores in an imaging capacity

	Advantages	Disadvantages
QDs	No photo-bleaching Broad excitation Narrow emission Large extinction coefficient[58]	Toxic Incompatible with water
Organic fluorophores	Water compatible	Photo-bleaching Narrow excitation Broad emission which could result in spectral overlap[58]

1.4. Cellular delivery of fluorescent-labelled polymer microspheres

Polymer microspheres are stable structures which have been found to enter cells without causing harm[59]. A diverse range of molecules can be attached to the microspheres, including biologically relevant cargo for cellular delivery[60]. Another advantage of the use of microspheres in relation to cells is that they are large enough to be visualised under standard microscopy techniques and microsphere-containing cells can be readily separated from other cells[61]. There is evidence of biocompatibility of polymer microspheres and combined with their biological inertness, these qualities allow their use in biological applications[59, 62-64]. Other benefits include the functionalisation of the microspheres either by the addition of a functional monomer into the polymerisation reaction or by a post polymerisation modification procedure.

The delivery of polymer microspheres into cells has previously been reported by the Sutherland group[59]. The process of microsphere entry into cells is known as beadfection and this process was shown to be highly efficient with neural stem cells (NSC). The presence of microspheres did not appear to negatively affect the NSC and was used to deliver biologically active proteins. Thiol-functionalised microspheres were first labelled with a thiol-reactive fluorescent dye and then encapsulated with a carboxyl-functionalised shell *via* a seeded emulsion polymerisation reaction. Proteins were loaded onto the carboxyl shell *via* a non-cleavable covalent bond. The resultant microspheres were incubated with NSC and results showed that microspheres were

readily internalised into both mouse and human NSC and no toxic effects were observed[59].

Further evidence for beadfection was reported by the Bradley group where efficient uptake of amino-functionalised microspheres by mouse melanoma cells was observed. Microspheres of sizes between 0.2–2 µm were incubated with a range of cell lines including mouse melanoma. Microsphere-containing cells were not found to exhibit any toxic effects and the viability of the cells appeared to be largely unchanged. Microspheres did not appear to have moved into the cell *via* active transport. It was also observed that uptake appeared to be influenced by longer incubation times and smaller microspheres (0.2 µm and 0.5 µm). Lower temperatures (20 °C, 4 °C) were found to significantly lower beadfection. It was suggested that the low temperatures could have reduced the fluidity of the cell membrane making beadfection more difficult[62].

More recently, Bradley *et al*[63] have reported evidence for compatibility of microspheres in HeLa cells. Amino-functionalised microspheres were modified to form thiol reactive microspheres which were then conjugated to thiolated fluorophores. These modified fluorescent microspheres were incubated with HeLa cells and it was observed that the fluorescence of the microspheres was at its highest after 12 hours and had decreased by 24 hours. This decrease in fluorescence was due to the reduction of disulfide bonds present on the microspheres by glutathione which is found to occur naturally in cells. The modified fluorescent microspheres were also conjugated to siRNA in order to assess their capability for gene suppression. The siRNA-containing microspheres were incubated with HeLa-GFP cells and after 72 hours, GFP expression was found to have reduced significantly. The silencing efficiency of GFP had reduced to 80 %. The process of beadfection was monitored by confocal microscopy. Both of these results supported the theory of beadfection[63].

Studies appear to indicate that the passage of microspheres into cells can also be used as a vehicle for drug delivery, transporting biologically relevant cargo to known target cells. The attachment of drugs to polymer microspheres is becoming more prevalent; however the delivery of microspheres into cells has not been extensively investigated. Further studies in this area would help improve the process of microsphere delivery and the transportation of vital drugs to areas of need.

1.5. Tear film

The tear film is a layered structure present over the ocular surface of the eye. The structure of the tear film has been widely discussed in literature with the most common theory, first put forward by Wolff, being a three layer model consisting of a mucin layer, aqueous layer and lipid layer[65-67] as shown in Figure 8[68]. However, the thickness of each layer of the tear film has also been disputed, with different thicknesses reported. The entire tear film is thought to be 7 µm thick, with the lipid layer accounting for 1-1.5 % of the total thickness, aqueous layer contributing to almost 98 % and the mucin layer comprising 0.5 % of the tear film[66, 67, 69].

Aston University

Illustration removed for copyright restrictions

Figure 8: A schematic representation of a cross-sectional view of the layers which comprise the tear film[68]

The lipid layer exists over the outermost surface of the eye and provides an oily surface through which vital ocular fluids cannot easily evaporate. Meibomian glands secrete the lipids that comprise this layer and these lipids pass through the duct openings situated at the inner corner of the eye[69]. The lipid layer contains a mixture of non-polar and polar lipids, the latter of which acts to reduce the interfacial tension between the non-polar lipids and the aqueous layer[70]. This layer also helps maintain the hydration of the eye[65, 66].

The aqueous layer, the central layer of the tear film, is secreted by the lacriminal glands[65, 69]. This layer is a solution containing organic compounds including urea, amino acids, glucose, proteins and inorganic electrolytes such as potassium and sodium ions[71]. This dilute solution is a source of nutrients for the ocular surface and is protected from evaporation due to the oily nature of the lipid layer[65, 66].

The innermost layer of the tear film is the mucin layer and this is secreted by the conjuctival and corneal goblet cells[67, 71]. This layer is composed of long chain glycoproteins and mucus as well as many of the compounds present in the aqueous layer. The presence of mucin provides protection from bacteria[65], increases the wettability of the eye and ensures a smooth, fluid surface for ocular movement[66, 67].

The function of the tear film as a whole involves protection of the cornea from entry of pathogens and microorganisms[65] whilst ensuring that the ocular surface is smooth, uniform and lubricated to provide a surface suitable for light refraction[70]. It also acts as a source of oxygen to help maintain the ocular environment conditions[65] and permits the entry of white blood cells[72] into the eye.

The presence of the tear film across the ocular surface is instigated by the blink action of the eyelid[65]. This action is facilitated by stimulation due to bright light, the presence of a foreign body on the ocular surface or simply due drying of the ocular surface[65]. This action is involuntary and is initiated by the closure of the eyelid. The closure of the lid leads to the distribution of tears and causes the secretion of lipid from the meibomian glands across the ocular surface[65, 67, 73]. Tear drainage through the puncta also occurs during blink action[66]. After blink action, the tear film immediately spreads across the ocular surface[65]. The formation of tear film after blinking is called tear build-up time[74, 75].

Before blinking, the tear film breaks up and this is known as non-invasive tear film break-up time[65].

Failure of the production or even distribution of the tear film across the ocular surface or the quality of the tear film can lead to quicker tear film break-up times, which can result in dry patches on the ocular surface[65]. Continuous occurrence of these dry patches can lead to dry eye syndrome. A method which would allow observation of tear film build-up or break-up time could help distinguish between normal and dry eye subjects.

Previous studies examining tear film break-up time involve non-invasive techniques such as thin film interferometry (TFI). TFI uses the presence of lipid on the outer layer of the tear film to measure the nature of the spread and stability of the tear film. The speed of the spreading of the lipid layer, measured using TFI, was found to be slower in dry eye subjects[76, 77].

The application of particles to the ocular surface is a way of potentially observing the spread of the tear film. Black carbon particles, 15 µm in diameter, have been applied to the ocular surface and the movement of these particles along the lid margin and across to the puncta was observed with high speed photography. Blink action caused the particles to travel across the cornea and towards the puncta[78].

A study using coloured polystyrene microspheres was found to yield similar results. The coloured microspheres were applied to the tear film of subjects wearing different contact lens types. The findings were similar to those with the carbon particles, in that the microspheres moved towards the puncta on blink action. However, the speed at which the microspheres moved was somewhat slower. The microspheres were found to move quickly to the lid margin (within 1–2 seconds), then slowly towards the puncta (5 minutes). For subjects wearing rigid lenses, the microspheres were not found to interact with or flow underneath the lens; however with soft lenses the microspheres were observed to move behind the contact lens *via* blink action. The microspheres were also found to partition into the three layers of the tear film, however the size of microspheres in each layer was not noted nor how the partitioning was achieved[79].

Given that tear film build-up and break-up time has yet to be accurately determined and the estimated thickness of the tear film has been disputed, the development of a method which could help to give a clearer indication of both parameters would be useful.

1.6. Red blood cells

Red blood cells (RBCs) are the simplest of human cells as they do not possess a nucleus or other organelles[80]. RBCs are approximately 8 μm in diameter[81-83] and contain haemoglobin-rich cytoplasm bound by a two-layered membrane. Haemoglobin is the major constituent of RBCs and allows transportation of oxygen from the lungs to the rest of the body, whilst also returning carbon dioxide back to the lungs[84]. The composition and behaviour of the cell membrane of RBCs is adapted to suit this function. To withstand constant circulation around the body, the membrane of RBCs has to be particularly robust and flexible. They must also be able to adapt their shape depending on the diameter of vessel that they must pass through.

Their membrane consists of two layers, an inner cytoskeleton layer and an outer lipid bilayer[85]. The cytoskeleton is mainly composed of spectrin. Spectrin is a cytoskeletal protein consisting of α and β subunits[86] and possesses regions from which it can bind to the other proteins present in the cytoskeleton, principally actin and ankyrin[86-89].

The cytoskeleton also contains protein 4.1, demantin, adducin, tropomyosin and tropomodulin[88, 89]. These proteins interact with other proteins and lipids present in the membrane to ensure attachment of the cytoskeleton to the lipid bilayer. Transport membrane proteins, which include band 3 and Glut1 interact with cytoskeleton proteins such as adducin and demantin to further aid cohesion of the cytoskeleton and lipid bilayer[89].

The lipid bilayer consists of phospholipids and cholesterol. Cholesterol is evenly distributed between the bilayer, whilst phospholipids are asymmetrically distributed[89, 90]. Phospholipids thought to be present in the bilayer are sphingomyelin, phosphatidylcholine, phosphatidylserine, phosphatidylinositol and phosphatidylethanolamine[89, 90]. A model of the two-layered nature of the RBC membrane and the interaction of tethering proteins between the two layers is shown in Figure 9[88].

Figure 9: A schematic representation of a model of the outer lipid bilayer and inner cytoskeleton layer which comprise the RBC membrane[88]

An important feature of RBCs is their ability to undergo a change in shape to enable their passage through a variety of diameters of blood vessels. Generally, there are two shapes associated with RBCs, biconcave and compressed ellipse[81, 82]. Initially, RBCs assume a biconcave shape, which is developed during the maturation of RBCs and takes place in the bone marrow. This shape is maintained during circulation until the RBCs meet narrow capillaries which are <1 μm in diameter[81]. As RBCs are too large to pass through these capillaries, they deform significantly and assume an ellipsoid shape[89, 91] as shown in Figure 10[89].

Figure 10: Biconcave RBCs (top image), ellipsoid-shaped RBCs (bottom image) generated by deformation of biconcave RBCs[89]

The exact mechanism by which shape change occurs is unknown[85, 86] but it is brought about by the highly elastic and flexible nature of the cell membrane of RBCs. It is thought that the surface tension and shear modulus of the cytoskeleton is altered in order to facilitate a shape change[85, 86]. It has also been reported that when RBCs undergo shear stress, *i.e.* when they deform to pass through a capillary smaller than their diameter, they release ATP[91]. This shape change also occurs when levels of ATP are depleted[85]. Low levels of ATP are thought to cause a change in protein interaction between the cytoskeleton and lipid bilayer[90]. Other energy sources include calcium extrusion and enzymes present in the membrane[88].

RBCs with a biconcave shape have 25 % more membrane surface area and this extra membrane allows successful change of shape to an ellipsoid[86, 90]. The cell membrane of RBCs is fluid due to lipid composition and coupled with excess membrane, a biconcave RBC is able to undergo successful deformation[86-88]. Membrane strength is also of vital importance in maintaining the structure of RBCs throughout its life span in the body[90]. Typically RBCs are broken down after 120 days in circulation.

RBCs are only slightly structurally different to eukaryotic cells, with the major difference being the absence of a nucleus. RBCs possess a nucleus during the maturation process in the bone marrow[92, 93] and lose their nucleus after maturation. As RBCs develop from a cell line which contains a nucleus, they can still be described as eukaryotic cells[84].

1.6.1. Red blood cell-mediated drug delivery

RBCs have been investigated as a possible vehicle for drug delivery. Their potential carrier ability is based on their biocompatibility, inertness, circulation throughout the body, long life-span and large capacity[83, 94-99]. It has also been suggested that the carrier capabilities of RBCs can be utilised for the delivery of microspheres imbued with drugs[83].

RBCs are known to interact with and metabolise drugs administered intravenously. These drugs include insulin, dopamine, nitroglycerin and epinephrine[97, 100].

Other biological molecules used for drug delivery include albumin and antibodies[97]. Liposomes have also been used previously as a biologically-occurring carrier in vaccines and for the transportation of drugs[101]. RBCs could be used in a similar manner to liposomes, which are utilised due to their compatibility with biological milieu. RBCs can either be used to deliver site-specific drugs or for the prolonged release of drugs[83, 94, 97].

One of the methods in which RBCs can be loaded with drugs is endocytosis. Drugs that have been successfully loaded into RBCs *via* this method include hydrocortisone, retinol and pravastatin[94]. Endocytosis is an attractive method for drug loading of RBCs as the cells simply engulf the drug and this process is not thought to vastly affect the membrane of the RBC.

Drugs selected for loading must not be prone to degradation once inside RBCs, must not interact with the RBC membrane and should be water soluble[83, 94]. Drugs of particular interest for cellular delivery are anti-inflammatory, anti-viral, anti-amoebic and anti-cancer drugs[83, 97, 99].

Anti-cancer agents, in particular anthracycline antibiotics such as doxorubicin[68], have been loaded into RBCs and used in the treatment of lymphoma patients. A similar anthracycline drug, daunorubicin, was encapsulated into RBCs in the same way and

used in the treatment of patients with acute leukaemia. Results from both studies seemed to indicate a marked improvement in the side effects when compared with administration of the drug on its own[97].

Other methods of drug-loading into RBCs are physical, chemical or osmosis-based[83, 96]. Osmosis methods involve subjecting RBCs to reduced osmotic pressure which allows the desired substance to enter RBCs through their membrane pores. The RBCs are then sealed with isotonic buffer[96]. Techniques such as the chemical perturbation of the membrane, hypotonic haemolysis, electro-insertion and the use of a red cell loader have also been investigated as potential drug loading mechanisms[83, 95, 97].

RBCs which have been filled with drugs and then resealed are known as resealed RBCs[83]. Resealed RBCs have been used successfully in applications which require targeting specific cells such as macrophages[95, 97] or organs such as the liver, treatment of cancer or diseases and the removal of foreign bodies[83].

Synthetic materials proposed as drug delivery vehicles are biodegradable polymer microspheres and polyelectrolyte capsules[96], however the use of these materials alone is not ideal in a biological environment. Perhaps when associated with a biologically-occurring structure, *in-vivo* use may be possible. RBC-membrane coated polymer nanoparticles have been reported for use as a drug delivery system[102].

Disadvantages of using RBCs as a cellular delivery system are the leakage of substances contained with the RBC and the weak nature of the RBC membrane after permeation of the membrane[96, 97]. However, this could be improved upon by coating RBC with polyelectrolytyes *via* a layer-by-layer procedure as reported by Luo et al[96].

1.7. Project aims

Polymer microspheres synthesised from either dispersion, emulsion or suspension polymerisation can be functionalised *via* the inclusion of a functional monomer into the polymerisation reaction.

Functional groups such as thiols are particularly useful for the immobilisation of fluorescent structures such as fluorescent dyes or QDs into polymer microspheres.

The resultant fluorescent-conjugates formed from this immobilisation reaction can be used as an analytical tool for the visualisation of cells, in particular RBCs. The

conjugates can also be used to analyse and visualise the tear film structure residing over the ocular surface of the eye.

The passage of these microspheres into RBCs can also serve as a delivery system, transporting biologically relevant cargo or site-specific drugs to areas of need.

The size of the microspheres for these applications is of importance in the visualisation of these biological structures. The diameter of RBCs is 8 µm which means that only microspheres smaller than this size would be capable of entry. The thickness of tear film is thought to be 7 µm and again, only microspheres smaller than this would be useful for successful visualisation of the tear film.

The development of microspheres with consideration of the aims described above has been explored in this project as well as investigation of the possibility of using these microspheres for visualisation purposes.

The development of functionalised polymeric material for interaction with another type of nanoparticle described in later sections, titanium dioxide nanoparticles, was also explored in this project.

Chapter 2
Results and Discussion

2.1. Synthesis of polymer microspheres

Functionalised polymer microspheres that can covalently attach to structures such as fluorescent dyes and quantum dots (QDs) were synthesised for evaluation in bio-related applications.

Selection and synthesis of a functional monomer was required to functionalise the microspheres. Thiol groups were selected as the moiety of choice as there is evidence of strong interaction with the sites of interest, fluorescent dyes and QDs. This thiol functionality was introduced *via* a thiouronium compound which was subsequently deprotected on-bead to yield the thiol group. The synthetic route to the thiouronium compound and thiol-functionalised microspheres has been previously reported by the Sutherland group[103].

2.1.1. Synthesis of chemically-functionalised polymer microspheres

4-Vinylbenzyl isothiouronium chloride (4-VBTU) **2** was synthesised by a S_N2 displacement reaction between 4-vinylbenzyl chloride **1** and thiourea shown in Scheme 2[103].
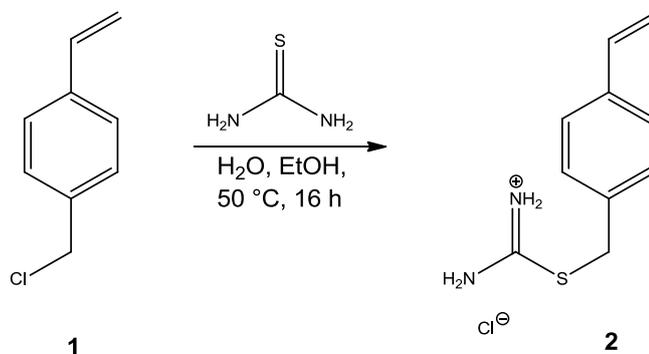
Scheme 2: Synthesis of 4-vinylbenzyl isothiouronium chloride **2** from 4-vinylbenzyl chloride **1**

4-VBTU **2** was synthesised in an 83 % yield and subsequently used as a co-monomer, along with styrene **3** and divinylbenzene (DVB) **4**, in the synthesis of thiouronium-functionalised microspheres **5** *via* a dispersion polymerisation reaction. This monomer mixture was combined with AIBN, a free radical initiator, to initiate the formation of thiouronium-functionalised microspheres **5** represented by Scheme 3[103].
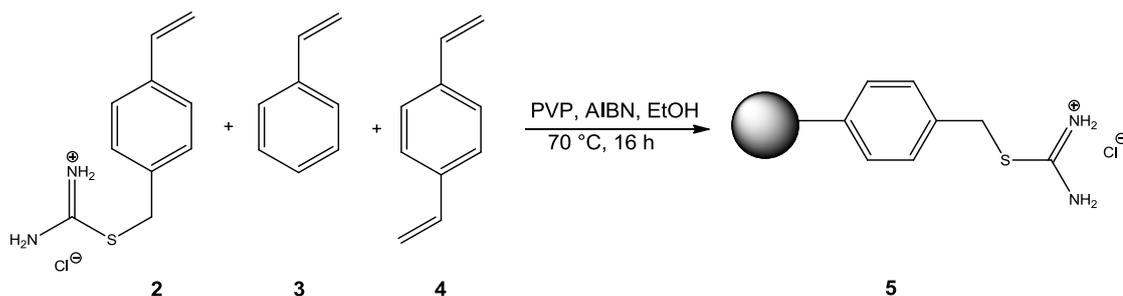
Scheme 3: Synthesis of thiouronium-functionalised microspheres **5** *via* a dispersion polymerisation reaction using 4-VBTU **2** as the functional co-monomer

4-VBTU **2** was used in a 1 % mmol ratio relative to styrene **3**. This was found to be the optimum ratio for yielding monodisperse microspheres within a 1 μm size range which was the diameter most appropriate for the desired applications. The microspheres remain relatively monodisperse with an increasing ratio of 4-VBTU **2**, up to 2 %, above which, the polymerisation reaction fails.

DVB **4**, a cross-linker, was also present in a 1 % mmol ratio relative to styrene **3**. The presence of a cross-linker afforded the microspheres with a microgel-like composition that enabled the polymer to be swollen in organic solvents. This also allowed the easy passage of structures such as fluorophores into the polymer matrix. Polyvinylpyrrolidone (PVP) is a stabiliser in the polymerisation process and was also present in a 0.02 % mmol amount relative to styrene **3**.

After the polymerisation reaction was complete, the resultant thiouronium-functionalised microspheres **5** were washed with methanol and water to remove any un-reacted monomer. The microspheres were obtained in an 86 % yield. Laser diffraction-based size analysis, performed on a Sympatec Helos Particle Size Analyser, showed that the microspheres had a mean diameter of 1.0 μm and a relatively uniform size distribution (standard deviation = 0.5 μm) as shown in Figure 11. Sample preparation and procedure for size analysis is described in section 4.2.1.

Combustion analysis of thiouronium-functionalised microspheres **5** was carried out to determine the elemental composition of the sample. The level of sulfur present in the microspheres was an indication of the loading of 4-VBTU **2**. The sulfur content for thiouronium-functionalised microspheres **5** was found to be <0.10 %, which is below the level of detection available to the analytical instrument. This suggests that the level of 4-VBTU **2** loading is very low, however, in later experiments, the level was found to be sufficient to anchor a high level of the desired structures. Combustion analysis data also indicated the level of nitrogen present in the microspheres, which

was found to be 0.36 %. This level cannot be used as a sole indicator of 4-VBTU **2** loading as AIBN used in the polymerisation will also be present in resultant microspheres, thus contributing to the nitrogen levels.
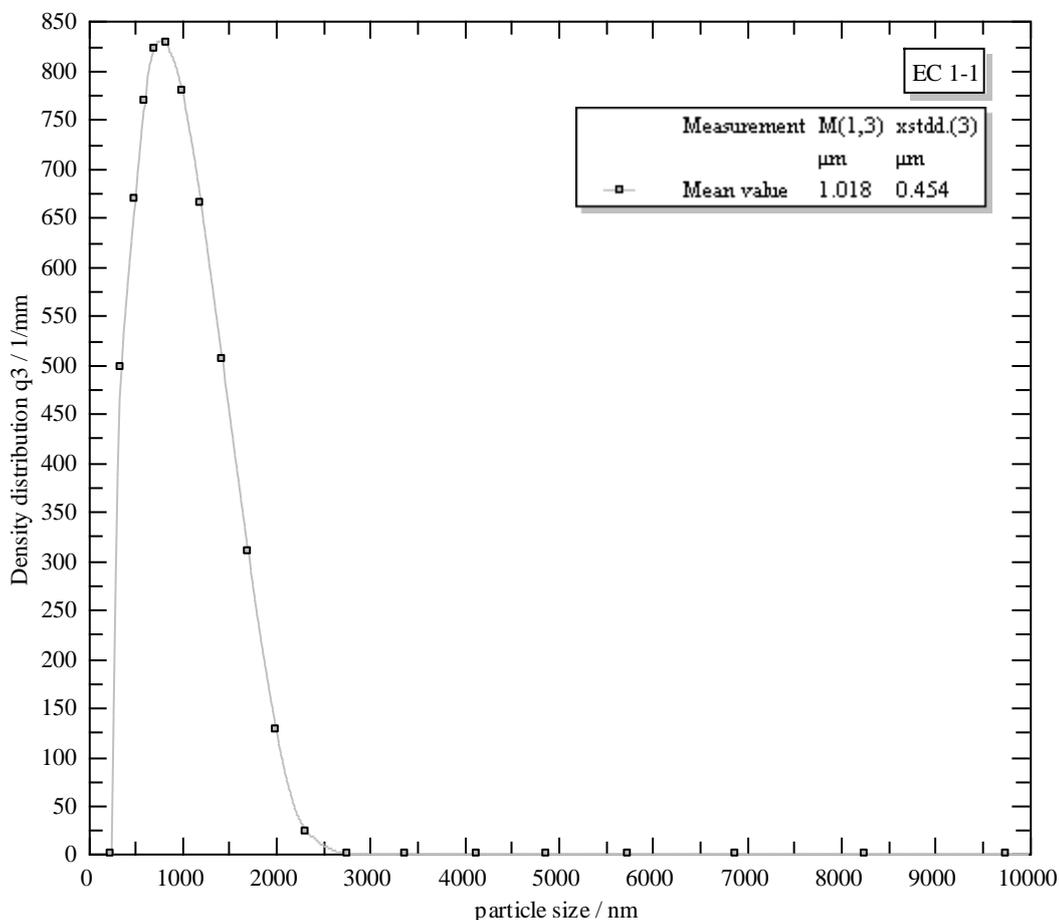
Figure 11: Distribution density curve for particle size of thiouronium-functionalised microspheres **5** suspended in distilled water, obtained by laser diffraction analysis after a 60 second period of ultrasonication

The thiouronium moieties within the microspheres **5** were then converted to the thiol functionality *via* deprotection with a base, tetramethylammonium hydroxide (TMAOH) as shown in Scheme 4.
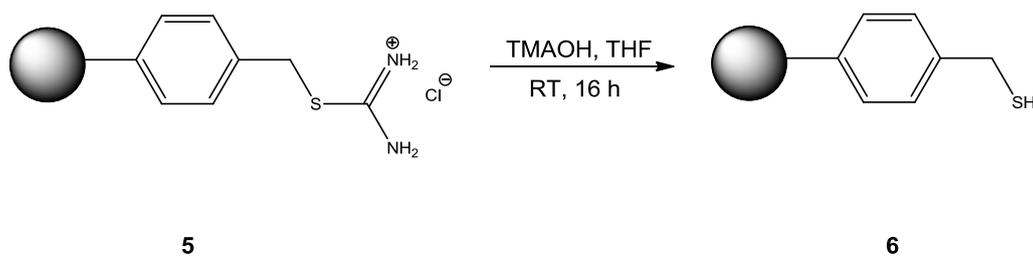
Scheme 4: Conversion of thiouronium-functionalised microspheres **5** to thiol-functionalised microspheres **6**

The microspheres were swollen in tetrahydrofuran (THF) to allow the base, TMAOH, better access to the thiouronium groups. After conversion of the thiouronium groups, the thiol-functionalised microspheres **6** were washed with THF and methanol to remove excess base and the cleaved urea molecule. The resultant thiol-functionalised microspheres **6** were recovered in a 96 % yield and their size distribution had not changed.

2.2. Immobilisation of QDs into thiol-functionalised microspheres 6

Work reported by Behrendt *et al*[103] found that thiol-functionalised microspheres **6**, can act as polymeric ligands for the immobilisation of nanoparticles such as QDs. QDs are electron poor and possess metal lewis acid sites which are able to form strong bonds with nucleophiles, in particular, thiol groups[104]. The reported immobilisation procedure was used to immobilise different types of QDs for this project.

There were two types of QDs that were immobilised into thiol-functionalised microspheres **6**, cadmium-free quantum dots (CFQDs) and cadmium-containing quantum dots (CdQDs).

CdQDs and CFQDs were each immobilised into thiol-functionalised microspheres **6** *via* a simple swelling/doping procedure as shown in Scheme 5.

6   **7**
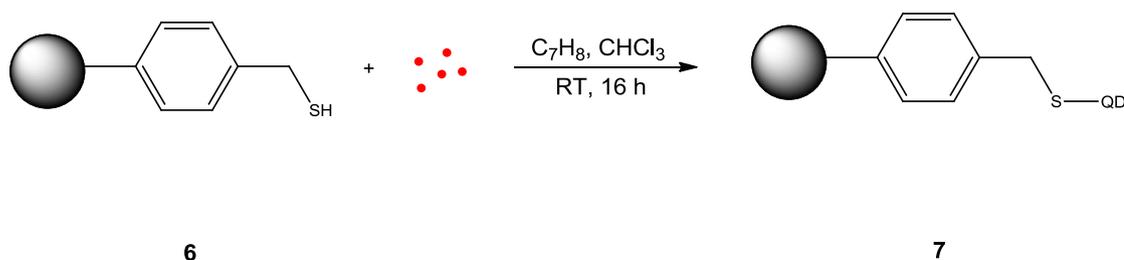
Scheme 5: Immobilisation of QDs into thiol-functionalised microspheres **6**

Thiol-functionalised microspheres **6** were swollen in toluene and chloroform, which allowed the easy passage of an excess amount of QDs into the polymer matrix of the microspheres. This also allowed QDs access to the sites of attachment, the thiol groups, to which they can covalently bind. The resultant "QD-microspheres" **7** were found to possess a high level of fluorescence which was assessed qualitatively with a fibre-optic fluorescent probe and under UV light.

After the immobilisation reaction, the resultant QD-microspheres **7** were washed with toluene and ethanol to remove excess unbound QDs. Following these organic washes, the QD-microspheres **7** were resuspended in water after suspension in a 0.01 wt % aqueous solution of PVP. PVP is an amphiphilic polymer which contains a polar amide group and a non-polar hydrocarbon backbone which gives rise to its hydrophobic and hydrophilic nature[46]. The hydrophobic region of the polymer surrounds the microspheres and is held by hydrophobic-hydrophobic interactions and the hydrophilic region projects outwards into the solution enabling QD-microspheres **7** to form stable suspensions in water[46].

QD-microspheres **7** underwent several water washes (to remove the excess PVP), whilst retaining the fluorescence of the QD-microspheres **7**.

The CFQDs were immobilised into thiol-functionalised microspheres **6** using the same method depicted in Scheme 5. Again, the CFQD-microspheres were washed with toluene and ethanol to remove any excess unbound QDs. However, unlike the procedure for CdQD immobilisation described above, the water and PVP washes were not carried out as a loss of fluorescence was observed when CFQD-microspheres were washed into water. The fluorescence of CFQDs was found to be less than that of CdQDs after immobilisation into thiol-functionalised microspheres **6**, therefore the development of a method to prevent loss of fluorescence would be advantageous if CFQDs are to be applied to further use.

2.3. Coating of QD-microspheres 7

The fluorescence of QDs and thus QD-microspheres **7** is thought to decrease in the presence of oxygen and moisture. The introduction of a physical barrier around QD-microspheres **7**, in the form of a coating or shell would be a possible method of prevention of the passage of oxygen or moisture to QDs. Ideally, the resultant QD-microspheres would be more stable and less prone to photo degradation thus enhancing the fluorescent lifetime of QD-microspheres **7**.

The potential coating material should act as a gas barrier, preventing the permeation of oxygen or moisture. A strong adhesion to the QD-microspheres **7** (either by covalent bonding or electrostatic attraction) will prevent the coating material from being displaced by solvents or processes such as ultrasonication or centrifugation.

Therefore, methods of increasing fluorescent lifetime by coating or shelling QD-microspheres **7** have been explored in this project.

2.3.1. Silica shelling of QD-microspheres **7**

Polysiloxanes have been reported to provide resistance to moisture and oxygen by successfully shelling polymer latexes. The strength of the Si-O bond (452 KJ mol^{-1}) provides durability to the shell and the bond has high resistance to heat, UV light and oxidation. A protocol for the silica shelling of polymer microspheres developed by Behrendt et al[105], was applied to the shelling of QD-microspheres **7**. A silica shell was synthesised around QD-microspheres **7** with a view to creating a gas barrier around the QDs.

Two silane monomers were used in the synthesis of the silica shell, tetraethylorthosilicate (TEOS) and aminopropylsilane (APS). TEOS and APS were used in a 1:1 ratio relative to each other and the ratio of silanes to microspheres was 2:1. TMAOH was also used in the reaction, which is shown in Scheme 6.

● represents QD-microspheres **7**
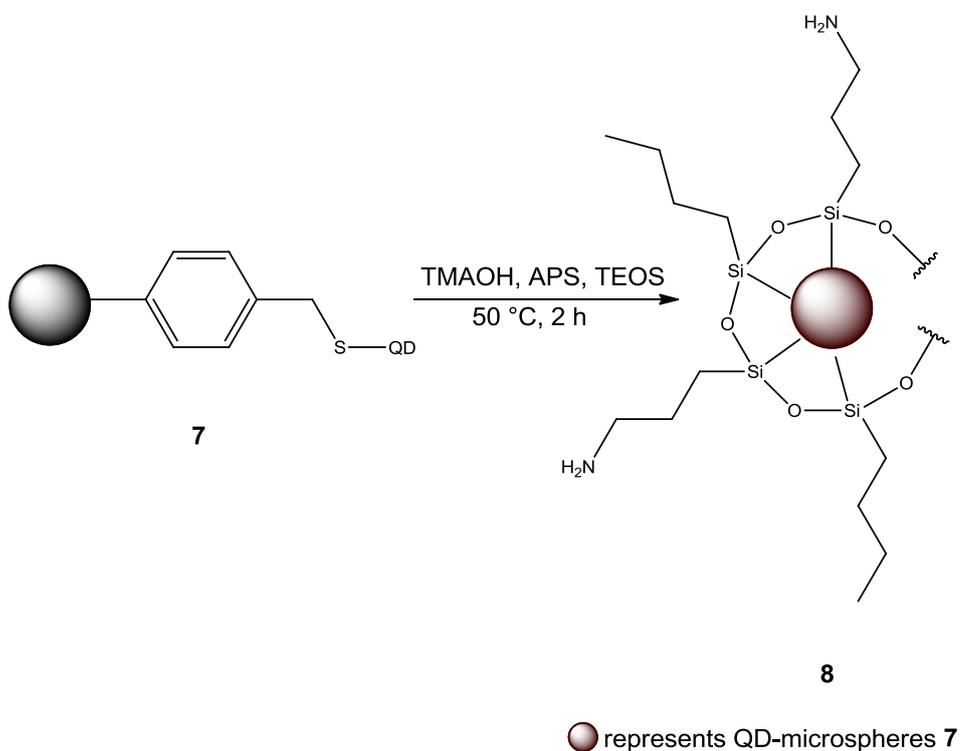
Scheme 6: Silica shelling of QD-microspheres **7**

Silica shelling of samples of both CdQD-microspheres and CFQD-microspheres was carried out. After silica shelling, the level of fluorescence of the silica shelled QD-microspheres **8** was assessed using a fibre-optic probe. Qualitative comparisons were carried out based on fluorescence levels for silica shelled and unshelled QD-microspheres. These results were then compared with QDs before they were associated with microspheres to give an indication of how well the QDs had retained their fluorescence after immobilisation and the subsequent shelling reaction.

Silica shelling of CFQD-microspheres was carried out in methanol, ethanol, isopropanol and toluene. The CFQD-microspheres exhibited a low level of fluorescence after shelling in toluene, ethanol and isopropanol. When silica shelled in methanol, the CFQD-microspheres exhibited a reasonable level of fluorescence after the reaction and subsequent washes. This sample of microspheres was then washed into water but this caused the fluorescence to reduce significantly.

Silica shelling of CdQD-microspheres was carried out in water. The resultant silica-shelled composites **8** displayed a high level of fluorescence after the reaction and subsequent washes in comparison with the unshelled CFQD-microspheres.

2.3.2. Summary

The results from this silica shelling study showed that the protocol was better suited to CdQDs, with a high level of fluorescence being obtained after the shelling procedure in water. CFQD-microspheres displayed a reasonable level of fluorescence after silica shelling in methanol but this level reduced on contact with water. This suggests that the shelling of the CFQD-microspheres did not work or was not sufficient to act as a barrier to oxygen and water. A further possibility is that CFQDs were degraded by the reaction conditions used to shell the microspheres.

2.3.3. PVDC coating of quantum dots

Another barrier material, polyvinylidene chloride, PVDC, was also investigated. PVDC was selected as a potential coating material as it is known to possess excellent barrier properties, superior to its counterparts as shown in Table 5[106]. The polymer displays high resistance to oxygen and moisture[107] and was most commonly used as a component of food packaging[108], particularly in the form of Saran wrap. Saran wrap

played a significant role in extending product shelf life by maintaining a low permeability to gas[109, 110].

Table 5: Water and oxygen permeability of polyethylene terephthalate (PET), Nylon and PVDC[106]

	Water permeability (g mmm^{-2} s^{-1})	Oxygen permeability (ml mm m^{-2} s^{-1} GPa^{-1})
PET	7.29×10^{-4} - 1.28×10^{-3}	2.25 - 4.05×10^{-1}
Nylon	2.73×10^{-3} - 1.00×10^{-2}	4.50×10^{-2} - 1.12×10^{-1}
PVDC	3.65×10^{-5} - 1.82×10^{-4}	6.75 - 8.99×10^{-4}

PVDC is synthesised from vinylidene chloride, and often contains another co-monomer, which helps contribute to the flexible nature of the polymer.

CdQDs were not directly coated with PVDC and were immobilised into thiol-functionalised microspheres **6** prior to coating because individual QDs are prone to aggregation and the use of QD-microspheres **7** would be more suited to future applications such as light-emitting diodes (LED), inks and beadfection agents.

An encapsulation approach was undertaken in attempting to coat QD-microspheres **7** with PVDC. The approach was similar to the one described in Kobayashi and Nagayama[111] and Akiyama and Kobayashi[112], in which scandium trifluoromethanesulfonate, Sc(OTf)$_3$, was coated using a microencapsulation technique. This coating approach was adapted for QD-microspheres **7** with PVDC.

A solution of PVDC in THF was added to QD-microspheres **7** which were suspended in THF. THF was selected as it was a solvent that both the core and coating material were compatible in, which allowed ease of mixing of the two. The mixture was then heated, which was followed by cooling down of the mixture to aid encapsulation of the microspheres. A hardening agent was then added to strengthen the coated layer.

The coating procedure was repeated with different conditions as discussed in the following sections.

2.3.3.1 PVDC coating of large microspheres

Microspheres which were 38 μm in diameter, synthesised *via* a suspension polymerisation reaction, were used to determine the effectiveness of the coating procedure on large microspheres. These microspheres were too heavy to suspend in THF, and were added directly to PVDC-THF coating medium. After the resultant mixture had been shaken on a shaker plate for one hour, PVDC was found to have aggregated and separated out from the microspheres. It was also observed that the microspheres had fragmented suggesting that they are not strong enough to undergo the level of agitation required in this protocol.

2.3.3.2 Mass of PVDC

The reaction was initially carried out with an excess of PVDC (5 g) to 1 g of thiol-functionalised microspheres **6** which were 1.0 μm in diameter. However, the majority of PVDC had precipitated out once the reaction was completed, which indicated that such an excess of PVDC was not required. A series of experiments were then carried out to determine the amount of PVDC which can be used without causing aggregation and precipitation to occur. Different quantities of PVDC, ranging from 2 g to 0.25 g were used, with the sizing data for each of these experiments outlined in Table 6. The diameter of each product was determined on a Sympatec Helos Particle Size Analyser and sample preparation and procedure for size analysis is described in section 4.2.1.

Table 6: Average diameter of PVDC-coated, thiol-functionalised microspheres formed with differing amounts of PVDC. The size of starting material was 1.0 μm, standard deviation was 0.5 μm. Data was obtained by laser diffraction analysis.

Mass of PVDC used (g)	Size (μm)
2.00	13.5 ± 25.0
1.50	2.7 ± 5.7
1.00	1.8 ± 1.2
0.50	10.0 ± 14.5
0.25	9.3 ± 13.5

Data from the experiment conducted with 1 g of PVDC looked the most promising, as size distribution was narrow and there did not appear to be any large aggregates present from the distribution curve. The size of thiol-functionalised microspheres **6**

before coating was 1.0 µm, suggesting the coated layer was 0.8 µm thick. Reactions carried out after this experiment utilised 1 g of PVDC as the optimum amount.

2.3.3.3   Hardening agent

Water was used to harden the PVDC layer, and the use of this solvent appeared to work well, as on addition, a precipitate began to form. The sizing data showed that it was possible that the microspheres had been successfully coated as they showed an increase in diameter. The volume of water used was varied as shown in Table 7 which yielded a range of different thicknesses of the PVDC layer.

Table 7: Average diameter of PVDC-coated, thiol-functionalised microspheres formed in the presence of different volumes of hardening agent. The size of starting material was 1.0 µm, standard deviation was 0.4 µm. Data was obtained by laser diffraction analysis.

Volume of hardening agent (mL)	Size (µm)
5.000	2.5 ± 3.0
0.720	30.0 ± 22.2
0.600	17.5 ± 13.3
0.440	7.9 ± 8.0
0.320	4.0 ± 4.6

As the volume of hardening agent was increased from 0.320 mL to 0.720 mL, sizing data appeared to show an increase in the diameter of the microspheres. This led to the assumption that the thickness of the coated PVDC layer increases with increasing hardening agent. However, on closer observation of this data, it appeared that this increase was not necessarily due to an increase in thickness of the PVDC layer.

The distribution curve in Figure 12 shows the average diameter of microspheres when 0.720 mL of water was added to the reaction. The bimodal nature of the distribution suggested that a number of large (10-80 µm) aggregates were present in the sample. The aggregates could have arisen from either the aggregation of PVDC or the aggregation of the microspheres themselves. These aggregates are likely to be responsible for the large increase in diameter from the starting material.

The 10 µm region of the curve in Figure 12 is displayed in Figure 13. From this expansion, it is apparent that the distribution of the majority of the sample appears to be around 1 µm (the peak of distribution is highlighted by the red line on the curve), with only a small proportion of microspheres larger than 2.5 µm.
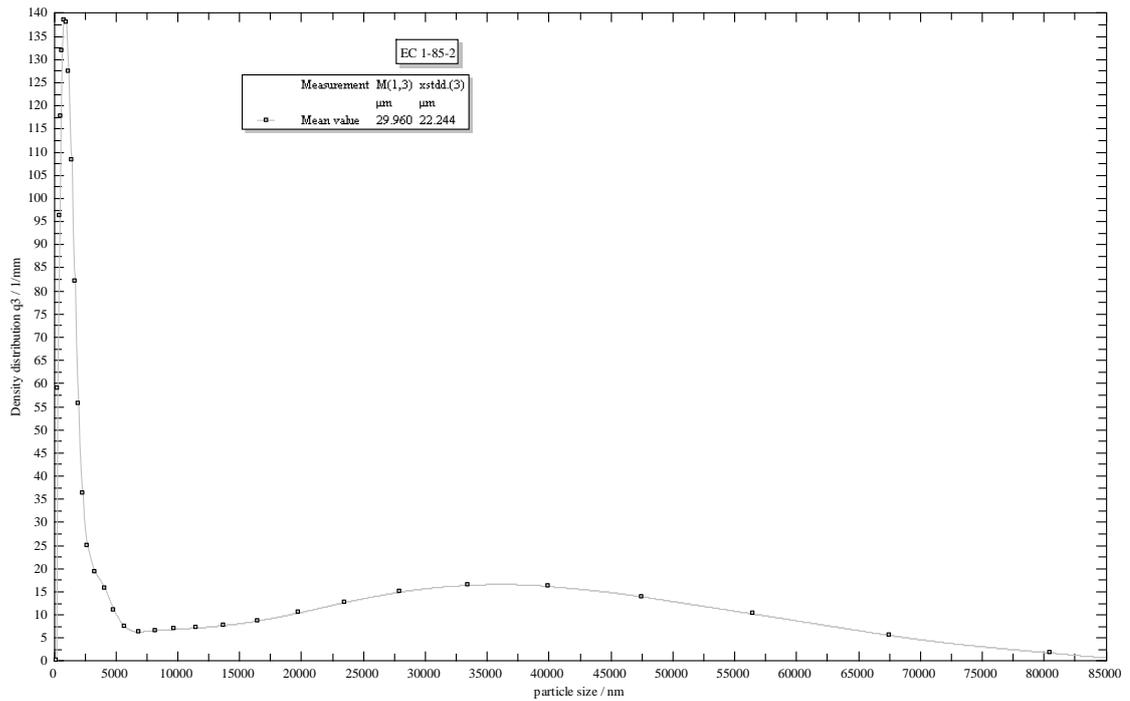
Figure 12: Distribution density curve for particle size of PVDC-coated, thiol-functionalised microspheres with the addition of 0.720 mL water, suspended in distilled water, obtained by laser diffraction analysis after a 60 second period of ultrasonication
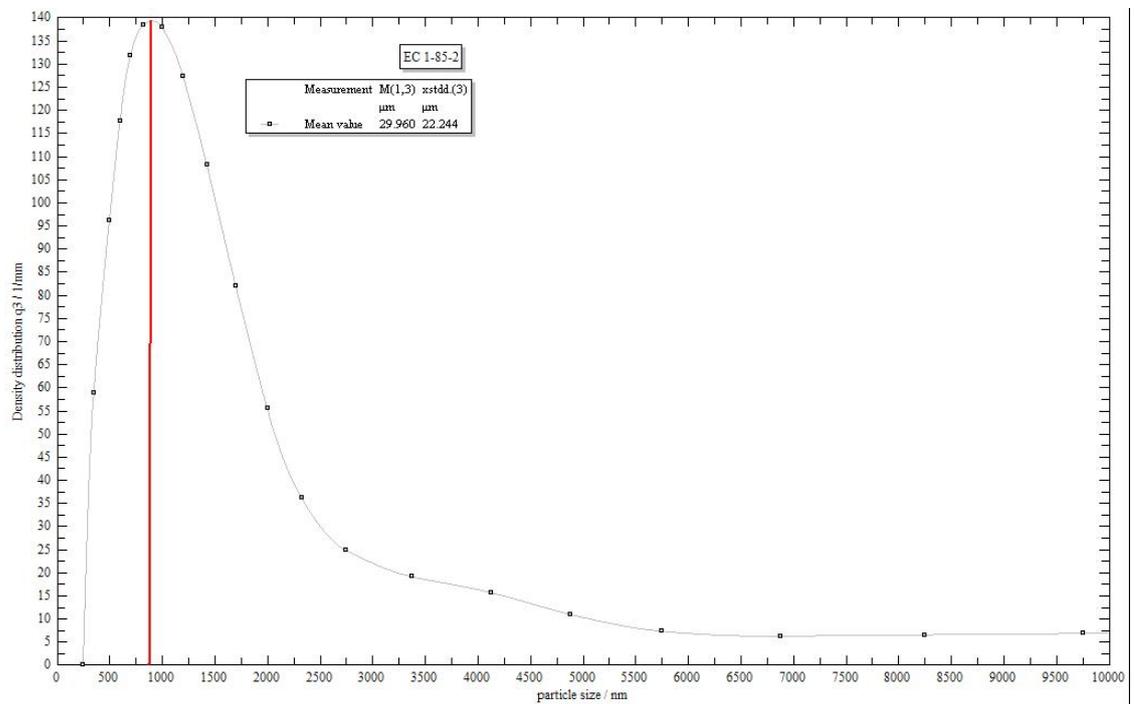
Figure 13: Distribution density curve for particle size of PVDC-coated, thiol-functionalised microspheres with the addition of 0.720 mL water, suspended in distilled water, obtained by laser diffraction analysis after a 60 second period of ultrasonication, zoomed to a region of 10 µm

The average size distribution for the microspheres in Figure 12 is around 1.0 μm which looked similar to the average size distribution for the uncoated microspheres **6** which was 1.0 μm as shown in Figure 14. This suggests that either the microspheres were not coated with PVDC or that the coated layer was not thick enough to observe an appreciable size difference.
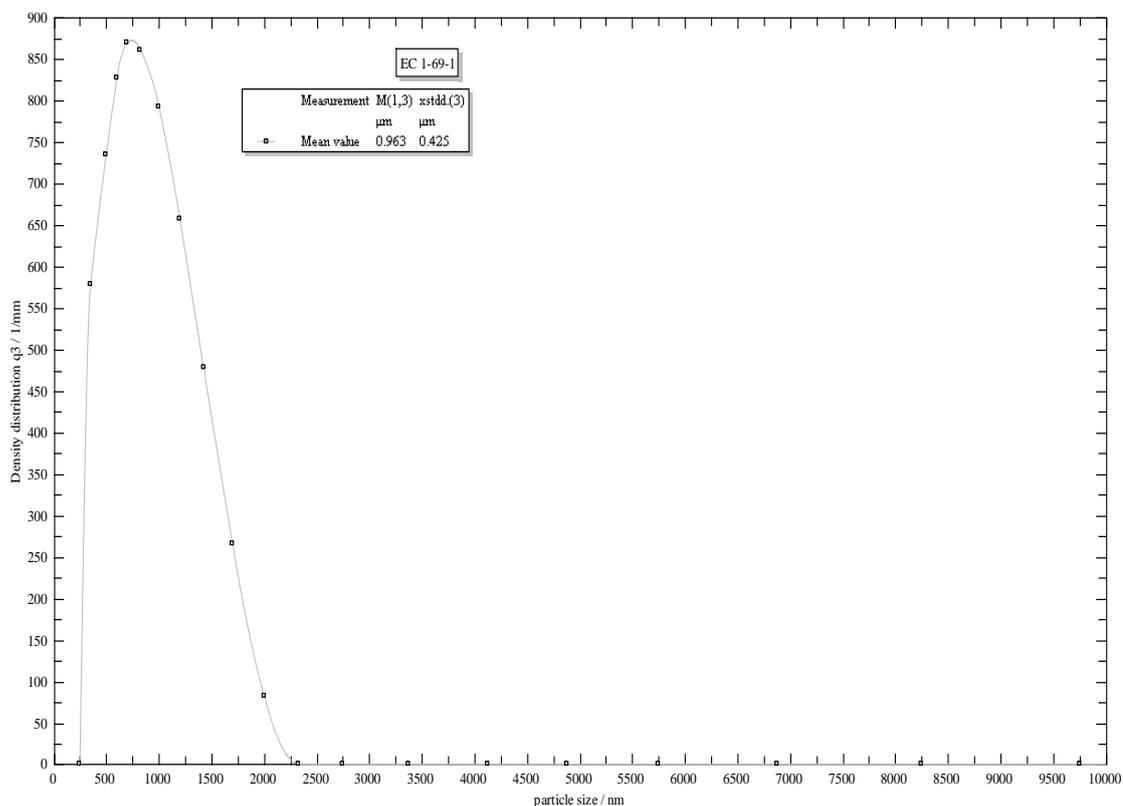
Figure 14: Distribution density curve for particle size of thiol-functionalised microspheres **6** suspended in distilled water obtained by laser diffraction analysis after a 60 second period of ultrasonication

The distribution curve for coated microspheres with 5 mL hardening agent shown in Figure 15 displayed a shift in the major size distribution peak, which suggested an increase in the average diameter of the microspheres. The average diameter of the microspheres was extrapolated at around 1.2 μm which was a 0.2 μm increase from the uncoated microspheres **6**.

The distribution curve for coated microspheres with 0.320 mL hardening agent, Figure 16, also appeared to show an increase in the average diameter of the microspheres. The bimodal distribution of size also indicated the presence of significant amounts of aggregates in the sample. These aggregates were probably similar to those found in the sample with 0.720 mL hardening agent.

58
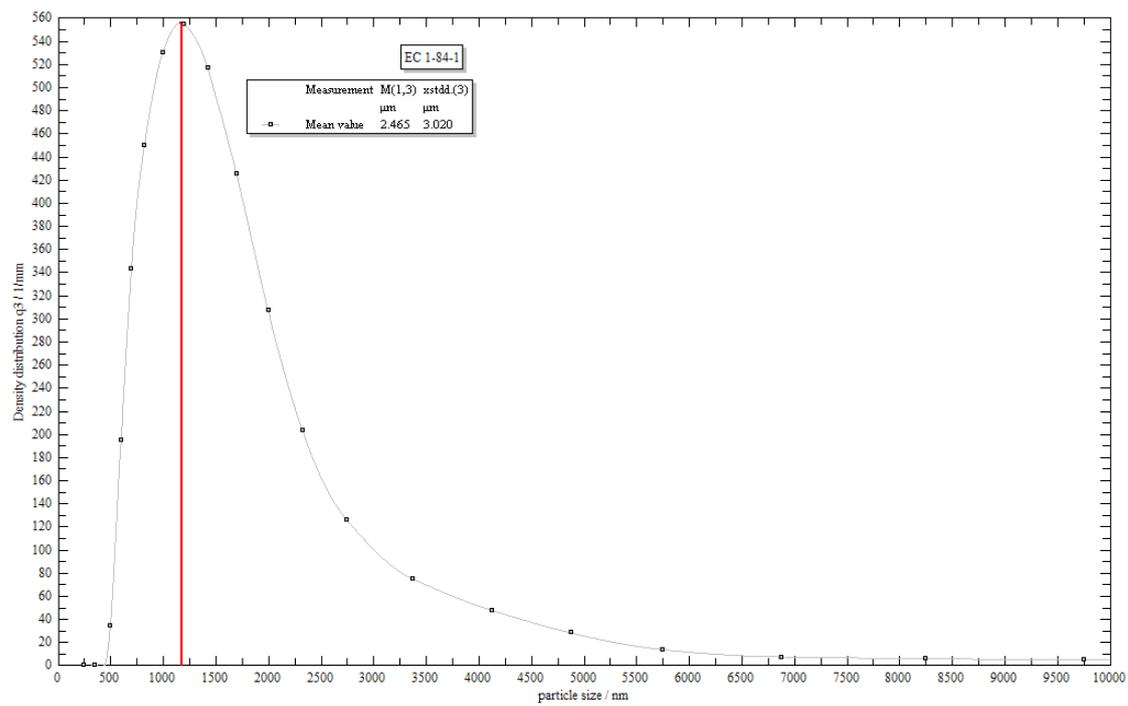
Figure 15: Distribution density curve for particle size of PVDC-coated, thiol-functionalised microspheres with the addition of 5 mL water, suspended in distilled water, obtained by laser diffraction analysis after a 60 second period of ultrasonication
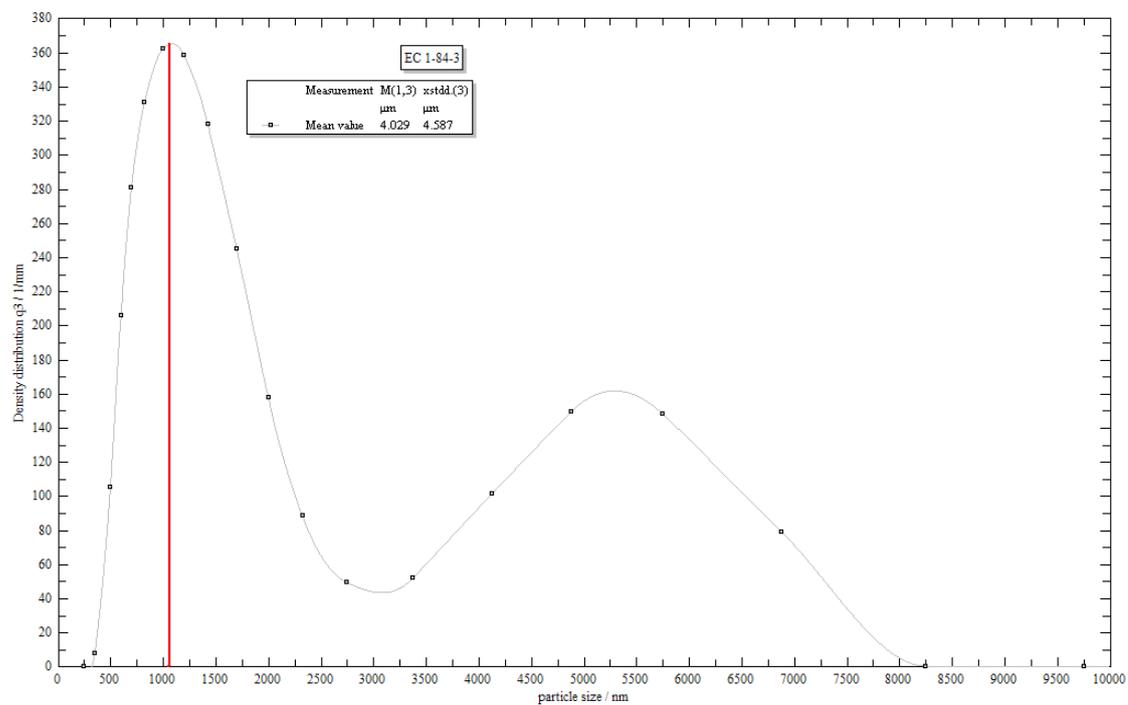
Figure 16: Distribution density curve for particle size of PVDC-coated, thiol-functionalised microspheres with the addition of 0.320 mL water, suspended in distilled water, obtained by laser diffraction analysis after a 60 second period of ultrasonication

The only two volumes in which a marked increase of the average diameter of the microspheres was observed were 5 mL and 0.320 mL. Therefore, these volumes were selected as the hardening agent volumes to be used in further experiments.

All other volumes of hardening agent did not seem to have an effect on the diameter of the microspheres, with the diameter remaining at a similar value to that of the uncoated sample. The extrapolated average diameter for each volume of hardening agent is summarised in Table 8.

Table 8: Extrapolated average diameter of PVDC-coated, thiol-functionalised microspheres formed in the presence of different volumes of hardening agent. The size of starting material was 1.0 μm, standard deviation was 0.4 μm.

Volume of hardening agent (mL)	Extrapolated average diameter (μm)
5	~1.2
0.720	<1
0.600	<1
0.440	<1
0.320	~1.1

Using the established hardening agent volumes, the experiment was repeated with thiol-functionalised microspheres **6** and QD-microspheres **7**, the results for which are presented in Table 9 and Table 10.

Table 9: Average diameter of PVDC-coated, thiol-functionalised microspheres formed with the chosen hardening conditions. The size of starting material was 1.0 μm, standard deviation was 0.4 μm. Data was obtained by laser diffraction analysis.

Volume of water (mL)	Run 1	Run 2	Run 3
5.000	2.5 ± 3.0	16.7 ± 20.1	2.1 ± 2.6
0.320	7.9 ± 8.0	7.7 ± 6.0	---

Table 10: Average diameter of PVDC-coated, QD-microspheres formed with the chosen hardening conditions. The size of starting material was 1.0 μm, standard deviation was 0.4 μm. Data was obtained by laser diffraction analysis.

Volume of water (mL)	Run 1	Run 2	Run 3
5.000	13.5 ± 25.0	7.5 ± 15.0	---
0.320	18.3 ± 16.6	12.0 ± 13.6	17.7 ± 22.2

The series of experiments for the PVDC coating of thiol-functionalised microspheres **6** seemed fairly reproducible with the selected hardening agents. However, the series of experiments with QD-microspheres **7** did not yield reproducible results. The presence of QDs may have affected microencapsulation, thus preventing PVDC from successfully coating the microspheres. This, in turn, could have led to the aggregation of PVDC into structures which caused an increase in the average diameter of the sample. The QD-microspheres **7** themselves could have aggregated which would also lead to an increase in the average diameter of the sample.

2.3.4. Summary

The aim of this work was to coat QD-microspheres **7** with a layer of PVDC. This was abandoned as it appeared that the formation of aggregates prevented the accurate analysis of the average diameter of coated samples. Perhaps in the future, greater understanding of the coating process might enable this to be revisited.

In summary, it appears that results indicated successful coating of thiol-functionalised microspheres **6** with PVDC could have taken place with appropriate reaction conditions. However, the sizing data obtained was not reproducible owing to the possible aggregation of PVDC and/or microspheres. Further work to confirm the viability of the procedure is needed, perhaps by investigation into other reaction conditions such as the temperature of the reaction mixture. Further characterisation of the coated layer, by labelling PVDC with a fluorescent dye and analysing the fluorescence under UV excitation, may help determine whether the coating was successful. The zeta potential of the PVDC coated layer could also be analysed to further examine the presence of the coated layer.

2.4. **Applications of QD-microspheres 7**

Beadfection work described in this section was conducted in collaboration with Professor Geoff Tansley and Dr Laura Leslie from the Mechanical Engineering and Design Group (EAS), Dr Lindsay Marshall and Dr Anna Hine. Beadfection studies were conducted by Dr Laura Leslie and Dr Lindsay Marshall.

QDs possess a high level of photo-stability, which along with their broadband excitation makes them an attractive prospect for use in imaging applications.

A possible application of QD-microspheres **7** explored in this project was the use of the fluorescence nature of the conjugates to help visualise and track the position of red blood cells (RBCs) in a haemolysis rig.

The purpose of the haemolysis rig was to mimic the action of a blood pump. When RBCs flow through a pump, they undergo shear stress which can damage the RBCs[113-117], so the intention of the rig is to mimic a pump and induce stress, but without damaging the RBCs.

In order to track RBCs, the first task was to determine whether it would be possible to internalise QD-microspheres **7** in RBCs. It was also important to internalise the microspheres without damaging the cells or changing their mechanical properties.

Initially, the idea was to use QDs without association with microspheres for RBCs visualisation. However, the majority of QDs that are commercially available and commonly used are only compatible in organic solvents. The use of QDs suspended in organic solvents could lyse RBCs and it is possible that naked QDs will not be stable in aqueous environments.

QDs are hydrophobic and cannot be readily made aqueous compatible; therefore, another possibility was to immobilise CdQDs into thiol-functionalised microspheres **6** as described in section 2.2. The resultant QD-microspheres can be made aqueous compatible by treatment with PVP, therefore QDs associated with microspheres was viewed as the best way of introducing QDs into RBCs.

2.4.1.   Internalisation of QD-microspheres **7** into red blood cells

There is evidence of polymer microsphere uptake by cells from previous group work and a protocol for bead entry into cells, which is known as beadfection, has already been established[59, 64]. This protocol involves the addition of microspheres to a layer of settled cells; the beads then settle on the cells and penetrate the RBC membrane. This protocol was applied to beadfection with RBCs.

All blood samples used were taken from healthy volunteers following the Aston University Blood Taking Policy and with University ethical approval.

Initial tests involved the suspension of RBCs in phosphate buffered saline (PBS), to which QD-microspheres **7** at a concentration of 3.00×10^{-3} g mL^{-1}, also suspended in PBS, were added. The microspheres and cells were then incubated for 24 hours, to

allow the process of beadfection to take effect. Previous studies have shown that 24-48 hours is sufficient to ensure microsphere uptake. The resultant cells/microspheres were then visualised under a confocal microscope, the images for which are shown in Figure 17. Sample preparation and procedure for confocal microscope analysis is described in section 4.2.2.

The test showed that microspheres appeared to be taken up by RBCs, although the longer the incubation time, the worse the uptake seemed. This could mean that RBCs were dying, either due to the length of incubation time or the presence of microspheres and/or QDs. Cell death due to the toxic effects of QDs could also be a possibility.
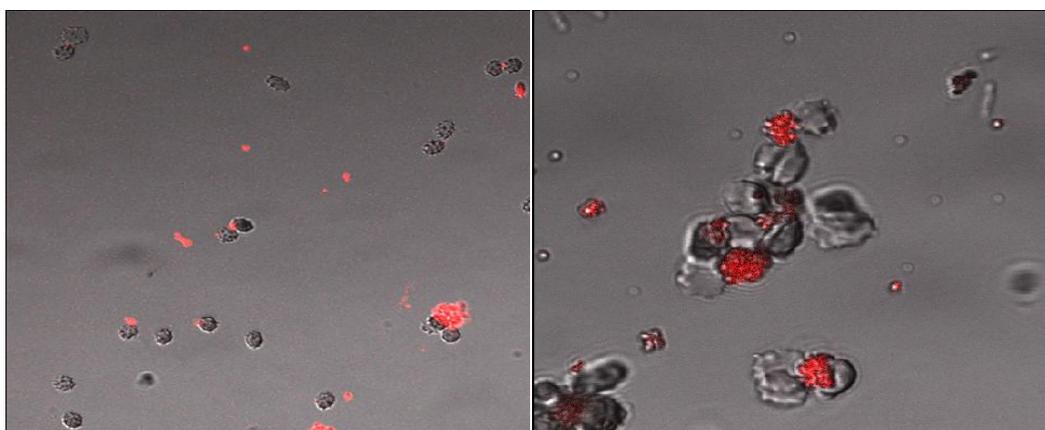
Figure 17: Confocal microscope images showing the interaction of QD-microspheres **7** (3.00×10^{-3} g mL^{-1}) with RBCs at a haematocrit of 40 % suspended in PBS. Images were taken using a helium-neon laser line with a wavelength of 594 nm.

An observation from the images in Figure 17 was that there appeared to be clumps of aggregated QD-microspheres **7** present in the sample visualised. This was further confirmed by a confocal image of QD-microspheres **7** in PBS, Figure 18, before they were internalised into RBCs.

Individual microspheres rather than clumps would be better to track as it would be easier to make an assumption of microsphere uptake based on the level of individual microspheres entering the RBCs. Furthermore, the movement of large clumps of microspheres into cells could damage the cell membrane; therefore an investigation into ways of combating aggregation was conducted.
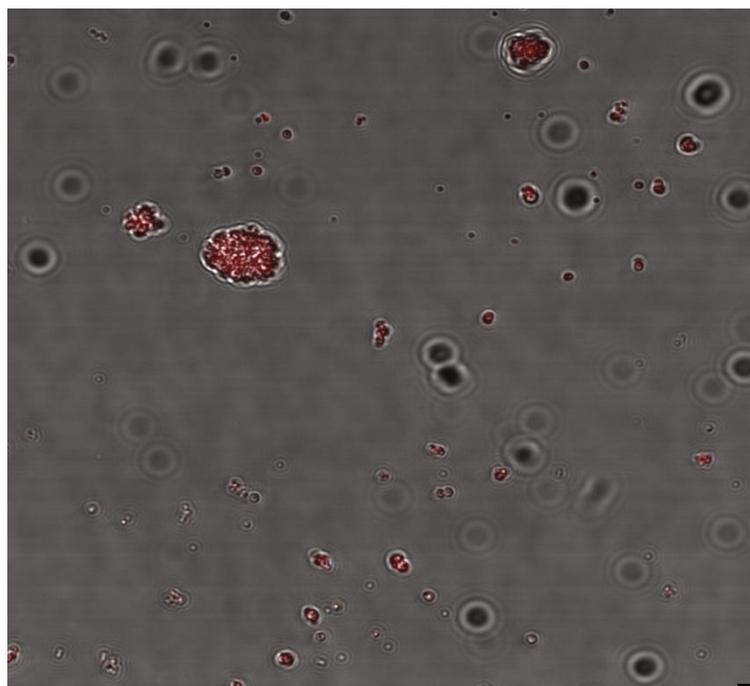
Figure 18: Confocal microscope image of QD-microspheres **7** (1.00×10^{-3} g mL^{-1}) suspended in PBS by ultrasonication. Image was taken using a helium-neon laser line with a wavelength of 594 nm.

2.4.1.1 Layer-by-layer assembly of charged polyelectrolytes

The layer-by-layer technique is an approach used to deposit thin film multilayers of oppositely charged materials onto a substrate. The multilayers are held together by electrostatic attraction or sometimes by hydrogen bonding. Coating materials used previously include polyelectrolytes and biological molecules[118-122].

The technique involves adsorption of the charged species onto a substrate. This is usually carried out by dipping the substrate into a charged solution, followed by the removal of excess charged solution with water washes to leave a thin layer of material ready for adsorption of the next oppositely charged layer[118].

This is a facile way of coating substrates in an efficient and effective manner and can also be employed as a means of introducing a gas barrier around the substrate. It also allows for the incorporation of structures such as nanoparticles, organic fluorophores or biologically relevant cargo[123]. The technique also enables the construction of multilayered structures in which the thickness of the composite layers can be controlled by the number of bilayers deposited onto the substrate. This becomes particularly important for the construction of gas barriers which require a sufficient thickness in order to be effective at preventing the permeation of gases[118].

As a wide range of substrates and coatings materials can be utilised, it is possible to tailor this approach to suit a particular study.

The aim of using the layer-by-layer technique in this study was to coat QD-microspheres **7** with a charged material to prevent aggregation[120]. The assembly of multilayers was not needed as one layer of charged material surrounding the microspheres should be adequate for the introduction of a charged surface to repel the microspheres from each other.

The coating materials selected for this study were weak polyelectrolytes, polyacrylic acid (PAA) and polyethyleneimine (PEI). Polyelectrolytes contain polymer chains with ionisable functional groups that can dissociate in aqueous solutions, dependent on pH, to leave a charged polymer coating and counter ions in solution[123].

PAA, an anionic polymer, is a weak polyelectrolyte as it partially dissociates in aqueous solutions yielding a negatively charged polymer. In basic conditions, most of the carboxylic acid groups are deprotonated, leaving the polymer highly charged. The structure of PAA is represented in Figure 19.
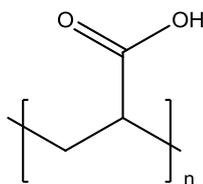
Figure 19: Structure of polyacrylic acid (PAA)

Branched polyethyleneimine, a branched cationic polymer, is also a weak polyelectrolyte and can gain charge at an appropriate pH, to yield a positively charged polymer. In acidic conditions, the primary, secondary and tertiary amine groups can all be protonated and thus the resulting polymer is positively charged. The structure of PEI is shown in Figure 20.
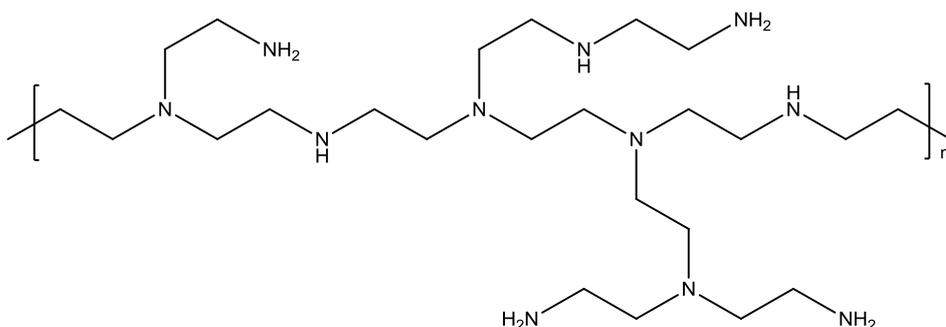
Figure 20: Structure of branched polyethyleneimine (PEI)

Weak polyelectrolytes are particularly useful when constructing bilayers as their charge can easily be altered by pH changes.

Many layer-by-layer studies have used PEI and PAA as the coating material of choice as it appears they have yielded sufficiently coated substrates[118, 121]. A similar protocol to the one described in Yang et al[118] was followed for the layer-by-layer coating of QD-microspheres **7**.

Thiol-functionalised microspheres **6** (7.50×10^{-3} g) were suspended in PEI solution (0.1 wt %, pH 10) by ultrasonication. This was to ensure that the microspheres were fully dispersed in the PEI solution. This suspension was sonicated for five minutes to prevent the microspheres from settling at the bottom of the centrifuge tube. This procedure was repeated with thiol-functionalised microspheres **6** in PAA solution. Both batches of microspheres treated with these conditions appeared to show a reduction in the level of aggregation. Figure 21 is a confocal image of thiol-functionalised microspheres **6** suspended in PEI solution.
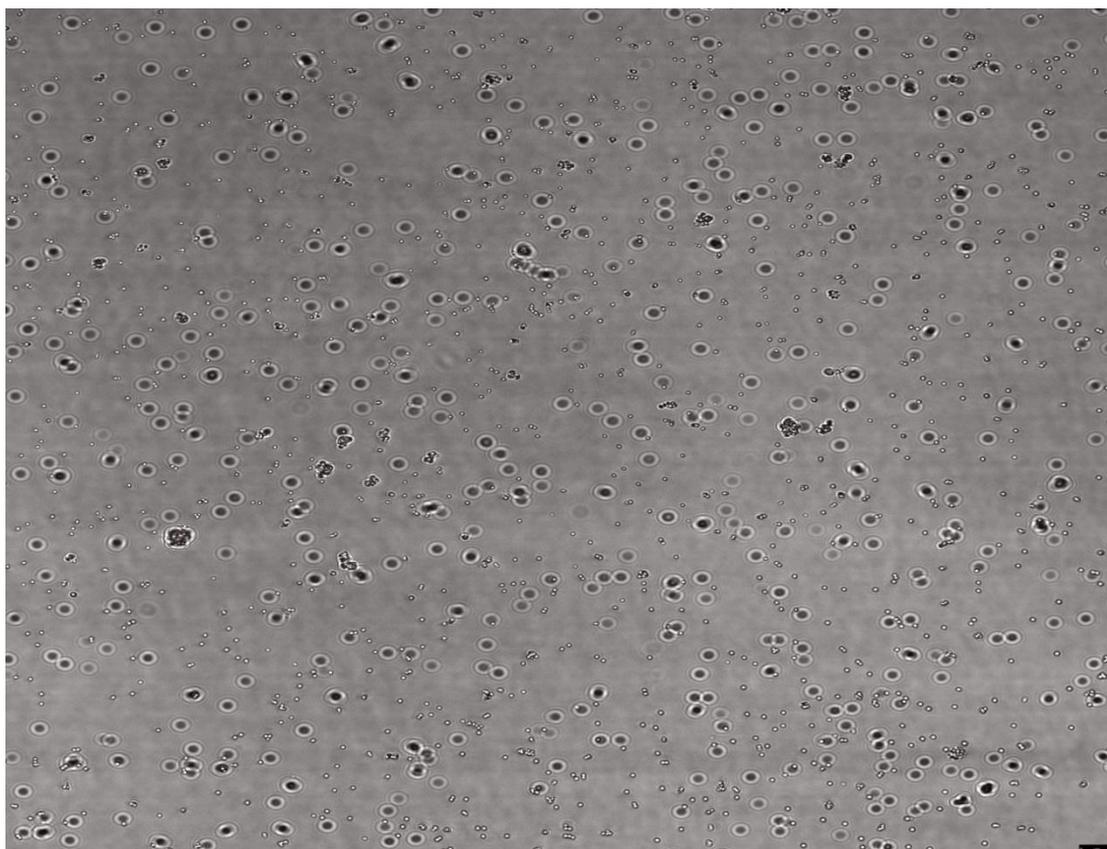
Figure 21: Confocal microscope image of thiol-functionalised microspheres **6** (1.00×10^{-3} g mL^{-1}) suspended in PEI solution (0.1 wt %, pH 10) by ultrasonication. The image was taken using an argon laser line with a wavelength of 488 nm.

From the image in Figure 21, the microspheres were shown to be well-dispersed with no large clumps of aggregated microspheres present. Figure 22 is a confocal image of thiol-functionalised microspheres **6** suspended in PAA solution, which again indicated that aggregation was reduced as many individual microspheres were present. Both these images seemed to show microspheres that were significantly less aggregated than the control sample of thiol-functionalised microspheres **6** before the layer-by-layer experiment, shown in Figure 23.
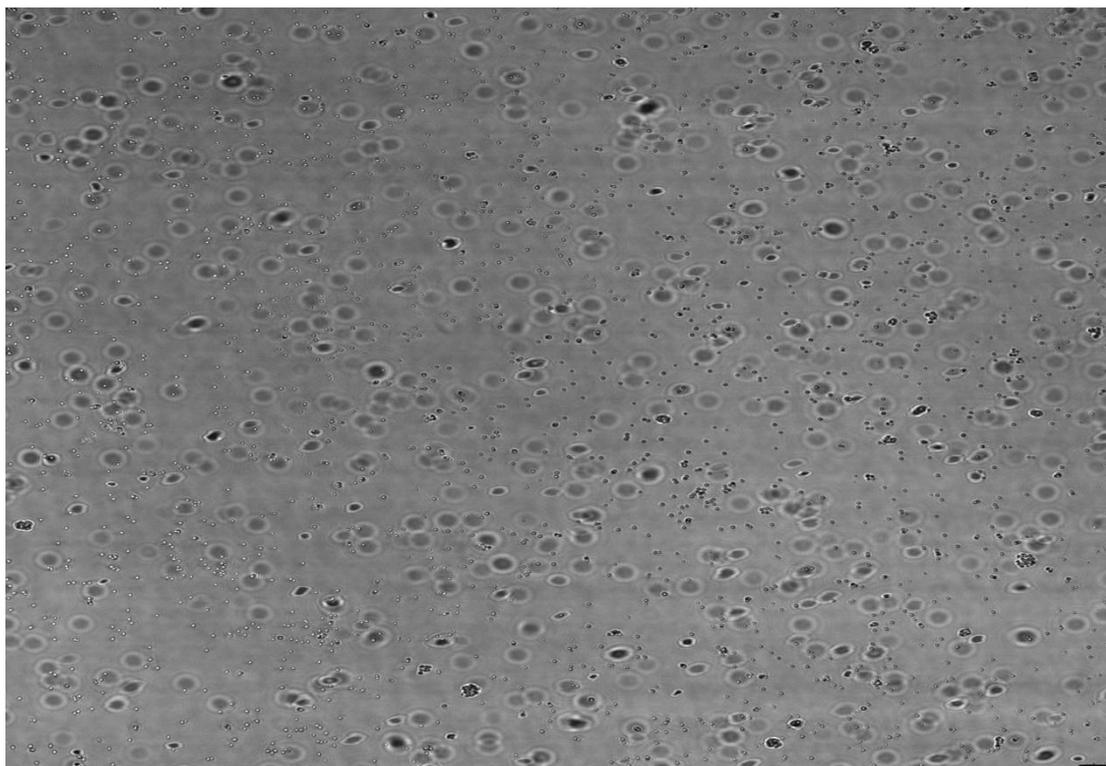
Figure 22: Confocal microscope image of thiol-functionalised microspheres **6** (1.00×10^{-3} g mL^{-1}) suspended in PAA solution (0.2 wt %, pH 4) by ultrasonication. The image was taken using an argon laser line with a wavelength of 488 nm.

However, there was some difficulty encountered in capturing these images as the strong fan associated with the confocal microscope caused the microspheres to continuously move and consequently, the microspheres did not settle easily. Nevertheless, images were clear enough to give an impression of the degree of aggregation in the sample.
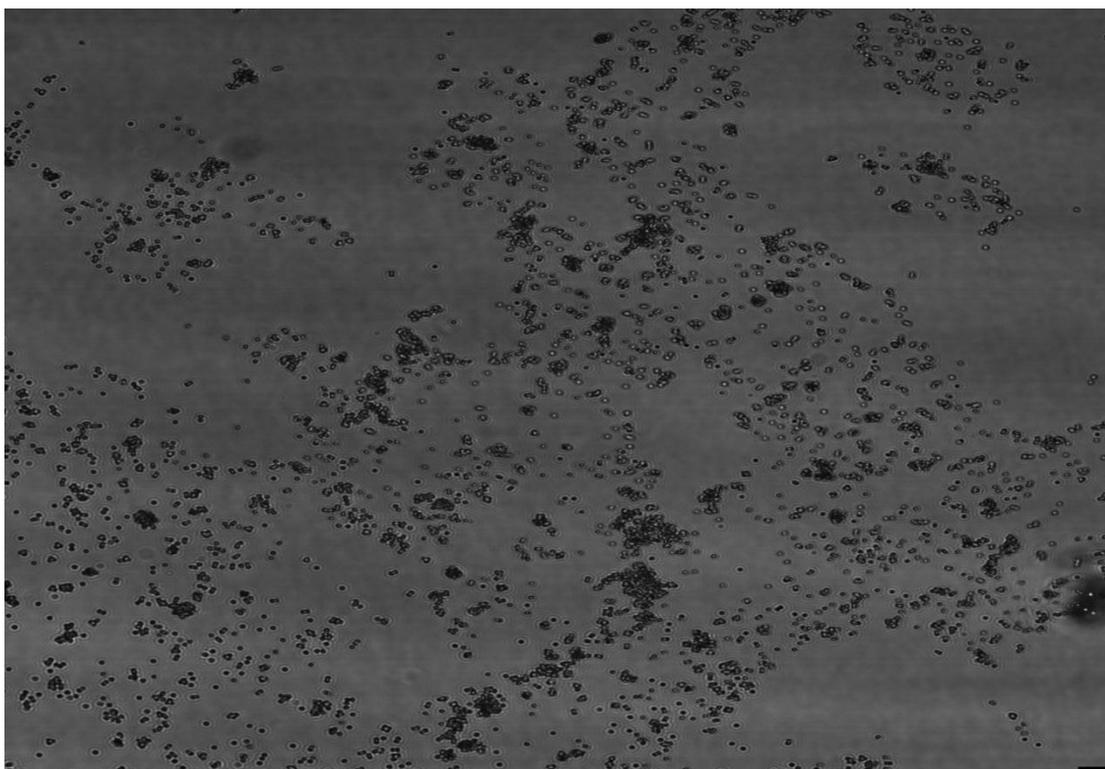
Figure 23: Confocal microscope image of thiol-functionalised microspheres **6** (1.00×10^{-3} g mL^{-1}) suspended in PBS by ultrasonication. The image was taken using an argon laser line with a wavelength of 488 nm.

Once the parameters for the production of non-aggregated microspheres had been established, the layer-by-layer experiment was repeated with QD-microspheres **7** and after coating, these microspheres were washed into PBS as this was the medium required for RBC incubation.

Unfortunately, the results obtained with thiol-functionalised microspheres **6** were not replicated with QD-microspheres **7**. Figure 24 and Figure 25 are confocal microscope images of QD-microspheres **7** washed into PBS after suspension in polyelectrolyte solution.

The samples appeared clumpy and did not look similar to the dispersed behaviour of thiol-functionalised microspheres **6** suspended in polyelectrolyte solution.

Thiol-functionalised microspheres **6** observed in Figure 21 and Figure 22 were also washed into PBS and visualised under the confocal microscope, as eventually, any microspheres coated by the layer-by-layer technique will have to be suspended in PBS.
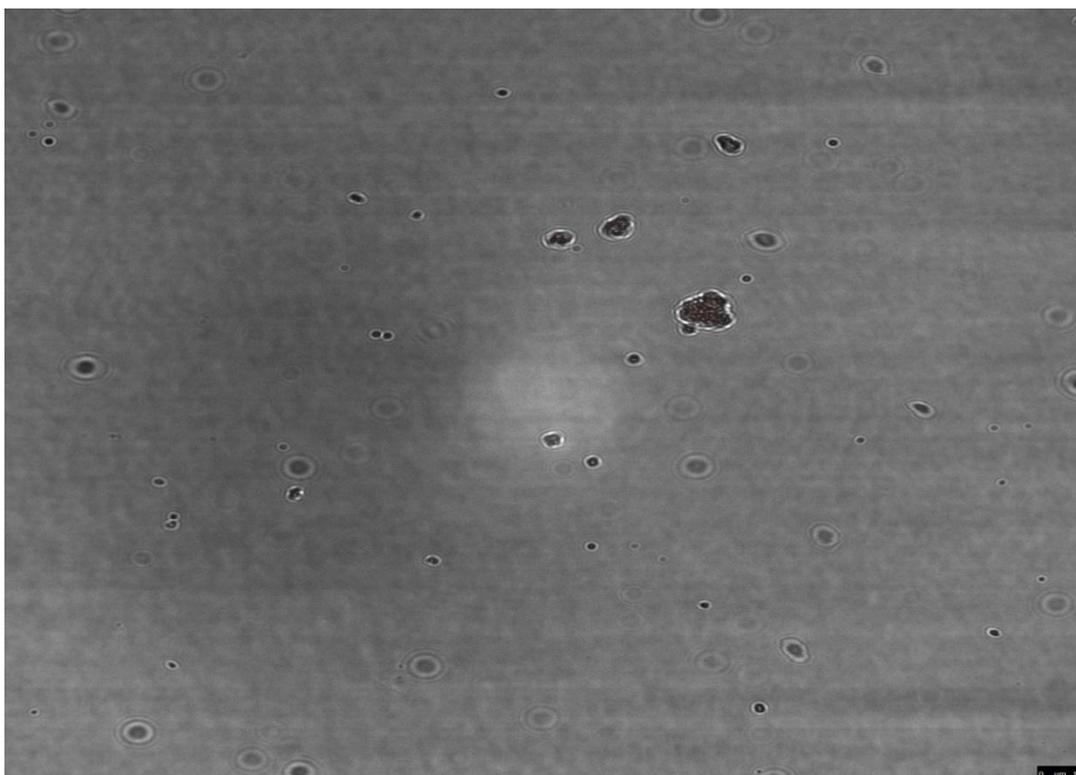
Figure 24: Confocal microscope image of QD-microspheres **7** (1.00×10^{-3} g mL^{-1}) suspended in PAA solution (0.2 wt %, pH 4). The image was taken using a helium-neon laser line with a wavelength of 594 nm.
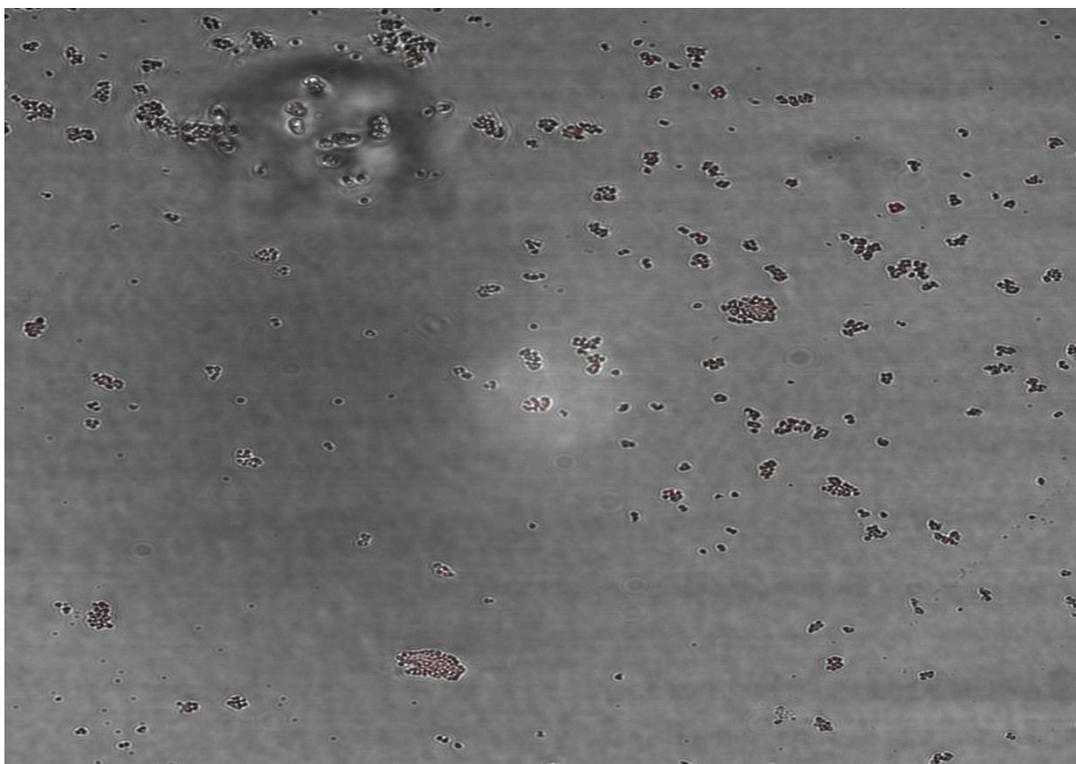
Figure 25: Confocal microscope image of QD-microspheres **7** (1.00×10^{-3} g mL^{-1}) suspended in PEI solution (0.1 wt %, pH 10). The image was taken using a helium-neon laser line with a wavelength of 594 nm.

Unfortunately, the non-aggregated appearance of the thiol-functionalised microspheres **6** disappeared on suspension in PBS. The microspheres became aggregated and formed large clusters as shown in Figure 26 and Figure 27. This suggests that the polyelectrolyte coating deposited on microspheres was removed when washed into PBS. This could possibly due the fact that the coated layer was not sufficiently adhered to the surface of the microspheres. PBS is a charged medium and the ions present in the buffer could have surrounded the polyelectrolyte layer thus negating the polyelectrolyte charge, leading to aggregation.
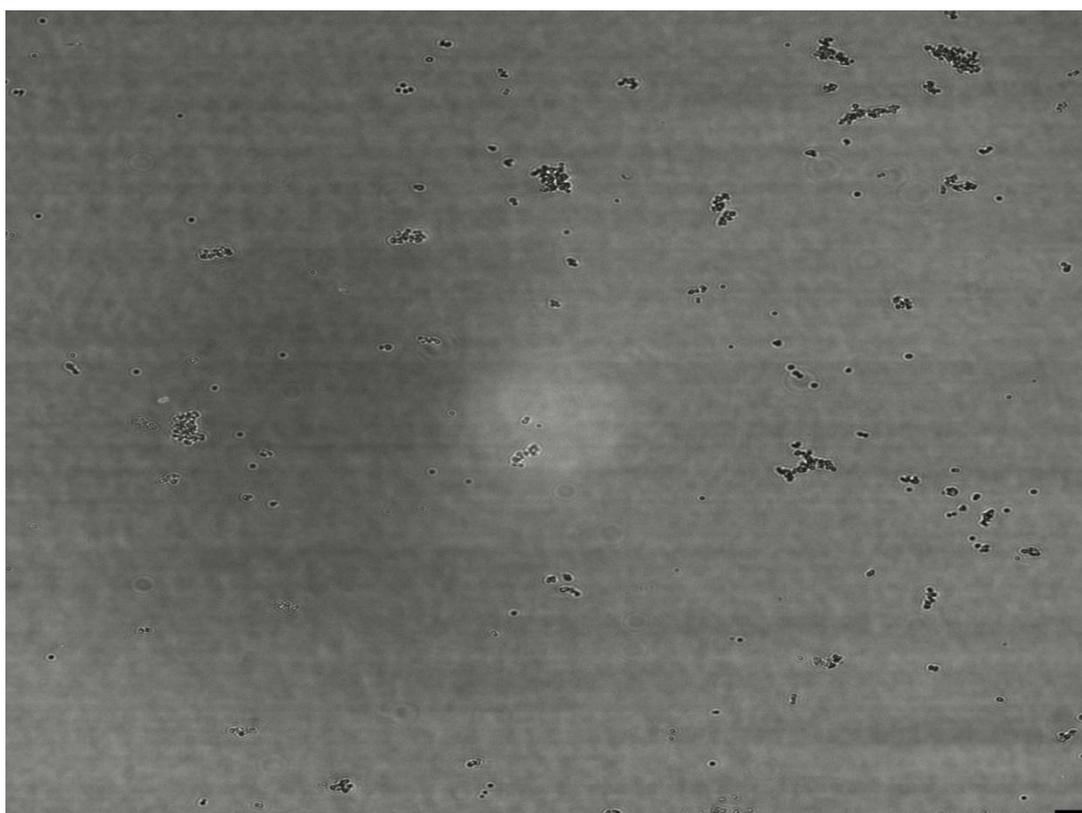
Figure 26: Confocal microscope image of PEI-coated, thiol-functionalised microspheres (1.00 × 10^{-3} g mL^{-1}) suspended in PBS. The image was taken using an argon laser line with a wavelength of 488 nm.

As thiol-functionalised microspheres **6** are not charged, it is possible that the coated layer would not be able to adhere to the microspheres by electrostatic attraction and could detach when agitated, i.e. either when the microspheres were sonicated to aid suspension in PBS or when the microspheres were centrifuged after suspension in the polyelectrolyte solution. A possible way to ensure attachment of the layer would be the addition of another layer of polyelectrolyte coating to the existing one to help anchor the coating beneath to the microsphere.
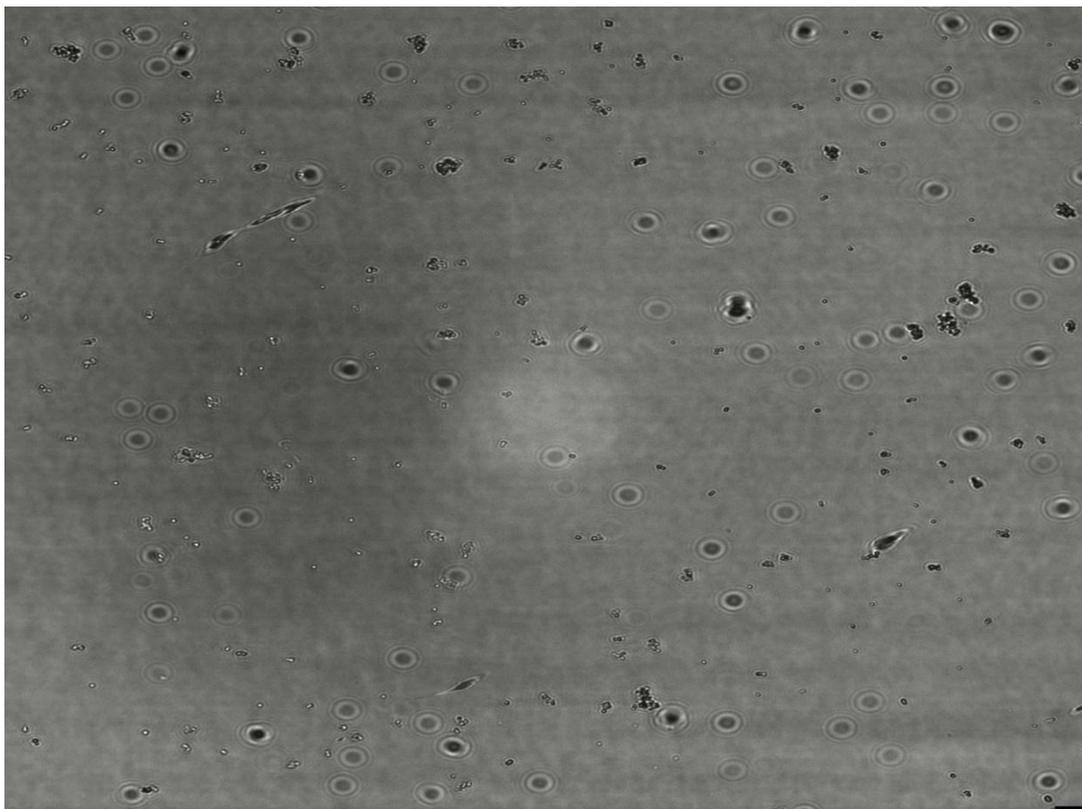
Figure 27: Confocal microscope image of PAA-coated, thiol-functionalised microspheres (1.00×10^{-3} g mL^{-1}) suspended in PBS. The image was taken using an argon laser line with a wavelength of 488 nm.

Accordingly, PEI-coated, thiol-functionalised microspheres were suspended in PAA solution by ultrasonication and visualised under a confocal microscope. The microspheres were observed to be slightly more aggregated than the PEI-coated, thiol-functionalised microspheres which suggested that the extra polyelectrolyte layer did not help to anchor the PEI layer to the microsphere. It is quite probable that the presence of PAA destabilised the microspheres and may have bound to the PEI layer by electrostatic attraction but because the PEI layer was not electrostatically attracted to the thiol-functionalised microspheres **6**, agitation required for suspension may have displaced the PEI layer from the microspheres. Thus, the aggregation of PEI-coated, thiol-functionalised microspheres was not reduced by suspension in PAA solution.

Unfortunately, the layer-by-layer approach was unsuccessful in the production of non-aggregated microspheres so another possibility of combating aggregation was sought. It was thought that the introduction of a charged layer of material to the microspheres by covalent attachment as opposed to electrostatic attraction might yield more promising results.

2.4.1.2   Covalent attachment of a charged polymeric shell

The attachment of a charged layer of polymer that is covalently bound to the microspheres was carried out by means of a seeded emulsion polymerisation reaction. This involved the synthesis of a polymeric shell containing an ionisable molecule, methacrylic acid **9**, which possesses ionisable carboxylic acid groups to provide repulsion between the microspheres and thus reduce aggregation. Styrene **3** provided a strong hydrocarbon backbone to ensure the shell is resistant to the stringent conditions required by subsequent reactions. DVB **4** was present as it crosslinks the shell causing it be physically stable. This seeded emulsion polymerisation reaction is represented in Scheme 7. The polymeric shell was synthesised around seed particles, which, in the case of this particular application, were thiol-functionalised microspheres **6**.
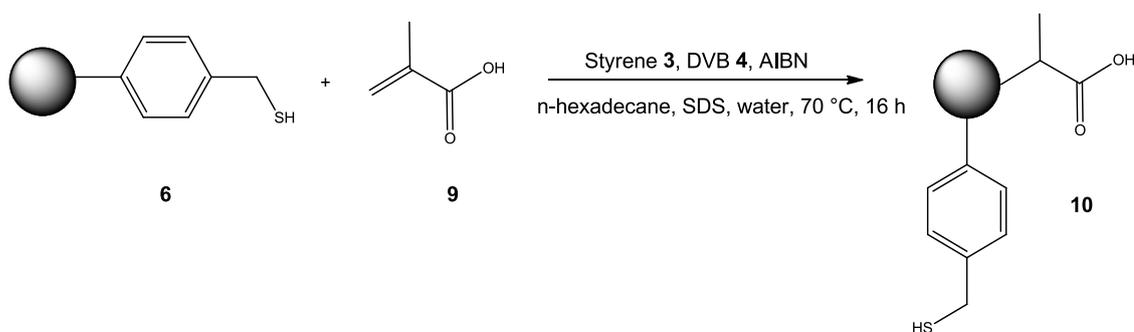
Scheme 7: Synthesis of thiol-core, carboxyl-shelled microspheres **10** by seeded emulsion polymerisation in which thiol-functionalised microspheres **6** were the seed particles

The charged microspheres **10** were assessed with zeta potential data which gives an indication of the potential stability of the colloid system and how well dispersed the system is. Particles with a high zeta potential value is an indication of high dispersion stability as the particles are charged enough to repel one another. Particles with a low zeta potential value indicate dispersion instability as the particles are not charged enough to repel each other. A colloidal system between +30 mV to −30 mV is considered unstable and the particles will be aggregated, anything above or below these values is generally considered stable and highly charged and is indicative of a highly dispersed system[124].

The dispersion stability of thiol-core, carboxyl-shelled microspheres **10** was confirmed by zeta potential measurements which indicated that the microspheres possessed a charge of −74.84 mV. This zeta potential value is confirmation of a highly dispersed system. The zeta potential value of thiol-functionalised microspheres **6** was +4.86 mV.

These zeta potential values indicated that the aggregation of the microspheres had been significantly reduced by the covalent attachment of the carboxyl-functionalised polymeric shell.

In order to ensure that the optimum level of microspheres was being taken up by cells, a number of parameters were explored to improve internalisation and aid visualisation of internalisation. Parameters such as the incubation time, level of haematocrit used and the effect of haemoglobin on the fluorescence of QD-microspheres **7** were also investigated for this study.

2.4.1.3   Effect of haematocrit levels on visualisation of red blood cells

Haematocrit is the percentage of RBCs present in a blood sample. The level of haemocrit initially tested was 40 % as this is percentage of haematocrit present in blood[125]. However, an observation from the confocal microscope image displayed in Figure 28 (image A) was that the haematocrit level was too high as there were too many RBCs present to ascertain effectively whether beadfection was occurring. Tests with haematocrit levels at 20 % and 10 % were also carried out before the level was reduced to 1 % and this was the level at which individual RBCs were best observed. RBCs at a haematocrit level of 1 % (image B) were imaged under a confocal microscope, as shown in Figure 28.
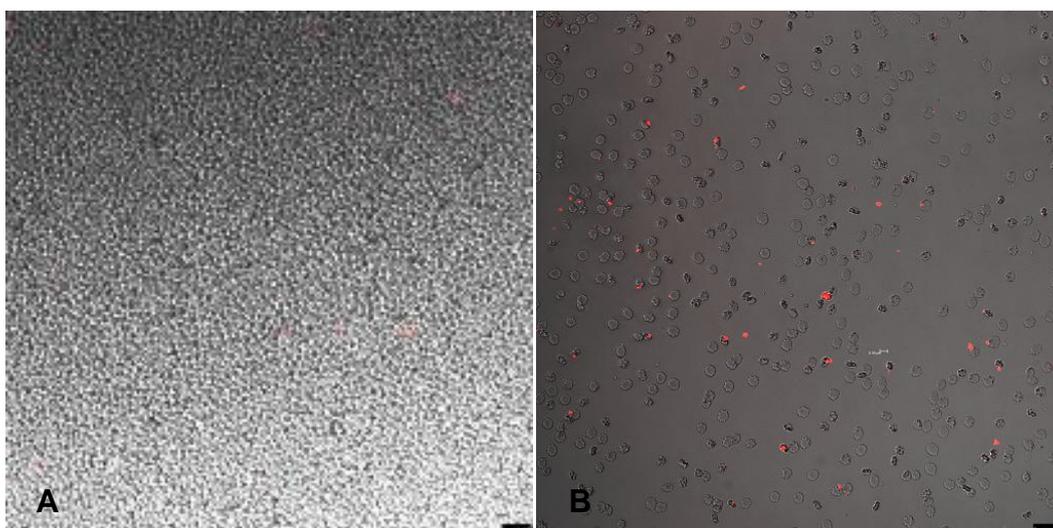
Figure 28: Confocal microscope images of beadfection with different haematocrit levels.
Image A: Red blood cells at a haematocrit of 40 % which were incubated with QD-microspheres **7** (3.00×10^{-3} g mL^{-1}) suspended in PBS for 1 hour
Image B: Red blood cells at a haematocrit of 1 % which were incubated with QD-microspheres **7** (3.00×10^{-3} g mL^{-1}) suspended in PBS for 1 hour

2.4.1.4   Effect of incubation time on beadfection

Incubation times of 1 hour, 5 hours, 24 hours were examined to find the optimum length of time for beadfection to occur. After 24 hours of incubation, the microspheres appeared to be entering RBCs as shown in Figure 29.
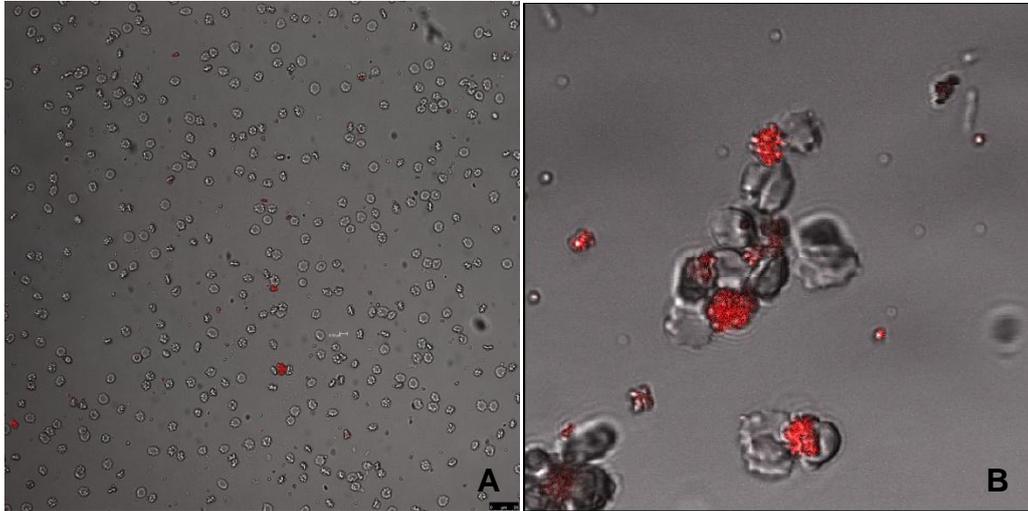
Figure 29: Confocal microscope image of RBCs incubated with QD-microspheres **7**
Image A: Red blood cells at a haematocrit of 1 % which were incubated with QD-microspheres **7** (3.00×10^{-3} g mL^{-1}) suspended in PBS for 1 hour
Image B: Red blood cells at a haematocrit of 1 % which were incubated with QD-microspheres **7** (3.00×10^{-3} g mL^{-1}) suspended in PBS for 24 hours

RBCs with an incubation time of 1 hour also appeared to show beadfection, however it is possible that a repeat of this test on different batches of RBCs may require a different incubation time for beadfection to occur.

2.4.1.5   Effect of QD-microspheres **7** on haemolysis levels

The possible negative effects of QD-microspheres **7** on blood, if any, were investigated by assessment of haemolysis levels (RBC death). Haemolysis levels were determined by measuring the level of plasma free haemoglobin (pfHb) which is released when a RBC lyses.

The haemolytic effects of QD-microspheres **7** and QDs were observed using the Harboe assay[126]. The methodology for this study is described in section 4.5.2.

The results for the measured haemolysis levels are shown in Figure 30 and indicated that for both the control and QD-microsphere sample, very low haemolysis levels were present for the first 40 hours of incubation. After 40 hours, the haemolysis level for the

QD-microsphere sample appears to rise rapidly from a static level of 100 mg mL^{-1} to 4000 mg mL^{-1} during 40 hour another period.
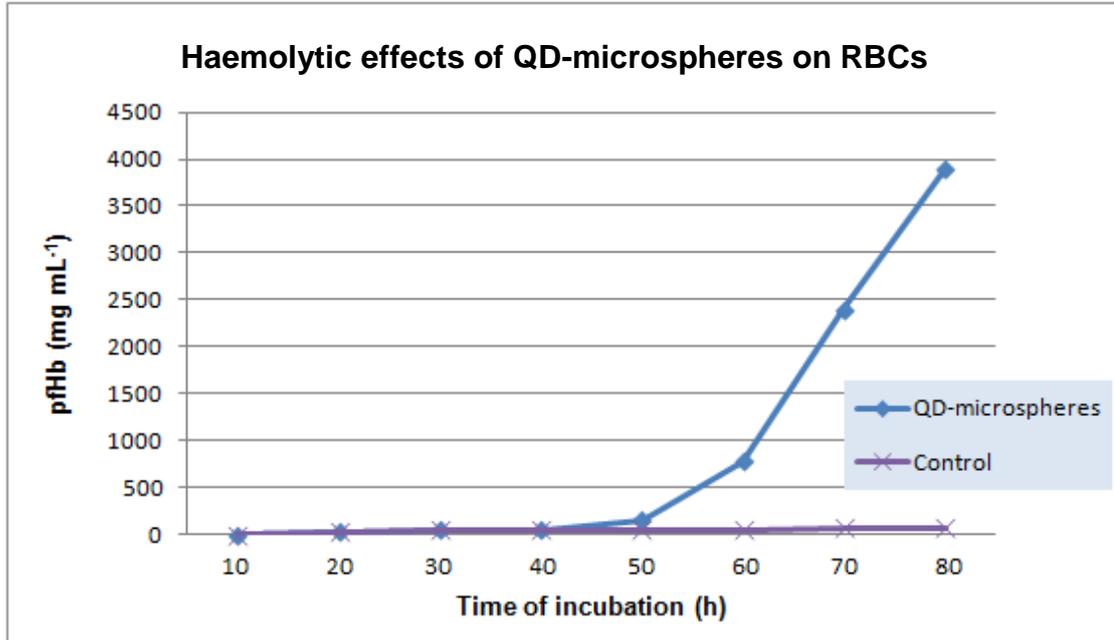
Figure 30: The effect of QD-microspheres **7** on the haemolysis levels of RBCs

A possible explanation for these results could be that the RBCs were taking up microspheres until they reached their capacity at 40 hours and then burst or the microspheres could enter the cells at 40 hours, causing the cells to burst on entry. It could also be possible that the microspheres were not entering the cells but the mere presence of microspheres in the vicinity of the cell may have weakened the cells, causing them to burst. This was an indication that QD-microspheres **7** are not biocompatible with RBCs.

A few variables to consider were that the same sample of blood and only one blood specimen was used in both tests. Different blood samples would be ideal for future tests as it would useful to see if haemolysis at 40 hours was consistent with other samples of blood. The blood sample had also been treated with dextran, which is a long chain polymer of glucose and is used to improve blood flow and reduce blood viscosity[127]. It is uncertain what effect, if any, dextran would have on microsphere uptake but it would be constructive to test a sample of blood which has not been treated with dextran.

2.4.1.6 The effect of haemoglobin on the fluorescence of quantum dots

The possible interaction of QDs with haemoglobin has been investigated by Shen et al[128]. Haemoglobin has been reported to exhibit fluorescence when excited around its characteristic bands of absorption, the Soret band, which has strong absorption at approximately 406 nm and the *Q*-band at approximately 580 nm[125, 129-131]. Shen et al[128] found that the fluorescence of haemoglobin was quenched in the presence of QDs. This notion was investigated in this study, in which the fluorescence of QDs was assessed when incubated together with haemoglobin. This assessment was carried out using a fluorescent plate reader. The methodology for this study is detailed in section 4.5.3.

Naked QDs and QD-microspheres **7** were incubated individually in a 1:1 ratio with RBCs in PBS and haemoglobin in PBS. Haemoglobin was obtained by lysing RBCs which caused its release. The fluorescence of each of these samples was analysed on a fluorescent plate reader, the results for which are shown in Figure 31.
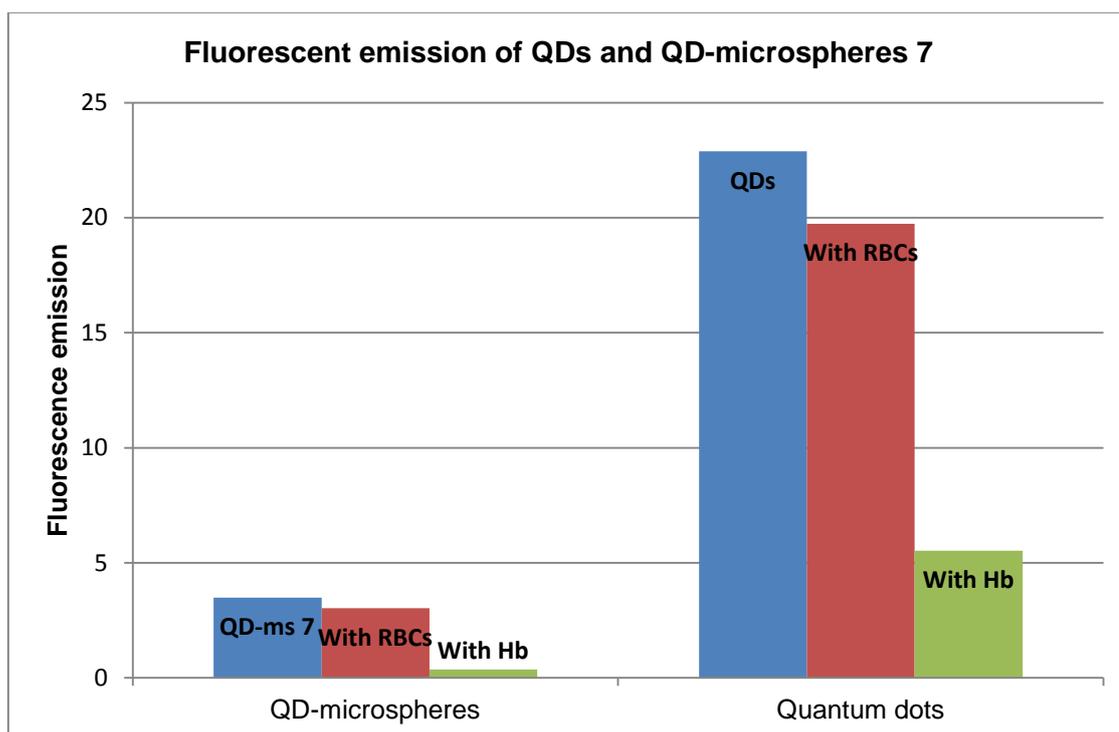
Figure 31: Fluorescent emission of QDs, QD-microspheres **7** alone and on interaction with haemoglobin and RBCs

The data shows that the fluorescence emission of both QDs and QD-microspheres slightly reduced when in contact with RBCs, but was significantly reduced when incubated with haemoglobin.

It is not certain why the fluorescence of QDs reduced so greatly when in contact with haemoglobin. A possible reason is that haemoglobin could be absorbing the energy required for QD excitation, thus preventing QDs from fluorescing. As mentioned earlier, haemoglobin has been found to absorb around 410 nm and 580 nm. The QDs used for this study emit at 610 nm and excite below 610 nm, so it may be possible that there is an overlap of excitation energy of QDs with the excitation bands of haemoglobin.

It is also possible that there is some form of interaction between haemoglobin and QDs, which may have led to a subsequent reduction in the emissive properties of QDs. Electrostatic attraction has been suggested as the possible interaction mechanism between QDs and haemoglobin[129]. Overall, the findings from this study meant that the use of QDs to track RBCs was no longer viable as QD fluorescence from either free QDs or QD-microspheres **7** is significantly reduced upon exposure to haemoglobin.

2.4.1.7   Use of fluorescent tag to visualise red blood cells

A difficulty faced in the visualisation of microspheres inside cells was the determination of whether the microspheres were inside the cell or simply stuck to the outside of the cell membrane. To give a more accurate image of the position of microspheres in relation to the cells, the cell membrane of RBCs were labelled with a fluorescent dye, PKH26, which has a maximum emission of 567 nm. A confocal microscope image of RBCs labelled with PKH26 can be found in Figure 32.

In order to clearly compare and contrast the position and colour of the microspheres and RBCs, a fluorescent dye complementary to PKH26 was selected. As previous work in section 2.4.1.6 had shown, it was no longer feasible to use QDs to track RBCs, hence the use of a fluorescent dye, DY-405 maleimide. DY-405 maleimide absorbs at 400 nm and emits at 423 nm. This fluorophore enabled a microscope set-up with a 4',6-diamino-2-phenylindole (DAPI) filter which would allow the emission wavelength of the microspheres, cell membrane dye and RBCs to be significantly independent of each other and thus easier to visualise.
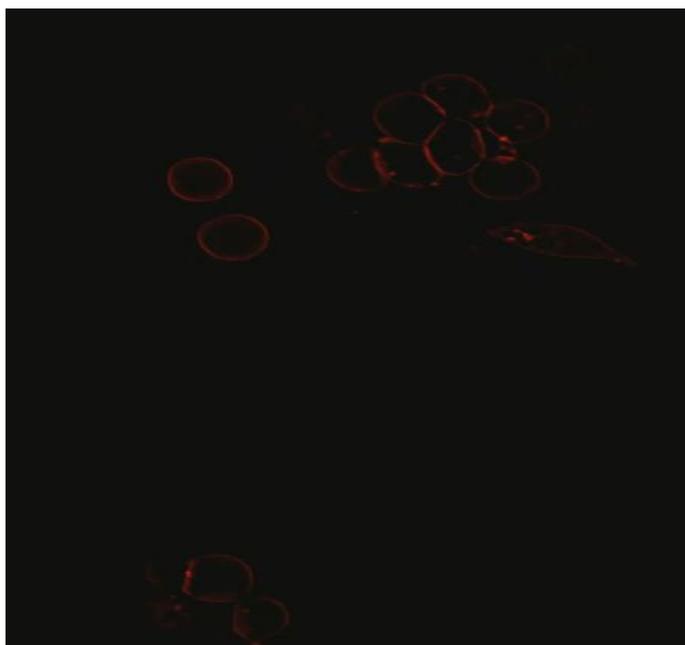
Figure 32: Confocal microscope image of RBCs with cell membrane labelled with PKH26

DY-405 maleimide, which is thiol reactive, was used to label thiol-functionalised microspheres **6** with the same procedure summarised in Scheme 8, section 2.5.1. However, the reaction failed and did not yield fluorescent microspheres. This was presumed to result from the fact that DY-405 is hydrophilic dye and was not able to penetrate the relatively hydrophobic thiol-functionalised microspheres **6**.

This reaction was then repeated with polar thiouronium-functionalised microspheres **5** in place of thiol-functionalised microspheres **6**, which yielded highly fluorescent microspheres. This reaction was successful presumably because the dye molecules were able to associate with the microspheres by electrostatic attraction of the positive charge on thiouronium-functionalised microspheres **5** with the negative charge of the dye. The labelled thiouronium-functionalised microspheres were shelled by the reaction summarised in Scheme 7 to yield DY-405 labelled thiouronium-core, carboxyl-shelled microspheres.

These microspheres were incubated with RBCs and results appeared to show positive signs of beadfection. An image of DY-405 labelled thiouronium-core, carboxyl-shelled microspheres inside cell membrane labelled RBCs was obtained as shown in Figure 33. This image appears to show the presence of microspheres that have moved through the membrane of the RBCs by the process of beadfection.
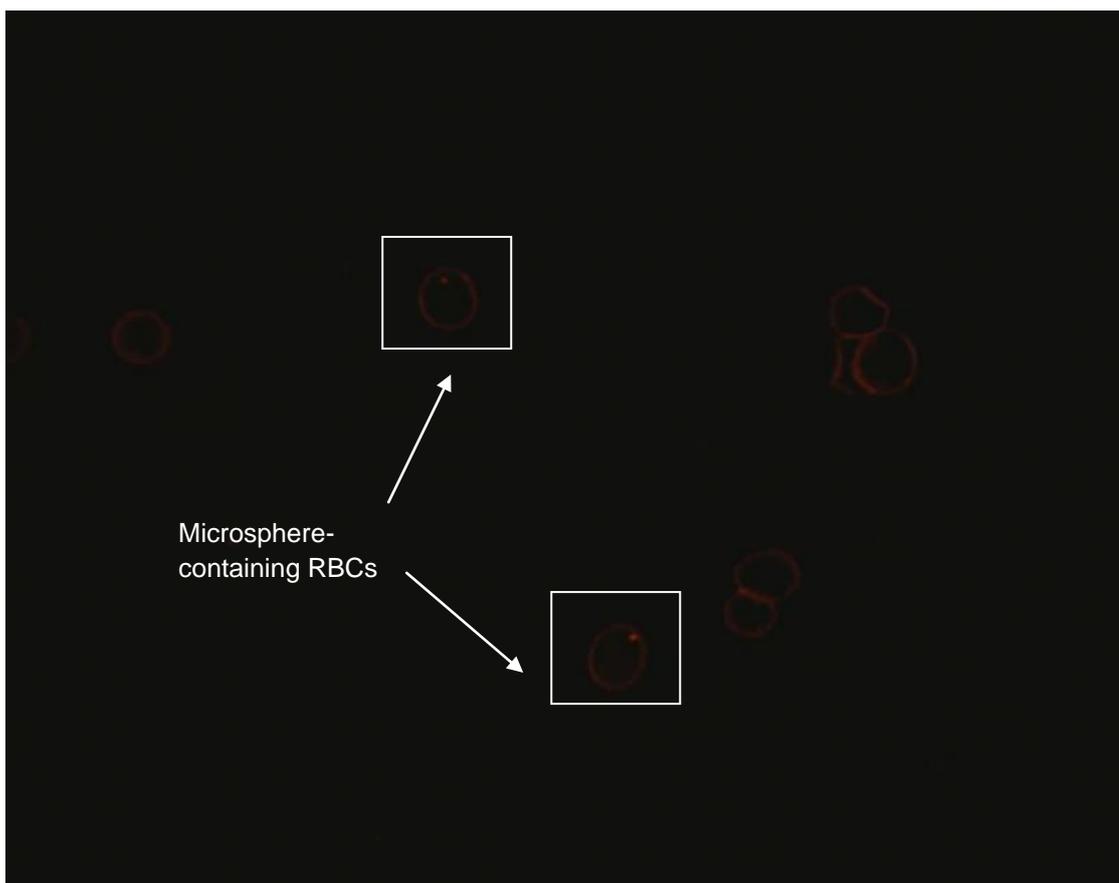
Figure 33: Confocal microscope image of DY-405 labelled thiouronium-core, carboxyl-shelled microspheres inside RBCs labelled with PKH26 suspended in PBS

2.4.2. Summary

Several parameters were explored in order to optimise the beadfection process. These parameters included haematocrit levels, incubation time and the effect of QDs on the haemolysis levels of RBCs. Results from these investigations gave rise to some key findings, one of which included the observation of large aggregates of QD-microspheres **7** present in samples visualised on a confocal microscope. This would make it difficult to visualise the passage of individual microspheres into RBCs. The problem was successfully combated by the covalent attachment of a charged layer of polymeric shell around the microspheres. This was found to greatly reduce the aggregation of the microspheres and was supported by zeta potential data which indicated a charged surface.

Another significant finding was the effect of QD-microspheres **7** on the haemolysis level of RBCs. When RBCs were incubated with QD-microspheres **7**, the haemolysis level was found to increase significantly in comparison with the control sample. This

rapid increase in haemolysis was observed after an incubation period of 40 hours. Reasons for rapid haemolysis could relate to the presence of microspheres either inside or around the RBCs.

A turning point of the investigation was the observation that the presence of haemoglobin has a deleterious effect on the fluorescence of QDs. For reasons not yet fully understood, the fluorescence of QDs appeared to reduce significantly when in the presence of haemoglobin. Therefore, it was decided that microspheres labelled with fluorescent dyes were better suited to RBC visualisation.

In order to evaluate the use of fluorescent microspheres to image RBCs, it had to be determined whether the fluorescent microspheres could be successfully internalised into RBCs. A confocal image of microspheres labelled with DY-405 maleimide incubated with RBCs indicated that the microspheres appeared to have been successfully internalised. This is a preliminary finding and further work is required to optimise the process of beadfection, nevertheless, this is compelling evidence to suggest that visualisation of RBCs *via* the internalisation of fluorescent microspheres is possible.

2.4.3. Future developmental work to internalisation process

Further work will involve the use of micromanipulators to watch the interaction of a microsphere which has been placed on a single cell. This would be a method of assessment of beadfection into a single cell.

To increase the chances of internalisation of microspheres into RBCs, a method incorporating active transport of microspheres instead of the passive transport approach might be another route of investigation. It was suggested that microspheres coated with potassium or calcium could exhibit increased uptake when placed in a calcium-depleted environment containing RBCs.

As internalisation of microspheres appears to occur with a small number of RBCs in a sample of blood, fluorescence activated cell sorting (FACS) could be employed to separate the fluorescent microsphere-containing cells from non-fluorescent cells. This method would give a clearer indication of the number of cells internalising microspheres.

Atomic force microscopy (AFM) could also be used to further examine beadfection. AFM would give an indication of the shape and properties of RBCs and the RBCs containing QD-microspheres **7**. The effect of QD-microspheres **7** on the properties of RBCs, if any, can be determined *via* this method.

Should internalisation into RBCs progress, the passage of the microspheres into cells can serve as a delivery system, possibly transporting biologically relevant cargo to blood-rich sites such as tumours.

2.5. Labelling of polymer microspheres with fluorescent dyes

Polymer microspheres labelled with a fluorescent dye can be used as an analytical tool for other bioimaging purposes. Another application of these fluorescent microspheres was to visualise the tear film of the eye.

As the microspheres were to be applied directly to the eye, the study was restricted to fluorescent dyes as QDs contain a potentially harmful heavy metal core.

The tear film is of particular interest as the thickness of each of the three layers that it is composed of is uncertain. A means of accurately determining the thickness of each layer would be ideal, hence the development of fluorescent microspheres for this purpose. The proposed tasks were to synthesis fluorescent microspheres in a range of diameters and observe their behaviour in the tear film. The presence of the fluorescent microspheres within the eye could serve as a tracking system, with the fluorescent nature of the microspheres allowing their path to be followed across the tear film.

The hypothesis was based on the idea that the larger the diameter of the microsphere, the more likely it is to partition into the denser layers of the tear film, *i.e.* the aqueous or mucin layer.

The first task was to attempt to successfully label previously synthesised thiol-functionalised microspheres **6** with a range of fluorescent dyes. This labelling reaction is described in more detail in the next section.

2.5.1. Labelling of thiol-functionalised microspheres **6** with maleimide-functionalised fluorescent dye

Thiol-functionalised microspheres **6** can be labelled with maleimide-functionalised, thiol-reactive fluorescent dyes by a Michael addition reaction. This involves the addition of a Michael donor, in this case a non-enolate nucleophile - the thiol group, to a Michael acceptor, the electrophilic maleimide functionality. Maleimides possess two carbonyl groups conjugated to the ring structure, which yields an electron-poor double bond. This bond is susceptible to nucleophilic attack. The activated double bond attracts electrons from the thiol group which adds to the maleimide unit ultimately forming a stable thio-ether bond[132].

To enable the reaction to occur, thiol-functionalised microspheres **6** were swollen with *N-N*-dimethylformamide (DMF) to allow the easy passage of the maleimide-functionalised dye into the polymer matrix. Successful conjugation of the dye was indicated by a strong fluorescent signal possessed by the microspheres under UV excitation. The fluorescence of the microspheres was analysed either under UV light or with a fibre-optic fluorescent probe.

This reaction is summarised in Scheme 8.

X = Texas Red,
PyMPO,
Pacific Blue,
Alexa Fluor 546,
Fluorescein diacetate
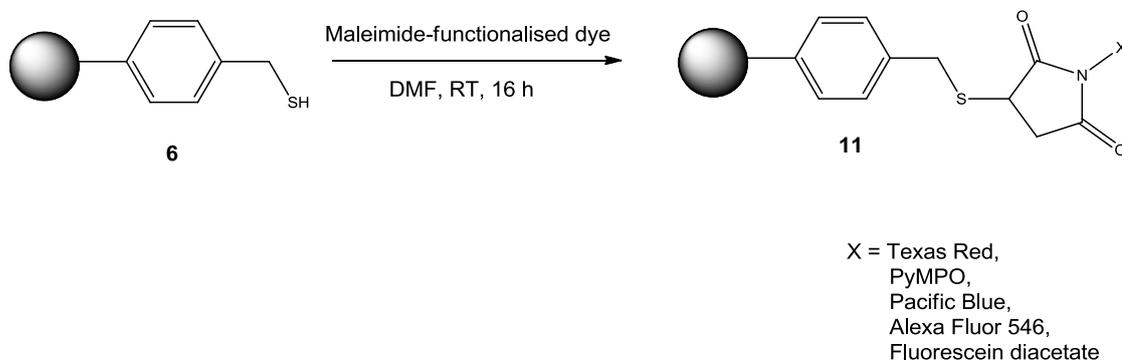
Scheme 8: Synthesis of fluorescent thiol-functionalised microspheres **11** with maleimide-functionalised dyes. The molecular structure of the maleimide-functionalised dyes is shown in Table 12.

The reaction of microspheres with fluorescein diacetate-5-maleimide also required the addition of TMAOH, in a 1:1 ratio to the fluorescent dye. This addition served to cleave the diacetate protecting group, thus activating the fluorescein ring and enabling the fluorescein molecule to fluoresce. This reaction was efficient and yielded highly fluorescent microspheres **11**, an image for which was taken on a fluorescent

microscope and shown in Figure 34. Sample preparation and procedure for fluorescent microscope analysis is described in section 4.2.2.
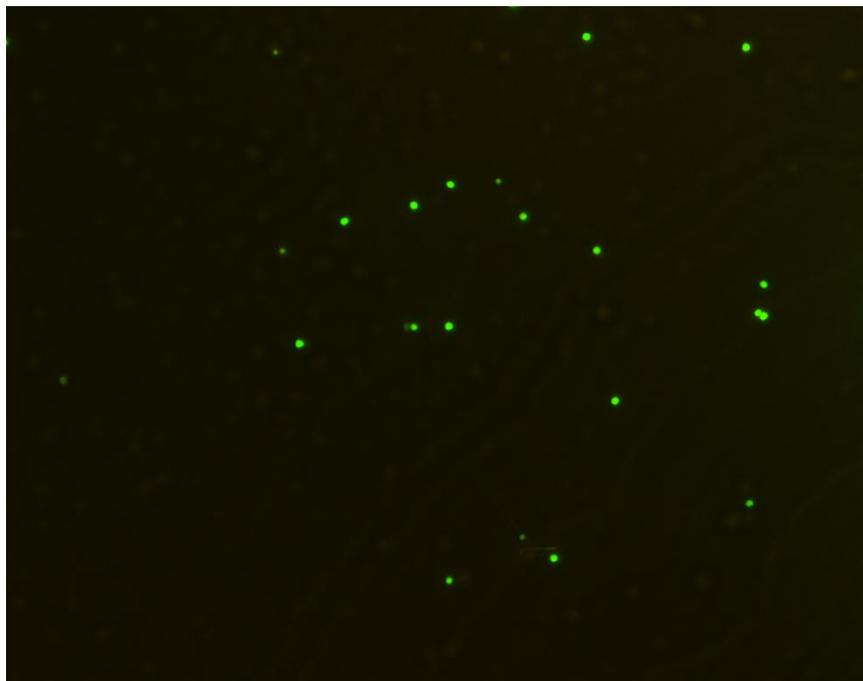
Figure 34: Fluorescent microscope image of thiol-functionalised microspheres **6** (5.00 × 10^{-3} g mL^{-1}) labelled with fluorescein diacetate maleimide suspended in distilled water by ultrasonication.

The reaction in Scheme 8 was repeated with four additional maleimide-functionalised fluorescent dyes, listed in Table 11.

Table 11: Excitation and emission wavelengths for maleimide-functionalised fluorescent dyes used to label thiol-functionalised microspheres **6**

Maleimide-functionalised dye	Excitation wavelength (nm)	Emission wavelength (nm)
Texas Red	595	615
Alexa Fluor 546	556	575
Pacific Blue	410	455
PyMPO	415	561

Each dye selected had an excitation and emission wavelength which was different from one another. The purpose of using these four dyes was to produce four batches of fluorescent microspheres of different colours, which would allow easy identification between the different sets of microspheres when used simultaneously in the eye.

83

Two of the dyes, Texas Red and PyMPO, successfully labelled thiol-functionalised microspheres **6**, yielding highly fluorescent microspheres. These microspheres were visualised on a fluorescent microscope, with an image of the microspheres labelled with Texas Red displayed in Figure 35.
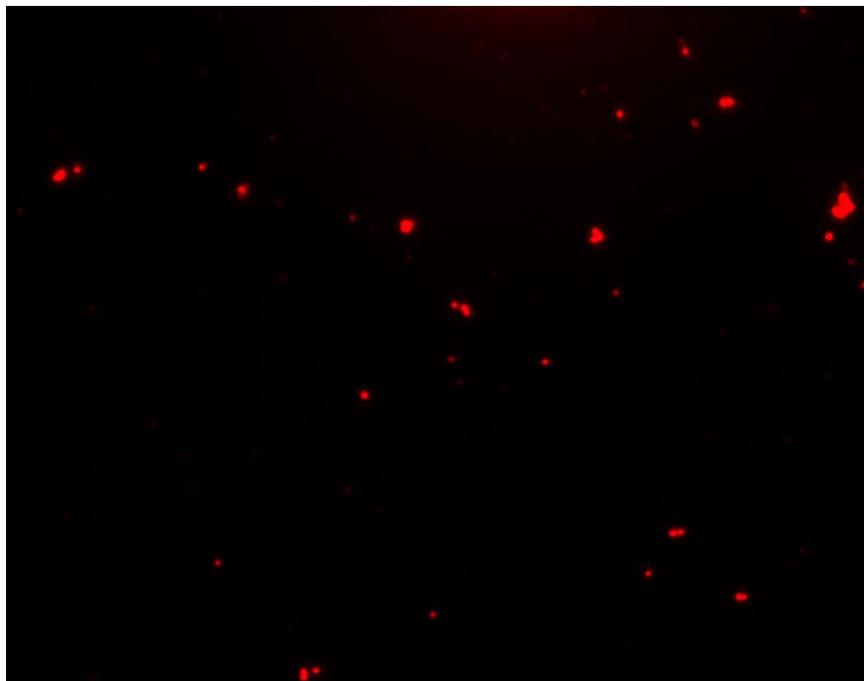
Figure 35: Fluorescent microscope image of thiol-functionalised microspheres **6** (5.00×10^{-3} g mL^{-1}) labelled with Texas Red maleimide suspended in distilled water by ultrasonication.

The two other dyes, Pacific Blue and Alexa Fluor 546 did not successfully label the microspheres, with the microspheres exhibiting a very low level of fluorescence post labelling.

This can possibly be explained by looking at the structures of the dyes, shown in Table 12.

Texas Red and PyMPO are relatively hydrophobic structures, which means that they are able to associate well with the microspheres which are also hydrophobic. The compatibility between dye and microsphere is favourable and the dye is able to penetrate the polymer matrix and react with the thiol groups present within the microspheres.

Table 12: Molecular structures of the maleimide-functionalised fluorescent dyes used to label thiol-functionalised microspheres **6**

	Molecular structure of fluorescent dye
PyMPO	
Texas Red	
Pacific Blue	
Alexa Fluor 546	
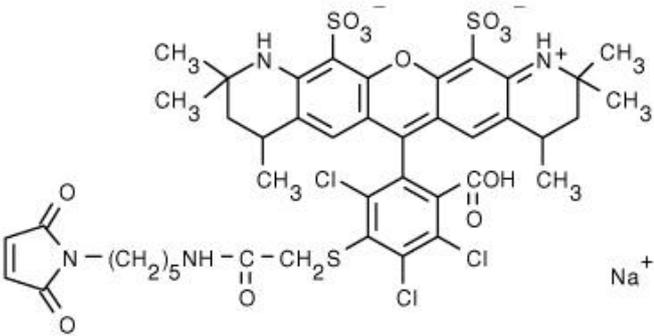
In contrast, Pacific Blue and Alexa Fluor 546 appear to be quite hydrophilic which presented a problem with microsphere association. It is possible that the relatively apolar microspheres would repel the polar, negatively charged dyes and restrict interactions between the microspheres and the dye. This, in turn, would prevent the

hydrophilic dyes from reacting with the thiol groups resulting in non-fluorescent microspheres.

In order to make conjugation of Pacific Blue and Alexa Fluor 546 more successful, the next step was to synthesise microspheres with a hydrophilic nature to aid attachment of the hydrophilic dyes.

This was achieved by a seeded emulsion polymerisation reaction using thiol-functionalised microspheres **6** as the seed particles.

2.5.1.1 Synthesis of thiol-core, carboxyl-shelled microspheres **10**

The desired hydrophilic nature was introduced *via* a carboxylated polymer shell which was synthesised around thiol-functionalised microspheres **6**, as shown in Scheme 7 and previously described in section 2.4.1.2.

The carboxyl groups were provided by a monomer, methacrylic acid **9**, which formed part of the polymeric shell along with styrene **3** and DVB **4**. The molar ratio of styrene **3** compared with methacrylic acid **9** was 7:3, and this provided microspheres with a uniform shell and a relatively monodisperse size distribution. DVB **4** enabled the microspheres to be swollen in the presence of organic solvents, allowing fluorescent dyes to readily enter the polymer matrix to react with the thiol groups. Sodium dodecyl sulfate (SDS) was used as a surfactant to aid the formation of uniform particles.

The resultant thiol-core, carboxyl-shelled microspheres **10** were synthesised in a 64 % yield and were found to have increased slightly in mean diameter in comparison with the seed particles.

The sizing data indicated a shift in the average diameter of the seed particles from 0.8 µm (standard deviation = 0.4 µm) to an average diameter of 0.9 µm (standard deviation = 0.4 µm) for the thiol-core, carboxyl-shelled microspheres **10**.

The level of carboxyl groups present on the microspheres was assessed by the loading of an Fmoc protected amino acid onto the microspheres. Fmoc-diaminopropyl hydrochloride **12** was coupled to thiol-core, carboxyl-shelled microspheres **10** *via* the carboxyl functionality of the microsphere in the presence of a coupling agent, TBTU, as shown in Scheme 9.
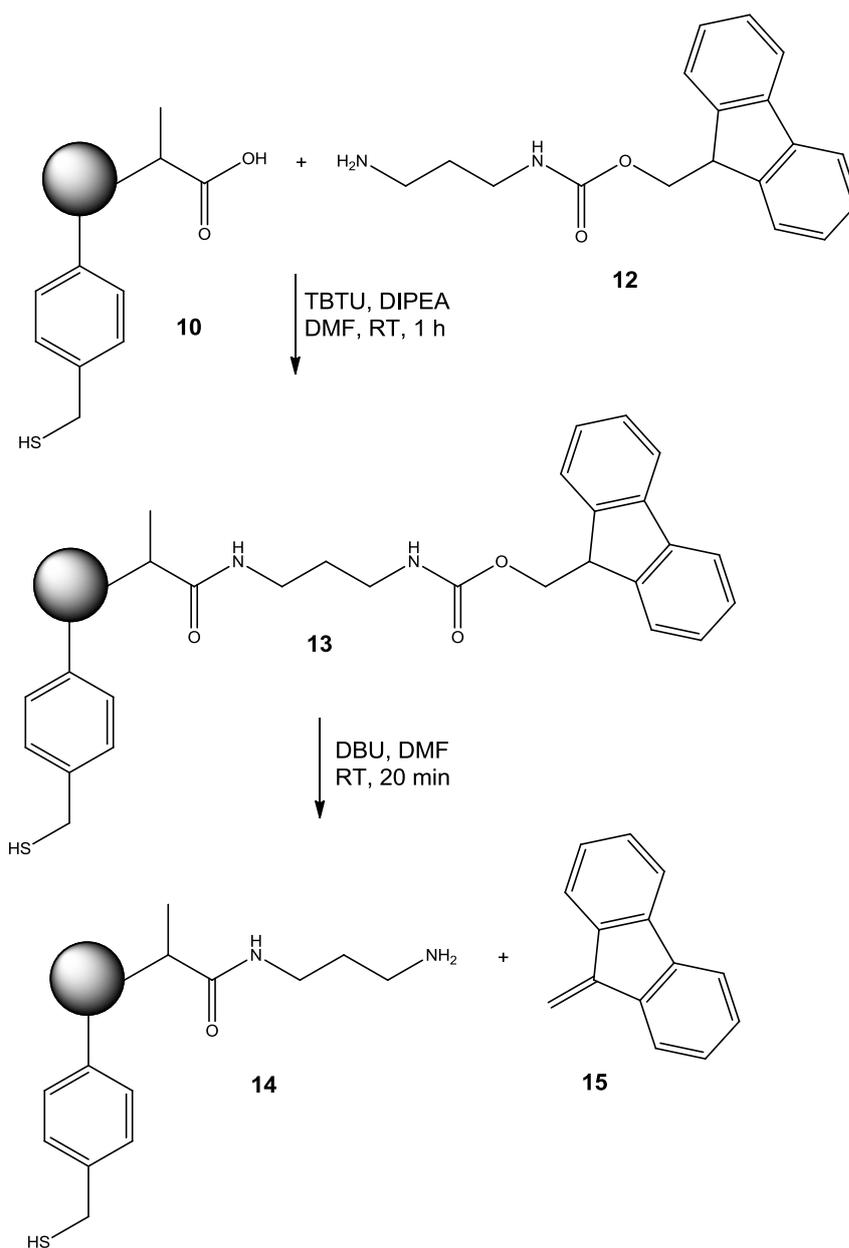
Scheme 9: Fmoc loading of diaminopropyl hydrochloride **12** to thiol-core, carboxyl-shelled microspheres **10** and subsequent cleavage of fulvene **15**

The resultant microspheres **13** were treated with 1,8-diazabicyclo[5.4.0]undec-7-ene (DBU) to mediate Fmoc cleavage. The UV absorbance of the cleaved fulvene adduct **15** was then measured at 294 nm and 304 nm. Each absorbance value was entered into equation 1 in order to calculate the experimental loading of the resin. The extinction coefficient value in equation 1[105] arises from the gradient of the calibration curve, Figure 36, constructed for UV absorbance at 294 nm and 304 nm of the fulvene adduct **15** from Fmoc-diaminopropyl hydrochloride **12**.
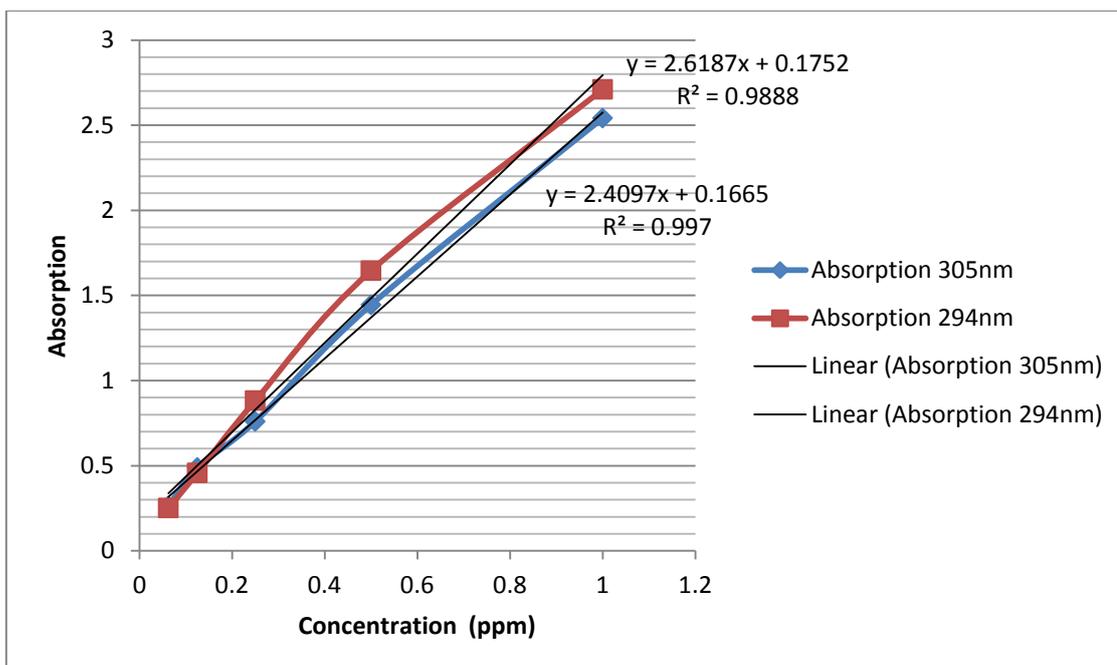
Figure 36: Calibration curve of the concentration of the fulvene adduct **15** cleaved from Fmoc-diaminopropyl hydrochloride **12** against UV absorbance at 294 nm and 304 nm

Equation 1: Equation for the calculation of carboxyl loading[105]

Carboxyl loading (mmol g^{-1}) = [(Abs/ε)*V]/mass of microspheres

An average of the loading value for both absorbances was taken as the final loading value. This was found to be 100 µmol g^{-1} for thiol-core, carboxyl-shelled microspheres **10** which was lower than the theoretical loading value of 390 µmol g^{-1}.

The thiol-core, carboxyl-shelled microspheres **10** were reacted with the two hydrophilic dyes, Alexa Fluor 546 and Pacific Blue maleimide, in the same way as described in section 2.5.1, in an attempt to fluorescently label the microspheres. Unfortunately, the reaction appeared to have failed as the microspheres were not fluorescent. Failure of this reaction may have been due to the inability of the fluorescent dyes to successfully penetrate the thiol core. Although the shell was hydrophilic, once the dye had penetrated the shell, the hydrophobic core may have meant that it was not possible for the dye to reach the thiol groups.

Therefore, the development of another route to label the microspheres with the two hydrophilic fluorescent dyes was investigated. This new route involved the modification of thiol-core, carboxyl-shelled microspheres **10**.

2.5.1.2 Modification of thiol-core, carboxyl-shelled microspheres **10** and subsequent labelling

A new approach involved the use of the carboxyl groups as a route for attachment of the maleimide-functionalised dyes. This involved the synthesis of a molecule with a moiety that was capable of reaction with the carboxyl groups and another moiety that was capable of reaction with the maleimide functionality of the dye thus linking the dye to the thiol-core, carboxyl-shelled microspheres **10**.

The molecule selected was *S*-trityl cysteamine **18** as it is a thiol amine with a simple synthetic route shown in Scheme 10[133]. The molecule has two reactive ends, an amine group for reaction with the carboxyl functionality on the microspheres and a thiol group for reaction with the maleimide dyes. However, it is possible for both ends to react with the carboxyl group, therefore to circumvent this; the thiol group was protected with a trityl protecting group. The idea being that the trityl group could be cleaved with a strong acid, trifluoroacetic acid (TFA), once coupling of *S*-trityl cysteamine **18** to the microspheres **10** was complete.
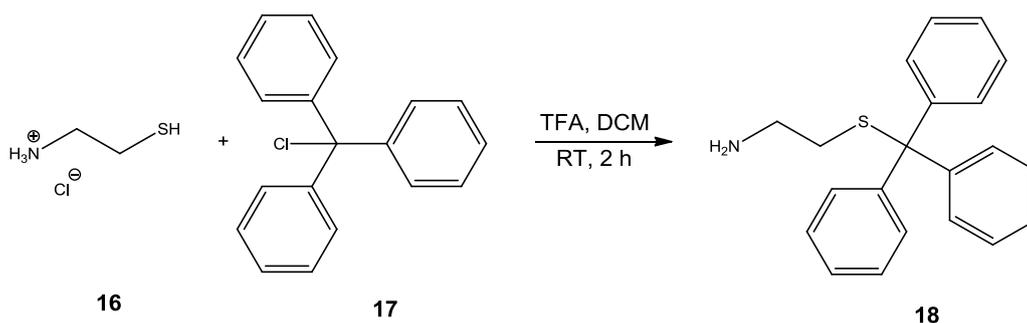
Scheme 10: Synthesis of *S*-trityl cysteamine **18** from cysteamine hydrochloride **16** and trityl chloride **17**

S-trityl cysteamine **18** was synthesised *via* a S_N1 displacement reaction with cysteamine hydrochloride **16** dissolved in dichloromethane (DCM) to which TFA and trityl chloride **17** were added.

Formation of the product was monitored by thin layer chromatography (TLC) (10 % ethyl acetate in hexane) and aqueous work-up provided *S*-trityl cysteamine **18**. Further purification of the product was not required.

^{1}H NMR analysis indicated successful formation of the product. Two triplets integrated at 2 protons were found at ∂ 2.320 ppm and ∂ 2.598 ppm which represented the two CH$_2$ groups in the aliphatic carbon chain. The aromatic region of *S*-trityl cysteamine **18** was accounted for by the presence of a multiplet with an

integration of 9 protons found at ∂ 7.204 ppm. This corresponded to the *para* and *meta* protons in the trityl group. A doublet with an integration of 6 protons and a chemical shift of ∂ 7.303 ppm, arose from the *ortho* protons in the trityl group.

^{13}C NMR analysis also confirmed the formation of *S*-trityl cysteamine **18**. Peaks related to the two CH_2 groups in the compound were found at δ 36.398 and δ 41.140. The tertiary carbon joined to sulfur was found at δ 66.593 ppm. The *para* carbons had a chemical shift of δ 126.711 ppm, *ortho* at δ 127.928 ppm, and *meta* at δ 129.653 ppm. Lastly, the *para* carbons joined to the tertiary carbon-sulfur bond were placed at δ 144.953 ppm.

FTIR and mass spectroscopy analysis listed in section 4.7.6 further confirmed the identity of the product.

S-tritylcysteamine **18** was then reacted with thiol-core, carboxyl-shelled microspheres **10** using the same coupling procedure described in the previous section. The trityl group was then deprotected with TFA and the maleimide-functionalised fluorescent dye was incubated with the resultant microspheres. Unfortunately, this did not yield fluorescent microspheres. This series of reactions is summarised in Scheme 11.
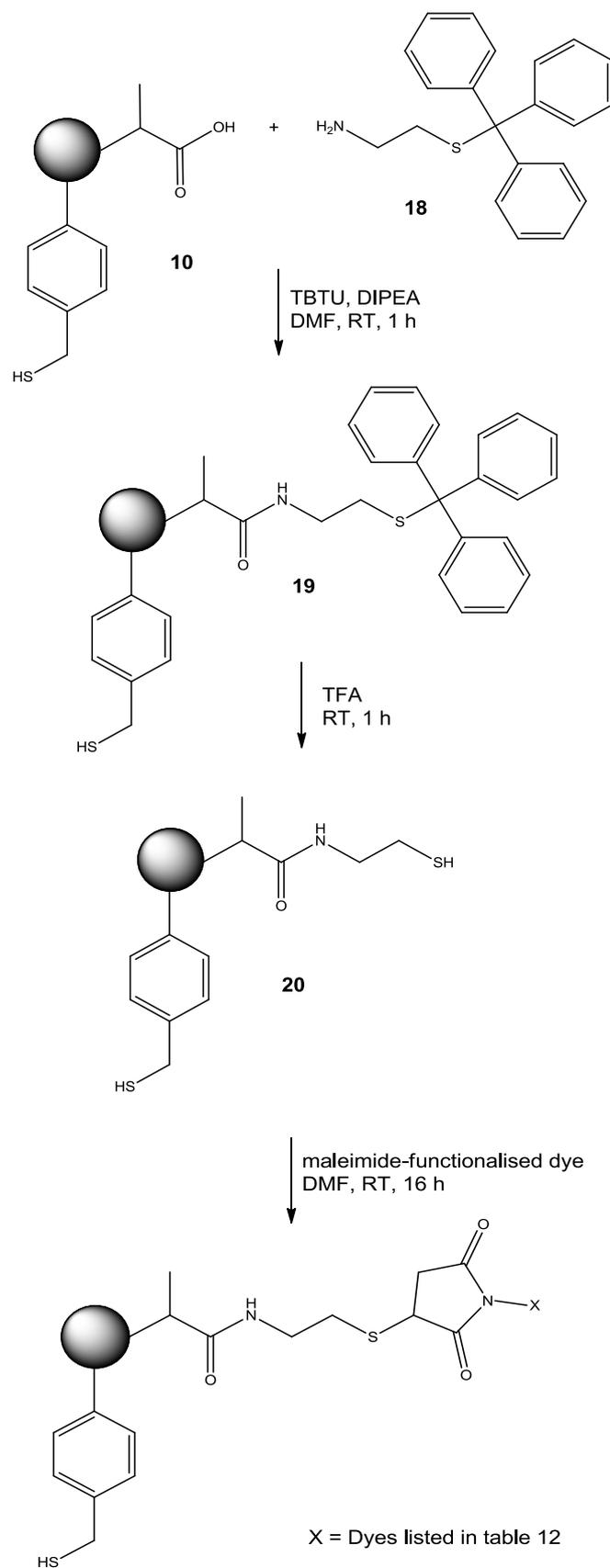
Scheme 11: Coupling of *S*-trityl cysteamine **18** to thiol-core, carboxyl-shelled microspheres **10** and the subsequent cleavage of the trityl group, followed by labelling of the resultant microspheres **20** with a maleimide-functionalised dye

There are three points where this reaction scheme could have failed upon, the first being that *S*-tritylcysteamine **18** did not successfully couple onto the microspheres. This point was investigated by coupling *S*-trityl cysteamine **18** to a carboxylic acid, acetic acid, in order to determine whether the thiol amine was capable of successfully coupling to a carboxyl group.

S-trityl cysteamine **18** was reacted with acetic acid **21** under the same coupling conditions as the reaction of *S*-trityl cysteamine **18** with thiol-core, carboxyl-shelled microspheres **10**. The formation of the product was monitored by TLC (20 % ethyl acetate in hexane). Aqueous work-up yielded the product, *N*-acetyl, *S*-trityl cysteamine **22** shown in Scheme 12 in a 22 % yield. The identity of the product was confirmed by ^{1}H and ^{13}C NMR analysis.
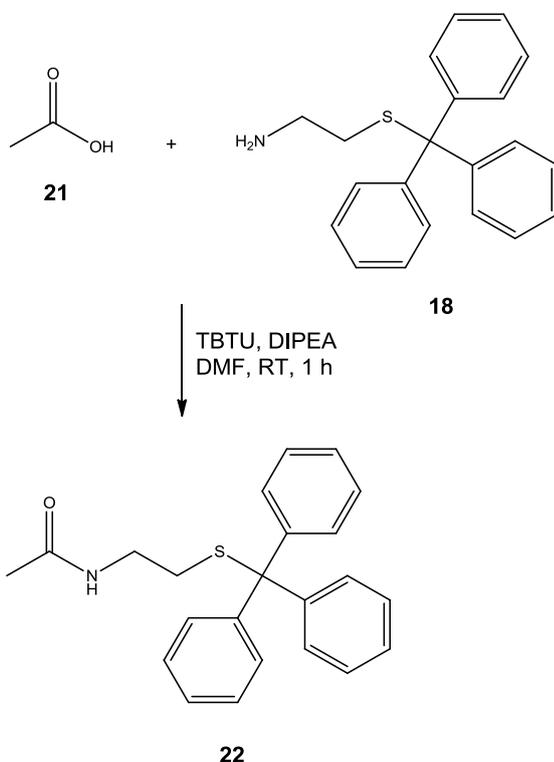
Scheme 12: Coupling of acetic acid **21** to *S*-trityl cysteamine **18** to form *N*-acetyl, *S*-trityl cysteamine **22** using the standard coupling protocol described in section 4.7.9

Specifically, ^{1}H NMR data indicated the presence of the two protons in the CH_2 groups in the aliphatic chain, which were found at ∂ 2.316 ppm and ∂ 3.024 ppm, both of which had an integration of 2 protons. The methyl group present due to the addition of acetic acid had a chemical shift of ∂ 1.886 ppm and integrated at 3 protons. The *para* and *meta* protons in the trityl group had a chemical shift of ∂ 7.205 ppm and integrated at 9 protons. The *ortho* protons had an integration of 6 protons and were found at ∂ 7.325 ppm.

^{13}C NMR analysis also indicated the formation of *N*-acetyl, *S*-trityl cysteamine **22**. The methyl group had a chemical shift of δ 23.328 ppm, followed by the two CH_2 groups at δ 32.022 ppm and δ 38.246 ppm. The tertiary carbon atom joined to sulfur was found at δ 66.914 ppm. The *para* carbons had a chemical shift of δ 126.911 ppm, *ortho* at δ 128.075 ppm, and *meta* at δ129.565 ppm. The *para* carbons joined to the tertiary carbon-sulfur bond were placed at δ144.657 ppm. The carbon present in the carbonyl bond was found at δ 169.854 ppm.

The success of this reaction indicated that the trityl cysteamine derivative could react successfully with carboxylic acid residues. Thus the reason for the failure of reaction scheme outlined in Scheme 11 was ascribed to a different failure point. There was a possibility that treatment of modified thiol-core, carboxyl-shelled microspheres **10** with TFA did not successfully cleave the trityl group to leave the thiol group free to react with the maleimide-functionalised dye. Successful cleavage of the trityl group should give rise to a yellow solution due to the cleaved trityl cation. Since a yellow solution was observed during the on-bead detritylation procedure, this indicated that successful detritylation did take place and this failure point was considered unlikely.

Another issue may have been that the level of carboxyl groups present on the microspheres was too low to load a sufficient amount of *S*-tritylcysteamine **18**. This would mean that the number of thiol groups for the maleimide dye to react with was also low, leading to non-fluorescent microspheres.

This is the most likely possibility as the loading assay on the thiol-core, carboxyl-shelled microspheres **10** provided a carboxyl loading value of 100 µmol g^{-1} which was not as high as the theoretical value of 390 µmol g^{-1}. This indicated that perhaps the amount of carboxyl groups was not high enough to anchor a sufficient level of *S*-trityl cysteamine **18** to yield fluorescent microspheres.

A possible solution would be to increase the carboxyl loading by increasing the ratio of methacrylic acid **9** in the seeded emulsion polymerisation reaction.

Another more feasible option was the use of amino-functionalised microspheres instead of thiol-core, carboxyl-shelled microspheres **10** as an attachment point for the hydrophilic dyes. Accordingly, a modified strategy employing amino-functionalised microspheres was evaluated.

2.5.1.3 Labelling of modified amino-functionalised microspheres 27

Amino-functionalised microspheres were synthesised in an analogous manner to thiouronium-functionalised microspheres **5** described in section 2.1.1.

4-Vinylbenzyl amine hydrochloride (4-VBAH) **23** was synthesised from 4-vinylbenzyl chloride **1** in the presence of sodium azide and triphenylphosphine (TPP) as shown in Scheme 13[134].
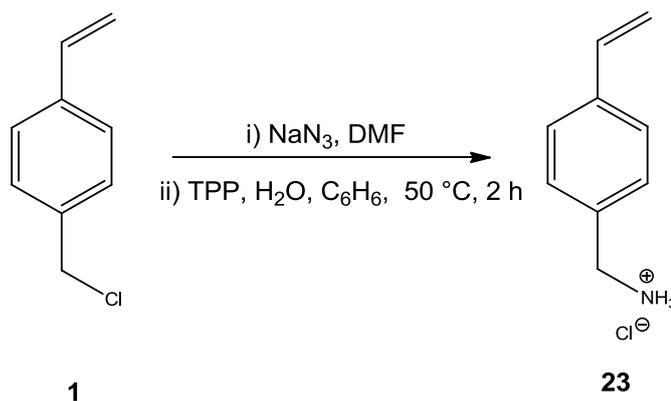
Scheme 13: Synthesis of 4-vinylbenzyl amine hydrochloride **23**[134] from 4-vinylbenzyl chloride **1**

4-Vinylbenzyl chloride **1** was converted into the corresponding azide derivative which was then subjected to a TPP-mediated Staudinger reaction to generate 4-VBAH **23** in a yield of 28 %. 4-VBAH **23** was then used in the synthesis of amino-functionalised microspheres **24** *via* a dispersion polymerisation reaction. AIBN was dissolved in a monomer mixture of 4-VBAH **23**, styrene **3** and DVB **4** and the reaction is shown in Scheme 14.
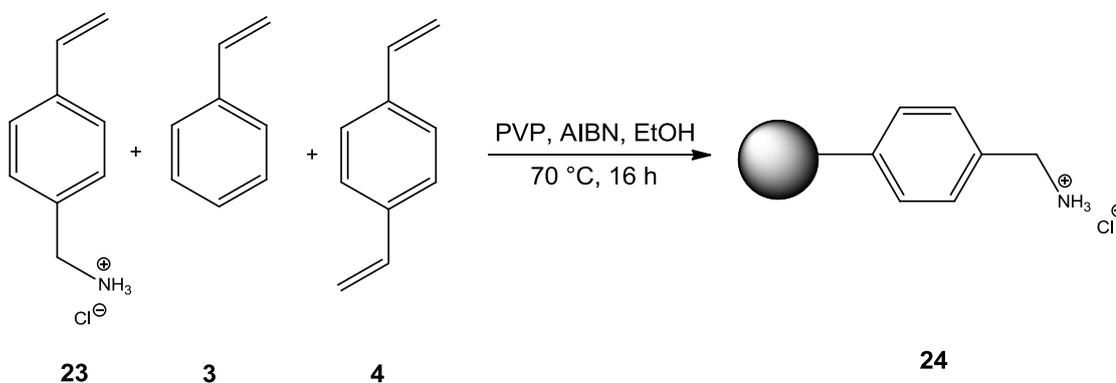
Scheme 14: Synthesis of amino-functionalised microspheres **24** *via* a dispersion polymerisation reaction using 4-VBAH **23** as the functional co-monomer

The resultant microspheres were washed with methanol and water to remove any un-reacted monomers.

The microspheres were synthesised in a 40 % yield. To confirm the successful synthesis of amino-functionalised microspheres **24**, the microspheres were labelled with fluorescein isocyanate, which reacts with primary amines to form a thiourea complex. The resultant microspheres possessed a green hue when excited with UV light which indicated the presence of amino groups on the microspheres.

The amino-functionalised microspheres **24** were then modified in a similar way to the thiol-core, carboxyl-shelled microspheres **10**, in which an amino acid capable of reaction with the maleimide dye as well as the amino groups was coupled onto the microsphere.

The amino acid selected was Fmoc-*S*-trityl, *L*-cysteine **25** as it possesses a thiol group for reaction with the maleimide-functionalised dye and a free carboxyl group to couple to the amino functionality of the microsphere.

Fmoc-*S*-trityl, *L*-cysteine **25** was reacted with amino-functionalised microspheres **24** in the same manner as the coupling reaction of *S*-trityl cysteamine **18** with thiol-core, carboxyl-shelled microspheres **10**.

The trityl group was then cleaved by treatment with TFA to leave the thiol group free to react with the maleimide-functionalised dye, as shown in Scheme 15.

Unfortunately, the dye labelling reaction did not yield fluorescent microspheres either. Neither hydrophilic dye successfully labelled the modified amino-functionalised microspheres **27**. Due to time constraints, establishment of the failure of the reaction, which may have been due to incomplete peptide coupling or incomplete detritylation, was circumvented and the study was pushed forward with microspheres that had been labelled successfully.

Microspheres successfully labelled with the hydrophobic fluorescent dyes, Texas Red and PyMPO, along with the microspheres labelled with fluorescein were used to visualise the tear film. The next stage in the study was the synthesis of microspheres in a range of diameters in order to try to investigate the different thicknesses of the layers that comprise the tear film.
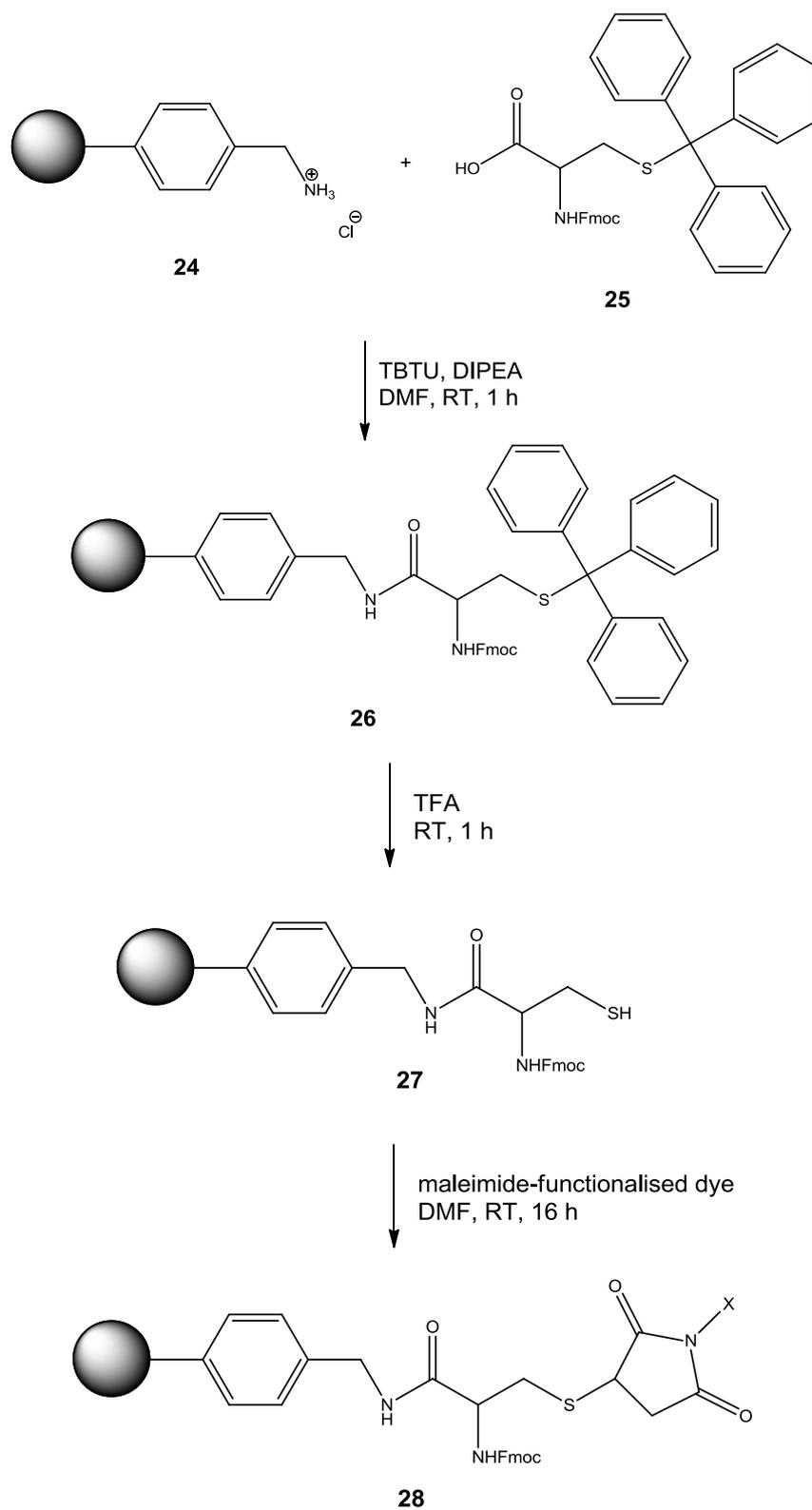
Scheme 15: Coupling of Fmoc-*S*-trityl-*L*-cysteine **25** to amino-functionalised microspheres **24**, cleavage of trityl protecting group from modified amino-functionalised microspheres **26** with TFA and subsequent labelling of microspheres **27** with maleimide-functionalised dye

2.5.2. Synthesis of different sized microspheres for tear film visualisation

The tear film is composed of a lipid layer (~2 μm), an aqueous layer (~4 μm) and finally a mucin layer (~1 μm)[66, 67, 69]. The work proposed was to synthesise microspheres that were ~0.5, 1, 1.5, 2 and 5 μm in diameter and observe their behaviour within the layers of the tear film. Different diameters of polymer microspheres were obtained by dispersion, suspension and emulsion polymerisation reactions.

To synthesise smaller microspheres, water was added to the dispersion polymerisation reaction medium. Water was present in a small quantity (5 % v/v in ethanol). Typically, the presence of water in a dispersion polymerisation reaction medium yields smaller particle sizes due to the differences in solubility between the monomers and solvent medium[9]. After the reaction has been initiated and monomer molecules react with the initiator to form oligomers, the oligomers of increasing molecular weight become insoluble in the ethanol-water medium more rapidly than in the ethanol medium alone[9]. This means that they precipitate out of the solvent medium quickly and have less time to aggregate with other insoluble oligomers, a process which causes an increase in size. Therefore, the final polymer particles formed in the ethanol/water medium are smaller than those formed in ethanol only.

The smallest microspheres were synthesised with 4-VBTU **2** to ensure that the microspheres could react with maleimide-functionalised dyes. These microspheres were 0.7 μm in diameter (standard deviation = 0.3 μm), the distribution curve for which is shown in Figure 37. The microspheres formed were relatively monodisperse and the subsequent fluorescent microspheres from the labelling reaction were highly fluorescent as shown in Figure 38.
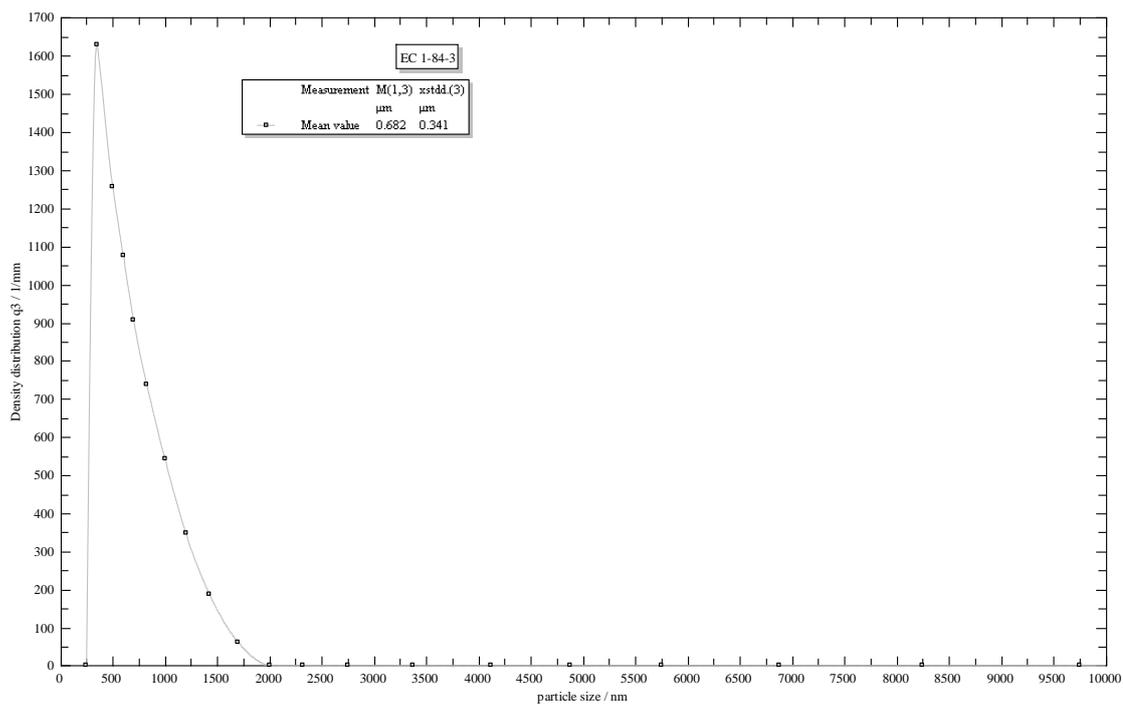
Figure 37: Distribution density curve for particle size of thiol-functionalised microspheres **6** synthesised by dispersion polymerisation with the addition of water to the reaction medium, suspended in distilled water, obtained by laser diffraction analysis after a 60 second period of ultrasonication
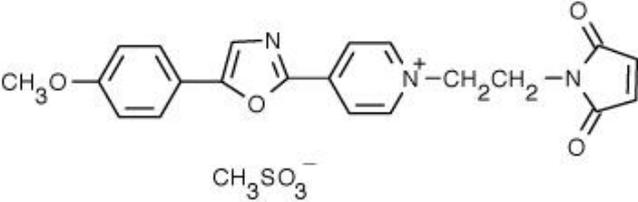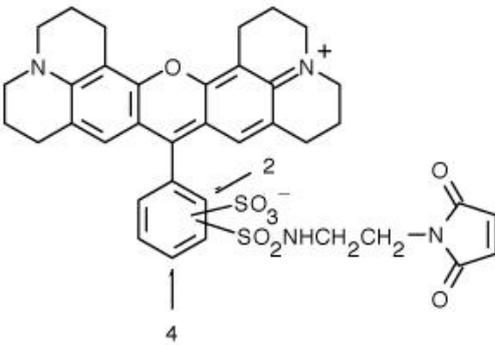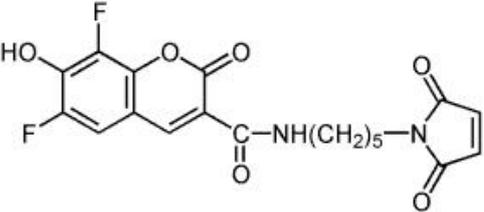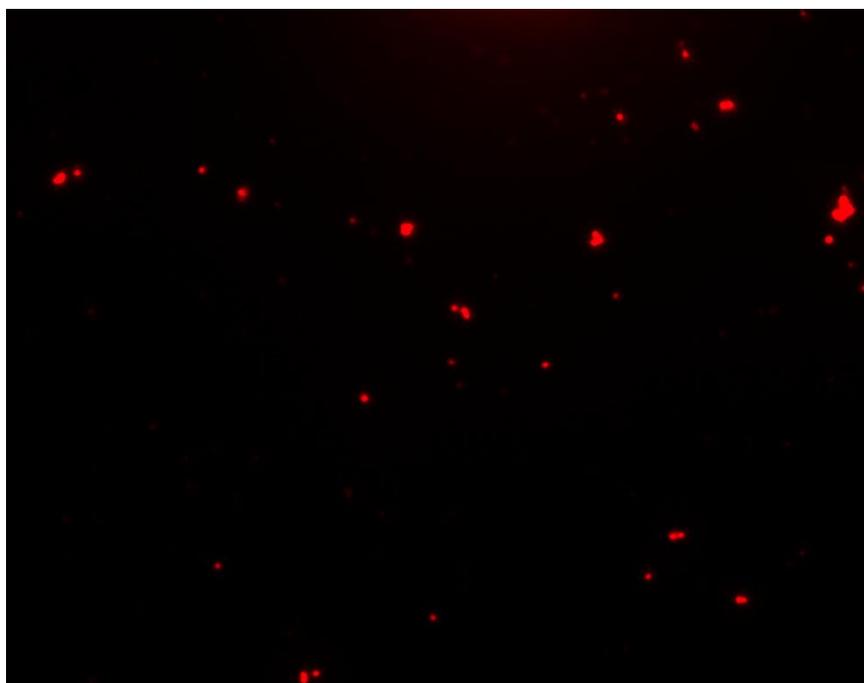

Figure 38: Fluorescent microscope image of small thiol-functionalised microspheres **6** (5.00×10^{-3} g mL^{-1}) labelled with Texas Red maleimide suspended in distilled water by ultrasonication.

Larger fluorescent crosslinked polystyrene microspheres **29** were synthesised by employing an emulsion polymerisation reaction shown in Scheme 16, in which the monomer was suspended in an aqueous solution of SDS with the aid of an ultrasonic probe. The probe promoted the dispersion of the monomer mixture within the aqueous phase and instigated the formation of small monomer droplets within the aqueous medium. This mixture was then stirred vigorously and polymerised at 70 °C, which led to the formation of microspheres between a size range of 1.5–5 µm.

3   4   29
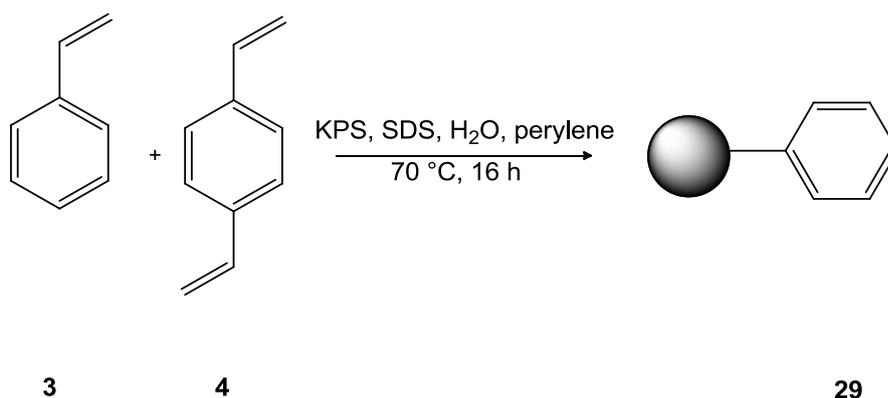
Scheme 16: Synthesis of fluorescent crosslinked polystyrene microspheres **29** *via* an emulsion polymerisation reaction

Another fluorescent dye, perylene, was used to label these microspheres. Perylene has is a polycyclic hydrocarbon structure which is shown in Table 13. It was selected for use as it emits in the blue region of the visible spectrum and was hence used as a replacement for the Pacific Blue maleimide dye that did not successfully label the thiol-functionalised microspheres **6** (see section 2.5.1.2).

Table 13: Excitation, emission wavelength and molecular structure of perylene

Structure of perylene	Excitation wavelength (nm)	Emission wavelength (nm)
	410	455
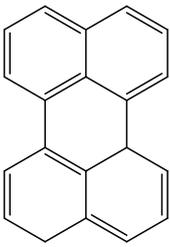
Perylene was added to the monomer mixture before sonication with the ultrasonic probe. The hydrophobic nature of the perylene molecule meant that it was able to associate with the hydrophobic monomers and subsequently remained in solution to form highly fluorescent microspheres as shown in the fluorescent image in Figure 39.
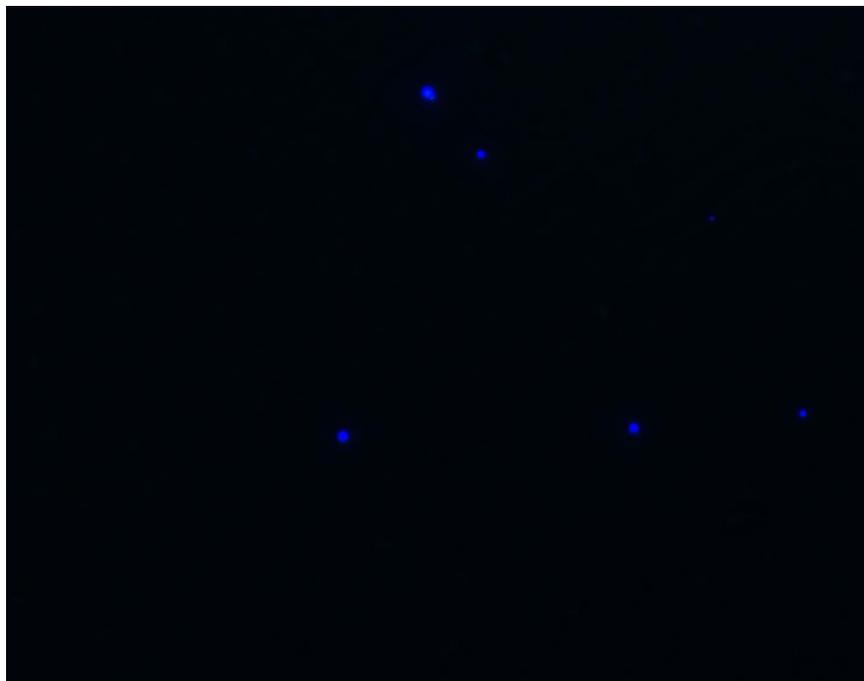
Figure 39: Fluorescent microscope image of crosslinked polystyrene microspheres (5.00 × 10^{-3} g mL^{-1}) labelled with perylene **29** suspended in distilled water by ultrasonication.

Large polymer microspheres **30** were also synthesised by employing a suspension polymerisation reaction. The monomers, styrene **3**, DVB **4** and 4-VBC **1** were combined with AIBN, shown in Scheme 17, to form the organic phase. This monomer mixture was then stirred vigorously in an aqueous solution of 1 wt % PVA solution[135].
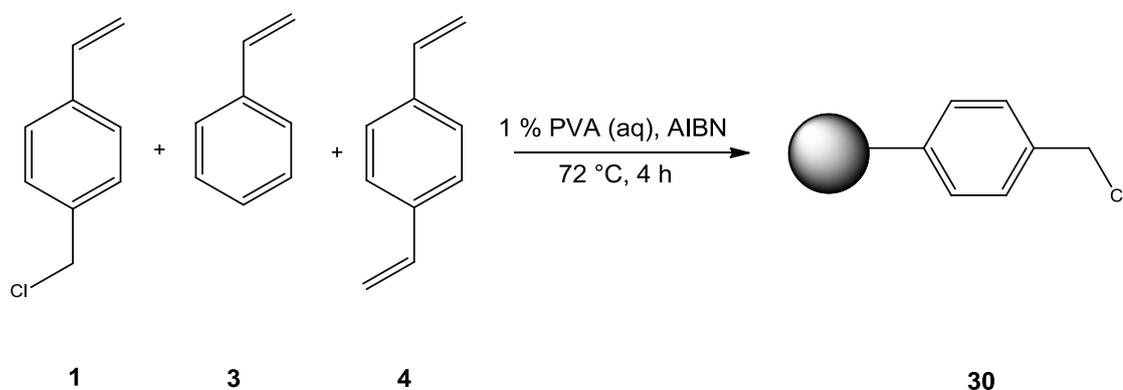
Scheme 17: Synthesis of large chloromethyl-functionalised polystyrene microspheres **30** *via* a suspension polymerisation reaction

The resultant microspheres **30** were washed with copious amounts of water to remove the excess PVA solution. The microspheres were also washed with methanol and THF to remove any un-reacted monomer or small polymer microspheres that may have fragmented in reaction vessel.

The final polymer product was then shaken on a shaker plate to separate out the microspheres into a range of diameters. The diameter required from this reaction was 0-38 µm and the yield of microspheres collected within this range was 3 %. It was deemed that microspheres with a diameter larger than 38 µm could potentially block the puncta (tear drainage duct positioned at the inner corner of the eye).

The microspheres were suspended in DMF and incubated with perylene as shown in Scheme 18 to yield microspheres which displayed a high level of fluorescence.
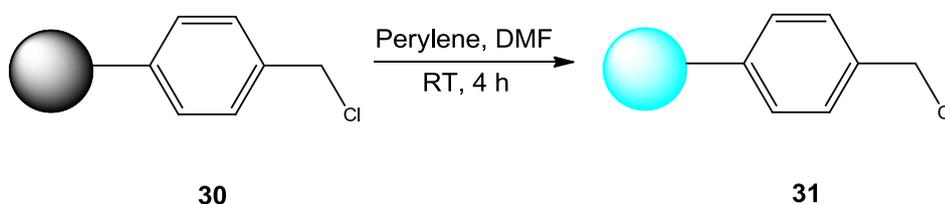
Scheme 18: Labelling of large chloromethyl-functionalised polystyrene microspheres **30** with perylene

Another dye, rose bengal was also used to label the microspheres. Rose bengal is a water-soluble, sodium salt which does not emit fluorescence and is seen under visible light. It is used as a stain; therefore a stringent labelling process was not required. The sodium salt was simply dissolved in water at 1 % w/v and an aliquot of this solution (30 µl) was added to the microspheres. The microspheres were then washed with water to remove any excess dye.

The range of fluorescent microspheres synthesised for this study is shown in Table 14.

Table 14: Summary of fluorescent microspheres synthesised for tear film visualisation

Type of microsphere	Size / µm	Fluorescent dye used
Thiol-PS dispersion	1.0 ± 0.4	Texas Red maleimide
Thiol-PS dispersion	1.0 ± 0.4	PyMPO maleimide
Thiol-PS dispersion	1.0 ± 0.4	Fluorescein diacetate maleimide
PS emulsion	4.7 ± 1.2	Texas Red maleimide
Thiol-PS dispersion	0.7 ± 0.3	Texas Red maleimide
Thiol-PS dispersion	0.8 ± 0.4	Texas Red maleimide
Thiol-PS dispersion	2.0 ± 0.9	Texas Red maleimide
PS emulsion	1.5 ± 0.6	Perylene
PS emulsion	2.1 ± 1.1	Perylene
Thiol-PS dispersion	1.0 ± 0.4	Rose Bengal
Thiol-PS dispersion	0.7 ± 0.3	Rose Bengal
Thiol-carboxyl	1.5 ± 0.6	Rose Bengal
Thiol-carboxyl	1.5 ± 0.6	Perylene
Crosslinked polystyrene	0 - 38	Perylene

2.5.3.   Visualisation of tear film using fluorescent microspheres

Tear film visualisation using fluorescent microspheres was performed by Paramdeep Bilkhu and Professor James Wolffsohn in Vision Sciences, Aston University.

Initial tests were carried out with 1 µm thiol-functionalised microspheres **6** labelled with PyMPO, fluorescein and Texas Red (highlighted in red in Table 14). The fluorescent microspheres were applied to the tear film with a cotton bud and the spread of the microspheres across the tear film was observed using a digital slit lamp microscope. Findings were encouraging as it was possible to visualise the fluorescence of the microspheres against the white/red eye background and it was also possible to track the movement of individual microspheres along the tear meniscus towards the puncta using the microscope.

The study was then expanded to the different sized microspheres with the aim being to track the distribution of fluorescent microspheres based on the size difference between the lipid, aqueous and mucous layers.

The next set of microspheres tested is highlighted in green in Table 14. The behaviour of the large (4.7 µm) microspheres was observed under the slit lamp. The microspheres seemed to have a tendency to clump together and quickly settled along the lid margin. The smaller microspheres (<2 µm) appeared difficult to visualise as they moved quickly across the tear film.

The transference of microspheres to the tear film proved to be difficult as the cotton bud absorbed the PBS solution leaving the microspheres stuck to the cotton, and out of solution. Microspheres labelled with fluorescein were then applied to the eye with a fluoret, which is a sterile strip of paper impreganated with fluorescein[136], instead of a cotton bud. The fluoret was moistened with a sterile buffer and gently brushed against the tear film to stain it. The fluoret strip appeared to be a useful method to apply microspheres directly to eye whilst also reducing the loss of microspheres transferred with the cotton bud. However, background fluorescence in the eye due to the fluoret appeared to mask the fluorescence of the fluorescein-labelled microspheres making it difficult to distinguish the microspheres from the background. There was also a possibility that the fluorescein provided by the strip could destabilise the tear film which could lead to compromised results.

Further tests with the batch of microspheres in the green and red section of Table 14 were carried out and an attempt was made to standardise the application procedure. Due to difficulties in applying the microspheres to the tear film with a cotton bud and fluoret, a micropipette was used instead. A known volume of the suspension of microspheres (0.020 mL) was taken up by the micropipette and dropped into each eye. There was 5 minute gap between application of microspheres to each eye.

Of the five different sized microspheres labelled with Texas Red, the largest size was the easiest to visualise, however the large microspheres tended to clump together towards the inner canthus. They also settled along the tear meniscus. The small microspheres (<1 µm) were difficult to track and visualise and a few were found to settle along the tear meniscus. Images for these tests are shown in Figure 40 and Figure 41.
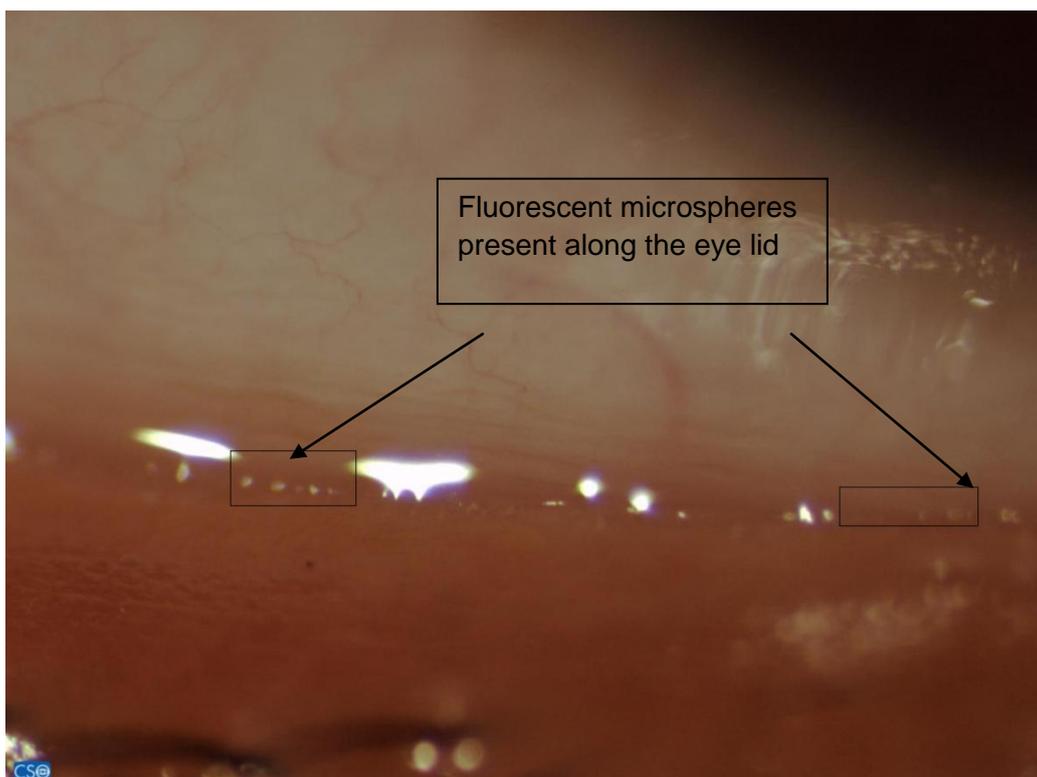
Figure 40: Fluorescent image of thiol-functionalised microspheres **6** (2.0 µm) labelled with Texas Red maleimide taken using a digital slit lamp
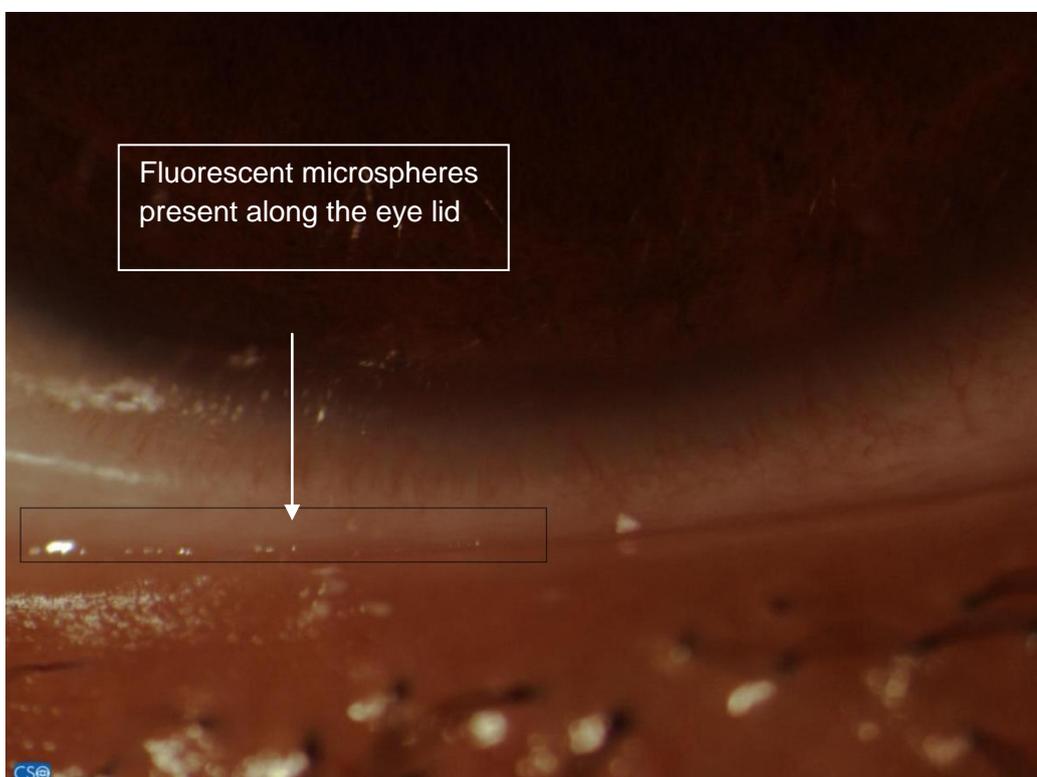
Figure 41: Fluorescent image of thiol-functionalised microspheres **6** (0.7 µm) labelled with Texas red maleimide taken using a digital slit lamp

The findings from these tests indicated that analysis of the behaviour of different sized microspheres in relation to the three layers of the tear film was difficult. This was due to the fact that the larger microspheres did not partition into the thicker aqueous and mucin layers as expected. Therefore, based on these findings, another angle that was investigated was the hydrophilic/hydrophobic nature of the tear film.

The tear film model suggests that the tear film is composed of a thin hydrophobic outer layer, a thick hydrophilic layer followed by another thin hydrophobic inner layer. Therefore, the polarity of the microspheres is another factor to consider in the investigation of the different components of the tear film. Rather than to use the size and weight of the microspheres alone, the polarity of the microspheres was altered to determine the layer in which the microspheres would settle within the tear film.

From the previous tests, it was found that larger microspheres were easier to visualise but individual microspheres were difficult to track due to clumping. Therefore, the next step was to synthesise larger fluorescent microspheres as they would be easier to track and visualise individually. This would also make it easier to differentiate the microspheres from air bubbles, debris and lipid present in the tear film. A lower magnification was also used as this allowed greater depth of focus and better identification of the location of the microsphere on the tear film.

A further improvement to the visualisation process was to reduce the aggregation of the microspheres to make it possible to track individual microspheres.

A batch of microspheres which fulfilled this purpose were the microspheres synthesised for compatibility with the hydrophilic maleimide-functionalised dyes, the thiol-core, carboxyl-shelled microspheres **10** described in section 2.5.1.1. These microspheres were found to be highly non-aggregated.

2.5.3.1   Non-aggregated fluorescent microspheres

Thiol-core, carboxyl-shelled microspheres **10** were non-aggregated due to their carboxyl shell. The incorporation of methacrylic acid **9** into the shell provided the important carboxyl groups which, when ionised, possess a negative charge. The carboxyl groups were present on the microsphere as indicated by loading data and elemental analysis data. This means that there was a sufficient amount of carboxyl groups to provide a strong negative charge to cause repulsion between the microspheres.

The non-aggregated nature of the microspheres was further confirmed with zeta potential data, from which the microspheres were found to possess a charge of −74.84 mV which is indicative of a highly dispersed system. The relevance of zeta potential data is summarised in section 2.4.1.2.

These non-aggregated microspheres were suspended in DMF and incubated individually with perylene and rose bengal overnight. The microspheres were successfully labelled and displayed a high level of fluorescence. These microspheres are highlighted in blue in Table 14 and were used in the visualisation of the tear film.

These microspheres did not aggregate as easily when in contact with the tear film; however they were difficult to track as they quickly moved towards the puncta. The next step was to visualise the tear film with the large microspheres synthesised by the suspension polymerisation reaction. Unfortunately, due to time constraints, this was not possible; however this should be carried out in future work.

2.5.4. Summary

The reaction of hydrophilic maleimide-functionalised fluorescent dyes with thiol-functionalised microspheres **6** synthesised by a dispersion polymerisation reaction and thiol-core, carboxyl-shelled microspheres **10** synthesised by a seeded emulsion polymerisation reaction which were modified for hydrophilic dye attachment did not yield fluorescent microspheres. Amino-functionalised microspheres **27** synthesised by a dispersion polymerisation reaction which were also modified for hydrophilic dye attachment did not yield fluorescent microspheres. Possible reasons for failure of the reaction include lack of association of the hydrophilic fluorescent dyes with the relatively hydrophobic thiol-functionalised microspheres **6**. Other reasons relate to the lack of penetration of the hydrophilic dyes through the core of thiol-core, carboxyl-shelled microspheres **10**.

Fluorescent microspheres were obtained from reaction of the hydrophobic maleimide-functionalised fluorescent dyes with thiol-functionalised microspheres **6** synthesised by a dispersion polymerisation reaction. These microspheres were used for visualisation of the tear film along with polymer microspheres synthesised from an emulsion polymerisation reaction, which were labelled with perylene to yield highly fluorescent microspheres. Core-shell microspheres synthesised by a seeded emulsion

polymerisation reaction were also used for their non-aggregated nature in the visualisation of the tear film.

The results from the tear film visualisation study indicated that fluorescent microspheres were useful in tracking the movement of fluid along the tear meniscus. It was observed that smaller microspheres were difficult to track on the tear film as they moved quickly along the tear meniscus and towards the puncta. Non-aggregated, small microspheres also travelled quickly along the tear meniscus and were problematical to track. Larger microspheres were easier to track as they moved more slowly and were easier to detect. Overall, the use of fluorescent microspheres seemed particularly useful in tracking the flow of tears along the tear meniscus.

2.5.5. Future work on visualisation of tear film using large fluorescent microspheres

Unfortunately, the large microspheres (highlighted in orange in Table 14) synthesised by a suspension polymerisation reaction, labelled with perylene, were not tested for tear film visualisation due to time constraints. However, future work should include the use of these large microspheres as results from tear film visualisation studies conducted in this project appear to indicate that large microspheres are easier to track and visualise on the tear film.

However, a factor to consider is that the microspheres leave the ocular surface *via* the puncta and pass through the drainage canal which is 300-500 μm wide[137]. The microspheres synthesised were 0-38 μm and it is unlikely that the passage of microspheres through the puncta would block the drainage canal. However, temporary punctual plugs could be used as a precaution to prevent the passage of microspheres through the puncta. The microspheres could also be sterilised with UV light to remove the presence of any bacterium which could be harmful to the eye.

In previous studies involving the use of large microspheres to visualise the tear film, no side effects have been reported and punctal plugs were not used. Saline was used to wash out any remaining microspheres and irrigate the eye, and one particular study received ethical approval from St George's Hospital, UK.

A suggestion of another possible application was to track the flow rate of tears along the menisci as it was observed that fluorescent microspheres would be useful to track the spread and distribution of tears across the tear film, which could be different

between normal and dry eye subjects. It has also been proposed that the microspheres could be used to observe tear flow behind a contact lens.

2.6. Interaction of titanium dioxide with polymeric materials

Another potential application of polymeric materials was based on their interaction with another nanoparticle, titanium dioxide (TiO_2).

Useful properties of TiO_2 include non-toxicity, photochemical stability, high specific surface area and a high refractive index[138]. TiO_2 nanoparticles are commonly used as pigment in paint and as a component in sunscreen. The role of TiO_2 in sunscreen is to absorb and reflect the harmful UVA (320–400 nm) and UVB (290–320 nm) rays from the sun[139]. A potential use is the possibility for TiO_2 nanoparticles to become an alternative to silicon which is currently used in photovoltaic cells.

Work discussed in previous sections of this chapter has shown that polymer microspheres containing thiol groups have been successfully used to immobilise QDs and maleimide-functionalised fluorescent dyes. To expand the scope of nanoparticle interaction with polymeric materials, TiO_2 nanoparticles were assessed for their binding capability to functionalised polymeric materials.

The polymeric material utilised in this section of the study was crosslinked thiol-functionalised polymethyl methacrylate. Once this polymer was synthesised, interaction between TiO_2 and thiol groups was assessed.

2.6.1. Interaction of titanium dioxide with bulk thiol-functionalised polymer

A polymer with a high loading of thiol groups was deemed preferable as this could mean a greater chance of interaction with TiO_2 nanoparticles.

Thiouronium-functionalised polystyrene **32** was synthesised *via* a bulk polymerisation reaction with monomers, styrene **3**, DVB **4** and 4-VBTU **2** which were combined with a free-radical initiator, AIBN, as shown in general Scheme 19, Table 15. Only a low level of 4-VBTU **2**, a ~2 % molar ratio relative to styrene **3**, was capable of dissolving into the monomer mixture. This reaction mixture was thermally initiated to yield a glassy polymer with a cloudy appearance.
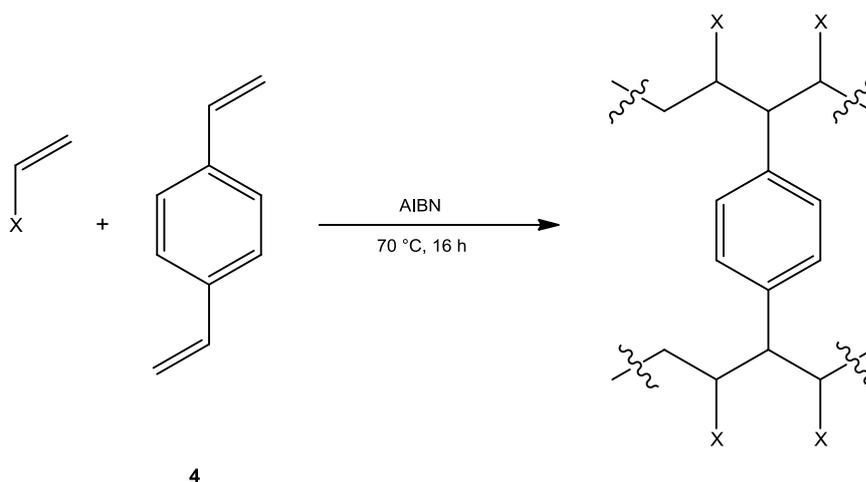
Scheme 19: Synthesis of crosslinked polymer by bulk polymerisation

Table 15: Monomer composition of polymers formed by bulk polymerisation

	Functional monomer / mol %			
Polymer	MMA **33**	Styrene **3**	4-VBTU **2**	DVB **4**
32	-	96	2	2
34	93	-	5	2

Methodology for the synthesis of polymers listed in Table 15 can be found in section 4.8.1.

Preparation of thiouronium-functionalised polystyrene **32** proved difficult as a high level of 4-VBTU **2** would not dissolve in styrene **3**. This may have been because 4-VBTU **2** is a charged ionic compound which would not have been easily solvated by styrene **3** as styrene **3** is hydrophobic and is likely to repel the charged monomer.

For this reason, another monomer was utilised for this study. Methyl methacrylate (MMA) **33** is a polar molecule and was able to dissolve a relatively higher level of 4-VBTU **2**. Therefore, thiouronium-functionalised polymethyl methacrylate **34** would yield a higher level of thiol groups promoting enhanced interaction with TiO_2 nanoparticles.

2.6.1.1   Investigation of the effect of porogens on the synthesis of polymers
           suitable for TiO_2 interaction

A high surface area of the polymer may increase interaction between the putative ligand groups (thiol moieties) and TiO_2 nanoparticles. Therefore, the use of a porogen was employed in this study to effectively create gaps within the structure of the polymer, increasing its surface area.

Porogens are small, organic molecules which can be used in polymerisations to increase the surface area of the polymer. The region of space occupied by a porogen is an area in which polymerisation does not takes place. Therefore, when the polymer is formed, there are voids present in the polymer where the porogen was situated during the polymerisation reaction.

A suspension of the monomers, MMA **33**, DVB **4** and 4-VBTU **2**, was added to a range of porogens in a 1:1 molar ratio, listed in Table 16, along with AIBN for the purpose of polymerisation.

Table 16: Porogens assessed for their effect on the successful synthesis of thiouronium-functionalised polymethyl methacrylate

Porogen	Polymer
THF	Failed reaction
Methanol	**36**
DMF	**37**
Acetonitrile	Failed reaction
Toluene	Failed reaction

The polymerisation reactions were carried out with each of the five porogens listed in Table 16, however only two reactions successfully gave rise to polymeric products. Reactions with methanol and DMF, described in section 4.8.3, yielded polymer **36** and **37**. The other porogens seemed to have a negative effect on the polymerisation process as polymer was not obtained.

The polymers that formed successfully were glassy and crystalline and were broken down into smaller pieces using a coffee grinder. These small pieces were subsequently milled using a planetary mill for 12 hours and this is further described in section 4.8.4. The purpose of milling was to reduce the size of the pieces of polymer, which would mean that the surface area of the material was further increased.

After milling, the polymer synthesised with methanol as a porogen yielded a fine crystalline powder, shown in image A in Figure 42, however the polymer synthesised with DMF appeared to have coagulated after milling and produced a sticky agglomeration shown in image B in Figure 42.
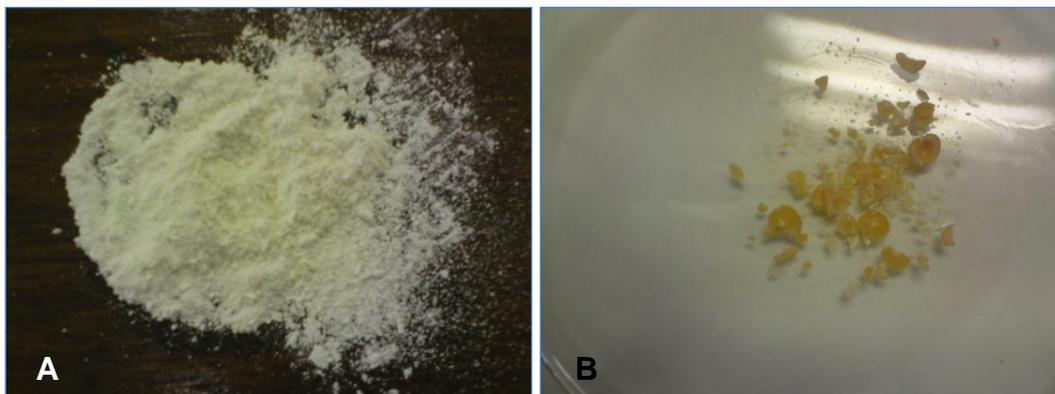
Figure 42: A - Thiouronium-functionalised polymethyl methacrylate with methanol as a porogen **36** after milling at 400 rpm for 12 hours.
B - Thiouronium-functionalised polymethyl methacrylate with DMF as a porogen **37** after milling at 400 rpm for 12 hours.

Based on this finding, only methanol was used a porogen in subsequent work as it yielded a fine polymer powder which would be easier to assess in TiO_2 interaction assays.

A sample of porogenic polymethyl methacrylate without 4-VBTU **35** was also prepared by bulk polymerisation. Preparation of this polymer is detailed in section 4.8.2. This sample was milled with the same milling conditions described in 4.8.4 and served as a control in this study.

Milled porogenic thiouronium-functionalised polymethyl methacrylate **36** was then converted to its thiol form by deprotection with a base, TMAOH, to form milled porogenic thiol-functionalised polymethyl methacrylate **38**. This reaction is described in section 4.8.4.

2.6.1.2 Investigation of the suspension of milled porogenic thiol-functionalised polymethyl methacrylate **38** and TiO$_2$ nanoparticles in solvent

Before interaction between milled porogenic thiol-functionalised polymethyl methacrylate **38** and TiO$_2$ nanoparticles could be tested, another factor investigated was the identification of a solvent in which both TiO$_2$ and the thiol-containing polymer could be suspended in. This was essential to ensure ease of mixing and interaction of the two. A range of solvents of different polarities, listed in Table 17, were tested for their ability to suspend TiO$_2$ nanoparticles.

Table 17: Solvents assessed for suspension of TiO$_2$ nanoparticles

Solvent	Suspension with ultrasonic probe	Successfully centrifuged
DCM	No	Yes
DMF	Yes	Yes
THF	Yes	No
Ethanol	Yes	No
Methanol	Yes	No
Water	Yes	No

TiO$_2$ nanoparticles were suspended in the solvent by sonication with an ultrasonic probe. The purpose of the probe was to help disperse the nanoparticles more evenly in the solvent. This enabled better observation of the solvent most appropriate for the suspension of TiO$_2$ nanoparticles.

Each solvent apart from DCM appeared to successfully suspend TiO$_2$, with the aid of the ultrasonic probe. To determine how effectively TiO$_2$ had been suspended, each sample was centrifuged. If the TiO$_2$ nanoparticles were not compatible with the solvent, the nanoparticles would separate out after centrifugation and collect at the bottom of the centrifuge tube. Should the particles have been fully suspended in the solvent then it would not easily separate by centrifugation. The suspension of TiO$_2$ in THF, ethanol, methanol and water were all difficult to successfully separate by centrifugation and the suspension retained a cloudy appearance which indicated that the nanoparticles had been fully suspended by the solvent. TiO$_2$ and DMF proved to be incompatible, as when centrifuged, the nanoparticles separated from the solvent and a pellet of TiO$_2$ was collected at the bottom of the centrifuge tube.

A similar study was carried out with milled porogenic thiol-functionalised polymethyl methacrylate **38**, the results for which are shown in Table 18. The polymer suspension

was also sonicated with the ultrasonic probe to ensure even distribution and aid suspension.

DCM, DMF, THF, methanol, ethanol and water appeared to have all successfully suspended the polymer with the aid of the ultrasonic probe and to further test this assumption, the samples were centrifuged.

Table 18: Solvents assessed for suspension of milled porogenic thiol-functionalised polymethyl methacrylate **38**

Solvent	Suspension with ultrasonic probe	Successfully centrifuged
DCM	Yes	Yes
DMF	Yes	No
THF	Yes	No
Methanol	Yes	No
Ethanol	Yes	No
Water	Yes	No

Polymer suspended in DCM was the only sample to be separated by centrifugation and a pellet of the polymer was collected at the bottom of the centrifuge tube. The centrifugation results indicated that the polymer was fully suspended in the other solvents.

Therefore, viable solvents for suspension of milled porogenic thiol-functionalised polymethyl methacrylate **38** and TiO_2 were THF, methanol, ethanol and water as they were good solvents for both binding parties.

2.6.1.3   Interaction of titanium dioxide with thiol-functionalised polymethyl methacrylate

TiO_2 nanoparticles were sonicated with one of the viable solvents, methanol, as was milled porogenic thiol-functionalised polymethyl methacrylate **38**. The two suspensions were then combined to allow interaction between the nanoparticles and the polymer to take place. The resulting mixture was centrifuged to test the association if any, between the polymer and nanoparticle. Details of the protocol for this study can be found in section 4.8.5. The mixture did not appear to have separated after centrifugation. This indicated that there was some interaction between the thiol groups and TiO_2, which was strong enough to withstand separation by centrifugation.

Milled porogenic polymethyl methacrylate **35** without any thiol groups present was used as a control to assess for interaction with TiO$_2$ nanoparticles. Milled porogenic polymethyl methacrylate **35** was also suspended in methanol by sonication with the ultrasonic probe and added to TiO$_2$ nanoparticles which had also been suspended in methanol with the aid of the ultrasonic probe. The resultant mixture was then centrifuged. This was found to yield a clear supernatant with a solid pellet of milled porogenic polymethyl methacrylate **35** and TiO$_2$ nanoparticles collected at the bottom of the centrifuge tube. The result of both the control and the thiol-functionalised polymer after centrifugation is shown in Figure 43.
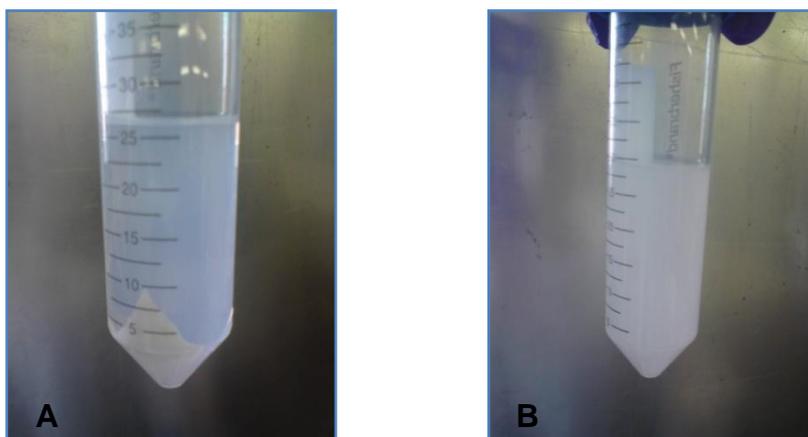
Figure 43: A - Milled porogenic polymethyl methacrylate **35** and TiO$_2$ both suspended in methanol by sonication with an ultrasonic probe, after centrifugation (6000 rpm, 10 minutes)

B - Milled porogenic thiol-functionalised polymethyl methacrylate **38** and TiO$_2$ both suspended in methanol by sonication with an ultrasonic probe, after centrifugation (6000 rpm, 10 minutes)

2.6.2. Summary

Results from these experiments suggest that it is possible that the presence of the thiol groups in milled porogenic thiol-functionalised polymethyl methacrylate **38** promoted the attachment of TiO$_2$ nanoparticles. Further indication of the importance of thiol groups in the interaction of TiO$_2$ was the control experiment, in which thiol groups were not present in milled porogenic polymethyl methacrylate **35**. The control polymer was found to display no interaction with TiO$_2$ after centrifugation and separated from the solvent, collecting at the bottom of the centrifuge tube.

This study gave promising results indicating likely interaction between thiol groups and TiO$_2$ nanoparticles. It was now desirous to look at thin polymer films to observe whether they could similarly interact with TiO$_2$ nanoparticles.

2.6.3. Investigation of interaction of TiO$_2$ with spin coated thiouronium-functionalised polystyrene

To further investigate the interaction between TiO$_2$ and functional groups, a similar thiol-containing polymer to that used in section 2.6.1.2 was synthesised. This polymer was then spin coated to assess a different morphology of polymer in relation to TiO$_2$ nanoparticle interaction. A planar polymer morphology was desirable for the assessment of interactions that may have utility in devices such as organic solar cells.

Thiouronium-functionalised polystyrene was synthesised by bulk polymerisation in which 4-VBTU **2** and AIBN were dissolved in styrene **3**. As the polymer had to be prepared for spin-coating applications, which involves dissolving the polymer in an appropriate solvent in order to form a thin film layer, DVB **4** was omitted from the polymerisation as the presence of the cross-linking agent would render dissolution of the polymer impossible.

Four types of polymer were prepared in this way and the method is described in more detail in section 4.8.6. The molar compositions for these polymers are shown in Table 19.

Table 19: Monomer composition of polymer **39-42**

Polymer	Styrene **3** / mol %	4-VBTU **2** / mol %
39	99.8	0.2
40	97	3
41	93	7
42	100	0

Thiouronium-functionalised polymer was not converted into its thiol form as it would be difficult to remove the base from the polymer once the subsequent deprotection reaction had taken place. It was also desirable to establish if the thiouronium moiety itself could act as a ligand for TiO$_2$ nanoparticle interaction.

The hard, glassy polymer yielded from these reactions was subsequently dissolved in THF by ultrasonication in a 0.1 % w/v solution. THF was selected as it is volatile and would readily evaporate to leave a thin layer of polymer suitable for spin coating.

The principle of spin-coating involves the deposition of a thin, uniform film of liquid onto a substrate which moves in a circular motion. Excess fluid is added to ensure

that the total area of the substrate is covered without any defects. Once the substrate has been completely coated, the excess fluid is removed by centrifugal forces. These forces also contribute to the even distribution of the liquid[140, 141].

The dissolved polymers were spin-coated onto a square glass substrate which was 2 mm thick and 5 cm in length and width. An initial trial was carried out at 500 rpm for 6 seconds, but the polymer film obtained was very thick and had an uneven distribution, particularly at the centre of the substrate.

As theory dictates that the lower the spinning time and speed, the thicker the layer of film deposited on the substrate[140], the coating was repeated with an increase in both of these parameters. The speed was increased to 1500 rpm and the substrate was spun for 9 seconds. The volume of polymer coated onto the substrate was 0.4 mL, which was the same as the initial trial. These conditions were found to be optimum in producing a thin film with an even surface.

However, once coated, it was difficult to remove the polymer film from the substrate without damaging the film. The only option was to scrape the film off the substrate but this reduced the film to small pieces, ruling out this option. As it was important for the assay to be carried out on a thin film, it was decided to use the polymer film whilst still coated to the glass substrate.

The thickness of the polymer was measured using a Talystep to ensure reproducibility of the polymer film. The results in Table 20 show that the polymer films were largely reproducible as the thicknesses differed by <1 µm.

Table 20: Thickness of spin-coated polymer films, measured using a Talystep

Polymer used for spin coating	Thickness (µm)
39	5.2
40	4.0
41	4.0
42	4.8
Average	4.5

Interaction of the polymer films with TiO_2 nanoparticles was facilitated by dipping the polymer film into a suspension of TiO_2 nanoparticles. This was a facile way of ensuring that the whole area of the polymer film was in contact with TiO_2 and had sufficient time for interaction.

In this study, the polymer was non-crosslinked and so a solvent that could suspend the TiO_2 nanoparticles but did not dissolve the polymer was required. The obvious choice was ethanol as it produced a cloudy suspension which would be easier to visualise on the polymer film compared with other solvents which gave rise to a less cloudy suspension. TiO_2 nanoparticles in ethanol was prepared in 3×10^{-3} % w/v suspension.

The polymer films were dipped into the ethanolic suspension of TiO_2 nanoparticles for 30 seconds, then removed to dry for 2 minutes. The films were then washed with ethanol to remove any excess TiO_2.

Methodology for this spin-coating assay is described in further detail in section 4.8.7.

2.6.3.1 Analysis of the interaction of TiO_2 with polymer films by FTIR analysis

To assess the interaction of TiO_2 nanoparticles with polymer films, Fourier Transform Infrared Spectroscopy (FTIR) was considered as a means of determining the presence of TiO_2 on the polymer. However, it was difficult to transfer the polymer film to a sodium chloride plate or peel off the film and incorporate it into a KBr disc. Therefore, to avoid this problem, the film was spun directly onto a sodium chloride plate instead of the glass substrate.

The spin-coating procedure was repeated, but this time the polymer film was dipped into a 1 % w/v TiO_2 ethanolic suspension. The concentration of the TiO_2 suspension was increased to enhance the possibility of interaction with the thiouronium groups and to boost the chances of visualisation of bound TiO_2 by FTIR spectroscopy.

After spin-coating, the polymer film was left to dry for 30 minutes to ensure that there was not any THF present, the film was then analysed by FTIR spectroscopy. The film was then dipped into a suspension of TiO_2 nanoparticles. The sodium chloride plate was dried in an oven at 110 °C for 30 minutes to remove any ethanol which may have been present. The polymer film was re-analysed by FTIR spectroscopy.

FTIR analysis showed that peaks due to the presence of the thiouronium moiety in the polymer did not seem to be visible in the spectrum obtained for polymer **39**. The peaks for the amine groups present in thiouronium should appear between 3300-3500 cm^{-1} and the carbon-sulfur bond in thiouronium should be present between 600-700 cm^{-1}. The absence of both these peaks could be due to the small quantity of thiouronium present in polymer **39**.

A similar spectrum was observed for polymer **40**. The absence of peaks attributed to the thiouronium moiety also indicated that the level of 4-VBTU **2** was not high enough to be analysed with FTIR.

Polymer **41** possessed a peak attributed to the N-H bond, normally found between 1560-1640 cm^{-1}, which appeared at 1649 cm^{-1} on the spectrum. Another peak at 666 cm^{-1} was also present, which may have been an indication of the presence of thiouronium.

Unfortunately, due to the cloudy nature of the KBR disc, only a poor quality spectrum was obtained for TiO_2 nanoparticles as it would not grind easily into a powder.

The control sample, polymer **42**, was analysed by FTIR spectroscopy before and after dipping in the TiO_2 suspension. There were no peaks after dipping that could be attributed to the presence of TiO_2. The spectra before and after largely remained the same.

The spectra for polymer **39** also did not show much difference before and after exposure to the suspension of TiO_2 nanoparticles. It is quite possible that the level of thiouronium was not high enough to successfully immobilise TiO_2 nanoparticles.

The spectra for polymer **40** did not show a marked difference before and after dipping in the suspension of TiO_2 nanoparticles.

The spectra obtained for polymer **41** was similar to the rest, with no noticeable difference in data. A slight increase in intensity for the peak assigned to the N-H stretch could have been due to higher thiouronium levels in the particular part of the sample analysed.

As such, no real conclusions could be drawn from the analysis of the films by FTIR spectroscopy. Specifically, there was difficultly in firmly assigning a peak due to the presence of TiO_2 in any of the films post dipping. There was some evidence to suggest that the thiouronium group was present in the polymer, but again it was difficult to assign all the peaks which relate to the structure of the thiouronium group. Both of these issues could due to the level of thiouronium moieties and TiO_2 nanoparticles not being high enough to register in the FTIR spectra. Therefore, other assays for the interaction of TiO_2 with thiouronium-functionalised polystyrene were explored.

2.6.3.2   Observation of polymer films after association with TiO_2 to assess for interaction

Further interaction assays were based on observation of the polymer films before and after dipping in the suspension of TiO_2 nanoparticles.

A spin-coated film prepared from polymer **42** was observed and a photograph of the polymer film was taken before and after dipping in the TiO_2 suspension, the images for which are shown in Figure 44.
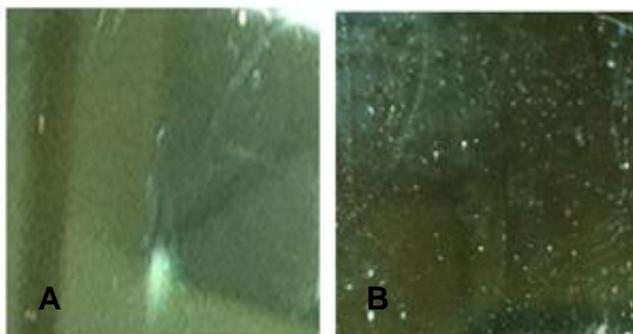
Figure 44: A - Spin-coated film of polymer **42** before dipping in an ethanolic
suspension of TiO_2
B - Spin-coated film of polymer **42** after dipping in an ethanolic
suspension of TiO_2 for 30 seconds

The polymer film made from polymer **42** did not appear significantly different after it had been dipped in the TiO_2 suspension. Before dipping, the film was clear and after dipping, it remained largely clear excluding a few white specks. This was expected for this particular film as there were no thiouronium groups present in the polymer and thus it had no ligands present to interact with the TiO_2 nanoparticles.

The spin-coated film prepared from polymer **39** was also observed, the images for which are shown in Figure 45. The film before dipping was clear, but after dipping in the TiO_2 suspension, the film appeared slightly cloudier and a white substance could be observed on the film. This result suggested that the presence of the thiouronium functionality within the film may have aided interaction with TiO_2 nanoparticles.
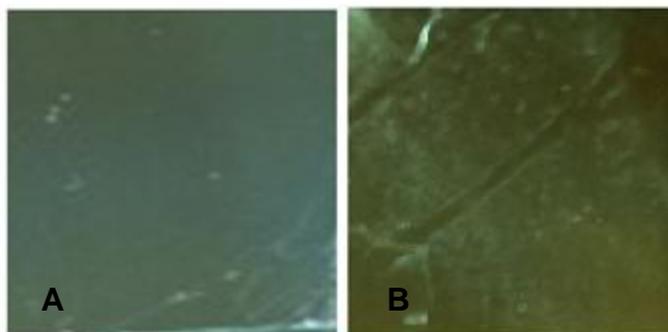
Figure 45: A - Spin-coated film of polymer **39** before dipping in an ethanolic suspension of TiO_2

B - Spin-coated film of polymer **39** after dipping in an ethanolic suspension of TiO_2 for 30 seconds

The spin-coated film prepared from polymer **40** appeared clear before dipping and was found to be very cloudy with the appearance of a white substance deposited over the surface of the film after dipping, as shown in Figure 46. The ethanolic suspension of TiO_2 nanoparticles was white and the white colouring of the film post dipping indicated that elements of this suspension were present on the film. The film had been washed with ethanol after dipping (as were the films made from the other polymers) to ensure that any excess TiO_2 was removed from the film. The difference between the two films before and after dipping in the TiO_2 suspension was more evident than for the film prepared from polymer **39**. The appearance of the film for polymer **40** after dipping indicated a marked interaction of the polymer with TiO_2 nanoparticles.
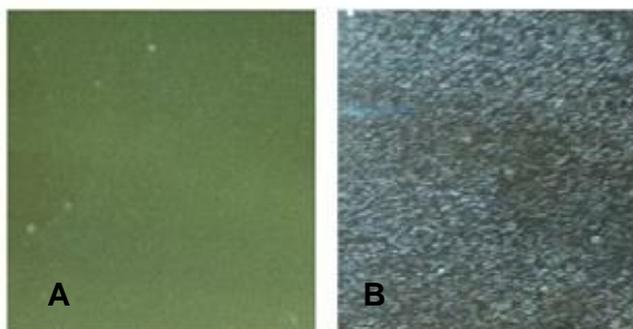
Figure 46: A - Spin-coated film of polymer **40** before dipping in an ethanolic suspension of TiO_2

B - Spin-coated film of polymer **40** after dipping in an ethanolic suspension of TiO_2 for 30 seconds

The spin-coated film prepared from polymer **41** was also clear before dipping and was cloudy after dipping in the suspension of TiO_2 nanoparticles, the images for which are shown in Figure 47. The film appeared to have interacted with TiO_2 nanoparticles as there was a white substance deposited on the film which correlated to white, cloudy appearance of the TiO_2 suspension. This was further evidence to suggest that the thiouronium groups played a significant role in the immobilisation of TiO_2 nanoparticles. As the level of thiouronium was significantly increased, it appeared that interaction with TiO_2 nanoparticles also increased.
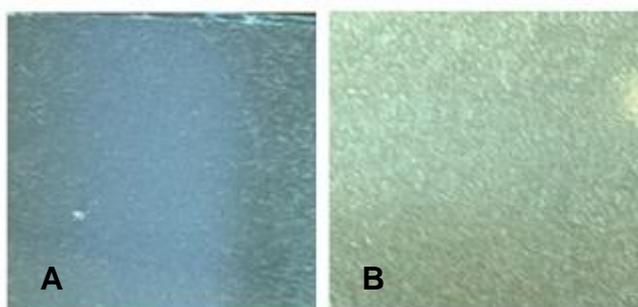
Figure 47: A - Spin-coated film of polymer **41** before dipping in an ethanolic
suspension of TiO_2
B - Spin-coated film of polymer **41** after dipping in an ethanolic suspension
of TiO_2 for 30 seconds

The polymer films made from polymer **40** and **41** did not look significantly different from each other after dipping in the TiO_2 suspension, indicating that the optimum level of thiouronium needed to immobilise TiO_2 may have been reached.

This observation assay seemed to indicate that the level of thiouronium present was relative to the level of interaction of TiO_2 nanoparticles. This is further evidence, albeit assessed non-qualitatively by eye, to suggest that thiouronium groups act as ligands for the attachment of TiO_2 nanoparticles.

2.6.3.3   Use of XPS to assess the interaction of TiO_2 with thiouronium-functionalised polystyrene

Another method for characterising the interaction of polymer films with TiO_2 nanoparticles was X-ray Photoelectron Spectroscopy (XPS). XPS is a technique used for the analysis of elements and chemical bonds by examination of the surface of the sample[141]. Sample preparation and XPS analysis conditions are detailed in section 4.2.1.

The two polymer films analysed by XPS were prepared in the same manner as described in section 2.6.3, however the dipping time for one film was 2 minutes and the dipping time for the other was 5 seconds. The XPS data is displayed in Table 21 and Table 22.

Table 21: XPS analysis of spin-coated film prepared from polymer **41**, dipped in an ethanolic suspension of TiO_2 nanoparticles for 2 minutes

Element	Peak Binding Energy (eV)	Atomic %
C (1s)	285.0	76.1
Ca (2p)	348.0	0.5
Cl (2p)	198.2	3.0
Mg (1s)	1305.3	0.1
N (1s)	400.5	4.8
Na (1s)	1072.0	0.3
O (1s)	532.4	9.8
S (2p)	164.6	3.5
Si (2p)	102.1	1.7
Ti $(2p^3)$	459.2	0.2

Table 22: XPS analysis of spin-coated film prepared from polymer **41**, dipped in an ethanolic suspension of TiO_2 nanoparticles for 5 seconds

Element	Peak Binding Energy (eV)	Atomic %
C (1s)	285.0	70.1
Ca (2p)	348.0	0.3
Cl (2p)	198.2	4.3
Mg (1s)	1305.2	0.2
N (1s)	400.5	6.1
Na (1s)	1072.0	0.4
O (1s)	532.4	12.1
S (2p)	164.5	4.7
Si (2p)	102.0	1.9
Ti $(2p^3)$	459.1	0.04

XPS data for the polymer film dipped for 2 minutes indicated that the percentage of titanium present in the film was 0.2 %. This is significantly higher than the figure obtained for the film that had been dipped for 5 seconds, which was 0.04 %. The high

percentage of nitrogen present in both films was most likely to be due to the presence of the thiouronium groups within the polymer. The level of carbon present in both samples was due the presence of carbon in polystyrene. Calcium, chlorine, magnesium, sodium and silicon were also detected and this was deemed likely to arise from the glass substrate onto which the film was coated.

This quantitative data provides compelling evidence to further indicate that TiO_2 nanoparticles were present on the polymer film post dipping. This also suggests that the longer the polymer film is dipped in the TiO_2 suspension, the higher the level of attachment of TiO_2 nanoparticles.

2.6.4. Summary

Observations of the polymer films before and after dipping in the suspension of TiO_2 nanoparticles indicated that TiO_2 was absorbed onto the surface of the polymer. This was particularly evident when the level of thiouronium in the polymer was increased from 0.2 mol % to 3 mol % relative to styrene **3**.

FTIR analysis was not useful for characterisation of the presence of TiO_2 nanoparticles on polymer films, however, there appeared to be some data to indicate the presence of thiouronium groups when the level of 4-VBTU **2** was increased. Attempts were made to record an FTIR spectrum for TiO_2 nanoparticles used in this study but it was not easily incorporated into a KBr disc as it was difficult to grind into a fine powder and the subsequent disc was cloudy.

XPS was the only form of characterisation which gave a qualitative indication that TiO_2 was present on the spin-coated film prepared from polymer **41**.

Given the results obtained from the analysis of the polymer films post dipping, especially the XPS data, it is reasonable to assume that the presence of thiouronium groups within the polymer films facilitate the attachment of TiO_2 nanoparticles.

2.6.5. Interaction of titanium dioxide with a catechol

Work described in the earlier sections was based on the interaction between TiO_2 nanoparticles and thiouronium and thiol groups. Another avenue investigated was the possible interaction of TiO_2 nanoparticles with hydroxyl groups, which has been discussed in literature[142-145]. This study involved the development of a suitable hydroxyl-containing compound for the attachment to TiO_2.

A means of controlling the distribution of TiO_2 nanoparticles by attachment to a hydroxyl-functionalised polymer would be a useful approach to controlling the position of TiO_2 within a solar cell. The polymer could be used to control the position of TiO_2 at specific layers within a cell. The amount of TiO_2-binding polymer within the cell could also be controlled meaning that the level of nanoparticles within the cell and indeed their distribution throughout the cell could be regulated.

The synthesis of a hydroxyl-containing polymer that can successfully interact with and immobilise TiO_2 nanoparticles would be another step towards investigation of the interaction of TiO_2 with polymeric materials.

A catechol was selected as a structure capable of interaction with TiO_2 as it possesses two hydroxyl groups which have been noted for their interaction with TiO_2 nanoparticles. There is evidence in literature to suggest that interaction between TiO_2 and catechols does occur[144, 145]. TiO_2 is thought to form stable chelates with catechols and the adsorption of TiO_2 onto a catechol has been reported to yield a bright orange colour[145-148].

As the aim was to polymerise the structure, 4-vinyl catechol **43** was used. Once the 4-vinyl catechol **43** units have been polymerised, this should leave a chain of TiO_2 running through the centre of the polymer. The two hydroxyl groups at positions 3 and 4 would act as a ligand binding site to which TiO_2 could covalently attach, to form a coordination complex **44** as shown in Scheme 20.
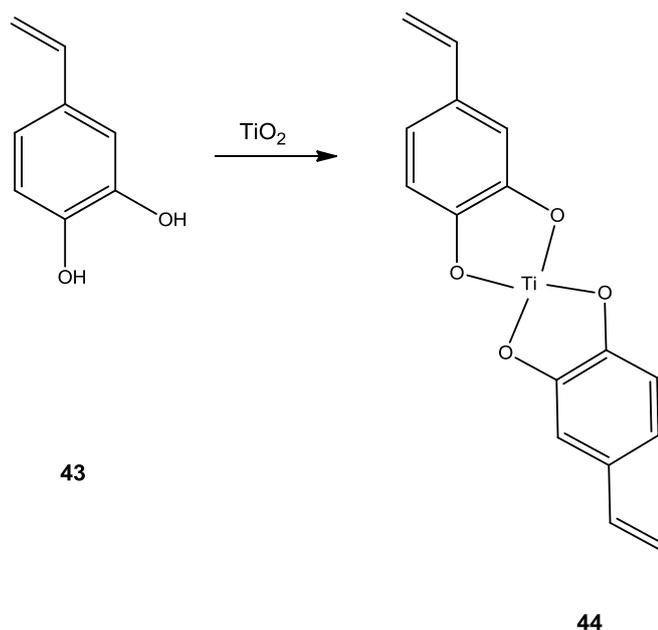
Scheme 20: Use of 4-vinyl catechol **43** as a ligand binding site to form a coordination complex **44** with TiO$_2$

Catechols are commonly used as polymerisation inhibitors[149], so the one of the benefits of binding of TiO$_2$ to the hydroxyl groups is that the molecule would no longer be a catechol structure and will not inhibit free-radical mediated polymerisation of itself or indeed other monomers.

2.6.5.1   Synthesis of 4-vinyl catechol **43**

The starting material, 3,4-dihydroxybenzaldehyde **45**, was reacted with malonic acid **46** in the presence of a weak base, piperidine, which is represented in Scheme 21, with a view to synthesising 4-vinyl catechol **43**[150].
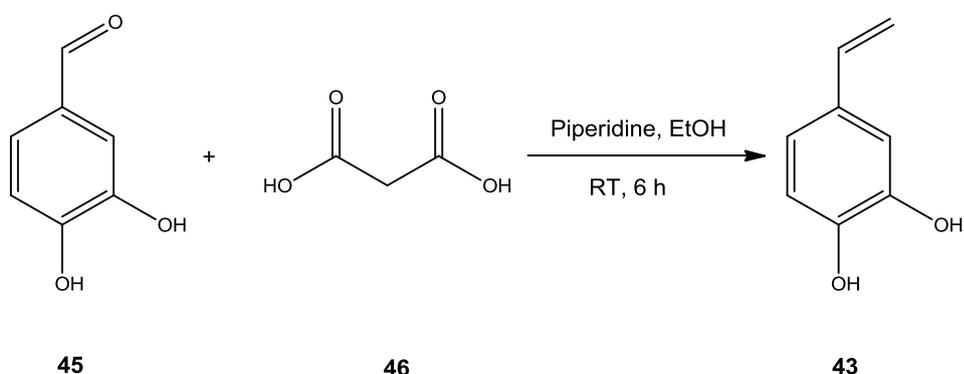
Scheme 21: Synthesis of 4-vinyl catechol **45** from 3,4-dihydroxybenzaldehyde **43**

The crude product obtained from the reaction was purified to yield a dark brown oil in a yield of 30 %.

^{1}H NMR analysis of the purified product indicated the presence of the aldehydic proton which had a chemical shift of ∂ 9.638 ppm. There was also an indication of the vinylic protons which were represented by two doublets at ∂ 5.473 ppm and ∂ 6.133 ppm. The peak heights for the vinyl protons were very low; indicating the yield of the product was low. There were many unaccounted peaks between 1-4 ppm which suggested that the product was impure.

A multiplet unrelated to the structure of the product, found at ∂ 3.267 ppm, was likely to be malonic acid **46** as it was shown to have a chemical shift around this area (ca. ∂ 3.2 ppm) when analysed by ^{1}H NMR as a starting material. There are a few peaks in the aromatic region of the spectrum which also remain unaccounted for and could be due to un-reacted 3,4-dihydroxybenzalehyde.

Overall, this data suggests that the reaction may have proceeded partially, resulting in an impure product.

To try and improve product formation, the reaction was repeated with a different base, tetramethylethylenediamine (TMEDA) and left to react overnight. The product was purified to furnish a dark brown oil with a yield of 11 %.

Analysis of the product by ^{1}H NMR showed the possible presence of a vinylic proton at ∂ 6.137 ppm, however the aldehydic proton was also present which suggested that the reaction may not have gone to completion. There were many peaks throughout the spectrum which could not be related to the structure of the expected product. This was an indication of the presence of impurities which were not removed by column purification. At this point, a decision was made to abandon this approach.

It was thought that the two hydroxyl groups may have prevented the clean formation of 4-vinyl catechol **43**. Therefore, another synthetic route to 4-vinyl catechol **43** was explored, once again with the use of 3,4-dihydroxybenzaldehyde **45** as the starting material.

2.6.5.2 Synthesis of 3,4-bis(*tert*-butyldimethylsilyl-oxy)benzaldehyde **47**

The new synthetic route with 3,4-dihydroxybenzaldehyde **45** first required the protection of the hydroxyl groups to prevent them from undergoing side reactions. This reaction was carried out using a silyl-protecting reagent, *tert*-butyldimethylchlorosilane (TBDMS-Cl), in which the hydroxyl groups were protected by the formation of a silyl ether. TBDMS is one of the most stable silyl protecting groups, around 10^4 times more stable than tetramethylsilane (TMS)[151].

After this reaction, the next step envisaged involved the conversion of the carbonyl group present in 3,4-dihydroxybenzaldehyde **45** to a vinyl group. This conversion would allow polymerisation of the molecule.

The mechanism for TBDMS protection first involves reaction between the base, imidazole, and the silyl-protecting reagent. The resulting compound deprotonates the hydroxyl groups present in 3,4-dihydroxybenzaldehyde **45** to form a Si-O bond. Imidazole is also reformed in this step.

The reaction was initially carried out in DCM at 0 °C according to a procedure developed by Faler and Joullie[152].

^{1}H NMR data for the product of the reaction carried out in DCM indicated the presence of the silyl groups at ∂ 0.170 ppm and ∂ 0.916 ppm as well as the protons present on the benzene ring. However, there were some peaks unrelated to the structure of the product around the silyl region and also between ∂ 6.5–8 ppm. This could be related to imidazole which has a chemical shift of ∂ 7.14 and ∂ 7.71 ppm and TBDMS-Cl which would be found between ∂ 0–1 ppm. As this product was deemed impure, an alternative solvent, DMF, was employed as it had been noted that the reagents were not readily soluble in DCM.

A solution of the silyl chloride and imidazole in DMF was stirred with 3,4-dihydroxybenzaldeyde **45** as shown in Scheme 22[153]. This is a standard procedure for protecting hydroxyls with TBDMS-Cl as reported by Corey and Venkateswarlu[151].
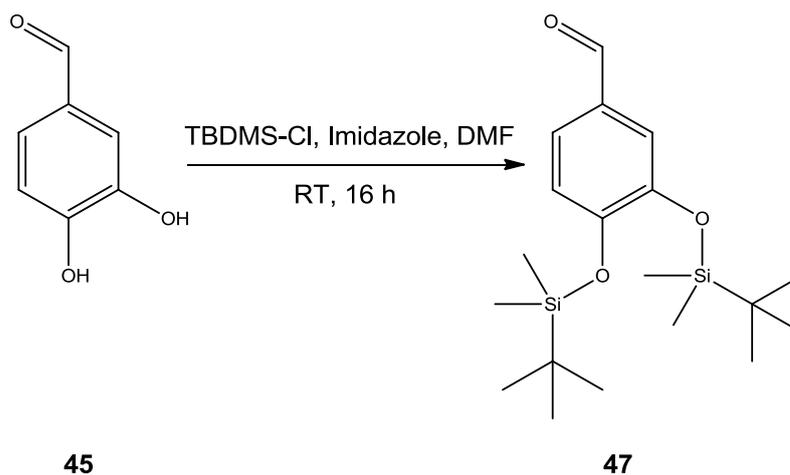
Scheme 22: Synthesis of 3,4-*bis*(*tert*-butyldimethylsilyl-oxy)benzaldehyde **47**

The formation of the product was monitored by TLC (5 % ethyl acetate in hexane) and the crude product obtained from the reaction was purified to furnish a golden yellow oil in a 54 % yield.

Analysis of the purified product by ^{1}H NMR, ^{13}C NMR, FTIR and mass spectroscopy was consistent with the structure of 3,4-*bis*(*tert*-butyldimethylsilyl-oxy)benzaldehyde **47**. FTIR and mass spectroscopy data can be found in section 4.9.4.

^{1}H NMR analysis showed that peaks due to the silyl protecting groups were present in the spectrum indicating that the silyl groups had been successfully introduced into the compound. The doublet at ∂ 0.205 ppm, which had an integration of 12 protons, corresponded to the two methyl groups attached to each silicon atom. A doublet at ∂ 0.941 pm represented the two *tert*-butyl groups also attached to silicon and had an integration of 18 protons. Further downfield, peaks relating to the aromatic region of the compound were observed. Specifically, the proton at the *meta* position of the benzene ring was evidenced by a doublet at ∂ 6.889 ppm which integrated at one proton and the two protons at the *ortho* position of the benzene ring were evidenced as multiplet signal at ∂ 7.327 ppm, which integrated at two protons. Lastly, the aldehydic proton was evidenced by a singlet at ∂ 9.752 ppm, which again integrated at one proton. Overall, the ^{1}H NMR data was consistent with the structure of the desired product, confirming successful synthesis of the product.

^{13}C NMR analysis was similarly unambiguous in the identity of the product. The spectrum displayed a doublet at ∂ −4.085 ppm which represented the two carbons present in the two methyl groups attached to silicon (C8 shown in Figure 48). A doublet at ∂ 18.456 ppm arose from the two carbons joined to silicon (C9). The

doublet at ∂ 25.855 ppm represented the terminal carbon atoms present in the *tert*-butyl groups (C10). Two peaks which arose from the carbon atoms present in the aromatic structure, C2 and C5, were located at ∂ 120.553 ppm and ∂ 120.831 ppm, followed by C6 at ∂ 125.360 ppm and C1 at ∂ 130.768 ppm. Peaks which corresponded to C3 and C4 (joined to the TBDMS ether groups) were found at ∂ 147.690 ppm and ∂ 153.358 ppm. Finally, the carbonyl carbon was evidenced by a signal at ∂ 190.831 ppm.
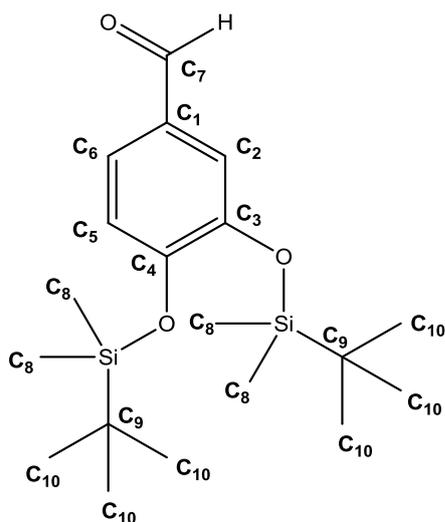
Figure 48: Structure of 3,4-*bis*(*tert*-butyldimethylsilyl-oxy)benzaldehyde **47**

2.6.5.3   Attempted olefination of 3,4-*bis*(*tert*-butyldimethylsilyl-oxy)benzaldehyde **47**

The next step was to convert the carbonyl group in 3,4-*bis*(*tert*-butyldimethylsilyl-oxy)benzaldehyde **47** to a vinyl group. This was attempted by a Wittig reaction which involves the generation of a phosphonium ylide for nucleophilic attack of the carbonyl group.

To generate a ylide, n-butyl lithium was added drop wise to a solution of the phosphonium salt, methyltriphenylphosphonium bromide, in THF. 3,4-*bis*(*tert*-butyldimethylsilyl-oxy)benzaldehyde **47** was added to the resultant yellow solution which turned a cream colour on addition. This mixture was stirred for two hours at −78 °C and the reaction is summarised in Scheme 23[152].

Aston University

Illustration removed for copyright restrictions

Scheme 23: Attempted Wittig olefination of 3,4-*bis*(*tert*-butyldimethylsilyl-oxy)benzaldehyde **47**[152]

The use of n-butyl lithium, a strong base, deprotonates the weakly acidic phosphonium salt to generate a ylide, which is prevented from reaction with moisture or oxygen by the presence of an inert environment[154]. The carbonyl group undergoes nucleophillic attack by the ylide, which yields a dipolar intermediate. The intermediate loses triphenylphosphine oxide to yield an alkene[155].

However, ^{1}H NMR analysis of the crude product from the Wittig reaction indicated the presence of the carbonyl group, which suggested that the reaction had not worked. A peak correlating to the aldehydic proton was found at ∂ 9.731 ppm in the crude product which was comparable with ∂ 9.752 ppm for the starting material. However, the product (Rf = 0.77) appeared to be different from the starting material (Rf = 0.26) by TLC analysis but this could be due to the presence of impurities or the by-product of this reaction, triphenylphosphine oxide.

This Wittig reaction was also repeated with cyclohexanone **49** and benzaldehyde **50** as the starting material, to serve as a control to determine whether 3,4-*bis*(*tert*-butyldimethylsilyl-oxy)benzaldehyde **47** was the reason for the failed reaction. However, neither reaction yielded the desired product.

Should cyclohexanone **49** have undergone the Wittig reaction successfully, the product formed should have been methylenecyclohexane **51** as shown in Scheme 24.
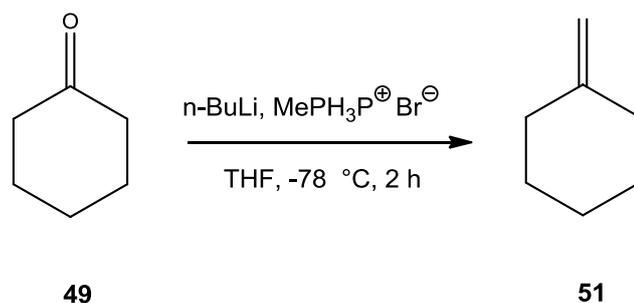
Scheme 24: Attempted Wittig olefination of cyclohexanone **49** to methylenecyclohexane **51**

The product formed did not correlate with data relating to methylenecyclohexane **51**. If the reaction had worked, a peak due to the CH$_2$ in the vinyl group would be observed between ∂ 4-5 ppm in ^{1}H NMR and between ∂ 100-110 ppm in ^{13}C NMR. However, this was not present in either the ^{1}H NMR data or ^{13}C NMR data of the crude product. ^{1}H NMR and ^{13}C NMR analysis of the crude product found peaks relating to the aliphatic structure found in either methylenecyclohexane **51** or cyclohexanone **49**. These peaks were more likely to be due to the starting material, cyclohexanone **49** as there did not seem to be evidence of the vinyl group.

^{1}H NMR spectrum for the product of the attempted Wittig olefination of benzaldehyde **50**, in Scheme 25, showed that the aldehydic proton was still present at ∂ 9.968 ppm which was comparable with the aldehydic proton in the benzaldehyde **50** found at ∂ 9.929 ppm. However, the presence of two doublets at ∂ 5.146 ppm and ∂ 5.701 ppm, as well as a quartet at ∂ 6.654 ppm seemed to indicate the formation of a vinyl group. The integration for these peaks was low, which suggested that the yield of the olefin was also low. The aromatic region for the product was more complicated than what would be expected for a spectrum relating simply to styrene **52**.
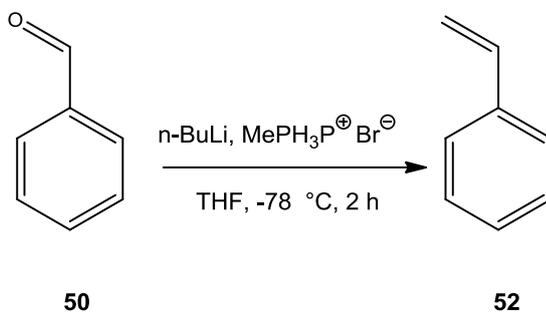
Scheme 25: Attempted Wittig olefination of benzaldehyde **50**

FTIR analysis also showed a weak signal at 1696 cm^{-1}, which again indicated the presence of the carbonyl group, which was comparable with the carbonyl group in benzaldehyde **50** found at 1685 cm^{-1}. Overall, the spectroscopic data suggested that the reaction had possibly worked, but in a very low yield, with much of the starting material still present.

Since olefination using n-BuLi and methyltriphenylphosphonium bromide was proving problematic, the Wittig reaction was repeated again with benzalydehyde **50**, a different base and Wittig reagent as shown in Scheme 26.
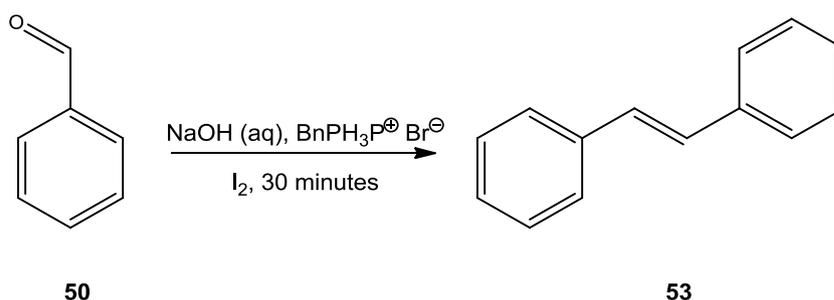
Scheme 26: Synthesis of trans-stilbene **53** by an alternative Wittig procedure[156]

This Wittig procedure used aqueous sodium hydroxide instead of n-BuLi to deprotonate the phosphonium salt[156]. The reaction took place in a two-phase system and utilised a phase-transfer catalyst. A phase-transfer catalyst ensures the efficiency of a reaction by facilitating the transfer of a reagent from one phase to another. In this case, the catalyst is benzyltriphenylphosphonium chloride. The catalyst exchanges chloride ions for hydroxide ions in the aqueous phase. The new phosphonium salt containing hydroxide ions is then deprotonated in the organic layer, yielding a neutral ylide compound which is free to react with benzaldehyde **50**, also in the organic layer. Deprotonation of the compound occurs in the organic layer as the hydroxide ion is a stronger base in the organic phase due the lack of water solvation. In this case, the phase transfer catalyst acts as the reagent as well as the catalyst[156, 157].

Benzaldehyde **50** is readily oxidised to benzoic acid in air, so any benzoic acid that might have been present was removed prior to the reaction by a wash with potassium carbonate solution.

The reaction appeared to work well and ^{1}H NMR confirmed the identity of the product, trans-stilbene **53**.

FTIR analysis also showed the disappearance of the carbonyl peak relating to the starting material. However, the yield of the product was very low, which may be due to the two-phase nature of this reaction.

The reaction which yielded trans-stilbene **53** was repeated with a different phosphonium salt used in earlier reactions, methyltriphenylphosphonium bromide. It was important to repeat the reaction with this particular phosphonium salt as it would yield a product with a carbon-carbon double bond which was essential for the formation of the desired monomeric structure, 3,4-*bis*(*tert*-butyldimethylsilyl-oxy)-vinyl benzene **48**. This proposed reaction with methyltriphenylphosphonium bromide, summarised in Scheme 27, should have yielded styrene **52** as the product.

50   **52**
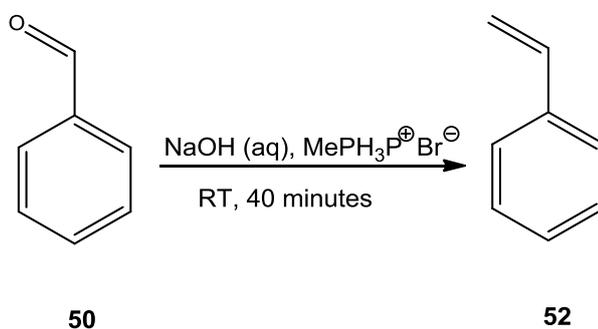
Scheme 27: Attempted olefination of benzaldehyde **50** *via* an alternative Wittig reaction

^{1}H NMR evidence indicated that the reaction had not worked as there was an absence of the vinylic peaks which would indicate successful olefination of benzaldehyde **50**. There was also a peak due to the aldehydic proton, found at ∂ 9.968 ppm, which was in accordance with the peak due to the aldehydic proton found in benzaldehyde **50** at ∂ 9.929 ppm. The aromatic region of the product obtained also matched the aromatic region of benzaldehyde **50**. Overall, the evidence suggested that the starting material had not reacted.

This Wittig reaction was also repeated with 3,4-*bis*(*tert*-butyldimethylsilyl-oxy)benzaldehyde **47** and is summarised in Scheme 28. However, this reaction did not appear to the yield the desired product either. ^{1}H NMR analysis indicated an absence of signals due to the vinylic protons. The vinylic protons for this molecule should be present at approximately ∂ 5.1 ppm and ∂ 5.6 ppm, each with an integration of one proton, and a quartet at around ∂ 6.6 ppm, again with an integral of one proton. The aldehydic proton was still present at ∂ 9.968 ppm, albeit with a moderately low intensity. FTIR analysis also showed the presence of a carbonyl group at 1693 cm^{-1},

comparable with the carbonyl stretch related to 3,4-*bis*(*tert*-butyldimethylsilyl-oxy)benzaldehyde **47** at 1696 cm^{-1}, which was further indication that the reaction had not worked.
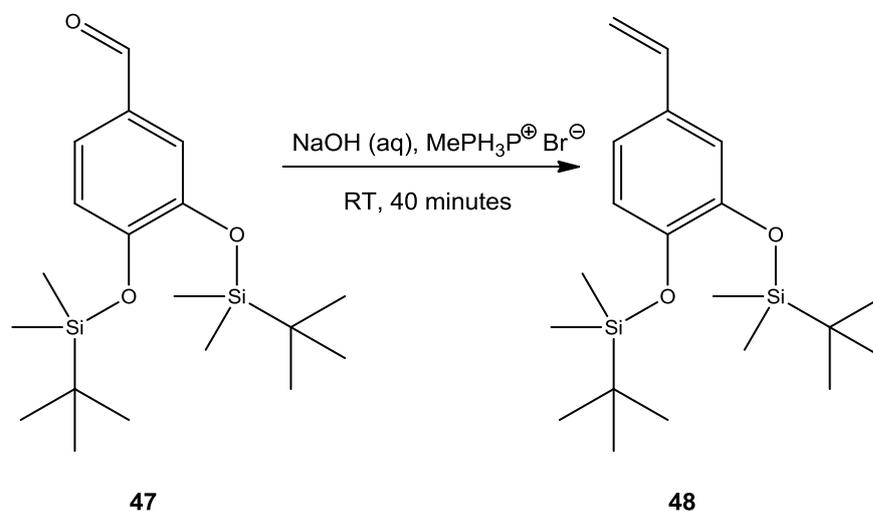
Scheme 28: Attempted olefination of 3,4-*bis*(*tert*-butyldimethylsilyl-oxy)benzaldehyde **47** *via* an alternative Wittig reaction

After several failed attempts at the Wittig reaction, a new approach to the olefination of the carbonyl group was undertaken. This approach utilises the formation of a gem-dimetal compound, which is a compound that has two carbon-metal bonds on the same carbon[154].

The reaction mixture consisted of zinc, diiodomethane and titanium tetrachloride which was successful in the olefination of 3,4-*bis*(*tert*-butyldimethylsilyl-oxy)benzaldehyde **47**, shown in Scheme 29.
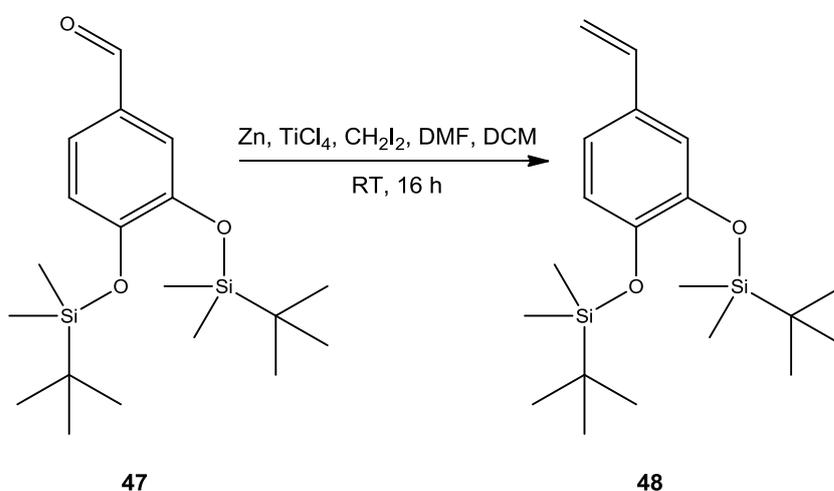
Scheme 29: Synthesis of 3,4-*bis*(*tert*-butyldimethylsilyl-oxy)vinyl benzene **48**

The identity of the product, 3,4-*bis*(*tert*-butyldimethylsilyl-oxy)vinyl benzene **48**, was confirmed by ^{1}H NMR, ^{13}C NMR, FTIR and mass spectroscopy analysis. FTIR and mass spectroscopy analysis data is described in section 4.9.8. The product was formed in a 21 % yield.

^{1}H NMR analysis of the product showed that the peaks arising from the silyl protecting groups were present and unchanged. The doublet at ∂ 0.286 ppm which integrated at 12 protons represented the two methyl groups attached to the two silicon atoms; a doublet at ∂ 1.046 ppm, integrated at 18 protons and represented the two *tert*-butyl groups also attached to silicon. Further downfield were the vinyl signals which indicated the successful formation of the olefin. Two doublets which represent the two protons on C8 in Figure 49 were present at ∂ 5.153 ppm and ∂ 5.610 ppm and each integrated at one proton. The proton on C7 in the vinyl group had a chemical shift of ∂ 6.666 ppm and also integrated at one proton. The peaks relating to the aromatic region of the compound were found further downfield. The proton at the *ortho* position (C2) had a chemical shift of ∂ 6.820 ppm and integrated at one proton. The proton at C5 had a chemical shift of ∂ 6.890 ppm and also integrated at one proton. The last proton at C6 was found to possess a chemical shift of ∂ 6.917 ppm and integrated at one proton. The ^{1}H NMR data was entirely consistent with the structure of the desired product, confirming successful synthesis of the product.
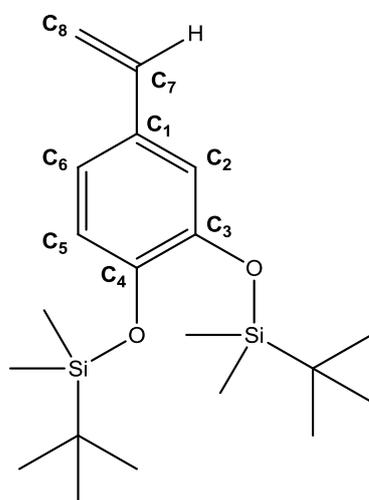
Figure 49: Structure of 3,4-*bis*(*tert*-butyldimethylsilyl-oxy)vinyl benzene **48**

^{13}C NMR analysis showed a doublet at ∂ −4.046 ppm which represented the four carbons present in the two methyl groups attached to silicon. A peak at ∂ 18.524 ppm arose from the tertiary carbon atoms which join silicon to the *tert*-butyl groups. A doublet found at ∂ 25.993 ppm correlated to the terminal carbon atoms present in the

tert-butyl groups. The signal due to the terminal carbon in the vinyl group, labelled C8 in Figure 49, was located at ∂ 111.650 ppm and the next three carbons in the aromatic part of the structure were found at ∂ 118.755 (C2), ∂ 119.738 (C5) and ∂ 121.002 (C6) ppm. The *para* carbon (C1) was found at ∂ 131.392 ppm. The next peak at ∂ 136.487 ppm represented the first carbon present in the vinyl group (C7). The last two carbons to account for were the final two peaks at ∂ 146.882 and ∂ 146.942 ppm which represented the carbons at positions C3 and C4, to which the TBDMS-ether groups are joined.

To generate a hydroxyl-containing compound which was capable of interaction with TiO$_2$ nanoparticles, it was desirous to remove the TBDMS group from 3,4-*bis*(*tert*-butyldimethylsilyl-oxy)vinyl benzene **48** to unmask the hydroxyl groups. Therefore, desilylation of 3,4-*bis*(*tert*-butyldimethylsilyl-oxy)vinyl benzene **48** was carried out.

2.6.5.4   Attempted desilylation of 3,4-*bis*(*tert*-butyldimethylsilyl-oxy)vinyl benzene **48**

Desilylation was attempted as shown in Scheme 30, using a common deprotection agent for silyl protecting groups, tetra-*n*-ammonium fluoride solution (TBAF). TBAF is a useful deprotection agent as the fluoride ion is able to form a strong SI-F bond (819 KJ mol^{-1}) which is stronger than the Si-O bond (530 KJ mol^{-1}) and typically allows easy cleavage of the silyl-ether [151, 153].
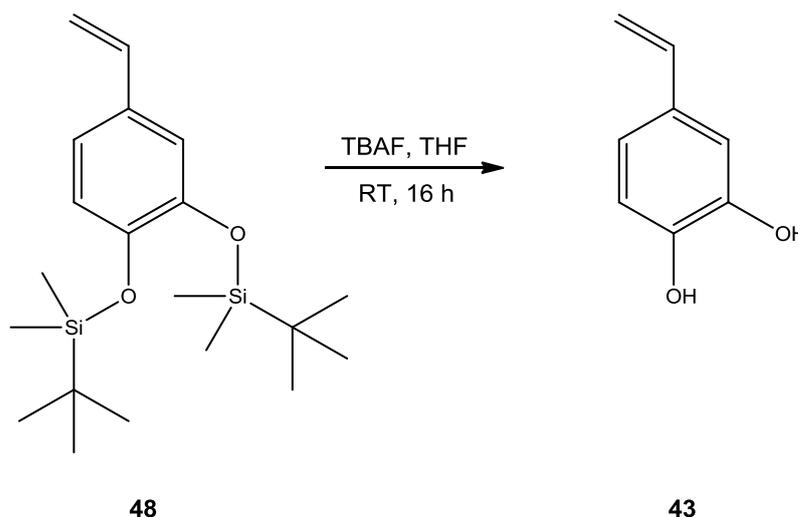
Scheme 30: Attempted desilylation of 3,4-*bis*(*tert*-butyldimethylsilyl-oxy)vinyl benzene **48** with TBAF

Deprotection using TBAF was carried out in standard and excess conditions however; the deprotection agent was not able to cleave the TBDMS groups.

^{1}H NMR analysis of the crude product from the attempted desilylation of 3,4-*bis*(*tert*-butyldimethylsilyl-oxy)vinyl benzene **48** showed that the TBDMS groups were still present in the compound, however their integration had reduced from 18 and 12 protons to 3 and 2 respectively. This suggests that 15-27 % of the silyl group was still present indicating that the reaction had not gone to completion.

Problems may have arisen in deprotection as TBDMS groups are known to be stable to many reaction conditions. Although acid labile and susceptible to attack by the basic fluoride ion, TBDMS groups are a popular choice of protective groups as they provide sufficiently strong protection from a variety of reaction conditions.

The protection of the hydroxyl groups in 3,4-*bis*(*tert*-butyldimethylsilyl-oxy)vinyl benzene **48** could not be circumvented as the reaction to convert the carbonyl group in 3,4-dihydroxybenzaldehyde **45** to a vinyl group had a very low yield in the presence of the free hydroxyl groups.

Another desilylation reaction was carried out with $TiCl_4$ in ethyl acetate and DCM as shown in Scheme 31[158]. It was hoped that after the deprotection reaction with excess $TiCl_4$, this might additionally yield the Ti coordination complex **44**.
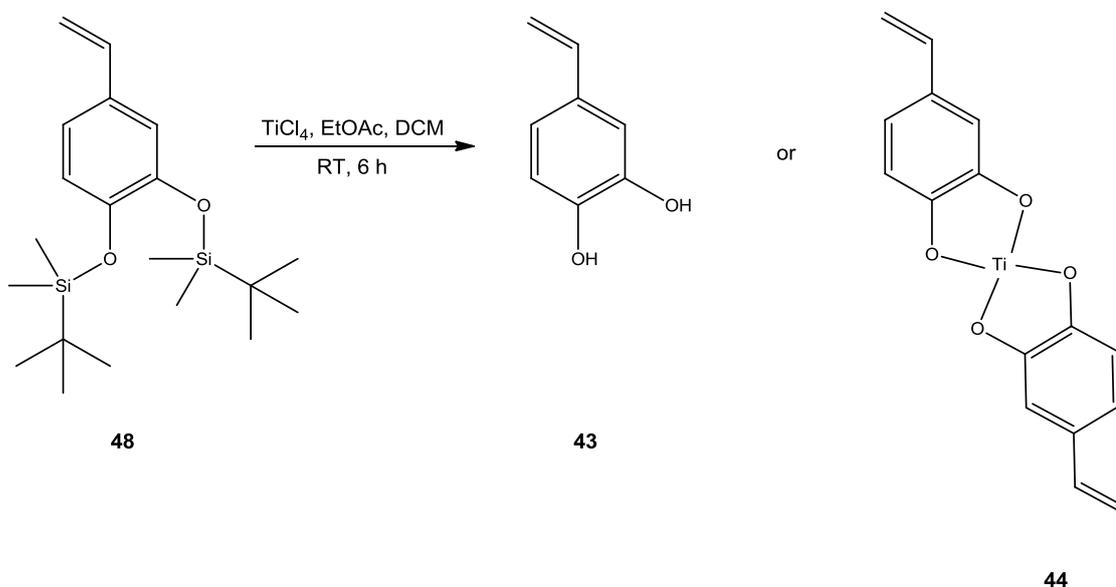
Scheme 31: Attempted desilylation of 3,4-*bis*(*tert*-butyldimethylsilyl-oxy)vinyl benzene **48** with $TiCl_4$, DCM and EtOAc

The attempted desilylation of 3,4-*bis*(*tert*-butyldimethylsilyl-oxy)vinyl benzene **48** did not yield 4-vinyl catechol **43** as the TBDMS groups did not seem to have been successfully removed, as evidenced by ^{1}H NMR spectroscopy.

Consequently, it was not possible to react TiO$_2$ nanoparticles with hydroxyl groups as the formation of 4-vinyl catechol **43** was unsuccessful.

2.6.6. Summary

The synthesis of 4-vinyl catechol **43** was required in order to form a coordination complex with TiO$_2$, after which, the complex could be polymerised. Formation of 4-vinyl catechol **43** from 3,4-dihydroxybenzaldeyde **45** and malonic acid **46** may have worked, however the crude product obtained was highly impure so this synthetic route was abandoned.

A new synthetic route involved the successful protection of the hydroxyl groups present on 3,4-dihydroxybenzaldeyde **45** to yield 3,4-*bis*(*tert*-butyldimethylsilyl-oxy)benzaldehyde **47**. Subsequent olefination of 3,4-*bis*(*tert*-butyldimethylsilyl-oxy)benzaldehyde **47** led to the successful formation of 3,4-*bis*(*tert*-butyldimethylsilyl-oxy)vinyl benzene **48**. The olefination of 3,4-*bis*(*tert*-butyldimethylsilyl-oxy)benzaldehyde **47** *via* a Wittig reaction was attempted with different Wittig reagents and carbonyl-containing compounds but none of the reactions appeared to have yielded the product.

Deprotection of the TBDMS groups in 3,4-*bis*(*tert*-butyldimethylsilyl-oxy)vinyl benzene **48** was required in order to leave the hydroxyl groups free for the coordination of TiO$_2$ nanoparticles. Different deprotection reagents such as TBAF and TiCl$_4$ were used but unfortunately, deprotection did not appear to have taken place as evidenced by ^{1}H NMR analysis.

Chapter 3
Conclusion

3.1. Coating / application of QD-thiol microspheres

Thiol-functionalised microspheres **6** were successfully synthesised by a dispersion polymerisation reaction for interaction with fluorescent dyes and nanoparticles, in particular QDs. The resultant conjugates were assessed for their utility in the imaging of biological systems.

Due to the loss of QD fluorescence over time, an approach was undertaken to encapsulate QD-microspheres **7** with a shell or coating to make the QDs more stable and prolong their lifetime.

Two types of QDs (Cd-containing, CdQDs, and non-Cd containing, CFQDs) were immobilised into thiol-functionalised microspheres **6** *via* a previously reported immobilisation procedure. The resultant QD-microspheres **7** were shelled with polysiloxanes in an attempt to provide resistance to the entry of oxygen or moisture.

Silica-shelled, CdQD-microspheres were observed to retain fluorescence on contact with water which suggested that the shell afforded some level of protection against quenching. However, silica-shelled CFQD-microspheres did not retain a high level of fluorescence after contact with water.

Further investigation into the shelling procedure for CFQDs is required as these QDs appear to be less stable than CdQDs which may make them more susceptible to quenching. In future work, an increase in the thickness of the polysiloxane layer may yield more favourable results in the ability of CFQDs to maintain fluorescence.

QD-microspheres **7** were also coated with PVDC, a polymer known to possess excellent water and oxygen barrier properties *via* a microencapsulation reaction. Conditions of the reaction such as the hardening agent and quantities of PVDC were varied in order to find the optimum condition. However, results obtained were not reproducible, possibly due to aggregation of PVDC and/or microspheres. In future work, an assessment of other factors which could influence the reaction such as temperature and reaction time is needed.

A potential application of QD-microspheres **7** involved the use of their fluorescent nature in the visualisation of RBCs. Firstly, in order to successfully visualise RBCs, determination of whether RBCs can internalise QD-microspheres **7** was required. Microsphere uptake by the process of beadfection was visualised by confocal microscopy, which appeared to show evidence of internalisation. However, an issue affecting visualisation was the tendency of the microspheres to aggregate.

A layer-by-layer technique was employed to prevent aggregation by coating microspheres with charged polyelectrolytyes. Confocal microscope images appeared to indicate a significant reduction in aggregation with the addition of one layer of charged polyelectrolyte. However, after washes with PBS, the medium in which beadfection with RBCs would take place, the microspheres became aggregated. This may have been due to the presence of ions in PBS which could have surrounded the polyelectrolyte layer and counteracted its charge, causing the aggregation of the microspheres.

Therefore, a covalent strategy was utilised for the attachment of charged material to the microspheres. A polymeric shell containing carboxylic acid groups was synthesised around the microspheres *via* a seeded emulsion polymerisation reaction to yield core-shell particles which were sufficiently charged to avoid aggregation. The presence of the carboxylic acid groups was indicated by the loading of Fmoc-diaminopropyl hydrochloride **12** which yielded a loading value of 100 µmol g^{-1}. Elemental analysis indicated the level of oxygen present in a sample of the core-shell particles was 3.71 % and combined with a zeta potential value of −74.84 mV, this further confirmed the presence of carboxyl groups and the charged nature of the surface of thiol-core, carboxyl-shelled microspheres **10**.

During investigation into the parameters affecting beadfection, it was found that the presence of haemoglobin had a deleterious effect on QD fluorescence. The exact mechanism by which fluorescence loss occurs was not determined however, it is possible that either haemoglobin absorbed the excitation energy for required for QD excitation, which prevented QD emission or there is some form of interaction between haemoglobin and QDs.

Consequently, QDs were replaced with fluorescent dyes for microsphere internalisation in RBCs. Thiol-core, carboxyl-shelled microspheres **10** labelled with a fluorescent dye were incubated with RBCs and confocal microscope images appeared to show the presence of microspheres successfully internalised into a few RBCs. This is a preliminary finding but nevertheless an encouraging result. Optimisation of beadfection in RBCs is required to progress this work.

3.2. Interaction of polymer microspheres with fluorescent dyes

The interaction of thiol-functionalised microspheres **6** with fluorescent dyes was explored for another potential application, the analysis of the tear film of the eye. Four thiol-reactive, maleimide-functionalised fluorescent dyes were selected for reaction with thiol-functionalised microspheres **6**. Two of the four dyes were hydrophobic and were able to successfully label the slightly hydrophobic microspheres, which was subsequently confirmed by fluorescent microscope images. The other two dyes were hydrophilic and did not label the microspheres. Thiol-core, carboxyl-shelled microspheres **10** which possessed a hydrophilic outer layer were reacted with the hydrophilic dyes however, this reaction failed, possibly due to the lack of association of the dye with the thiol core.

The carboxyl groups were then used as a point of attachment for the hydrophilic dyes. *S*-trityl cysteamine **18**, a compound capable of reaction with carboxyl groups and the thiol-reactive dyes, was successfully synthesised. This compound was coupled onto the thiol-core, carboxyl-shelled microspheres **10**, followed by deprotection of the trityl group. These modified microspheres were then reacted with the hydrophilic dyes however; the reaction also failed and did not yield fluorescent microspheres. The reason for failure may be due to the level of carboxyl groups which was not high enough to anchor a sufficient amount of *S*-trityl cysteamine **18** to the microspheres to enable a high level of dye conjugation.

Amino-functionalised microspheres **24** were also synthesised, to which Fmoc-*S*-trityl, *L*-cysteine **25** was coupled. The hydrophilic dyes were reacted with these modified amino-functionalised microspheres **27**, however, this reaction also failed.

Different diameters of polymer microspheres required for visualisation of the three layers of the tear film were synthesised by suspension, emulsion and dispersion polymerisation reactions. These microspheres were successfully labelled with the two hydrophobic fluorescent dyes as well as other organic fluorophores. The fluorescent conjugates were then used to visualise the tear film.

Results appeared to indicate that the microspheres were particularly useful for tracking the movement of fluid along the tear meniscus. It was also noted that small fluorescent microspheres (i.e. 0.5–5 μm) were difficult track on the tear film as they would quickly spread towards the puncta. Larger fluorescent microspheres were developed which would be easier to track as they move more slowly on the tear film.

Future work will involve the use of the developed fluorescent microspheres to provide an insight into tear flow behind a contact lens.

3.3. Interaction of titanium dioxide with functional groups

The interaction of thiol and thiouronium groups with another nanoparticle, titanium dioxide (TiO_2) was investigated. Thiol and thiouronium-functionalised polymeric material with different morphologies was assessed for interaction with TiO_2 nanoparticles.

Both milled porogenic thiol-functionalised polymethyl methacrylate **38** and TiO_2 nanoparticles were individually suspended in methanol with the use of an ultrasonic probe. Centrifugation of the mixture of these suspensions did not yield a clear supernatant or the separation of the polymer or nanoparticles. Unsuccessful separation suggested a level of interaction between the nanoparticle and polymer. In contrast, a clear supernatant was obtained for a control experiment which did not possess any thiol groups in the polymer.

A planar morphology was investigated with a film of spin-coated thiouronium-functionalised polystyrene **39**-**41**. These films were dipped into a suspension of TiO_2 nanoparticles to facilitate interaction. Visual observation of the films before and after dipping indicated that TiO_2 nanoparticles had been absorbed onto the surface. The level of bound TiO_2 nanoparticles appeared to increase with an increasing level of thiouronium groups.

Analysis of the presence of TiO_2 nanoparticles with FTIR spectroscopy was not viable as it was not possible to assign a peak specifically to TiO_2. However, XPS analysis indicated the presence of TiO_2 on the spin-coated film.

Interaction of TiO_2 nanoparticles with hydroxyl groups was also explored with the synthesis of a hydroxyl-containing compound which could act as a ligand binding site for TiO_2 nanoparticles. 4-Vinyl catechol **43** was selected for this purpose, with the eventual aim being to polymerise the compound to form a polymer containing TiO_2 nanoparticles immobilised by hydroxyl groups.

Different synthetic routes for 4-vinyl catechol **43** were investigated. Attempts to synthesise 4-vinyl catechol **43** from 3,4-dihydroxybenzaldehyde **45** and malonic acid **46** did not prove successful as indicated by NMR analysis. The yield of the product

was low and a large amount of impurities were present, therefore this synthetic route was not deemed to be viable.

A new approach was taken which first involved the protection of the hydroxyl groups in 3,4-dihydroxybenzaldehyde **45** with TBDMS-Cl. After the successful synthesis of 3,4-bis(*tert*-butyldimethylsilyl-oxy)benzaldehyde **47**, attempts were made to convert the carbonyl group present in the compound to a vinyl group.

Initially, olefination of the carbonyl group was carried out *via* a Wittig reaction. Different conditions for the Wittig reaction were investigated (*i.e.* different temperatures, Wittig reagents and carbonyl-containing compounds), however attempts at this reaction with 3,4-*bis*(*tert*-butyldimethylsilyl-oxy)benzaldehyde **47** failed.

Successful conversion of the carbonyl group was achieved by a zinc-mediated olefination reaction. The synthesis of 3,4-*bis*(*tert*-butyldimethylsilyl-oxy)vinyl benzene **48** was confirmed by ^{1}H NMR, ^{13}C NMR, FTIR and mass spectroscopy analysis.

Difficulties arose in the removal of the TBDMS protecting groups. Cleavage of the TBDMS groups with TBAF and TiCl$_4$ was not successful. Failure of this deprotection step meant that interaction of TiO$_2$ nanoparticles with hydroxyl groups could not be assessed. Further investigation into methods of deprotection is required before the attachment of TiO$_2$ nanoparticles can take place.

Overall, there is good evidence to suggest a level of TiO$_2$ interaction with thiol and thiouronium groups. Further analysis and assays on the interaction between nanoparticle and polymer is required in order to optimise interaction.

Chapter 4
Experimental

4.1 Source of materials

Organic reagents were purchased from Sigma-Aldrich with the exception of *tert*-butyldimethylchlorosilane (TBDMS-Cl) which was purchased from Avocado. Peptide coupling reagents were obtained from Merck Biosciences and Avocado.

All solvents used were either laboratory reagent grade or analytical reagent grade and were used as received from Fisher with the exception of dichloromethane (DCM) which was distilled from calcium hydride and tetrahydrofuran (THF) which was distilled from a mixture of sodium and benzophenone.

All monomers were acquired from Sigma-Aldrich and used as received except for styrene which was washed with 1 M sodium hydroxide solution and water and dried over anhydrous magnesium sulfate before use.

Cadmium-free quantum dots (CFQDs) and cadmium-containing quantum dots (CdQDs) were supplied by Nanoco Technologies Ltd.

Qdot 655 ITK organic quantum dots was purchased from Invitrogen Ltd.

Polymers such as polyvinyl alcohol (87-89 % hydrolysed), poly(vinylidene chloride-*co*-acrylonitrile) (average M_w ~150,000 g mol^{-1}, average M_n ~80,000 g mol^{-1}), polyvinylpyrrolidone (M_n = 58,000 g mol^{-1}), branched polyethyleneimine (average M_w ~25,000 g mol^{-1} by LS, average M_n ~10,000 g mol^{-1} by GPC) and polyacrylic acid (35 wt % in H$_2$O, average M_w ~100,000 g mol^{-1}) were used as received from Sigma-Aldrich.

Maleimide-functionalised dyes were obtained from Invitrogen Ltd with the exception of DY-405 maleimide, which was acquired from Dyomics GMBH.

Titanium (IV) oxide anatase nanopowder (99.7 %, particle size <25 nm) was purchased from Sigma-Aldrich.

4.2. General Information

All reactions were stirred magnetically and conducted under an atmosphere of nitrogen. Moisture sensitive reactions were conducted in oven dried (120 °C) glassware. All polymerisation reactions were carried out using a Radleys Discovery Technologies Ltd. Carousel Reaction Station.

Organic reactions were monitored by thin layer chromatography (TLC) where possible; using Merck silica gel 60 RP-8 F_{254} glass plates which were visualised under UV light and then developed using a 10 % w/v solution of phosphomolybdic acid in methanol. Column chromatography was carried out using Fluka silica gel 60 (0.04-0.063 mm, 230-400 mesh).

4.2.1. Equipment details and methodology

^{1}H NMR and ^{13}C NMR spectroscopy were carried out using a Bruker AC300 spectrometer. ^{13}C NMR spectra were recorded using the PENDANT program. The deuterated solvents used were deuterated chloroform ($CDCl_3$), deuterated methanol (CD_3OD) and deuterium oxide (D_2O). Chemical shift (δ) values were measured relative to tetramethylsilane (TMS) in parts per million (ppm), relative to the residual signal of the deuterated solvent used. Coupling constants were measured in Hertz (Hz).

Fourier Transform Infrared Spectroscopy was recorded on a Perkin Elmer FTIR spectrometer spectrum RX I, either as a solid compressed within a potassium bromide disk or as a thin film between two sodium chloride plates.

High resolution mass spectroscopy measurements were carried out on a Waters LCT Premier Micromass Mass Spectrometer with electrospray ionisation and a Waters GCT Premier Micromass Mass Spectrometer with electron impact.

UV-Vis spectroscopy data was acquired on a Perkin-Elmer UV/VIS spectrophotometer Lambda 12, using two quartz glass cuvettes with 1 cm path length.

Elemental analyses were performed by Medac Ltd.

Sizing data for polymer microspheres was obtained on a Sympatec Helos Particle Size Analyser, equipped with a helium-neon laser with a wavelength of 632.8 nm and measurements were obtained with Windox 5 software. A R2 lens with a measuring range of 0.25/0.45-87.5 µm was used for all measurements.

All polymer samples were suspended in distilled water by ultrasonication prior to measurement. The polymer sample was then added to the active disperser, a 50 mL glass cuvette filled to two-thirds of the volume with distilled water, until the optical concentration of the suspension in the cuvette was between 8-10 %. The laser was then switched on to commence measurement and the suspension was sonicated for 60 seconds, whilst being stirred with a PTFE stirrer bar at a speed of 1200 rpm. Three successive diameter measurements were generated from which an average was obtained to give the final diameter reading.

Zeta potential measurements were acquired using a Beckmann Coulter Delta Nano C Particle Analyzer which was equipped with Delsa Nano 2.1 software. Samples were measured in a Delta Nano C Zeta Potential flow cell. The sample (1×10^{-3} g) was suspended in deionised water (1.00 mL) by ultrasonication, which was then injected into the flow cell using a 1.00 mL syringe.

The Beckmann Coulter Delta Nano C Particle Analyzer used in this research was obtained, through Birmingham Science City: Innovative Uses for Advanced Materials in the Modern World (West Midlands Centre for Advanced Materials Project 2), with support from Advantage West Midlands (AWM) and part funded by the European Regional Development Fund (ERDF).

XPS analysis was carried out on a Thermofisher ESCALAB 250 Electron Spectrometer, equipped with a hemispherical sector energy analyser. An analyser pass energy of 20 eV with a step size of 0.1 eV and dwell time of 50 ms was used throughout all measurements. A monochromatic aluminium K-α X-ray source at a source excitation energy of 15 eV with an emission current of 0.6 mA was also used. The base pressure during sample analysis was above 5×10^{-10} mbar which ensured that the signals were obtained from the surface of the sample. The analysis area of the sample had a 500 µm diameter. XPS survey scans were carried out to acquire elemental data which was followed by narrow region energy scans.

4.2.2. Microscope methodology and sample preparation

Fluorescent microscope images were obtained on a Zeiss Axioskop upright microscope equipped with a Zeiss AxioCam HRc and Axiovision 4.8 software. Images were captured with a 100x objective. Fluorescent microspheres suspended in distilled water (0.010 mL, 5.00×10^{-3} g mL^{-1}) by ultrasonication were pipetted onto a glass microscope slide (76 mm × 26 mm, 1.0-1.2 mm thick) and a borosilicate glass coverslip (24 mm × 50 mm) was mounted over the microsphere suspension. A drop of immersion oil was placed between the coverslip and microscope objective. The slide was immediately examined under the microscope.

Confocal microscopy was carried out on a Leica TCS SP5 II laser scanning microscope using a HCX PL APO CS 63.0x/1.40 Oil UV objective. Images were acquired with a scan speed ranging from 10-100 Hz.

Microspheres suspended in either a PBS or polyelectrolyte medium (0.010 mL, 1.00×10^{-3} g mL^{-1}) by ultrasonication were pipetted onto a glass microscope slide (76 mm × 26 mm, 1.0-1.2 mm thick) and a borosilicate glass coverslip (24 mm × 50 mm) was mounted over the microsphere suspension. A drop of immersion oil was placed between the coverslip and microscope objective. The slide was immediately examined under the microscope. Thiol-functionalised microspheres **6** and QD-microspheres **7** were observed using an argon laser line with a wavelength of 488 nm and a helium-neon laser line with a wavelength of 594 nm respectively.

Red blood cells (RBCs) suspended in PBS (0.010 mL) were also placed onto a glass slide and a coverslip (specifications mentioned above) was mounted over the cell suspension. A drop of immersion oil was placed between the coverslip and microscope objective. RBCs were visualised using a helium-neon laser line with a wavelength of 594 nm.

4.3 Synthesis of thiol-functionalised microspheres

4.3.1. Synthesis of 4-vinylbenzyl isothiouronium chloride **2**[103]

4-Vinylbenzyl chloride (4-VBC) **1** (11.4 mL, 12.3 g, 80.1 mmol) was added to a solution of thiourea (2.50 g, 32.8 mmol) in absolute ethanol (25.0 mL) and water (2.50 mL). This mixture was heated to 50 °C and stirred for 16 hours under an atmosphere of nitrogen. The reaction mixture was allowed to cool to room temperature, before ethanol was removed under reduced pressure. Water (50.0 mL) was then added in excess to dissolve the water-soluble product, along with the addition of chloroform (50.0 mL $\times$ 3) for the extraction of any un-reacted 4-VBC **1**. The collected aqueous layer was concentrated under reduced pressure to leave a wet slurry which was dissolved in absolute ethanol (10.0 mL) and once again concentrated under reduced pressure to yield a white, powdery solid (6.26 g, 27.4 mmol, 83 %). This was then dried *in vacuo* for two hours.

Yield: 6.26 g, 27.4 mmol, 83 %

IR (KBr disc): 3040 (s, C-H aromatic), 2711 (m, C-H aliphatic), 1653 (s, C=C vinyl), 1509 (m, C=C aromatic), 1437 (m), 1256 (m), 1205 (m), 1160 (m), 1112 (m), 1090 (w), 1016 (w), 989 (m), 902 (m), 830 (m), 727 (s)

^{1}H NMR (300 MHz, D_2O): δH 4.272 (s, 2H, CH_2), 5.205 (d, 1H, CH, J = 11.0), 5.718 (d, 1H, CH, J = 17.7), 6.610 (dd, 1H, CH, J = 11.0 and J = 11.0), 7.326 (d, 2H, CH, J = 8.3), 7.381 (d, 2H, CH, J = 8.3)

^{13}C NMR (75 MHz, D_2O, PENDANT): δC 34.818 (CH_2), 114.946 (CH_2), 126.659 (CH), 129.202 (CH), 133.624 (C), 135.911 (CH), 137.497 (C)

4.3.2. Synthesis of thiouronium-functionalised microspheres **5** by dispersion polymerisation[103]

A solution of azobis-*iso*-butyronitrile (AIBN) (0.172 g, 1.05 mmol) in styrene **3** (12.0 mL, 10.9 g, 105 mmol) and divinylbenzene (DVB) **4** (0.149 mL, 0.136 g, 1.05 mmol) was added to a solution of polyvinylpyrrolidone (PVP) (1.22 g, 0.0200 mmol) and 4-vinylbenzyl isothiouronium chloride (4-VBTU) **2** (0.240 g, 1.05 mmol) in absolute ethanol (100 mL). This mixture was degassed with nitrogen at room temperature for 30 minutes. The reaction mixture was then heated to 70 °C and stirred for 16 hours under an atmosphere of nitrogen. Once cooled, the resultant polymer microspheres were centrifuged (7000 rpm, 10 minutes). The supernatant was

decanted and the microspheres were resuspended in methanol (30.0 mL) by ultrasonication and centrifuged again. This washing procedure was repeated with methanol (30.0 mL) and twice with water (30.0 mL). Finally, the microspheres were resuspended in water (30.0 mL) by ultrasonication.

Yield: 9.72 g, 86 % by mass

Average diameter: 1.0 μm (standard deviation = 0.5 μm)

Combustion analysis: Carbon 91.61 %, Hydrogen 7.78 %, Nitrogen 0.36 %, Sulphur <0.10 %

Zeta potential: +9.86 mV

4.3.3. Conversion of thiouronium-functionalised microspheres **5** to thiol-functionalised microspheres **6**[103]

A suspension of thiouronium-functionalised microspheres **5** (1.00 g) was centrifuged (9700 rpm, 13 minutes). The supernatant from which was decanted and the microspheres were resuspended in methanol (30.0 mL) by ultrasonication and centrifuged again. This washing procedure was repeated once with methanol (30.0 mL), and twice with THF (30.0 mL). The microspheres were then resuspended in THF (30.0 mL), to which tetramethylammonium hydroxide solution (TMAOH) (0.0585 mL, 0.0510 g, 0.559 mmol) was added; this suspension was then shaken on a shaker plate for 16 hours at room temperature. The resultant microspheres, which possessed a pale yellow hue, were centrifuged (8000 rpm, 10 minutes). The supernatant was then decanted and the microspheres were resuspended in THF (30.0 mL) by ultrasonication and centrifuged again. This washing procedure was repeated once more with THF (30.0 mL) and twice with methanol (30.0 mL) to leave the microspheres suspended in methanol (30.0 mL).

Yield: 0.96 g, 96 % by mass

Average diameter: 1.0 μm (standard deviation = 0.4 μm)

4.4 Immobilisation and shelling of quantum dots

4.4.1. Immobilisation of cadmium-containing quantum dots (CdQDs) into thiol-functionalised microspheres 6[103]

A suspension of thiol-functionalised microspheres **6** (0.100 g) was centrifuged (9500 rpm, 13 minutes), the supernatant was decanted and the microspheres were resuspended in toluene (30.0 mL) by ultrasonication and centrifuged again. This washing procedure was repeated twice with toluene (30.0 mL). The microspheres were resuspended in toluene (30.0 mL) again, to which chloroform (10.0 mL) was also added. This mixture was degassed with nitrogen for 30 minutes whilst stirring at room temperature. CdQDs (5.00×10^{-3} g) were then added to the mixture which was stirred for 16 hours under an atmosphere of nitrogen. The resultant QD-microspheres were centrifuged (7000 rpm, 10 minutes), the supernatant was decanted and the fluorescent microspheres were resuspended in toluene (which had been degassed with nitrogen) (10.0 mL) by ultrasonication and centrifuged again. This washing procedure was repeated once more with degassed toluene (10.0 mL), twice with degassed absolute ethanol (10.0 mL), once with a degassed aqueous solution of PVP (10 mL, 0.0100 g mL^{-1}) and twice with degassed water (10.0 mL) to leave the microspheres resuspended in degassed water (10.0 mL).

Yield: 0.0760 g, 72 % by mass

4.4.2. Immobilisation of cadmium-free quantum dots (CFQDs) into thiol-functionalised microspheres 6

A suspension of thiol-functionalised microspheres **6** (0.100 g) was centrifuged (9500 rpm, 13 minutes), the supernatant was decanted and the microspheres were resuspended in toluene (30.0 mL) by ultrasonication and centrifuged again. This washing procedure was repeated twice with toluene (30.0 mL). The microspheres were resuspended in toluene (30.0 mL) again, to which chloroform (10.0 mL) was also added. This mixture was degassed with nitrogen for 30 minutes whilst stirring at room temperature. CFQDs (5.00×10^{-3} g) were then added to the mixture and stirred for 16 hours under an atmosphere of nitrogen. The resultant QD-microspheres were centrifuged (7000 rpm, 10 minutes), the supernatant was decanted and the microspheres were resuspended in toluene (which had been degassed with nitrogen) (10.0 mL) by ultrasonication and then centrifuged again. This washing procedure was repeated once more with degassed toluene (10.0 mL) and twice with degassed

absolute ethanol (10.0 mL) to leave the microspheres resuspended in degassed absolute ethanol (10.0 mL).

Yield: 0.0700 g, 67 % by mass

CFQDs were used only in two protocols, 4.4.2 and 4.4.3 (see Table 23). All other protocols which refer to QD-microspheres **7** were synthesised with CdQDs.

4.4.3. Silica shelling of QD-microspheres **7**

A suspension of QD-microspheres **7** (0.0500 g) was centrifuged (9700 rpm, 13 minutes), the supernatant was decanted and the microspheres were resuspended in water (10.0 mL). This suspension was degassed with nitrogen for 15 minutes, after which TMAOH (0.400 mL, 0.346 g, 3.80 mmol) was added. After five minutes, a mixture of tetraorthosilicate (TEOS) (0.0500 mL, 0.0467 g, 0.224 mmol) and aminopropyl silane (APS) (0.0500 mL, 0.0513 g, 0.286 mmol) was added to the microspheres and the mixture was heated to 50 °C and stirred for 2 hours under an atmosphere of nitrogen. The resultant microspheres were centrifuged (9700 rpm, 13 minutes), the supernatant was decanted and the microspheres were resuspended in water (10.0 mL) by ultrasonication and centrifuged again. This washing procedure was repeated once more with water (10.0 mL) to leave the microspheres suspended in water (10.0 mL).

Yield: 0.0240 g, 48 % by mass

The procedure above was repeated with different solvents and QDs, the details for which are listed in Table 23:

Table 23: Silica shelling conditions for CFQD-microspheres and CdQD-microspheres

Type of QD	Silica shelling conditions	
	Mass of microspheres **6** (g)	Solvents used
CFQDs	0.050	Methanol
CFQDs	0.050	Toluene
CFQDs	0.005	Absolute ethanol
CFQDs	0.020	Absolute ethanol
CFQDs	0.050	Isopropanol
CdQDs	0.050	Water

4.4.4. Coating of thiol-functionalised microspheres **6** with PVDC[111, 112]

A suspension of thiol-functionalised microspheres **6** (0.200 g) was centrifuged (9500 rpm, 13 minutes), the supernatant was decanted and the microspheres were resuspended in THF (20.0 mL) and centrifuged again. This washing procedure was repeated again with THF (20.0 mL). The microspheres were then resuspended in a solution of poly(vinylidene chloride-*co*-acrylonitrile) (1.000 g) in THF (20.0 mL) by ultrasonication. This suspension was heated to 40 °C and stirred for 1 hour under an atmosphere of nitrogen. The reaction mixture was then slowly cooled to 0 °C. Water, which acts as a hardening agent, (30.0 mL) was added, and stirred for a further 1 hour. The microspheres were centrifuged (6000 rpm, 10 minutes), the supernatant was decanted and the microspheres were resuspended in acetonitrile (20.0 mL) and centrifuged again. This washing procedure was repeated once more with acetonitrile (20.0 mL) to leave microspheres suspended in acetonitrile (20.0 mL).

This procedure was repeated using different reaction conditions, described in Table 24:

Table 24: Reaction conditions for PVDC coating of microspheres

Type of microsphere	Mass of microspheres (g)	Mass of PVDC (g)	Hardening agent	Volume of hardening agent (mL)	Volume of MeCN wash (mL)
Thiol **6**	0.200	1.00	H_2O	30.0	20.0
Thiol **6**	0.200	0.50	H_2O	30.0	20.0
Thiol **6**	0.200	2.00	H_2O	8.50	20.0
Thiol **6**	0.200	0.50	H_2O	22.0	20.0
Thiol **6**	0.200	0.25	H_2O	44.0	20.0
Thiol **6**	0.200	2.00	H_2O	8.50	20.0
Thiol **6**	0.200	2.00	H_2O	7.00	20.0
Thiol **6**	0.200	2.00	H_2O	7.00	20.0
Thiouronium **5**	0.100	0.21	H_2O	5.00	10.0
Thiouronium **5**	0.100	0.21	H_2O	0.60	10.0
Thiouronium **5**	0.100	0.21	H_2O	0.32	10.0
Thiouronium **5**	0.100	0.21	H_2O	5.00	10.0
Thiouronium **5**	0.100	0.21	H_2O	0.72	10.0
CdQD-thiol **7**	0.100	0.21	H_2O	5.00	10.0
CdQD-thiol **7**	0.100	0.21	H_2O	0.42	10.0
CdQD-thiol **7**	0.100	0.21	H_2O	5.00	10.0
CdQD-thiol **7**	0.100	0.21	H_2O	5.00	10.0
CdQD-thiol **7**	0.100	0.21	H_2O	0.20	10.0
CdQD-thiol **7**	0.100	0.21	H_2O	0.72	10.0
CdQDs	0.004	0.21	H_2O	0.42	1.00

4.5. Red blood cell assays

4.5.1. Internalisation of polymer microspheres into red blood cells (RBCs)

QD-microspheres **7** (3.00×10^{-3} g mL^{-1}, 0.200 mL) suspended in phosphate buffered saline (PBS) by ultrasonication were added to a suspension of RBCs in PBS (0.100 mL) at a haematocrit of 40 %. The microspheres and cells were then incubated in 24-well plates for 24 hours, to allow the process of beadfection to take effect.

4.5.2. Effect of QD-microspheres **7** on haemolysis levels

QD-microspheres **7** (3.00×10^{-3} g mL^{-1}, 0.200 mL) suspended in PBS by ultrasonication, were incubated with a suspension of RBCs in PBS (1:1, 0.200 mL) at a haematocrit of 40 %. A control which consisted of RBCs in PBS (1:1, 0.200 mL) was also incubated. An aliquot of each sample (0.045 mL) was extracted and centrifuged (4000 rpm, 5 minutes) after 1.5, 19.5, 26.5, 43.5, 50.5, 69.0, 73.5 and 80.0 hours. The supernatant from the aliquot was decanted and analysed for the presence of plasma free haemoglobin (pfHb). The level of pfHb was assessed using the Harboe assay[126]. This involved the measurement of the absorbance of light at a wavelength of 380, 415 and 450 nm using a 2800 UV/Vis Spectrophotometer (Cole Palmer).

4.5.3. Effect of haemoglobin on the fluorescence of QDs

QDs (3.00×10^{-3} g mL^{-1}) (these QDs were Qdot 655 ITK organic quantum dots purchased from Invitrogen) and QD-microspheres **7** (3.00×10^{-3} g mL^{-1}) were incubated with either RBCs or haemoglobin (Hb) in 1:1 ratio as described in Table 25. RBCs were lysed by dilution with distilled water which caused the release of Hb. The samples were transferred into a black 96-well plate and the fluorescence was analysed on a fluorescent plate reader, Spectramax Gemini XS (Molecular Devices, Berkshire, UK), at an excitation wavelength of 550 nm and emission wavelength of 610 nm for QD-microspheres **7** and an excitation wavelength of 500 nm and emission wavelength of 655 nm for the QDs.

Table 25: Volumes of QD-microspheres **7**, QDs, RBCs and Hb each suspended in PBS, used to assess the effect of Hb on QD fluorescence

Sample	QDs in PBS / mL	QD-microspheres **7** in PBS / mL	RBCs in PBS / mL	Hb in PBS / mL
1	-	0.200	-	-
2	-	0.200	0.200	-
3	-	0.200	-	0.200
4	0.200	-	-	-
5	0.200	-	0.200	-
6	0.200	-	-	0.200

4.6. Layer-by-layer coating of polymer microspheres

4.6.1. Bilayer coating of QD-microspheres **7**[118]

QD-microspheres **7** (2.10×10^{-3} g) were suspended in branched polyethyleneimine (PEI) solution (0.500 mL, 0.100 wt %, pH 10) by ultrasonication (5 minutes) and then centrifuged (13, 200 rpm, 2 minutes). The supernatant was decanted and the microspheres were resuspended in deionised water (0.500 mL) for 30 seconds and centrifuged again. The supernatant was decanted and the microspheres obtained by centrifugation were then dried with a stream of air for 1 minute. The above suspension/drying procedure was repeated again with polyacrylic acid (PAA) solution (0.500 mL, 0.200 wt %, pH 4) to complete the addition of one bilayer. This cycle was repeated using 1 minute suspension times for the polymer deposition stage.

This reaction was repeated with the reaction conditions described in Table 26.

Table 26: Different quantities of microspheres and bilayers used in layer-by-layer coating

Type of microsphere	Mass of microsphere (g)	Number of bilayers
Thiol **6**	0.0200	1
Thiol **6**	7.50×10^{-3}	4

4.6.2. Coating of thiol-functionalised microspheres 6 with branched PEI[118]

Thiol-functionalised microspheres **6** (7.50×10^{-3} g) were suspended in branched PEI solution (0.500 mL, 0.100 wt %, pH 10) by ultrasonication (5 minutes) and then centrifuged (13, 200 rpm, 2 minutes). The supernatant was decanted and the microspheres were resuspended in deionised water (0.500 mL) for 30 seconds and centrifuged again. The supernatant was decanted and the microspheres obtained by centrifugation were then dried with a stream of air for 1 minute before being resuspended in deionised water (0.500 mL).

Zeta Potential: +44.39 mV

4.6.3. Coating of thiol-functionalised microspheres 6 with PAA[118]

Thiol-functionalised microspheres **6** (7.50×10^{-3} g) were suspended in PAA solution (0.500 mL, 0.200 wt %, pH 4) by ultrasonication (5 minutes) and then centrifuged (13, 200 rpm, 2 minutes). The supernatant was decanted and the microspheres were resuspended in deionised water (0.500 mL) for 30 seconds then centrifuged again. The supernatant was decanted and the resulting pellet of microspheres obtained from centrifugation was dried with a stream of air for 1 minute before being resuspended in deionised water (0.500 mL).

Zeta Potential: −24.78 mV

4.7 Fluorescent labelling of microspheres

4.7.1. Synthesis of thiol-core, carboxyl-shelled microspheres 10 by seeded emulsion polymerisation[64]

A suspension of thiol-functionalised microspheres **6** (1.00 g) was centrifuged (9700 rpm, 13 minutes), the supernatant was decanted and the microspheres were resuspended in a solution of SDS (0.0400 g, 0.139 mmol) in water (48.0 mL). A solution of AIBN (0.0200 g, 0.122 mmol) in styrene **3** (1.54 mL, 1.40 g, 13.4 mmol), DVB **4** (0.109 mL, 0.0996 g, 0.765 mmol), methacrylic acid **9** (0.591 mL, 0.600 g, 7.00 mmol) and *n*-hexadecane (0.258 mL, 0.199 g, 0.879 mmol) was added to this polymer suspension and the resulting mixture was degassed for 30 minutes, whilst stirring. This mixture was then heated to 70 °C and stirred for 5 hours under an

atmosphere of nitrogen. The resultant microspheres were centrifuged (7000 rpm, 10 minutes), the supernatant was decanted and the microspheres were resuspended in water (30.0 mL) by ultrasonication and centrifuged again. This washing procedure was repeated once more with water (30.0 mL), twice with methanol (30.0 mL) and twice again with water (30.0 mL) to leave the microspheres suspended in water (30.0 mL).

Yield: 0.805 g, 24 % by mass

Average diameter: 0.9 μm (standard deviation = 0.4 μm)

Combustion analysis: Carbon 88.14 %, Hydrogen 7.79 %, Nitrogen 0.26 %, Oxygen 3.71 %, Sulphur <0.10 %

Zeta potential: −74.84 mV

This reaction was repeated with DY-405 labelled, thiouronium-functionalised microspheres in place of thiol-functionalised microspheres **6**.

4.7.2. Labelling of thiol-functionalised microspheres **6** with maleimide-functionalised fluorescent dyes[59, 105]

A suspension of thiol-functionalised microspheres **6** (0.0100 g) was centrifuged (13, 200 rpm, 2 minutes), the supernatant was decanted and the microspheres were resuspended in DMF (1.00 mL) and centrifuged again. This washing procedure was repeated twice with DMF (1.00 mL), to leave the microspheres suspended in DMF (1.00 mL). A solution of maleimide-functionalised fluorescent dye in DMF (0.0500 mL, 1.00×10^{-3} g mL^{-1}) was added to the microsphere suspension, which was then shaken on a shaker plate for 16 hours at room temperature. The resultant microspheres were centrifuged (13, 200 rpm, 2 minutes), the supernatant was decanted, and the microspheres were resuspended in DMF (1.00 mL) and centrifuged again. This washing procedure was repeated three more times with DMF (1.00 mL) and twice with water (1.00 mL) to leave the microspheres **11** suspended in water (1.00 mL).

The above procedure was also repeated using different maleimide-functionalised fluorescent dyes, listed in Table 27.

Table 27: Maleimide-functionalised fluorescent dyes used in procedure 4.7.2

Maleimide-functionalised fluorescent dye
Texas Red maleimide
PyMPO maleimide
Alexa Fluor 546 maleimide
Pacific Blue maleimide
Fluorescein diacetate maleimide
DY-405 maleimide

4.7.3. Labelling of thiol-core, carboxyl-shelled microspheres **10** with maleimide-functionalised dyes[105]

A suspension of thiol-core, carboxyl-shelled microspheres **10** (0.0100 g) was centrifuged (13, 200 rpm, 2 minutes), the supernatant was decanted, and the microspheres were resuspended in DMF (1.00 mL) and centrifuged again. This washing procedure was repeated twice, to leave the microspheres suspended in DMF (1.00 mL). A solution of fluorescent dye in DMF (0.0500 mL, 1.00×10^{-3} g mL^{-1}) was added to the microsphere suspension, which was then shaken on a shaker plate for 16 hours at room temperature. The resultant microspheres were centrifuged (13, 200 rpm, 2 minutes), the supernatant was decanted and the microspheres were resuspended in DMF (1.00 mL) and centrifuged again. This washing procedure was repeated three more times with DMF (1.00 mL) and twice with water (1.00 mL) to leave the microspheres suspended in water (1.00 mL).

The fluorescent dyes used in the above procedure were Alexa Fluor 546 maleimide, Pacific Blue maleimide and perylene.

4.7.4. Fmoc loading assay for thiol-core, carboxyl-shelled microspheres **10**[105]

A suspension of thiol-core, carboxyl-shelled microspheres **10** (0.0100 g) was centrifuged (13, 200 rpm, 2 minutes), the supernatant was decanted and the microspheres were resuspended in DMF (1.00 mL) by ultrasonication and centrifuged again. This washing procedure was repeated once more with DMF (1.00 mL). The microspheres were then resuspended in a solution of Fmoc-diaminopropyl hydrochloride **12** (0.0113 g, 0.0390 mmol) and TBTU (0.0130 g, 0.0405 mmol) in *N-N*-di*iso*propylethylamine (0.0130 mL, 9.65×10^{-3} g, 0.0747 mmol) and DMF (1 mL).

This mixture was shaken on a shaker plate for 1 hour at room temperature. The microspheres were then centrifuged (13, 200 rpm, 2 minutes), the supernatant was decanted and the microspheres were resuspended in DMF (1.00 mL) by ultrasonication and centrifuged again. This washing procedure was repeated with DMF (1.00 mL × 5) and methanol (1.00 mL × 2). The microspheres were then dried *in vacuo* to determine the mass of the microspheres remaining. Once dried, the microspheres were resuspended in DMF (1.00 mL) to which 1,8-diazabicyclo [5.4.0] undec-7-ene (DBU) (0.0200 mL, 0.0200 g, 0.134 mmol) was added. This mixture was shaken on a shaker plate for 20 minutes at room temperature. The microspheres were then transferred to a volumetric flask, diluted to 5.00 mL with acetonitrile and centrifuged (8000 rpm, 15 minutes). The supernatant was collected, placed in a cuvette and analysed with a UV spectrophotometer. UV signals corresponding to the absorbance of the cleaved fulvene **15** adduct at 294 nm and 304 nm were observed and quantified.

4.7.5. DBU-mediated cleavage of Fmoc-diaminopropyl hydrochloride **12** for the Fmoc loading assay[105]

A solution of Fmoc-diaminopropyl hydrochloride **12** (0.0100 g, 0.0300 mmol) in DBU (0.0400 mL, 0.0407 g, 0.267 mmol) and DMF (2.00 mL) was shaken on a shaker plate for 20 minutes at room temperature. The solution was then transferred to a volumetric flask and diluted to 10.0 mL with acetonitrile. Four serial dilutions were carried out using 5.00 mL of the preceding solution and diluting with acetonitrile (5.00 mL). A background solution of DBU (0.0400 mL, 0.0407 g, 0.267 mmol) in DMF (2.00 mL), diluted to 10.0 mL with acetonitrile, in a volumetric flask, was also prepared. For each dilution, absorbance at 294 nm and 304 nm was measured on a UV/Vis spectrophotometer against the reference sample (background solution). The absorbance was then plotted against the concentration of the solution to produce a calibration curve with a gradient which corresponded to the extinction coefficient, ε, for that particular wavelength. The carboxyl loading of the microspheres could then be quantified by the following equation:

Carboxyl loading (mmol g^{-1}) = $\dfrac{[(\text{Absorbance of sample}/\varepsilon)*\text{volume of sample}]}{\text{mass of microspheres}}$

4.7.6. Synthesis of *S*-trityl cysteamine **18**[133]

Trifluoroacetic acid (TFA) (1.60 mL, 2.46 g, 21.5 mmol) was added to a solution of cysteamine hydrochloride **16** (1.05 g, 9.30 × 10^{-3} mmol) and trityl chloride **17** (2.23 g, 8.00 × 10^{-3} mmol) in freshly distilled DCM (4.00 mL). This solution was stirred for 2 hours at room temperature, under an atmosphere of nitrogen. The reaction was quenched with sodium hydroxide solution (1 M, 12.0 mL); the resulting slurry was extracted with ethyl acetate (40.0 mL) and washed with brine (20.0 mL × 3), followed by a mixture of brine and 1 M sodium hydroxide solution (2:1, 150 mL × 2). The organic layer was then dried over anhydrous sodium sulfate, filtered and concentrated under reduced pressure to yield a yellow oil which was dried *in vacuo* to form a beige solid (1.84 g, 5.76 mmol, 32 %). This product was used without any need for further purification.

Yield: 1.84 g, 5.76 mmol, 32 %

IR (KBr disc): 4044 (w), 3376 (w, N-H stretch), 3052 (w, C-H aromatic), 2925 (w, C-H aliphatic), 1958 (w), 1898 (w), 1811 (w), 1734 (w), 1722 (w), 1591 (w, C=C aromatic), 1484 (m), 1440 (m), 1179 (w), 1077 (w), 1033 (w), 850 (w, C-H aromatic bend), 743 (m, C-H aromatic bend), 700 (m, C-H aromatic bend), 625 (m)

^{1}H NMR (300 MHz, CDCl$_3$): δH 2.320 (t, 2H, CH$_2$, *J* = 13.0), 2.598 (d, 2H, CH$_2$, *J* = 13.055), 7.204 (m, 9H, CH), 7.303 (d, 6H, CH, *J* = 8.164)

^{13}C NMR (75 MHz, CDCl$_3$, PENDANT): δC 36.398 (s, CH$_2$), 41.140 (s, CH$_2$), 66.593 (s, C) 126.711 (s, CH), 127.928 (s, CH), 129.653 (s, CH), 144.953 (s, C)

MS (ESI-): m/z 322 (100 %, [M + H]$^+$), calculated 319

4.7.7. Attempted coupling of *S*-trityl cysteamine **18** to thiol-core, carboxyl-shelled microspheres **10** and subsequent detritylation of trityl protecting group

A suspension of thiol-core, carboxyl-shelled microspheres **10** (0.0100 g) was centrifuged (13, 200 rpm, 2 minutes), the supernatant was decanted and the microspheres were resuspended in DMF (1.00 mL) by ultrasonication and centrifuged again. This washing procedure was repeated once more with DMF (1.00 mL). The microspheres were then resuspended in a solution of *S*-trityl cysteamine **18** (0.100 g, 0.156 mmol) and TBTU (0.0554 g, 0.172 mmol) in *N-N*-di*iso*propylethylamine (0.0273 mL, 0.0203 g, 0.157 mmol) and DMF (1.00 mL). This mixture was shaken on a shaker plate for 1 hour at room temperature. The microspheres were then

centrifuged (13, 200 rpm, 2 minutes), the supernatant was decanted and the microspheres were resuspended in DMF (1.00 mL) by ultrasonication and centrifuged again. This washing procedure was repeated with DMF (1.00 mL × 5) and methanol (1.00 mL × 2) to leave the microspheres suspended in DMF (1.00 mL). TFA (0.0300 mL, 0.0461 g, 0.404 mmol) was added to the microspheres and this suspension was shaken on the shaker plate for 1 hour at room temperature. The microspheres were then centrifuged, the supernatant was decanted and the microspheres were resuspended in DMF (1.00 mL) by ultrasonication and centrifuged again. This washing procedure was repeated with DMF (1.00 mL × 4) to leave the microspheres **20** in DMF (1.00 mL).

4.7.8. Labelling of modified thiol-core, carboxyl-shelled microspheres **20** with maleimide-functionalised dye

A solution of maleimide-functionalised dye (0.0500 mL, 1.00×10^{-3} g mL^{-1}) in DMF was added to the modified thiol-core, carboxyl-shelled microspheres **20** (0.0100 g) which were suspended in DMF (1.00 mL). This suspension was shaken on a shaker plate for 16 hours at room temperature. The microspheres were then centrifuged (13, 200 rpm, 2 minutes), the supernatant was decanted and the microspheres were resuspended in DMF (1.00 mL) by ultrasonication and centrifuged again. This washing procedure was repeated with DMF (1.00 mL × 3) and water (1.00 mL × 2) to leave the microspheres suspended in water (1.00 mL).

4.7.9. Synthesis of *N*-acetyl, *S*-trityl cysteamine **22**

A solution of *S*-trityl cysteamine **18** (0.100 g, 0.313 mmol) and TBTU (0.111 g, 0.344 mmol) in *N-N*-di*iso*propylethylamine (0.273 mL, 0.202 g, 1.57 mmol), acetic acid **21** (0.0358 mL, 0.0376 g, 0.626 mmol) and DMF (5.00 mL) was stirred for 2 hours at room temperature, under an atmosphere of nitrogen. The reaction was quenched with a mixture of brine and 1 M sodium hydroxide solution (1:1, 100 mL) and the crude product was extracted with diethyl ether (50.0 mL). The organic layer was washed with a mixture of brine and citric acid (1 M, 100 mL), followed by brine (100 mL × 5). The organic layer was then dried over anhydrous sodium sulfate, filtered and concentrated under reduced pressure to yield a white crystalline solid (0.0245 g, 0.0679 mmol, 22 %).

Yield: 0.0245 g, 0.0679 mmol, 22 %

IR (KBr disc): 4051 (w), 3275 (m, N-H stretch), 3059 (w, C-H aromatic stretch), 2926 (w, C-H aliphatic), 2361 (w), 1954 (w), 1810 (w), 1636 (m, C=O), 1549 (m, C=C aromatic), 1487 (m), 1443 (m), 1373 (w), 1295 (m), 1185 (w), 1033 (w), 859 (w, C-H aromatic bend), 746 (m, C-H aromatic bend), 700 (m, C-H aromatic bend), 619 (w)

^{1}H NMR (300 MHz, CDCl$_3$): δH 1.886 (s, 3H, CH$_3$), 2.316 (d, 2H, CH$_2$, J = 14.0), 3.024 (d, 2H, CH$_2$, 14.1), 7.205 (m, 9H, CH), 7.325 (d, 6H, CH, J = 7.9)

^{13}C NMR (75 MHz, CDCl$_3$, PENDANT): δC 23.328 (s, CH$_3$), 32.022 (s, CH$_2$), 38.246 (s, CH$_2$), 66.914 (s, C), 126.911 (s, CH), 128.075 (s, CH), 129.565 (s, CH), 144.657 (s, C), 169.854 (s, C=O)

4.7.10. Synthesis of 4-vinylbenzylamine hydrochloride (4-VBAH) **23**[134]

A solution of sodium azide (0.426 g, 6.57 mmol) in 4-VBC **1** (0.462 mL, 0.500 g, 3.28 mmol) and DMF (8.33 mL) was stirred for 1 hour at room temperature. Water (30.0 mL) was then added to the reaction mixture and the crude product was extracted with diethyl ether (30.0 mL). This organic layer was washed with brine (30.0 mL) and dried over anhydrous magnesium sulfate, filtered and concentrated under reduced pressure to yield a brown oil. A solution of triphenylphosphine (1.29 g, 4.92 mmol) in benzene (3.30 mL, 5.78 g, 74.0 mmol) and water (8.30 mL) was added to this oil and the resultant mixture was heated to 70 °C and stirred for 3 hours under an atmosphere of nitrogen. The reaction was quenched with dilute hydrochloric acid (2 M, 50.0 mL) and any organic impurities were extracted with DCM (50.0 mL). Sodium hydroxide solution (2 M, 50.0 mL) was added to the aqueous layer, to which DCM (50.0 mL) was also added, to extract the product. This organic layer was then dried over anhydrous magnesium sulfate, filtered and concentrated under reduced pressure to yield an oil which was subsequently dissolved in diethyl ether (10.0 mL). The product was then precipitated out of diethyl ether with concentrated hydrochloric acid. The resulting precipitate was filtered and dried *in vacuo* to yield a white solid (0.153 g, 0.904 mmol, 28 %)

Yield: 0.153 g, 0.904 mmol, 28 %

IR (KBr disc): 3003 (s, C-H aromatic stretch), 2755 (m), 2576 (m), 2352 (m), 2047 (m), 1919 (m), 1811 (m), 1627 (m, C=C vinyl), 1598 (s, C=C aromatic), 1514 (m, C=C aromatic), 1479 (s), 1465 (m), 1407 (m), 1383 (m), 1220 (m), 1117 (m), 1083 (m), 988 (m), 970 (m), 900 (s), 880 (m), 847 (s), 712 (w), 646 (w)

^{1}H NMR (300 MHz, DMSO): δH 4.000 (s, 2H, CH$_2$), 5.281 (d, 1H, CH, J = 11.015), 5.854 (d, 1H, CH, J = 17.6), 6.700 (dd, 1H, CH, J = 11.0 and J = 11.0), 7.471 (d, 2H, CH, J = 8.2), 7.5364 (d, 2H, CH, J = 8.3)

^{13}C NMR (75 MHz, DMSO, PENDANT): δC 42.313 (s, CH$_2$), 115.465 (s, CH$_2$), 126.713 (s, CH), 129.741 (s, CH), 134.155 (s, C), 136.573 (s, CH), 137.667 (s, C)

MS (EI+): m/z 133 (100 %, [M - HCl]$^+$), calculated 133.193 for C$_9$H$_{11}$N

4.7.11. Synthesis of amino-functionalised microspheres **24** by dispersion polymerisation

A solution of AIBN (8.61 × 10^{-3} g, 0.0524 mmol) in styrene **3** (0.600 mL, 0.545 g, 5.20 × 10^{-3} mmol) and DVB **4** (7.46 × 10^{-3} mL, 6.82 × 10^{-3} g, 0.0524 mmol) was added to a solution of PVP (0.06078 g, 1.05 × 10^{-3} mmol) and 4-VBAH **23** (4.45 × 10^{-3} g, 0.0262 mmol) in absolute ethanol (5.00 mL). This mixture was degassed with nitrogen at room temperature for 30 minutes. The reaction mixture was then heated to 70 °C and stirred for 16 hours under an atmosphere of nitrogen. Once cooled, the resultant polymer microspheres were centrifuged (7000 rpm, 10 minutes). The supernatant was decanted and the microspheres were resuspended in methanol (5.00 mL) by ultrasonication and centrifuged again. This washing procedure was repeated again with methanol (5.00 mL) and twice with water (5.00 mL). Finally, the microspheres were resuspended in water (5.00 mL) by ultrasonication.

Yield: 0.200 g, 40 % by mass

Average diameter: 2.2 μm (standard deviation = 4.2 μm)

4.7.12. Coupling of Fmoc-*S*-trityl-*L*-cysteine **25** to amino-functionalised microspheres **24**

A suspension of amino-functionalised microspheres **24** (5.00 × 10^{-3} g) was centrifuged (13, 200 rpm, 2 minutes), the supernatant was decanted and the microspheres were resuspended in DMF (1.00 mL) by ultrasonication and centrifuged again. This washing procedure was repeated once more with DMF (1.00 mL). The microspheres were then resuspended in a solution of Fmoc-*S*-trityl-*L*-cysteine **25** (0.0250 g, 0.0430 mmol) and TBTU (0.0158 g, 0.0460 mmol) in *N*-*N*-di*iso*propylethylamine

(7.49 × 10^{-3} mL, 5.56 × 10^{-3} g, 0.0430 mmol) and DMF (1.00 mL). This mixture was shaken on a shaker plate for 1 hour at room temperature. The microspheres were then centrifuged (13, 200 rpm, 2 minutes), the supernatant was decanted and the microspheres were resuspended in DMF (1.00 mL) by ultrasonication and centrifuged again. This washing procedure was repeated with DMF (1.00 mL × 5) and methanol (1.00 mL × 2) to leave the microspheres suspended in DMF (1.00 mL). TFA (0.015 mL, 0.0230 g, 0.202 mmol) was then added to the microspheres and this mixture was shaken on the shaker plate for 1 hour at room temperature. The microspheres were then centrifuged, the supernatant was decanted and the microspheres were resuspended in DMF (1.00 mL) by ultrasonication and centrifuged again. This washing procedure was repeated with DMF (1.00 mL × 4) to leave the microspheres **26** in DMF (1.00 mL).

4.7.13. Labelling of modified amino-functionalised microspheres **26** with maleimide-functionalised dye

A solution of maleimide-functionalised dye (0.0250 mL, 1.00 × 10^{-3} g mL^{-1}) in DMF was added to the modified amino-functionalised microspheres **26** (5.00 × 10^{-3} g) which were suspended in DMF (0.500 mL). This suspension was shaken on a shaker plate for 16 hours at room temperature. The microspheres were then centrifuged (13, 200 rpm, 2 minutes), the supernatant was decanted and the microspheres were resuspended in DMF (0.500 mL) by ultrasonication and centrifuged again. This washing procedure was repeated with DMF (0.500 mL × 3) and water (0.500 mL × 2) to leave the microspheres **28** suspended in water (0.500 mL).

4.7.14. Labelling of amino-functionalised microspheres **24** with fluorescein isocyanate

A suspension of amino-functionalised microspheres **24** (0.0100 g) was centrifuged (13, 200 rpm, 2 minutes), the supernatant was decanted and the microspheres were resuspended in DMF (1.00 mL) and centrifuged again. This washing procedure was repeated twice to leave the microspheres suspended in DMF (1.00 mL). A solution of fluorescein isocyanate in DMF (0.0500 mL, 1.00 × 10^{-3} g mL^{-1}) was added to the microsphere suspension along with TMAOH (0.0500 mL, 0.0433 g, 0.475 mmol) and the resultant mixture was shaken on a shaker plate for 16 hours at room temperature. The microspheres were then centrifuged (13, 200 rpm, 2 minutes), the supernatant was decanted and the microspheres were resuspended in DMF (1.00 mL) and centrifuged again. This washing procedure was repeated three more times with DMF

(1.00 mL) and twice with water (1.00 mL) to leave the microspheres suspended in water (1.00 mL).

4.7.15. Synthesis of fluorescent crosslinked polystyrene microspheres **29** by emulsion polymerisation

A solution of SDS (0.317 g, 0.110 mmol) in water (10.0 mL) was combined with a solution of potassium persulfate (0.0400 g, 0.147 mmol) in water (2.00 mL) and added to a solution of perylene (1.00 × 10^{-3} g, 3.69 × 10^{-3} mmol) in styrene **3** (2.52 mL, 2.29 g, 219 mmol) and DVB **4** (1.09 mL, 0.996 g, 7.65 mmol). The resultant mixture was sonicated with an ultrasonic processor (75 % amplitude, 0.5 cycle, 2 × 10 repetitions), then degassed with nitrogen for 30 minutes, whilst stirring. This mixture was then heated to 70 °C and stirred for 16 hours under an atmosphere of nitrogen. The resultant microspheres were centrifuged (7000 rpm, 10 minutes), the supernatant was decanted and the microspheres were resuspended in water (30.0 mL) by ultrasonication and centrifuged again. This washing procedure was repeated once more with water (30.0 mL), twice with methanol (30.0 mL) and twice again with water (30.0 mL) to leave the microspheres suspended in water (30.0 mL).

Yield: 0.390 g, 12 % by mass

Average diameter: 1.5 μm (standard deviation = 1.2 μm)

4.7.16. Synthesis of chloromethyl-functionalised polystyrene microspheres **30** by suspension polymerisation[135]

A solution of AIBN (0.700 g, 4.26 mmol) in styrene **3** (63 mL, 57.3 g, 550 mmol), DVB **4** (2.30 mL, 2.10 g, 16.1 mmol) and 4-VBC **1** (9.90 mL, 10.7 g, 70.3 mmol) was degassed for 40 minutes, and added to an aqueous solution of PVA (1 %, 700 mL) which had been degassed with nitrogen for one hour. This resultant mixture was stirred at 1080 rpm for 10 minutes, before the temperature was increased to 72 °C and stirred for 16 hours under an atmosphere of nitrogen. Once cooled, the resultant polymer microspheres were washed with a large volume of distilled water until the effluent was clear. The polymer microspheres were then washed with distilled water (600 mL × 2), methanol (600 mL), methanol/THF (600 mL, 1:1), THF (600 mL), methanol/THF (600 mL, 1:1) and finally methanol (600 mL). The polymer microspheres were dried under vacuum for 2 hours, then extracted with 1,4-dioxane for 16 hours. The microspheres were then washed with methanol/THF (600 mL, 1:1)

and methanol (600 mL), after which the microspheres were dried under reduced pressure to a constant mass. The dried polymer microspheres were sieved with a sieve shaker to yield polymer microspheres ranging from <38-212 μm in diameter.

Yield: <38 μm (1.81 g, 3 % by mass), 38-212 μm (22.6 g, 32 % by mass)

4.7.17. Labelling of chloromethyl-functionalised polystyrene microspheres **30** with perylene

Chloromethyl-functionalised polystyrene microspheres **30** (0.0100 g) were suspended in a solution of perylene in DMF (1.00×10^{-3} g mL^{-1} in 1.00 mL). This suspension was shaken on a shaker plate for 4 hours at room temperature. The microspheres were then centrifuged (13, 200 rpm, 2 minutes), the supernatant was decanted; the microspheres were resuspended in DMF (1.00 mL) and centrifuged again. This washing procedure was repeated twice more with DMF (1.00 mL), twice with water (1.00 mL) and twice with PBS (1.00 mL) to leave the fluorescent chloromethyl-functionalised polystyrene microspheres **31** suspended in PBS (1.00 mL).

4.8 Interaction of titanium dioxide with functionalised polymeric material

4.8.1. Synthesis of thiouronium-functionalised polystyrene **32** by bulk polymerisation

A solution of 4-VBTU **2** (0.120 g, 0.524 mmol) and AIBN (0.0600 g, 0.360 mmol) in styrene **3** (3.00 mL, 2.72 g, 26.2 mmol) and DVB **4** (0.112 mL, 0.102 g, 0.786 mmol) was degassed with nitrogen at room temperature for 15 minutes, whilst stirring. The reaction mixture was then heated to 70 °C and stirred for 16 hours under an atmosphere of nitrogen to yield a hard, cloudy polymer **32** (1.81 g, 60 % by mass).

The above polymerisation was repeated with methyl methacrylate **33** to yield thiouronium-functionalised polymethyl methacrylate **34**. The % molar ratio of the monomers can be found in Table 15 below.

Table 15: Monomer composition of polymers formed by bulk polymerisation

Polymer	Functional monomer / mol %			
	MMA **33**	Styrene **3**	4-VBTU **2**	DVB **4**
32	-	96	2	2
34	93	-	5	2

4.8.2. Synthesis of porogenic polymethyl methacrylate 35

Methanol (1.18 mL, 0.933 g, 29.1 mmol) was added to a solution of AIBN (0.0600 g, 0.360 mmol) in methyl methacrylate **34** (3.00 mL, 2.82 g, 28.2 mmol) and DVB **4** (0.0780 mL, 0.0730 g, 0.564 mmol). This mixture was degassed with nitrogen at room temperature for 15 minutes, whilst stirring. The reaction mixture was then heated to 70 °C and stirred for 16 hours under an atmosphere of nitrogen to yield polymer **35** (2.54 g, 65 % by mass).

4.8.3. Synthesis of porogenic thiouronium-functionalised polymethyl methacrylate 36

Methanol (1.24 mL, 0.978 g, 30.5 mmol) was added to a solution of 4-VBTU **2** (0.323 g, 1.41 mmol) and AIBN (0.0600 g, 0.360 mmol) in methyl methacrylate **34** (3.00 mL, 2.82 g, 28.2 mmol) and DVB **4** (0.0780 mL, 0.0730 g, 0.564 mmol). This mixture was degassed with nitrogen at room temperature for 15 minutes, whilst stirring. The reaction mixture was then heated to 70 °C and stirred for 16 hours under an atmosphere of nitrogen to yield polymer **36** (2.62 g, 62 % by mass).

This reaction was repeated with DMF in place of methanol to yield polymer **37**.

4.8.4. Milling of porogenic thiouronium-functionalised polymethyl methacrylate 36, followed by conversion to milled porogenic thiol-functionalised polymethyl methacrylate 38

Porogenic thiouronium-functionalised polymethyl methacrylate **36** (2.62 g) was broken down in small pieces (1-10 mm) using a coffee grinder. These pieces were then milled (400 rpm, 12 h) using a Planetary Micro Mill (Pulverisette 7 classic line).

The fine polymer particles obtained from milling were suspended in THF (6.00 mL) to which TMAOH (0.148 mL, 0.129 g, 1.41 mmol) was added. This suspension was shaken on a shaker plate for 16 hours at room temperature. The resultant polymer was centrifuged (500 rpm, 2 minutes), the supernatant was decanted and the polymer was resuspended in THF (30.0 mL) by ultrasonication and centrifuged again. This washing procedure was repeated once more with THF (30.0 mL) to yield a polymer **38** (1.89 g, 67 % by mass).

4.8.5. Interaction assay of milled porogenic thiol-functionalised polymethyl methacrylate **38** with titanium dioxide nanoparticles

Milled porogenic thiol-functionalised polymethyl methacrylate **38** (0.0150 g) was suspended in methanol (5.00 mL) by sonication with an ultrasonic processor (75 % amplitude, 0.5 cycle, 10 × 10 repetitions). The resultant mixture was centrifuged (6000 rpm, 10 minutes) to yield a cloudy suspension of polymer.

Titanium dioxide nanoparticles (0.0150 g) were suspended in methanol (5.00 mL) by sonication with an ultrasonic processor (75 % amplitude, 0.5 cycle, 10 × 10 repetitions). The resultant mixture was centrifuged (6000 rpm, 10 minutes) to yield a white, cloudy suspension of titanium dioxide nanoparticles.

The two suspensions were combined and sonicated in an ultrasonic bath for 10 minutes. The resultant mixture was centrifuged (6000 rpm, 10 minutes) to yield a cloudy suspension of polymer/titanium dioxide nanoparticles.

4.8.6. Synthesis of thiouronium-functionalised polystyrene **39** by bulk polymerisation

A solution of 4-VBTU **2** (0.0144 g, 0.0630 mmol) and AIBN (0.0600 g, 0.360 mmol) in styrene **3** (3.00 mL, 2.72 g, 26.2 mmol) was degassed with nitrogen at room temperature for 15 minutes, whilst stirring. The reaction mixture was then heated to 70 °C and stirred for 16 hours under an atmosphere of nitrogen to yield polymer **39** (1.72 g, 62 % by mass).

The above polymerisation was repeated with different quantities of 4-VBTU **2** listed in Table 29 below.

Table 29: Monomer composition of polymers formed by bulk polymerisation

Polymer	Styrene **3** (mol %)	4-VBTU **2** (mol %)
40	97	3
41	93	7
42	100	0

4.8.7. Spin-coating of polymer and interaction with titanium dioxide nanoparticles

A solution of thiouronium-functionalised polystyrene **39** in THF (0.400 mL, 0.100 w/v %) was applied to a sodium chloride plate and spun (1500 rpm, 9 seconds). The resultant polymer film was dipped into an ethanolic suspension of titanium dioxide nanoparticles (5.00 mL, 3.00×10^{-3} w/v %) for 30 seconds, then removed to dry for 2 minutes before analysis.

This procedure was also repeated with polymers **40-42**.

4.9. Attempted synthetic route to 4-vinyl catechol 43

4.9.1. First attempted synthesis of 4-vinyl catechol **43**[150]

Piperidine (2.00×10^{-3} mL, 2.32×10^{-3} g, 0.272 mmol) was added to a solution of 3,4-dihydroxybenzaldehyde **45** (1.01 g, 7.30 mmol) and malonic acid **46** (1.32 g, 12.8 mmol) in absolute ethanol (16.7 mL). The resultant mixture was refluxed for 6 hours whilst being stirred under an atmosphere of nitrogen. Water (167 mL) was added to the reaction and the product was extracted with diethyl ether (100 mL × 3). The combined organic extracts were dried over anhydrous magnesium sulfate, filtered and concentrated under reduced pressure to yield a dark brown oil. The crude product was then purified by flash column chromatography (80 % DCM, 20 % diethyl ether) to yield the product as a light brown oil (0.309 g, 2.20 mmol, 30 %).

Yield: 0.309 g, 2.20 mmol, 30 %

IR (thin film, NaCl plate): 3392 (m, O-H), 2978 (m, C-H aliphatic), 1605 (m, C=C aromatic), 1447 (m), 1266 m), 1194 (m), 1115 (w), 1046 (w), 975 (w), 878 (w), 816 (w), 739 (m)

^{1}H NMR (300 MHz, CD$_3$OD): δH 1.071, 1.236, 1.336, 2.010, 3.267, 3.646, 4.152, 4.989, 5.473 (d, 1H, CH, J = 17.527), 6.133 (d, 1H, CH, J = 15.937), 6.493 (dd, 1H, CH, J = 10.8 and J = 10.8), 6.608, 6.742, 6.42, 7.465, 7.519, 9.638

^{13}C NMR (75 MHz, CD$_3$OD, PENDANT): δC 13.332, 14.124, 14.259, 17.060, 22.631, 22.948, 57.023, 60.129, 63.265, 65.576, 77.577, 79.340, 109.465, 112.253 (s, CH$_2$), 112.807, 112.874, 113.764, 113.899, 114.313, 114.769,114.796, 114.876, 115.179 (s, CH), 117.589 (s, CH), 117.747, 118.376 (s, CH), 121.552 (s, CH), 121.615, 126.352, 126.446, 130.038 (s, C), 134.557, 135.232, 136.737 (s, C), 144.369,

144.511, 144.966, 145.021, 145.066, 145.136, 145.428 (s, C), 145.651 (s, C), 148.083, 148.184, 168.041, 169.844

4.9.2. Second attempted synthesis of 4-vinyl catechol **43**[150]

Tetramethylethylenediamine (0.450 mL, 0.347 g, 3.00 mmol) was added to a solution of malonic acid **46** (1.48 g, 14.3 mmol) and 3,4-dihydroxybenzaldehyde **45** (1.14 g, 8.25 mmol) in absolute ethanol (18.8 mL). The resultant mixture was refluxed for 6 hours whilst being stirred under an atmosphere of nitrogen. Water (167 mL) was added to the reaction, and the product was extracted with diethyl ether (100 mL × 3). The combined organic extracts were dried over anhydrous magnesium sulfate, filtered and concentrated under reduced pressure to yield a dark brown oil. The crude product was then purified by flash column chromatography (70 % hexane, 30 % ethyl acetate) to yield the product as a light brown oil (0.120 g, 0.882 mmol, 11 %).

Yield: 0.120 g, 0.882 mmol, 11 %

^{1}H NMR (300 MHz, CD$_3$OD): δH 1.121 (m, 2H), 1.929 (s, 0.22H), 3.996 (m, 0.27H), 4.182 (m, 0.6H), 6.137 (d, 1H, J = 15.8), 6.683 (m, 1.5H), 6.797 (m, 2H), 7.036 (s, 1H), 7.451 (d, 1H, J = 15.7), 9.604 (s, 0.30H)

4.9.3. Attempted silylation of 3,4-dihydroxybenzaldehyde **45**

A suspension of 3,4-dihydroxybenzaldehyde **45** (1.00 g, 7.24 mmol) in DCM (5.00 mL) was cooled to 0 °C. *Tert*-butyldimethylchlorosilane (TBDMS-Cl) (1.30 g, 8.64 mmol) and imidazole (1.47 g, 21.6 mmol) were added to this suspension, which was then allowed to warm to room temperature. This mixture was stirred for 5 hours under an atmosphere of nitrogen. The reaction was quenched by the addition of water (100 mL) and the crude product was extracted with DCM (100 mL × 2). The combined organic extracts were dried over anhydrous magnesium sulfate, filtered and concentrated under reduced pressure to yield a dark brown oil (2.58 g, 7.05 mmol, 98 %).

Yield: 2.58 g, 7.05 mmol, 98 %

IR (thin film, NaCl plate): 2931 (s, C-H aromatic), 2859 (s, C-H aliphatic), 1696 (s, C=O), 1592 (s, C=C aromatic), 1430 (m), 1390 (m), 1295 (s), 1256 (s), 1161 (m), 1124 (m), 993 (m), 902 (s), 841 (s), 801 (s), 783 (s)

^{1}H NMR (300 MHz, CDCl$_3$): δH 0.007, 0.022, 0.078, 0.088, 0.112, 0.149, 0.159, 0.170 (m, 12H) 0.782, 0.833, 0.841, 0.880, 0.897, 0.914, 0.916 (m, 18H,), 5.186, 6.404, 6.663, 6.670, 6.707, 6.735, 6.780, 6.786, 6.849, 6.863 (m, 1H, CH), 6.878, 6.953, 7.004, 7.267, 7.274, 7.281, 7.287, 7.295, 7.302 (m, 2H, CH), 7.544, 7.595, 9.723 (s, 1H, CO)

^{13}C NMR (75 MHz, CDCl$_3$, PENDANT): δC -4.010 (d, CH$_3$), 18.041, 18.433, 18.450 (d, C), 18.537, 25.680, 25.733, 25.795, 25.809, 25.825, 25.842 (d, CH$_3$), 25.886, 25.905, 25.933, 81.242, 117.056, 118.473, 118.843, 120.507 (d, CH), 120.823 (s, CH), 120.908, 121.891, 125.369 (s, CH), 129.272, 130.758 (s, C), 133.201, 135.234, 135.572, 146.970 (s, C), 147.674 (s, C), 153.343

4.9.4. Synthesis of 3,4-*bis*(*tert*-butyldimethylsilyl-oxy)benzaldehyde **47**[151]

A solution of 3,4-dihydroxybenzaldehyde **45** (3.00 g, 21.7 mmol) in DMF (15.0 mL) was added to a solution of TBDMS-Cl (7.85 g, 52.1 mmol) and imidazole (8.86 g, 130 mmol) in DMF (15.0 mL). The resultant mixture was stirred at room temperature for 16 hours under an atmosphere of nitrogen. The reaction mixture was quenched with the addition of brine (100 mL) and the product was extracted with ethyl acetate (100 mL). The organic extract was washed with brine (100 mL) a further four times and dried over anhydrous magnesium sulfate, filtered and concentrated under reduced pressure to yield a brown oil. This crude product was purified by flash column chromatography (90 % hexane, 10 % ethyl acetate) to yield the pure product as a golden yellow oil (4.25 g, 11.6 mmol, 54 %).

Yield: 4.25 g, 11.6 mmol, 54 %

IR (thin film, NaCl plate): 3697 (w), 3371 (w), 3067 (w, C-H aromatic), 2955 (s, C-H aliphatic), 2930 (s, C-H aliphatic), 2858 (s, C-H aliphatic), 2721 (w), 2595 (w), 2360 (w), 2341 (w), 1696 (s, C=O), 1592 (s, C=C aromatic), 1572 (s, C=C aromatic), 1508 (s, C=C aromatic), 1472 (m), 1430 (m), 1389 (m), 1362 (m), 1295 (s), 1254 (s), 1159 (m), 1123 (m), 994 (m), 980 (m), 901 (s), 840 (s), 783 (s), 735 (m), 706 (m), 694 (m), 668 (m)

^{1}H NMR (300 MHz, CDCl$_3$): δH 0.205 (d, 12H, CH$_3$, J = 6.1), 0.941 (d, 18H, CH$_3$, J = 0.8), 6.889 (d, 1H, CH, J = 8.6), 7.327 (m, 2H, CH), 9.752 (s, 1H, CO)

^{13}C NMR (75 MHz, CDCl$_3$, PENDANT): δC -4.085 (d, CH$_3$), 18.456 (d, C), 25.855 (d, CH$_3$), 120.553 (s, CH), 120.831 (s, CH), 125.360 (s, CH), 130.768 (s, C), 147.690 (s, C), 153.358 (s, C), 190.831 (s, C=O)

MS (ES+): m/z 389.1939 (100 %, [M + Na]$^+$), calculated 389.1944 for C$_{19}$H$_{34}$O$_3$Si$_2$Na

4.9.5. Attempted Wittig olefination of 3,4-*bis*(*tert*-butyldimethylsilyl-oxy)benzaldehyde 47[152]

n-Butyl lithium (0.250 mL, 0.173 g, 2.73 mmol) was added drop wise to a solution of methyltriphenylphosphonium bromide (0.990 g, 2.73 mmol) in THF (8.20 mL). The resultant yellow mixture was stirred under nitrogen for 15 minutes, followed by the slow addition of 3,4-*bis*(*tert*-butyldimethylsilyl-oxy)benzaldehyde 47 (1.00 g, 2.73 mmol). This mixture was then stirred for 2 hours at −78 °C under an atmosphere of nitrogen. The reaction mixture was allowed to warm to room temperature before being quenched by the addition of saturated ammonium chloride solution (100 mL) and the product was extracted with DCM (100 mL). The organic layer was dried over anhydrous magnesium sulfate, filtered and concentrated under reduced pressure to yield a white solid (0.433 g, 1.19 mmol, 44 %).

Yield: 0.433 g, 1.19 mmol, 44 %

IR (thin film, NaCl plate): 3292 (s), 3056 (s, C-H aromatic), 2954 (s, C-H aliphatic), 2928 (s, C-H aliphatic), 2855 (s, C-H aliphatic), 2714 (m), 2359 (w), 1969 (w), 1899 (w), 1820 (w), 1776 (w), 1683 (s, C=O), 1591 (s, C=C aromatic), 1512 (m, C=C aromatic), 1471 (m), 1419 (m), 1438 (s), 1361 (w), 1298 (s), 1254 (m), 1174 (s), 1123 (s), 1071 (m), 1028 (w), 997 (w), 885 (s), 834 (s), 771 (s), 742 (s), 714 (s), 694 (s)

^{1}H NMR (300 MHz, CDCl$_3$): δH 0.179 (d, 13H, CH$_3$, *J* = 6.7), 0.922 (s, 19H, CH$_3$), 3.238 (d, 11H, *J* = 13.6), 5.229 (s, 3H), 6.8332 (m, 4H), 7.304 (m, 3H), 7.711 (m, 56H), 9.731 (s, 1H, CO)

^{13}C NMR (75 MHz, CDCl$_3$, PENDANT): 15.217, 16.006, 16.982, 18.432, 57.883, 61.051, 101.573, 125.545, 126.628, 126.686, 128.136, 128.164, 128.287, 128.469, 128.562, 128.600, 128.621, 128.679, 128.759, 128.780, 128.795, 128.825, 129.013, 129.727, 130.402, 130.438, 130.533, 130.568, 130.890, 131.799, 131.835, 132.137, 133.194, 134.497, 136.362, 192.419 (s, C=O)

The above reaction was repeated with cyclohexanone 49 and benzaldehyde 50 in place of 3,4-bis(*tert*-butyldimethylsilyl-oxy)benzaldehyde 47.

4.9.6. Synthesis of trans-stilbene **53** by an alternative Wittig procedure[156]

Benzyltriphenylphosphonium chloride (3.89 g, 10.0 mmol) was stirred in DCM (7.5 mL) for 10 minutes, after which benzaldehyde **49** (1.02 mL, 1.01 g, 10.0 mmol) was added, followed by the addition of sodium hydroxide solution (25.0 g in 37.5 mL). This mixture was stirred vigorously for 40 minutes. Water (7.50 mL) was then added to the reaction mixture and the product was extracted with DCM (50.0 mL). The aqueous phase was extracted once more with DCM (20.0 mL) and the combined organic extracts were dried over anhydrous magnesium sulfate, filtered and concentrated under reduced pressure to yield a cream solid. This solid was triturated with hot petroleum ether (50.0 mL) and concentrated under reduced pressure to yield a cream solid which was then suspended in hot petroleum (12.5 mL). A crystal of iodine was added to this suspension which was refluxed for 30 minutes. Once cooled, the resultant mixture was washed with sodium metabisulfite solution (5 % w/v, 5.00 mL), and methanol (12.5 mL). Finally, the organic layer was dried over anhydrous magnesium sulfate, filtered and concentrated under reduced pressure to yield a white crystalline solid (0.0700 g, 0.388 mmol, 4 %).

IR (thin film, NaCl plate): 3054 (m, C-H aromatic), 3020 (m, C=C vinyl), 1949 (m), 1598 (m, C=C aromatic), 1493 (m), 1448 (m), 1118 (m), 1071 (m), 1028 (m), 960 (m), 924 (m), 779 (m), 763 (w), 693 (m)

^{1}H NMR (300 MHz, CDCl$_3$): δH 7.061 (s, 2H), 7.206 (t, 11H), 7.284 (t, 4H), 7.480 (d, 4H, J = 7.3)

^{13}C NMR (75 MHz, CDCl$_3$, PENDANT): δC 124.593 (s, CH), 126.706 (s, CH), 127.251 (s, CH), 127.746 (s, CH), 132.763 (s, C)

MS (EI+): m/z 180.0938 (100 %, [M]$^+$), calculated 180.0939 for C$_{14}$H$_{12}$

4.9.7. Attempted olefination of benzaldehyde **50** *via* alternative Wittig procedure[156]

Removal of benzoic acid from benzaldehyde

Benzaldehyde **50** (5.00 mL, 5.22 g, 49.2 mmol) was added to potassium carbonate solution (10 % w/v, 30.0 mL) and vigorously swirled for 1 minute. The organic layer was collected.

Methyltriphenylphosphonium bromide (7.14 g, 20.0 mmol) was stirred in DCM (15.0 mL) for 10 minutes, after which benzaldehyde **50** (2.00 mL, 2.10 g, 20.0 mmol)

was added, followed by the addition of sodium hydroxide solution (50.0 g in 75.0 mL). This mixture was stirred vigorously for 40 minutes. Water (15.0 mL) was then added to the reaction mixture and the product was extracted with DCM (100 mL). The aqueous phase was extracted once more with DCM (40.0 mL) and the combined organic extracts were dried over anhydrous magnesium sulfate, filtered and concentrated under reduced pressure to yield a cream solid. This was triturated with hot petroleum ether (50.0 mL) and concentrated under reduced pressure to yield a cream solid (0.75 g, 7.19 mmol, 38 %).

Yield: 0.75 g, 7.19 mmol, 38 %

IR (thin film, NaCl plate): 3414 (s), 3056 (s, C-H aromatic), 2794 (s, C-H aliphatic), 2915 (s, C-H aliphatic), 2740 (w), 1974 (w), 1905 (w), 1823 (w), 1697 (s, C=O), 1653 (m, C=C aromatic), 1596 (m, C=C aromatic), 1484 (m), 1438 (s), 1415 (m), 1333 (m), 1298 (m), 1169 (s), 1123 (s), 1107 (s), 1072 (m), 1027 (w), 997 (w), 885 (s), 828 (w), 745 (s), 714 (s), 695 (s), 650 (w)

^{1}H NMR (300 MHz, CDCl$_3$): δH 1.154 (t, 1H), 1.941 (d, 1H, J = 13.146), 3.501 (m, 1H), 7.205 (m, 5H), 9.968 (s, 0.20H)

^{13}C NMR (75 MHz, CDCl$_3$, PENDANT): δC 15.217, 16.006, 16.892, 18.432, 57.883, 61.051, 101.573, 125.545, 126.628, 126.686, 128.136, 128.164, 128.287, 128.469, 128.562, 128.600, 128.621, 128.679, 128.759, 128.780, 128.795, 128.825, 129.013, 129.727, 130.402, 130.438, 130.533, 130.568, 130.890, 131.799, 131.835, 132.137, 133.194, 134.497, 136.362, 192.419

This reaction procedure was repeated with 3,4-*bis*(*tert*-butyldimethylsilyl-oxy)benzaldehyde **47** in place of benzaldehyde **50**.

4.9.8. Synthesis of 3,4-*bis*(*tert*-butyldimethylsilyl-oxy)vinyl benzene **48**

Zinc powder (2.41 g, 36.9 mmol) was stirred in distilled THF (19.5 mL) at 0 °C. Diiodomethane (1.65 mL, 5.49 g, 20.5 mmol) was added to this slurry at a rate which maintained the temperature below 10 °C. After the addition, the resultant suspension was recooled to 0 °C. A solution of titanium tetrachloride (0.670 mL, 1.17 g, 6.15 mmol) in distilled DCM (2.60 mL) was added slowly to the suspension, whilst ensuring the temperature did not exceed 15 °C. This suspension was then cooled to 0 °C and stirred for 30 minutes, after which 3,4-*bis*(*tert*-butyldimethylsilyl-oxy)benzaldehyde **47** (1.50 g, 4.09 mmol) was added. The resultant green/black

mixture was stirred at room temperature for 16 hours under an atmosphere of nitrogen. The reaction was quenched by the addition of dilute hydrochloric acid (1 M, 350 mL) and the product was extracted with diethyl ether (100 mL). The organic layer was then washed with brine (100 mL × 2), dried over anhydrous magnesium sulfate, filtered and concentrated under reduced pressure to yield a yellow oil. This crude product was purified by flash column chromatography (100 % hexane) to yield a clear oil **48** (0.300 g, 0.825 mmol, 21 %).

Yield: 0.300 g, 0.825 mmol, 21 %

IR (thin film, NaCl plate): 3086 (w, C-H aromatic), 3037 (m, C=C aromatic), 3006 (m), 2956 (s), 2930 (s, C-H aliphatic), 2858 (s, C-H aliphatic), 2741 (w), 2711 (w), 2575 (w), 2360 (w), 1938 (w), 1799 (w), 1629 (m, C=C vinyl), 1599 (m, C=C aromatic), 1567 (m, C=C aromatic), 1509 (s, C=C aromatic), 1472 (m), 1416 (m), 1391 (m), 1362 (m), 1296 (s), 1254 (s), 1227 (m), 1163 (m), 1124 (m), 1006 (w), 970 (m), 903 (s), 839 (s), 781 (m), 689 (m)

^{1}H NMR (300 MHz, CDCl$_3$): δH 0.286 (d, 12H, CH$_3$, J = 2.3), 1.046 (d, 18H, CH$_3$, J = 3.8), 5.153 (d, 1H, CH, J = 10.9), 5.610 (d, 1H, CH, J = 17.6), 6.666 (dd, 1H, CH, J = 10.8 and J = 10.8), 6.820 (d, 1H, CH, J = 8.2), 6.890 (dd, 1H, CH, J = 10.8 and J = 10.8), 6.917 (d, 1H, CH, J = 1.9)

^{13}C NMR (75 MHz, CDCl$_3$, PENDANT): δC -4.056 (d, CH$_3$), 11.481, 14.169, 18.524 (d, C), 22.719, 25.993 (d, CH$_3$), 31.661, 111.650 (s, CH$_2$), 118.755 (s, CH), 119.738 (s, CH), 121.002 (s, CH), 131.392 (s, C), 136.487 (s, C), 146.882 (s, C), 146.942 (s, C)

MS (ES+): m/z 387.2145 (100 %, [M + Na]$^+$), calculated 387.2152 for C$_{20}$H$_{36}$O$_2$Si$_2$Na

4.9.9. Attempted desilylation of 3,4-*bis*(*tert*-butyldimethylsilyl-oxy)vinyl benzene **48**[151]

3,4-*bis*(*tert*-butyldimethylsilyl-oxy)vinyl benzene **48** (0.100 g, 0.275 mmol) was added to a solution of TBAF (0.178 mL, 0.605 mmol) in THF (1.00 mL). This mixture was stirred at room temperature for 16 hours under an atmosphere of nitrogen. The mixture was then poured into water (1.20 mL) and the product was extracted with ethyl acetate (1.00 mL × 2). The combined organic extracts were washed with saturated ammonium chloride solution (1.00 mL × 2) and brine (1.00 mL × 2), then

dried over anhydrous magnesium sulfate, filtered and concentrated under reduced pressure to yield a white solid (5.00×10^{-3} g, 0.0368 mmol, 13 %).

Yield: 5.00×10^{-3} g, 0.0368 mmol, 13 %

^{1}H NMR (300 MHz, CDCl$_3$): δH 0.215 (s, 2H), 0.938 (s, 3H), 5.110 (d, 1H, CH, J = 11.1), 5.556 (d, 1H, CH, J = 17.6), 6.557 (dd, 1H, CH, J = 10.8 and J = 10.8), 6.855 (d, 2H, CH), 7.001 (s, 1H, CH)

4.9.10. Further attempted desilylation of 3,4-*bis*(*tert*-butyldimethylsilyl-oxy)vinyl benzene **48**[158]

A solution of 3,4-*bis*(*tert*-butyldimethylsilyl-oxy)vinyl benzene **48** (0.0910 g, 0.250 mmol) in DCM (0.250 mL) was stirred at 30 °C for 20 minutes. A solution of TiCl$_4$ (0.0822 mL, 0.142 g, 0.750 mmol) in ethyl acetate (0.0822 mL) and DCM (0.375 mL) was added to the monomer mixture and the resultant mixture was stirred at 30 °C for 6 hours under an atmosphere of nitrogen. The reaction was quenched with water (20.0 mL) and the product was extracted with diethyl ether (20.0 mL × 2). The combined organic extracts were dried over magnesium sulfate, filtered and concentrated under reduced pressure to yield the product as a brown oil (0.0213 g, 0.157 mmol, 63 %) with a strong odour of TBDMS.

Yield: 0.0213 g, 0.157 mmol, 63 %

^{1}H NMR (300 MHz, CDCl$_3$): 0.088 (s, 1H), 0.896 (s, 1H), 1.273 (s, 1H), 1.580 (s, 1H)

Chapter 5
References

1. R. L. Huang, S. H. Goh and S. H. A. Ong, *The chemistry of free radicals*, 1974, Edward Arnold.
2. A. Ravve, *Principles of polymer chemistry*, vol. 1, 2000, Springer.
3. C. D. Anderson and E. S. Daniels, *Emulsion polymerisation and latex applications*, vol. 14, 2003, Rapra Technology.
4. K. Matyjaszewski and T. P. Davis, *Handbook of radical polymerization*, 2003, John Wiley & Sons.
5. K. N. N. Jayachandran and P. R. Chatterji, *Preparation of linear and crosslinked polymer microspheres by dispersion polymerization*, Polymer Reviews, 2001, **41**(1), 79-94.
6. W. Yang, D. Yang, J. Hu, C. Wang and S. Fu, *Dispersion copolymerization of styrene and other vinyl monomers in polar solvents*, Journal of Polymer Science: Part A: Polymer Chemistry, 2001, **39**, 555-561.
7. S. Deniz, N. Baran, M. Akgun, I. N. Uzun and S. Dincer, *Dispersion polymerization of methyl methacrylate in supercritical carbon dioxide using a silicone-containing fluoroacrylate stabilizer*, Polymer International, 2005, **54**, 1660-1668.
8. S. Shen, E. D. Sudol and M. S. El-Aasser, *Dispersion polymerization of methyl methacrylate: Mechanism of particle formation*, Journal of Polymer Science: Part A Polymer Chemistry, 1994, **32**, 1097-1100.
9. J. Hong, C. K. Hong and S. E. Shim, *Synthesis of polystyrene microspheres by dispersion polymerization using poly(vinyl alcohol) as a steric stabilizer in aqueous alcohol media*, Colloids and Surfaces A: Physicochem. Eng. Aspects, 2007, **302**, 225-233.
10. S. F. Ahmed and G. W. Poehlein, *Kinetics of dispersion polymerization of styrene in ethanol. 1. Model development*, Ind. Eng. Chem. Res. 1997, **36**, 2597-2604.
11. Z. Song, E. S. Daniels, E. D. Sudol, M. S. El-Aasser and A. Klein, *Mechanism of seeded dispersion polymerization of methyl methacrylate using submicron polystyrene seed particles*, Journal of Applied Polymer Science, 2011, **122**, 203-209.
12. D. Horak, *Uniform polymer beads of micrometer size*, Acta Polymer, 1996, **47**, 20-28.
13. K. D. Hermanson and E. W. Kaler, *Transition from microemulsion to emulsion polymerization: Mechanism and final properties*, Journal of Polymer Science: Part A: Polymer Chemistry, 2004, **42**, 5253-5261.
14. C. S. Chern, *Emulsion polymerization mechanisms and kinetics*, Prog. Polym. Sci., 2006, **31**, 443-486.
15. N. Friis, *A kinetic study of the emulsion polymerization of vinyl acetate*, 1973, Danish Atomic Energy Commission.
16. J. K. Oh, *Recent advances in controlled/living radical polymerization in emulsion and dispersion*, Journal of Polymer Science: Part A: Polymer Chemistry, 2008, **46**, 6983-7001.
17. T. J. Tulig and M. Tirrell, *On the onset of the trommsdorff effect*, Macromolecules, 1982, **15**(2), 459-463.
18. S. Hendrana, D. J. T. Hill, M. C. S. Perera and P. J. Pomery, *Copolymerization of methyl methacrylate and allyl acetate part i. Rate of reaction*, Polymer International, 2001, **50**, 597-605.
19. K. E. J. Barrett, *Dispersion polymerisation in organic media*, Br. Polym. J., 1973, **5**, 259-271.
20. P. R. Dvornic and M. S. Jacovic, *The viscosity effect on autoacceleration of the rate of free radical polymerisation*, Polymer engineering and science, 1981, **21**(12), 792-796.
21. E. Vivaldo-Lima, P. E. Wood and A. E. Hamielec, *An updated review on suspension polymerization*, Ind. Eng. Chem. Res., 1997, **36**(4), 939-965.

22. C-C. Lin and Y-F. Wang, *Suspension polymerization of methyl methacrylate. I. Modeling of reaction kinetics*, Journal of Applied Polymer Science, 1981, **26**, 3909-3915.

23. C. Guerrero-Sanchez, T. Erdmenger, P. Sereda, D. Wouters and U. S. Schubert, *Water-soluble ionic liquids as novel stabilizers in suspension polymerization reactions: Engineering polymer beads*, Chem. Eur. J., 2006, **12**, 9036-9045.

24. G. G. Odian, *Principles of polymerization*, 2004, Wiley-Interscience.

25. F. Jahanzada, S. Sajjadib and B. W. Brooks, *Characteristic intervals in suspension polymerisation reactors : An experimental and modelling study*, Chemical Engineering Science, 2005, **60**, 5574-5589.

26. H. Yuyama, T. Hashimoto, H-H. M, M. Nagai and S. Omi, *Mechanism of suspension polymerization of uniform monomer droplets prepared by glass membrane (shirasu porous glass) emulsification technique*, Journal of Applied Polymer Science, 2000, **73**, 1025-1043.

27. F. J. Schork, Y. Luo, W. Smulders, J. P. Russum, A. Butté and K. Fontenot, *Miniemulsion polymerization*, Adv. Polym. Sci., 2005, **175**, 129-255.

28. A. I. Cooper, W. P. Hems and A. B. Holmes, *Synthesis of highly cross-linked polymers in supercritical carbon dioxide by heterogeneous polymerization*, Macromolecules, 1999, **32**, 2156-2166.

29. M. Schmitt, R. Schulze-Pillotb and R. Hempelmann, *Kinetics of bulk polymerisation and gompertz's law*, Phys. Chem. Chem. Phys., 2011, **13**, 690-695.

30. J. W. Vanderhoff, *Mechanism of emulsion polymerisation*, Journal of Polymer Science: Polymer Symposium, 1985, **72**, 161-198.

31. S. Jiang, X. Fang, Q. Yu, J. Deng and W. Yang, *New route to monodispersed amphiphilic core-shell polymer nanoparticles: Polymerization of styrene from α-methylstyrene-containing macroinitiator*, Journal of Applied Polymer Science, 2012, **124**, 4121-4126.

32. A. J. Josea, S. Ogawab and M. Bradley, *Tuning the pore size and surface area of monodisperse poly(methyl acrylate) beads via parallel seeded polymerisation*, Polymer, 2005, **46**, 2880-2888.

33. K. Kobayashi and M. Senna, *Independent control of mechanical and chemical properties of monodispersed polystyrene-divinyl benzene microspheres by two-step polymerization*, Journal of Applied Polymer Science, 1992, **46**, 27-40.

34. S. Pathak, E. Cao, M. C. Davidson, S. Jin and G. A. Silva, *Quantum dot applications to neuroscience: New tools for probing neurons and glia*, The Journal of Neuroscience, 2006, **26**(7), 1893-1895.

35. R. Hardman, *A toxicologic review of quantum dots: Toxicity depends on physicochemical and environmental factors*, Environmental Health Perspectives, 2006, **114**(2), 165-172.

36. F. Pinaud, X. Michalet, L. A. Bentolila, J. M. Tsay, S. Doose, J. J. Li, G. Iyer and S. Weiss, *Advances in fluorescence imaging with quantum dot bio-probes*, Biomaterials, 2006, **27**, 1679-1687.

37. P. M. Naves, T. N. Gonzaga, A. F. G. Monte and N. O. Dantas, *Band gap energy of PbS quantum dots in oxide glasses as a function of concentration*, Journal of Non-Crystalline Solids, 2006, **352**, 3633-3635.

38. P. Alivisatos, U. Banin, J. S. Bradley and J. F. Corrigan, *Nanoparticles*, 2004, Wiley-VCH.

39. G. D. Scholes and G. Rumbles, *Excitons in nanoscale systems*, Nature materials, 2006, **5**, 683-696.

40. B. Pejova, A. Tanusevski and I. Grozdanov, *Semiconducting thin films of zinc selenide quantum dots*, Journal of Solid State Chemistry, 2004, **177**, 4785-4799.

41. P. Hui, *Quantum confinement effects on binding energies and optical properties of excitons in quantum dots*, Chin. Phys. Lett., 2004, **21**(1), 160-163.

42. C. Y. Wong, J. Kim, P. S. Nair, M. C. Nagy and G. D. Scholes, *Relaxation in the exciton fine structure of semiconductor nanocrystals*, J. Phys. Chem. C, 2008, **113**(3), 795-811.

43. B. O. Dabbousi, J. Rodriguez-Viejo, F. V. Mikulec, J. R. Heine, H. Mattoussi, R. Ober, K. F. Jensen and M. G. Bawendi, *(CdSe)ZnS core-shell quantum dots: Synthesis and characterization of a size series of highly luminescent nanocrystallites*, J. Phys. Chem. B, 1997, **101**(46), 9463-9475.

44. W. Cai, A. R. Hsu, Z-B. Li and X. Chen, *Are quantum dots ready for in vivo imaging in human subjects?*, Nanoscale Res. Lett., 2007, **2**, 265-281.

45. I. D. Tomlinson, H. A. Gussin, D. M. Little, M. R. Warnement, H. Qian, D. R. Pepperberg and S. J. Rosenthal, *Imaging gabac receptors with ligand-conjugated quantum dots*, Journal of Biomedicine and Biotechnology, 2007, 1-9.

46. R. Wilson, D. G. Spiller, I. A. Prior, R. Bhatt and A. Hutchinson, *Magnetic microspheres encoded with photoluminescent quantum dots for multiplexed detection*, Journal of Materials Chemistry, 2007, **17**, 4400-4406.

47. A. Bagga, P. K. Chattopadhyay and S. Ghosh, *Origin of stokes shift in InAs and CdSe quantum dots: Exchange splitting of excitonic states*, Physical B review, 2006, **74**, 1-7.

48. T. C. Lim, V. J. Bailey, Y-P. Ho and T-H. Wang, *Intercalating dye as an acceptor in quantum-dot-mediated fret*, Nanotechnology, 2008, **19**, 1-7.

49. B. A. Rzigalinski and J. S. Strobl, *Cadmium-containing nanoparticles: Perspectives on pharmacology and toxicology of quantum dots*, Toxicology and Applied Pharmacology, 2009, **238**, 280-288.

50. S. J. Cho, D. Maysinger, M. Jain, B. Roder, S. Hackbarth and F. M. Winnik, *Long-term exposure to CdTe quantum dots causes functional impairments in live cells*, Langmuir, 2007, **23**(4), 1974-1980.

51. E. Przybytkowski, M. Behrendt, D. Dubois and D. Maysinger, *Nanoparticles can induce changes in the intracellular metabolism of lipids without compromising cellular viability*, FEBS Journal, 2009, **276**, 6204-6217.

52. V. Karabanovas, E. Zakarevicius, A. Sukackaite, G. Streckytea and R. Rotomskis, *Examination of the stability of hydrophobic (CdSe)ZnS quantum dots in the digestive tract of rats*, Photochem. Photobiol. Sci., 2008, **7**, 725-729.

53. J. R. Lakowicz, *Principles of fluorescence spectroscopy*, vol. 1, 2006, Springer.

54. D. G. Patel, Y-Y. Ohnishi, Y. Yang, S-H. Eom, R. T. Farley, K. R. Graham, J. Xue, S. Hirata, K. S. Schanze and J. R. Reynolds, *Conjugated polymers for pure UV light emission: Poly(meta-phenylenes)*, Journal of polymer science Part B: polymer physics, 2011, **49**, 557-565.

55. E. Ripaud, Y. Olivier, P. Leriche, J. Cornil and J. Roncali, *Polarizability and internal charge transfer in thiophene-triphenylamine hybrid π-conjugated systems*, J. Phys. Chem. B, 2011, **115**, 9379-9386.

56. A. Fu, W. Gu, C. Larabell and P. Alivisatos, *Semiconductor nanocrystals for biological imaging*, Current Opinion in Neurobiology, 2005, **15**, 568-575.

57. W. W. Yu, E. Chang, R. Drezek and V. L. Colvin, *Water-soluble quantum dots for biomedical applications*, Biochemical and Biophysical Research Communications, 2006, **348**, 781-786.

58. K-H. Lee, *Quantum dots: A quantum jump for molecular imaging?*, The Journal of Nuclear Medicine, 2007, **48**(9), 1408-1410.

59. N. Gennet, L. M. Alexander, R. M. Sanchez-Martın, J. M. Behrendt, A. J. Sutherland, J. M. Brickman, M. Bradley and M. Li, *Microspheres as a*

vehicle for biomolecule delivery to neural stem cells, New Biotechnology, 2009, **25**(6), 442-449.

60. S. Jung, S. Huh, Y-P. Cheon and S. Park, *Intracellular protein delivery by glucose-coated polymeric beads*, Chem. Commun., 2009, 5003-5005.

61. R. M. Sanchez-Martin, L. Alexander, M. Muzerelle, J. M. Cardenas-Maestre, A. Tsakiridis, J. M. Brickman and M. Bradley, *Microsphere-mediated protein delivery into cells*, ChemBioChem, 2009, **10**, 1453-1456.

62. L. M. Alexander, S. Pernagallo, A. Livigni, R. M. Sanchez-Martın, J. M. Brickman and M. Bradley, *Investigation of microsphere-mediated cellular delivery by chemical, microscopic and gene expression analysis*, Molecular BioSystems, 2010, **6**, 399-409.

63. J. M. Cardenas-Maestre, S. Panadero-Fajardo, A. M. Perez-Lopez and R. M. Sanchez-Martin, *Sulfhydryl reactive microspheres for the efficient delivery of thiolated bioactive cargoes*, J. Mater. Chem., 2011, **21**, 12735-12743.

64. J. M. Behrendt, D. Nagel, E.Chundoo, L. M. Alexander, D. Dupin, A. V. Hine, M. Bradley and A. J. Sutherland, 2012, *Synthesis and characterization of dual-functionalized core-shell fluorescent microspheres for bioconjugation and cellular delivery*, Manuscript submitted for publication.

65. J. M. Tiffany, *The normal tear film*, Developments in Ophthalmology, 2008, **41**, 1-20.

66. U. Stahl, M. Willcox and F. Stapleton, *Osmolality and tear film dynamics*, Clin. Exp. Optom., 2012, **95**(1), 3-11.

67. A. Panaser and B. J. Tighe, *Function of lipids – their fate in contact lens wear: An interpretive review*, Contact Lens & Anterior Eye, 2012, 1-12.

68. A. J. Bron, J. M.Tiffanya, S. M. Gouveiaa, N. Yokoib and L. W. Voon, *Functional aspects of the tear film lipid layer*, Experimental Eye Research, 2004, **78**, 347-360.

69. H. Lorentz and L. Jones, *Lipid deposition on hydrogel contact lenses: How history can help us today*, Optometry and Vision Science, 2007, **84**(4), 286-295.

70. Y. Ohashi, M. Dogru and K. Tsubota, *Laboratory findings in tear fluid analysis*, Clinica Chimica Acta, 2006, **369**, 17-28.

71. R. Sariri and H. Ghafoori, *Tear proteins in health, disease, and contact lens wear*, Biochemistry (Moscow), 2008, **73**(4), 381-392.

72. K. A. McClellan, *Mucosal defence of the outer eye*, Survey of Ophthalmology, 1997, **42**(3), 233-246.

73. D. H. Szczesna and H. T. Kasprzak, *Numerical analysis of interferograms for evaluation of tear film build-up time*, Ophthalmic Physiol. Opt., 2009, **29**(3), 211-218.

74. J. Nemeth, B. Erdelyi, B. Csakany, P. Gaspar, A. Soumelidis, F. Kahlesz and Z. Lang, *High-speed videotopographic measurement of tear film build-up time*, Investigative Ophthalmology & Visual Science, 2002, **43**(6), 1783-1790.

75. D. H. Szczesna and H. T. Kasprzak, *Numerical analysis of interferograms for evaluation of tear film build-up time*, Ophthal. Physiol. Opt., 2009, **29**, 211-218.

76. E. Goto and S. C. Tseng, *Differentiation of lipid tear deficiency dry eye by kinetic analysis of tear interference images*, Archives of Ophthalmology, 2003, **121**, 173-180.

77. E. Goto and S. C. Tseng, *Kinetic analysis of tear interference images in aqueous deficiency dry eye before and after punctal occlusion*, Investigative Ophthalmology and Visual Science, 2003, **44**, 1897-1905.

78. M. A. Lemp and H. H. Weiler, *How do tears exit?*, Investigative Ophthalmology and Visual Science, 1983, **24**, 619-622.

79. M. G. Doane, *Interactions of the eyelids and tears in corneal wetting and the dynamics of the normal human eyeblink*, American Journal of Ophthalmology, 1980, **89**, 507-516.

80. P. H. Hinderling, *Red blood cells: A neglected compartment in pharmacokinetics and pharmacodynamics*, Pharmacological Reviews, 1997, **49**(3), 279-295.

81. S. R. Goodman, A. Kurdia, L. Ammann, D. Kakhniashvili and O. Daescu, *The human red blood cell proteome and interactome*, Experimental Biology and Medicine, 2007, **232**, 1391-1408.

82. M. Dao, C. T. Limb and S. Suresh, *Mechanics of the human red blood cell deformed by optical tweezers*, Journal of the Mechanics and Physics of Solids, 2003, **51**, 2259-2280.

83. A.V.Gothoskar, *Resealed erythrocytes : A review*, Pharmaceutical Technology, 2004, **28**(3), 140-158.

84. M. Y. B. Çimen, *Free radical metabolism in human erythrocytes*, Clinica Chimica Acta, 2008, **390**, 1-11.

85. N. S. Gov and S. A. Safrany, *Red blood cell membrane fluctuations and shape controlled by atp-induced cytoskeletal defects*, Biophysical Journal, 2005, **88**(3), 1859-1874.

86. Y-Z. Yoon, J. Kotar, G. Yoon and P. Cicuta, *The nonlinear mechanical response of the red blood cell*, Phys. Biol., 2008, **5**, 1-8.

87. D. S. Garbe, A. Das, R. R. Dubreuil and G. J. Bashaw, *β-spectrin functions independently of Ankyrin to regulate the establishment and maintenance of axon connections in the Drosophila embryonic CNS*, Development, 2007, **134**(2), 273-284.

88. E. M. Pasinia, H. U. Lutzb, M. Mannc and A. W. Thomasa, *Red blood cell (RBC) membrane proteomics — part i: Proteomics and RBC physiology*, Journal of Proteomics, 2010, **73**, 403-420.

89. N. Mohandas and P. G. Gallagher, *Red cell membrane: Past, present, and future*, Blood, 2008, **112**(10), 3939-3948.

90. J. E. Smith, *Erythrocyte membrane: Structure, function, and pathophysiology*, Vet. Pathol., 1987, **24**, 471-476.

91. J. Wan, A. M. Forsyth and H. A. Stone, *Red blood cell dynamics: From cell deformation to ATP release*, Integr. Biol., 2011, **3**, 972-981.

92. J-P. Marolleau, V. Vanneaux, D. Rea, B. Ternaux, V. Delasse, V. Hubert, E. Chantre, R. Traineau, M. Robin, M. Benbunan, G. Socié and J. Larghero, *Quantification of nucleated red blood cells in allogeneic marrow graft and impact of processing on recovery*, Transfusion, 2007, **47**, 266-271.

93. C. E. Stevens, J. Gladstone, P. E. Taylor, A. Scaradavou, A. R. Migliaccio, J.Visser, N. L. Dobrila, C. Carrier, M. Cabbad, P. Wernet, J. Kurtzberg and P. Rubinstein, *Placental/umbilical cord blood for unrelated-donor bone marrow reconstitution : Relevance of nucleated red blood cells*, Blood, 2002, **100**(7), 2662-2664.

94. G. El-Din, I. Harisa, M. F. Ibrahim and F. K. Alanazi, *Characterization of human erythrocytes as potential carrier for pravas-tatin: An in vitro study*, Int. J. Med. Sci., 2011, **8**(3), 222-230.

95. M. Magnani, L. Rossi, A. Fraternale, M. Bianchi, A. Antonelli, R. Crinelli and L. Chiarantini, *Erythrocyte-mediated delivery of drugs, peptides and modified oligonucleotides*, Gene Therapy, 2002, **9**, 749-751.

96. R. Luo, S. Mutukumaraswamy, S. S. Venkatraman and B. Neu, *Engineering of erythrocyte-based drug carriers: Control of protein release and bioactivity*, J. Mater. Sci.: Mater. Med., 2012, **23**, 63-71.

97. V. R. Muzykantov, *Drug delivery by red blood cells: Vascular carriers designed by mother nature*, Expert Opin. Drug Deliv., 2010, **7**(4), 403-427.

98. G. V. Shavi, R. C. Doijada, P. B. Deshpandea, M. Fva, S. R. Mekab, N. Udupab, O. R and D. K, *Erythrocytes as carrier for prednisolone: In vitro and in vivo evaluation*, Pak. J. Pharm. Sci. **23**(2), 194-200.

99. S. Biagiotti, M. F. Paoletti, A. Fraternale, L. Rossi and M. Magnani, *Drug delivery by red blood cells*, IUBMB Life, 2011, **63**(8), 621-631.

100. P. H. Hinderling, *Red blood cells: A neglected compartment in pharmacokinetics and pharmacodynamics*, Pharmalogical Reviews, 1997, **49**(3), 279-295.

101. W. T. Al-Jamal and K. Kostarelos, *Liposomes: From a clinically established drug delivery system to a nanoparticle platform for theranostic nanomedicine*, Accounts of Chemical Research, 2011, **44**(10), 1094-1104.

102. C-M. J. Hu, L. Zhang, S. Aryal, C. Cheung, R. H. Fang and L. Zhang, *Erythrocyte membrane-camouflaged polymeric nanoparticles as a biomimetic delivery platform*, PNAS, 2011, **108**(27), 10980-10985.

103. J. M. Behrendt, M. Afzaal, L. M. Alexander, M. Bradley, A. V. Hine, D. Nagel, P. O'Brien, K. Presland and A. J. Sutherland, *Thiol-containing microspheres as polymeric ligands for the immobilisation of quantum dots*, J. Mater. Chem., 2009, **19**, 215-221.

104. D. A. Navarro, S. Banerjee, D. S. Aga and D. F. Watson, *Partitioning of hydrophobic CdSe quantum dots into aqueous dispersions of humic substances: Influence of capping-group functionality on the phase-transfer mechanism*, Journal of Colloid and Interface Science, 2010, **348**, 119-128.

105. J. M. Behrendt, X. Fu, E. Chundoo, A. Hine, D. Nagel and A. J. Sutherland, 2012, *Synthesis of silica-shelled microspheres with covalently incorporated fluorescent dyes and reactive sites for surface functionalisation*, Manuscript submitted for publication.

106. T. Hwanga, L. Pua, S. W. Kimb, Y-S. Ohc and J-D. Nam, *Synthesis and barrier properties of poly(vinylidene chloride-co-acrylonitrile)/SiO$_2$ hybrid composites by sol–gel process*, Journal of Membrane Science, 2009, **345**, 90-96.

107. T. Hwang, L. Pu, S. W.Kim, Y-S. Oh and J.-D. Nam, *Synthesis and barrier properties of poly(vinylidene chloride-co-acrylonitrile)/SiO$_2$ hybrid composites by sol–gel process*, Journal of Membrane Science, 2009, **345**, 90-96.

108. M. A. Parada, A. de Almeida, P. N.Volpe, C. Muntele and D. Ila, *Damage effects of 1 MeV proton bombardment in PVDC polymeric film*, Surface & Coatings Technology, 2007, **201**, 8052-8054.

109. P. D. Zygoura, K. A. Riganakos and M. G. Kontominas, *Study of the migration behavior of acetyl tributyl citrate from PVDC/PVC film into fish fillets as affected by intermediate doses of electron beam radiation*, Eur. Food Res. Technol., 2011, **232**, 1017-1025.

110. T. Danno, K. Murakami and R. Ishikawa, *Preparation of carbyne-like films by dehydrochlorination of poly(vinylidene chloride)*, American Institute of Physics, 1999, 213-216.

111. S. Kobayashi and S. Nagayama, *A microencapsulated lewis acid. A new type of polymer-supported lewis acid catalyst of wide utility in organic synthesis*, J. Am. Chem. Soc., 1998, **120**, 2985-2986.

112. R. Akiyama and S. Kobayashi, *"Microencapsulated" and related catalysts for organic chemistry and organic synthesis*, Chem. Rev., 2009, **109**, 594-642.

113. H. M. Reul and M. Akdis, *Blood pumps for circulatory support*, Perfusion, 2000, **15**, 295-311.

114. H. Mizunuma and R. Nakajima, *Experimental study on shear stress distributions in a centrifugal blood pump*, Artificial Organs, 2007, **31**(7), 550-559.

115. T. Zhang, M. E. Taskin, H-B. Fang, A. Pampori, R. Jarvik, B. P. Griffith and Z. J. Wu, *Study of flow-induced hemolysis using novel couette-type blood-shearing devices*, Artificial Organs, 2011, **35**(12), 1180-1185.

116. N. Yokoyama, D. Sakota, E. Nagaoka and S. Takatani, *Alterations in red blood cell volume and hemoglobin concentration, viscoelastic properties and mechanical fragility caused by continuous flow pumping in calves*, Artificial Organs, 2011, **35**(8), 791-799.

117. H. Mizunuma and R. Nakajima, *Experimental study on shear stress distributions in a centrifugal blood pump*, Artificial Organs, 2011, **31**(7).

118. Y-H. Yang, M. Haile, Y. T. Park, F. A. Malek and J. C. Grunlan, *Super gas barrier of all-polymer multilayer thin films*, Macromolecules, 2011, **44**, 1450-1459.

119. A. Petukhova, A. S. Paton, Z. Wei, I. Gourevich, S. V. Nair, H. E. Ruda, A. Shik and E. Kumacheva, *Polymer multilayer microspheres loaded with semiconductor quantum dots*, Adv. Funct. Mater., 2008, **18**, 1961-1968.

120. J. Li, M. A. J. Mazumder, H. D. H. Stover, A. P. Hitchcock and I. M. Shirley, *Polyurea microcapsules: Surface modification and capsule size control*, Journal of Polymer Science Part A: Polymer Chemistry, 2011, **49**, 3038-3047.

121. D. P. Go, S. L. Gras, D. Mitra, T. H. Nguyen, G. W. Stevens, J. J. Cooper-White and A. J. O'Connor, *Multilayered microspheres for the controlled release of growth factors in tissue engineering*, Biomacromolecules, 2011, **12**, 1494-1503.

122. M. Martı, G. Fabregat, F. Estrany, C. Aleman and E. Armelin, *Nanostructured conducting polymer for dopamine detection*, J. Mater. Chem., 2010, **20**, 10652-10660.

123. A. N. Generalova, V. A. Oleinikov, M. M. Zarifullina, E. V. Lankina, S. V. Sizova, M. V. Artemyev and V. P. Zubov, *Optical sensing quantum dot-labeled polyacrolein particles prepared by layer-by-layer deposition technique*, Journal of Colloid and Interface Science, 2011, **357**, 265-272.

124. R. Wongsagonsup, S. Shobsngob, B. Oonkhanond and S. Varavinit, *Zeta potential (ζ) and pasting properties of phosphorylated or crosslinked rice starches*, Starch, 2005, **57**(1), 32-37.

125. W. Zheng, D. Li, Y. Zeng, Y. Luo and J. Y. Qu, *Two-photon excited hemoglobin fluorescence*, Biomedical Optics Express, 2011, **2**(1), 71-79.

126. M. Harboe, *A method for determination of hemoglobin in plasma by near-ultraviolet spectrophotometry*, Scandinavian journal of clinical and laboratory investigation, 1959, **11**, 66-70.

127. R. Mehvar, *Dextrans for targeted and sustained delivery of therapeutic and imaging agents*, Journal of Controlled Release, 2000, **69**, 1-25.

128. X-C. Shen, X-Y. Liou, L-P. Ye, H. Liang and Z-Y. Wang, *Spectroscopic studies on the interaction between human hemoglobin and CdS quantum dots*, Journal of Colloid and Interface Science, 2007, **311**, 400-406.

129. D-H. Hu, H-M. Wu, J-G. Liang and H-Y. Han, *Study on the interaction between CdSe quantum dots and hemoglobin*, Spectrochimica Acta Part A, 2008, **69** 830-834.

130. T. J. Difeo and A. W. Addison, *Haem-binding-site heterogeneity and haem cotton effects of glycera dibranchiata monomeric haemoglobins*, Biochem. J., 1989, **260**, 863-871.

131. W. Min, S. Lu, S. Chong, R. Roy, G. R. Holtom and S. Xie, *Imaging chromophores with undetectable fluorescence by stimulated emission microscopy*, Nature, 2009, **461**, 1105-1109.

132. B. D. Mather, K. Viswanathan, K. M. Miller and T. E. Long, *Michael addition reactions in macromolecular design for emerging technologies*, Prog. Polym. Sci., 2006, **31**, 487-531.

133.   R. Liu, R. Liew, J. Zhou and B. Xing, *A simple and specific assay for real-time colorimetric visualization of β-lactamase activity by using gold nanoparticles*, Angew. Chem. Int. Ed., 2007, **46**, 8799-8803.

134.   Y. A. Kim, A. Sharon, C. K. Chu, R. H. Rais, O. N. A. Safarjalani, F. N. M. Naguib and M. H. el Kouni, *Synthesis, biological evaluation and molecular modeling studies of N^6-benzyladenosine analogues as potential anti-toxoplasma agents*, Biochemical Pharmacology, 2007, **73**, 1558-1572.

135.   M. McCairn, Solid-phase combinatorial chemistry and scintillation proximity assays, PhD thesis, *CEAC*, Aston University, 2003.

136.   M. J. Doughty, *pH dependent spectral properties of sodium fluorescein ophthalmic solutions revisited*, 2010, Ophthalmic Physiol. Opt., **30**(2), 167-174.

137.   Y. B. Choy, J-H. Park and M. R. Prausnitz, *Mucoadhesive microparticles engineered for ophthalmic drug delivery*, J. Phys. Chem. Solids, 2008, **69** (5-6), 1533-1536.

138.   H. Xu and L. Zhang, *Controllable one-pot synthesis and enhanced photocatalytic activity of mixed-phase TiO_2 nanocrystals with tunable brookite/rutile ratios*, J. Phys. Chem. C, 2009, **113**, 1785-1790.

139.   A. Samontha, J. Shiowatana and A. Siripinyanond, *Particle size characterization of titanium dioxide in sunscreen products using sedimentation field-flow fractionation–inductively coupled plasma–mass spectrometry*, Anal. Bioanal. Chem., 2011, **399**, 973-978.

140.   E. Kontturi, P. C. Thune and J. W. Niemantsverdriet, *Novel method for preparing cellulose model surfaces by spin coating*, Polymer, 2003, **44**, 3621-3625.

141.   J. Song, J. Liang, X. Liu, W. E. Krause, J. P. Hinestroza and O. J. Rojas, *Development and characterization of thin polymer films relevant to fiber processing*, Thin Solid Films, 2009, **517**, 4348-4354.

142.   D. J. Cooke, D. Eder and J. A. Elliott, *Role of benzyl alcohol in controlling the growth of TiO_2 on carbon nanotubes*, J. Phys. Chem. C, 2010, **114**(6), 2462-2470.

143.   M. Aoyagi and M. Funaoka, *A new polymeric photosensitizer for dye-sensitized solar cell with porous TiO_2 from forest carbon resources*, Journal of Photochemistry and Photobiology A: Chemistry, 2004, **164**, 53-60.

144.   S. K. Lunsford, H. Choi, J. Stinson, A. Yeary and D. D. Dionysiou, *Voltammetric determination of catechol using a sonogel carbon electrode modified with nanostructured titanium dioxide*, Talanta, 2007, **73**, 172-177.

145.   D. Monllor-Satoca and R. Gómez, *A photoelectrochemical and spectroscopic study of phenol and catechol oxidation on titanium dioxide nanoporous electrodes*, Electrochimica Acta, 2010, **55**, 4661-4668.

146.   J. Moser, S. Punchihewa, P. P. Infelta and M. Gratzel, *Surface complexation of colloidal semiconductors strongly enhances interfacial electron-transfer rates*, Langmuir, 1991, **7**(12), 3012-3018.

147.   C. Creutz and M. H. Chou, *Binding of catechols to mononuclear titanium(iv) and to 1- and 5-nm TiO_2 nanoparticles*, Inorg. Chem., 2008, **47**(9), 3509-3514.

148.   I. A. Jankovic, Z. V. Saponjic, E. S. Dzunuzovic and J. M. Nedeljkovic, *New hybrid properties of TiO_2 nanoparticles surface modified with catecholate type ligands*, Nanoscale Res. Lett., 2010, **5**, 81-88.

149.   C. Wu, Y. Kong, F. Gao, Y. Wu, Y. Lu, J. Wang and L. Dong, *Synthesis, characterization and catalytic performance for phenol hydroxylation of Fe-mcm41 with high iron content*, Microporous and Mesoporous Materials, 2008, **113**, 163-170.

150.   M. Schwarz, T. C. Wabnitz and P. Winterhalter, *Pathway leading to the formation of anthocyanin-vinylphenol adducts and related pigments in red wines*, J. Agric. Food Chem., 2003, **51**(12), 3682-3687.

151. E. J. Corey and A. Venkateswarlu, *Protection of hydroxyl groups as tert-butyldimethylsilyl derivatives*, Journal of the American Chemical Society, 1972, **94**(17), 6190-6191.

152. C. A. Faler and M. M. Joullie, *The Kulinkovich reaction in the synthesis of constrained N,N-dialkyl neurotransmitter analogues*, Org. Lett., 2007, **9**(10), 1987-1990.

153. P. G. M. Wuts and T. W. Greene, *Greene's protective groups in organic synthesis*, 2006, John Wiley & Sons.

154. T. Takeda, *Modern carbonyl olefination: Methods and applications*, 2006, John Wiley & Sons.

155. B. E. Maryanoff and A. B. Reitz, *The Wittig olefination reaction and modifications involving selected synthetic aspects phosphoryl-stabilized carbanions. Stereochemistry, mechanism, and selected synthetic aspects*, Chem. Rev., 1989, **89**(4), 863-927.

156. L. M. Harwood, C. J. Moody and J. M. Percy, *Experimental organic chemistry: Standard and microscale*, 1999, Blackwell Science.

157. C. M. Starks, C. L. Liotta and M. Halpern, *Phase-transfer catalysis: Fundamentals, applications, and industrial perspectives*, 1994, Chapman & Hall.

158. A. Iida, H. Okazaki, T. Misaki, M. Sunagawa, A. Sasaki and Y. Tanabe, *Efficient method for the deprotection of tert-butyldimethylsilyl ethers with TiCl$_4$-lewis base complexes: Application to the synthesis of 1β-methylcarbapenems*, J. Org. Chem., 2006, **71**(14), 5380-5383.